Characterisation of Expression and Functional Properties of $P2X_7$ Receptors

Helen Joanne Bradley

Submitted in accordance with the requirements for the degree of Doctor of Philosophy

The University of Leeds
Institute of Membrane and Systems Biology

September 2010

The candidate confirms that the work submitted is her own, and that appropriate credit has been given where reference has been made to the work of others.

Acknowledgements

I would like to express my thanks to my supervisor, Dr. Lin-Hua Jiang for his expert guidance and support.

Thank you to Dr. Zhu-Zhong Mei, Dr. Xing Liu, Dr. Rong Xia, Dr. Wei Yang and Jie Zou, it has been great working with you! My thanks also go to members of the Beech, Rao and Lippiat groups for making our lab such an enjoyable place to work.

Finally, thank you to my family, friends and John Linley. The completion of this thesis would not have been possible without their love and support.

Abstract

$P2X_7$ receptors form non-selective cation channels at the plasma membrane and are gated by the binding of extracellular ATP. Prolonged $P2X_7$ receptor activation also leads to formation of a pore that allows permeation of large molecules. Many cell types express $P2X_7$ receptors. Expression is particularly high in cells of hematopoietic origin, where they have important roles in many biological processes, including release of pro-inflammatory cytokines and apoptosis. Furthermore, the properties of $P2X_7$ receptors, including their functional expression and pharmacology, exhibit striking species differences. However, the underlying molecular bases for these differences are not fully understood.

The gene encoding human $P2X_7$ receptors contains numerous single nucleotide polymorphisms (SNP), several of which are non-synonymous (ns-SNP). Two ns-SNP mutations, H155Y and A348T, were of particular interest due to their gain-of function effect on $P2X_7$ receptors. Furthermore, a previous study found ATP-induced secretion of cytokines was enhanced in immune cells from individuals harbouring the A348T mutation. These two mutations were therefore examined in detail. Whole-cell patch-clamp current recordings clearly showed both mutations increased agonist-induced maximal currents, with no or very mild effect on agonist sensitivity. Cells expressing human $P2X_7$ receptors had lower ATP-evoked maximal currents in comparison to the rat receptor. Mutations H155Y and A348T change the residues to those in the corresponding positions of the WT rat $P2X_7$ receptor. Introduction of reciprocal mutations, Y155H and T348A into the rat $P2X_7$ receptor reduced agonist-evoked current amplitudes. Substitution of residues surrounding His^{155} and Ala^{348} in the human $P2X_7$ receptor with the corresponding residues of the rat $P2X_7$ receptor did not result in gain-of-function, with the exception F353L. However, the reciprocal mutation L353F in the rat $P2X_7$ receptor had no effect. Taken together, these results strongly indicate that residues 155 and 348 are important in determining the functional expression of $P2X_7$ receptors. In addition, they reveal that the residues at these two positions contribute to the differences in functional expression of human and rat $P2X_7$ receptors.

Further investigations into the functional roles of His^{155} and Ala^{348} were performed by studying the effects of mutating to residues with side chains of distinct properties. Substitution of His^{155} with leucine and aspartic acid reduced

ATP-induced current amplitudes, whilst phenylalanine, arginine and alanine had no significant effect. Mutation of Ala^{348} revealed a discernible effect on the human $P2X_7$ receptor in that substitution with residues with larger side chains reduced, whereas changes to residues with small side chains increased, the amplitude of ATP-evoked currents. Immunostaining and biotin labelling revealed the H155Y mutation of human $P2X_7$ receptors increased, whilst Y155H of rat receptors decreased surface expression. No such effect on surface expression resulted from reciprocal mutations at position 348. A human $P2X_7$ receptor model, based on the recently determined crystal structure of the zebrafish $P2X_4$ receptor, indicates that His^{155} is in the extracellular region, distant from the agonist-binding site and ion-permeating pore, whilst Ala^{348} is located immediately intracellular to the narrowest part of the ion-conducting pathway. Therefore, the simple and most consistent explanation for the effects of mutating residues at 155 and 348 is that the residue at 155 is important in determining receptor surface expression, and the residue at 348 is involved in single channel function.

The monkey $P2X_7$ receptor, which shares 96% sequence homology with the human $P2X_7$ receptor, has been functionally characterised, and its pharmacological properties were similar to that of the human receptor. The monkey $P2X_7$ receptor had a 14-fold higher sensitivity to BzATP over ATP. Furthermore, the sensitivity to ATP and BzATP was slightly lower than in comparison to human $P2X_7$ receptors (2.5- and 2-fold, respectively). The sensitivity of the monkey $P2X_7$ receptor to the $P2X_7$ receptor antagonists KN-62, AZ11645373 and A-438079 was virtually indistinguishable from that of the human $P2X_7$ receptor. Therefore the five amino acids in the extracellular domain that differ between human and monkey $P2X_7$ receptors do not critically interact with these antagonists. The similar pharmacological profiles of human and monkey $P2X_7$ receptors suggests the monkey provides a suitable model for to investigate $P2X_7$ receptor involvement in human diseases.

Table of contents

List of figures

Chapter 1

Chapter 2

Chapter 3

Chapter 4

Chapter 5

Chapter 6

Chapter 7

List of tables

Chapter 1

Chapter 2

Chapter 7

Chapter 8

Abbreviations

αβmeATP	αβ-methylene-ATP
ADP	Adenosine 5'-diphosphate
AMP	Adenosine monophosphate
ATP	Adenosine 5'-triphosphate
BBG	Brilliant blue G
BCA	Bicinchoninic acid
BCG	*Bacille Calmette-Guérin*
BN-PAGE	Blue native-polyacrylamide gel electrophoresis
BSA	Bovine serum albumin
BzATP	Benzoyl-benzoyl-ATP
C-	Carboxyl
CaM	Calmodulin
CaMKII	Calmodulin-dependent protein kinase II
cAMP	Cyclic AMP
cDNA	Complementary DNA
CNS	Central nervous system
DAG	Diacylglycerol
DMEM	Dulbecco's modified Eagle's medium
DMSO	Dimethylsulphoxide
DRG	Dorsal root ganglion
EAE	Experimental autoimmune encephalomyelitis
EC_{50}	Agonist concentration producing half of the maximal response
E. Coli	*Escherichia coli*
EDTA	Ethylenediaminetetraacetic acid
eGFP	Enhanced green fluorescent protein
E-NPP	Ecto-nucleotide pyrophosphatase/phosphodiesterase
E-NTPDase	Ecto-nucleoside 5'-triphosphate diphosphohydrolase
ER	Endoplasmic reticulum
Et^+	Ethidium
FBS	Foetal bovine serum
HEK293	Human embryonic kidney 293
HRP	Horseradish peroxidase
IC_{50}	Antagonist concentration producing half of the maximal inhibition

IL-1β	Interleukin-1β
IP_3	Inositol-3-phosphate
kb	Kilobase
KO	Knock out
LPS	Lipopolysaccharide
LTP	Long-term potentiation
MOG_{35-55}	Myelin oligodendrocyte glycoprotein peptide 35-55
mRNA	Messenger RNA
MS	Multiple sclerosis
MTS	Methanethiosulphate
MTSEA	2-aminoethyl methanethiosulfonate hydrobromide
N-	Amino-
NADPH	Nicotinamide adenine dinucleotide phosphate
NMDG	N-methyl-D-glucamine
ns-SNP	Non-synonymous SNP
oATP	Oxidised ATP
PBS	Phosphate buffered saline
PCR	Polymerase chain reaction
PIP_2	Phosphatidylinositol 4,5-bisphosphate
PLC	Phospholipase C
p38 MAPK	p38 mitogen-activated protein kinase
PPADS	Pyridoxyl-5'-phosphate-6-azo-phenyl-2,4-disulphonate
ROS	Reactive oxygen species
RT-PCR	Reverse transcription-PCR
rpm	Revolutions per minute
RPTP-β	Receptor protein tyrosine phosphatase-β
SDS	Sodium dodecyl sulphate
SDS-PAGE	SDS-polyacrylamide gel electrophoresis
siRNA	Short interfering RNA
SNP	Single nucleotide polymorphism
TBST	Tris-buffered saline-Tween
TM	Transmembrane (TM)
TNP-ATP	Trinitrophenyl-ATP
WT	Wild type

Amino acid abbreviations:

A	Alanine	Ala
C	Cysteine	Cys
D	Aspartic acid	Asp
E	Glutamic acid	Glu
F	Phenylalanine	Phe
G	Glycine	Gly
H	Histidine	His
I	Isoleucine	Ile
K	Lysine	Lys
L	Leucine	Leu
M	Methionine	Met
N	Asparagine	Asn
P	Proline	Pro
Q	Glutamine	Gln
R	Arginine	Arg
S	Serine	Ser
T	Threonine	Thr
V	Valine	Val
W	Tryptophan	Trp
Y	Tyrosine	Tyr

Chapter 1

General introduction

1.1 Purinergic signalling

1.1.1 History of purinergic signalling

The first evidence that purines have extracellular actions came in 1929 when Drury and Szent-Gyrögyi reported that intravenous injection of adenine compounds affects the activity of the mammalian heart (Drury and Szent-Györgyi, 1929). In 1972, Burnstock put forward the hypothesis that adenosine 5'-triphosphate (ATP) acts as a neurotransmitter and accounts for the non-adrenergic, non-cholinergic responses in the gut and bladder, which he called 'purinergic' (Burnstock, 1972). In 1978 purinergic receptors were separated into two groups, P1 for those activated by adenosine and P2 for those by ATP and adenosine 5'-diphosphate (ADP) (Burnstock, 1978). P2 receptors divide into two subfamilies based on their structural features and signal transduction mechanisms. The P2Y receptor family contains the seven-transmembrane (TM) metabotropic G-protein coupled receptors and the P2X receptor family contains the two-TM ligand gated ion channels (Abbracchio *et al.*, 2009; Ralevic and Burnstock, 1998). The first P2Y receptors were cloned in 1993 (Lustig *et al.*, 1993; Webb *et al.*, 1993) and the first P2X receptors a year later (Brake *et al.*, 1994; Valera *et al.*, 1994).

1.1.2 ATP release

ATP is a critical source of energy within cells, and therefore the concept that a molecule so important to cell physiology could be released into the extracellular space was initially difficult for many researchers to comprehend. Due to its size and charge, ATP is unable to cross the plasma membrane by simple diffusion (Bodin and Burnstock, 2001). ATP is released by cell lysis in response to injury, inflammation and traumatic shock (Abbracchio *et al.*, 2009; Bodin and Burnstock, 2001; Yegutkin, 2008). A number of cell types release low concentrations of ATP under basal conditions and in response to shear stress, hypotonic swelling, hydrostatic pressure, hypoxia and stretching. There are numerous ATP release mechanisms under physiological conditions (Abbracchio *et al.*, 2009; Bodin and Burnstock, 2001; Yegutkin, 2008).

Release of ATP in response to nerve stimulation was first shown in 1959 (Holton, 1959). The idea that ATP acts as a neurotransmitter came from the observations made in 1970 that ATP accounts for the non-adrenergic, non-cholinergic transmission in the gut (Burnstock *et al.*, 1970). It is now well

established that ATP is a neurotransmitter or co-transmitter released with other neurotransmitters such as noradrenaline and acetylcholine (Abbracchio *et al.*, 2009). ATP is synthesised and packaged into vesicles at the presynaptic terminals and, upon nerve stimulation, released into the synaptic cleft by exocytosis, where it is degraded by ectonucleotidases (see below).

1.1.3 Ectonucleotidases

Once released into the extracellular space, ATP is rapidly metabolised by ectonucleotidases (Goding *et al.*, 2003; Yegutkin, 2008). There are three different families of these enzymes: ecto-nucleoside 5'-triphosphate diphosphohydrolase (E-NTPDase), ecto-nucleotide pyrophosphatase/phosphodiesterase (E-NPP) and ecto-5'nucleotidase (Figure 1.1) (Goding *et al.*, 2003; Yegutkin, 2008).

The E-NTPDase family has eight members, four of which express at the cell surface (ENTPDase 1 to 3 and 8). E-NTPDases dephosphorylate both ATP and ADP (Figure 1.1). E-NTPDase 1 has been identified as the B-cell activation marker, cell activation antigen CD39 and has a wide expression pattern. E-NTPDase 2 expression is mainly in the mesodermal and endodermal layers, E-NTPDase 3 in the central nervous system (CNS) and E-NTPDase 8 in the liver (Yegutkin, 2008).

The E-NPP ectonucleotidase family has seven members (E-NPP1 to 7). Only E-NPP1 to 3 are capable of hydrolysing nucleotides, and convert ATP into adenosine monophosphate (AMP) and pyrophosphate (Figure 1.1). E-NPPs can be detected in almost all tissues (Goding *et al.*, 2003; Yegutkin, 2008).

The ecto-5'-nucleotidase family also has seven members, which hydrolyse AMP to adenosine and phosphate (Figure 1.1). Only one member of this family, also known as CD73, is located in the outer plasma membrane and therefore capable of hydrolysing extracellular AMP (Yegutkin, 2008).

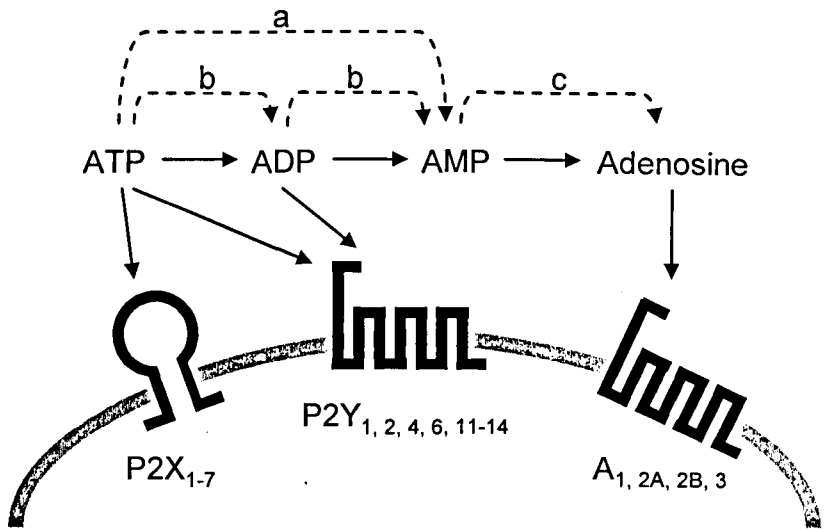

Figure 1.1 ATP Signalling

ATP is metabolised to ADP, AMP and adenosine by ectonucleotidase enzymes. ATP activates P2X and some P2Y receptors, ADP activates some P2Y receptors, and adenosine activated adenosine receptors. (a) E-NPP (b) E-NTPDase (c) ecto-5'-nucleotidase. This diagram has been adapted from Khakh and North, 2006 and Yegutkin, 2008.

1.1.4 Purinergic receptors

Adenosine/P1 receptors

P1 receptors, more often referred to as adenosine receptors, are activated by adenosine. Four members of the P1 receptor family have been identified, A_1, A_{2A}, A_{2B} and A_3 (Burnstock, 2007; Ralevic and Burnstock, 1998; von Kügelgen, 2006). They are metabotropic receptors coupling to G proteins, resulting in initiation of intracellular signalling cascades. A_1 and A_3 receptors couple to $G_{i/o}$ proteins, leading to inhibition of adenylate cyclase and a fall in levels of the second messenger cyclic AMP (cAMP). In contrast, A_{2A} and A_{2B} receptors primarily couple to G_s proteins, which stimulate adenylate cyclase and cause an increase in cAMP production. Interestingly, A_3 receptors can also couple to $G_{q/11}$ proteins resulting in activation of phospholipase C (PLC) which hydrolyses the membrane phospholipid phosphatidylinositol 4,5-bisphosphate (PIP_2) to produce diacylyglycerol (DAG) and inositol-3-phosphate (IP_3). It is therefore clear that the actions of adenosine depend on the complement of receptors expressed at the plasma membrane of the cell, resulting in diverse cellular signalling cascades (Burnstock, 2007; Ralevic and Burnstock, 1998; von Kügelgen, 2006).

P2Y receptors

To date, eight mammalian P2Y subunits have been identified, $P2Y_{1, 2, 4, 6, 11\text{-}14}$. Like adenosine receptors, they couple to G proteins (Burnstock, 2007; Ralevic and Burnstock, 1998; von Kügelgen, 2006) and can be divided into three groups according to the agonists which activate them. $P2Y_{1, 11\text{-}13}$ are activated by adenine nucleotides, $P2Y_{2, 4 \& 6}$ are activated by uracil nucleotides and $P2Y_{14}$ is activated by uracil diphosphate (UDP)-sugar derivatives. $P2Y_{1, 2, 4, 6, 11 \& 14}$ receptor activation stimulates PLC activity via coupling to $G_{q/11}$ proteins. This leads to conversion of PIP_2 to DAG and IP_3 and subsequent Ca^{2+} mobilisation from intracellular stores. $P2Y_{11}$ also couples to G_s proteins, resulting in adenylate cyclase activation and an increase in cAMP production. Conversely, $P2Y_{2, 4, 12, 13}$ receptors couple to $G_{i/o}$ proteins and inhibit adenylate cyclase (Burnstock, 2007; Ralevic and Burnstock, 1998; von Kügelgen, 2006).

P2X receptors

Seven P2X receptor subunits have been cloned to date, $P2X_{1-7}$ (North, 2002; Ralevic and Burnstock, 1998). P2X receptors form ATP-gated, cation selective ion channels at the plasma membrane (North, 2002; Valera *et al.*, 1994). The studies presented in this thesis focus on P2X receptors, and therefore the following sections will discuss the properties of these receptors in more detail.

1.2 Cloning and tissue distribution of vertebrate P2X subunits

1.2.1 $P2X_1$

The first complementary DNA (cDNA) encoding a P2X receptor subunit ($P2X_1$) was cloned from the rat vas deferens (Valera *et al.*, 1994). cDNAs encoding the $P2X_1$ subunit were subsequently isolated from human and mouse urinary bladders and chicken brain (Soto *et al.*, 1997; Soto *et al.*, 2003; Valera *et al.*, 1995). The human gene encoding the $P2X_1$ subunit has been mapped to chromosome 17 by *in situ* hybridisation (Valera *et al.*, 1995). The rat, human and mouse $P2X_1$ subunits are 399 amino acids long, whilst the chicken subunit has 392 residues (Soto *et al.*, 2003; Valera *et al.*, 1994; Valera *et al.*, 1995).

$P2X_1$ messenger RNA (mRNA) has been detected in the spinal cord, sensory ganglia, superior cervical ganglia and coeliac ganglia, and in smooth muscle of the vas deferens, bladder and peripheral arteries (Collo *et al.*, 1996; Valera *et al.*, 1994).

1.2.2 $P2X_2$

The $P2X_2$ receptor subunit was first cloned from rat pheochromocytoma (PC12) cells (Brake *et al.*, 1994). Human $P2X_2$ cDNA has been cloned from pituitary gland, and a number of splice variants were isolated, including $P2X_{2b}$ (internal splicing within exon 11), $P2X_{2c}$ (removal of exon 3), and $P2X_{2d}$ (inclusion of intron 11) (Lynch *et al.*, 1999). The rat $P2X_2$ subunit contains 472 amino acids, and the full-length human $P2X_2$ subunit is one amino acid shorter (Brake *et al.*, 1994; Lynch *et al.*, 1999).

$P2X_2$ receptor subunits are widely expressed in the CNS, including the thalamus, hypothalamus, preoptic area and spinal cord. They are also found in sensory ganglia, superior ganglion, adrenal medulla, bladder, pituitary, vas deferens and intestine (Brake *et al.*, 1994; Collo *et al.*, 1996; Lynch *et al.*, 1999).

1.2.3 $P2X_3$

The cDNA for the $P2X_3$ receptor subunit was simultaneously cloned by two groups from rat dorsal root ganglion (DRG) (Chen *et al.*, 1995; Lewis *et al.*, 1995). The human, mouse and zebrafish $P2X_3$ receptor subunits have subsequently been cloned (Boué-Grabot *et al.*, 2000; Garcia-Guzman *et al.*, 1997b; Souslova *et al.*, 1997), and the human $P2X_3$ receptor gene has been mapped to region q12 of chromosome 11 (Garcia-Guzman *et al.*, 1997b). The human, rat and mouse $P2X_3$ subunits contain 397 amino acids (Chen *et al.*, 1995; Garcia-Guzman *et al.*, 1997b; Lewis *et al.*, 1995; Souslova *et al.*, 1997), whilst the zebrafish $P2X_3$ is 410 residues long (Boué-Grabot *et al.*, 2000).

Despite analysis of numerous tissue types, studies have only shown rat $P2X_3$ receptor mRNA in sensory neurones (Chen *et al.*, 1995; Collo *et al.*, 1996), whilst human $P2X_3$ receptor mRNA is detected in the heart and spinal cord (Garcia-Guzman *et al.*, 1997b).

1.2.4 $P2X_4$

The $P2X_4$ receptor subunit was first cloned from rat brain (Bo *et al.*, 1995; Buell *et al.*, 1996), and the human, mouse, zebrafish and *Xenopus laevis* subunits were cloned soon after (Diaz-Hernandez *et al.*, 2002; Garcia-Guzman *et al.*, 1997a; Juranka *et al.*, 2001; Townsend-Nicholson *et al.*, 1999). The human $P2X_4$ receptor gene has been mapped to region q24.32 of chromosome 12 (Garcia-Guzman *et al.*, 1997a). The rat, human, mouse and zebrafish $P2X_4$ subunits have 388 amino acids, and the *Xenopus laevis* $P2X_4$ subunits consists of 391 residues (Bo *et al.*, 1995; Buell *et al.*, 1996; Garcia-Guzman *et al.*, 1997a; Townsend-Nicholson *et al.*, 1999).

$P2X_4$ receptors have a wide expression pattern. $P2X_4$ receptor mRNA has been detected in the brain, heart, spinal cord, adrenal gland, liver, kidney, skeletal muscle, trachea, lung, vas deferens, bladders, testis, thymus, salivary gland, sensory ganglia, pancreas, arterial smooth muscle, osteoclasts, kidney vascular endothelial cells and human B lymphocytes (Bo *et al.*, 1995; Buell *et al.*, 1996; Collo *et al.*, 1996; Garcia-Guzman *et al.*, 1997a).

1.2.5 $P2X_5$

$P2X_5$ receptor cDNA was cloned from rat celiac ganglia (Collo *et al.*, 1996) and heart (Garcia-Guzman *et al.*, 1996; Haines *et al.*, 1999). The $P2X_5$

subunit has been also cloned from human and mouse (Bo *et al.*, 2003; Cox *et al.*, 2001). The human $P2X_5$ subunit gene is located on chromosome 17p13.3 (Lê *et al.*, 1997). The rat and mouse $P2X_5$ subunits are 455 amino acid residues long, whilst the full-length human receptor contains 444 residues (Bo *et al.*, 2003; Collo *et al.*, 1996; Garcia-Guzman *et al.*, 1996).

In situ hybridisation shows little evidence of $P2X_5$ receptor RNA in the brain, however mRNA for this receptor could be detected in the spinal cord and sensory ganglia (Collo *et al.*, 1996). Southern blot analysis, however, shows $P2X_5$ mRNA expression in the brain as well as in heart, spinal cord and adrenal gland (Garcia-Guzman *et al.*, 1996). $P2X_5$ receptors are also expressed in satellite skeletal muscle cells (Ryten *et al.*, 2002).

1.2.6 $P2X_6$

The $P2X_6$ receptor subunit was first cloned from rat brain (Collo *et al.*, 1996; Soto *et al.*, 1996). The human and mouse homologues were subsequently cloned from human peripheral lymphocytes (Urano *et al.*, 1997), and from mouse skeletal muscle (Nawa *et al.*, 1998), respectively. The human $P2X_6$ gene is located on chromosome 22q11 (Urano *et al.*, 1997). The rat and mouse subunits are 379 amino acids in length, whilst the human $P2X_6$ comprises of 431 residues (Collo *et al.*, 1996; Soto *et al.*, 1996).

$P2X_6$ receptor mRNA was detected by *in situ* hybridisation in neurones of the CNS, several laminae of the spinal cord, superior cervical ganglion, salivary gland, sensory ganglia and bronchial epithelium (Collo *et al.*, 1996). Furthermore mRNA for $P2X_6$ was detected by RT-PCR (reverse transcription-polymerase chain reaction) in the brain, spinal cord, heart, trachea, uterus, lungs testis, liver and astrocytes, and in secretory tissues such as the pituitary and adrenal gland (Soto *et al.*, 1996).

1.2.7 $P2X_7$

The $P2X_7$ receptor is the main focus of this work, therefore the cloning and expression will be discussed in detail in section 1.6.

1.2.8 Invertebrate P2X subunits

Genomic analysis indicates P2X subunits are also found in many invertebrate species (Fountain and Burnstock, 2009) (Figure 1.2). The first was

cloned from *Schistosoma mansoni* (Agboh *et al.*, 2004). In 2007, Fountain *et al.* identified a *Dictyostelium discoideum* P2X receptor. This receptor is localised to membranes of the contractile vacuole, an intracellular organelle, and is important in regulating cell volume in hypotonic conditions (Fountain *et al.*, 2007). A P2X receptor subunit has also been cloned from the green algae *Ostreococcus tauri* (Fountain *et al.*, 2008).

1.3 Biophysical properties and functions of P2X receptors

This section describes the biophysical properties and physiological functions of six vertebrate P2X receptors ($P2X_{1-6}$). These properties of the $P2X_7$ receptor are discussed in detail in section 1.6.

1.3.1 $P2X_1$ receptors

Agonist-evoked currents mediated by $P2X_1$ receptors have fast activation and desensitisation kinetics (Figure 1.3) and the recovery from receptor desensitisation following agonist removal is slow (North, 2002; Soto *et al.*, 2003; Valera *et al.*, 1994).

The generation of $P2X_1$ receptor deficient mice has allowed the roles of P2X receptors containing the $P2X_1$ subunit to be determined. The first such study showed that disruption of the $P2X_1$ receptor function led to a dramatic reduction in fertility of male mice due to reduced contraction of the vas deferens in response to sympathetic nerve stimulation, thereby reducing the number of sperm in the ejaculate (Mulryan *et al.*, 2000). The amplitude of bladder detrusor muscle contractions in response to nerve stimulation was also reduced in $P2X_1$ deficient mice, indicating a role for the $P2X_1$ receptor in urinary bladder function (Vial and Evans, 2000). Furthermore, a role for the $P2X_1$ receptor in arterial vasoconstriction has been studied (Vial and Evans, 2002). It has been shown that constriction of mesenteric arteries from $P2X_1$ deficient mice in response to sympathetic nerve stimulation is attenuated. However, $P2X_1$ deficient mice had normal or only slightly elevated blood pressure, although it has been suggested that during increased sympathetic tone the contribution of the $P2X_1$ receptor to blood pressure may be altered (Mulryan *et al.*, 2000; Vial and Evans, 2002). Finally, collagen and adrenaline infused into the jugular vein induced intravascular thrombi formation and acute vascular occlusion, and led to death of the majority of wild type (WT) mice (Hechler *et al.*, 2003). However, $P2X_1$

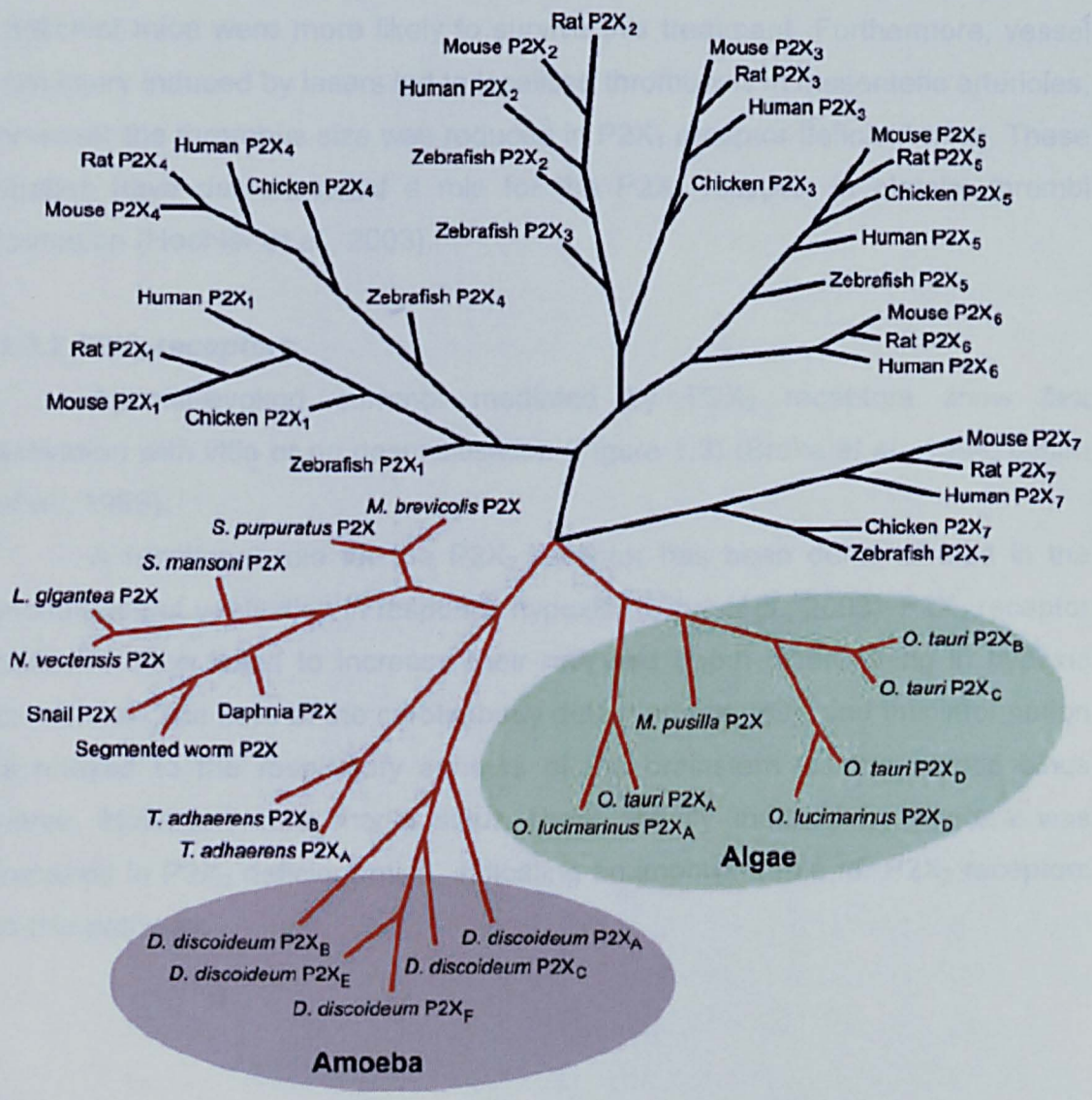

Figure 1.2 Phylogenetic tree showing the relationship between vertebrate and invertebrate P2X receptors

Black lines indicate vertebrate P2X receptor subunits, whilst red lines indicate invertebrate P2X receptors. Amoeba and Algae families are highlight grey and green respectively. This diagram has been taken from Fountain and Burnstock, 2009.

deficient mice were more likely to survive this treatment. Furthermore, vessel wall injury induced by lasers led to localised thrombosis in mesenteric arterioles, however the thrombus size was reduced in $P2X_1$ receptor deficient mice. These studies have demonstrated a role for the $P2X_1$ receptor in platelet thrombi formation (Hechler *et al.*, 2003).

1.3.2 $P2X_2$ receptors

Agonist-evoked currents mediated by $P2X_2$ receptors show fast activation with little or no desensitisation (Figure 1.3) (Brake *et al.*, 1994; Lynch *et al.*, 1999).

A functional role for the $P2X_2$ receptor has been demonstrated in the modulation of ventilation in response hypoxia (Rong *et al.*, 2003). $P2X_2$ receptor deficient mice failed to increase their rate and depth of breathing in hypoxic conditions. The cells of the carotid body detect arterial PO_2, and this information is relayed to the respiratory sensors of the brainstem via the carotid sinus nerve. However, in a model sinus nerve activity induced by hypoxia was impaired in $P2X_2$ deficient mice, indicating an important role for $P2X_2$ receptors in this pathway.

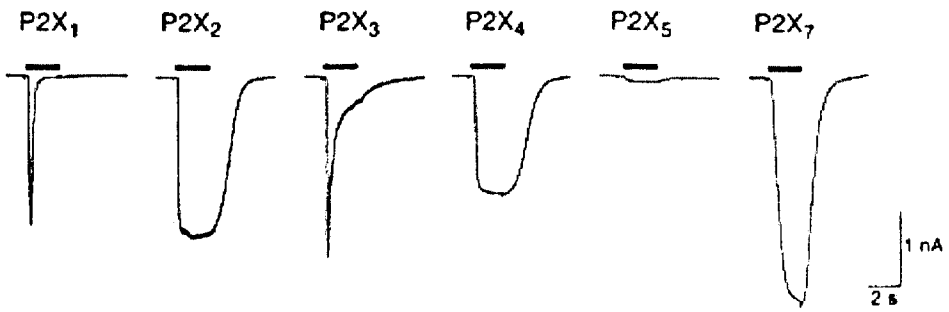

Figure 1.3 Comparison of ATP-evoked currents of P2X receptors
Whole-cell recordings made from HEK293 cells expressing indicated homomeric P2X receptors in response to a 2 s application of 30 μM ATP (or 1 mM for $P2X_7$). This figure has been taken from North, 2002.

1.3.3 $P2X_3$ receptors

Agonist-evoked currents mediated by $P2X_3$ receptors display rapid activation, rapid desensitisation (Figure 1.3), and slow recovery from desensitisation (Chen *et al.*, 1995; Garcia-Guzman *et al.*, 1997b).

$P2X_3$ receptors are highly expressed in nociceptive or "pain sensing" DRG neurons and there is strong evidence that it contributes to a number of pain states including neuropathic and inflammatory pain. Reduction of $P2X_3$ receptor protein expression using short interfering RNA (siRNA) attenuated agonist-induced hyperalgesia (enhanced pain sensation to a normally painful stimulus) and tactile allodynia (pain sensation to a normally innocuous stimulus) in the partial sciatic ligation model of neuropathic pain (Dorn *et al.*, 2004), indicating that $P2X_3$ contributes to neuropathic pain. Interestingly, mice lacking the $P2X_3$ receptor subunit display increased thermal hyperalgesia in response to chronic inflammation (Souslova *et al.*, 2000). However, in contrast, A-317491, a selective inhibitor for $P2X_3$ and $P2X_{2/3}$ receptors (see section 1.5.2), attenuated thermal hyperalgesia in models of inflammatory pain (Jarvis *et al.*, 2002). $P2X_3$ deficient mice displayed symptoms of urinary bladder hyporeflexia, including decreased bladder contractions in response to distension, decreased urination and increased bladder capacity, supporting a role for the $P2X_3$ receptor in controlling the bladder volume reflexes (Cockayne *et al.*, 2000).

Following cloning of the $P2X_3$ subunit from DRG neurons, Lewis and colleagues observed that the properties of αβ-methylene-ATP- (αβmeATP) evoked currents of $P2X_3$ receptors expressed in HEK293 (human embryonic kidney 293) cells were different from sensory neurons. They found that agonist-evoked currents of HEK293 cells co-expressing $P2X_2$ and $P2X_3$ resembled those of sensory neurons, and concluded that sensory neurons express $P2X_{2/3}$ heteromers (Lewis *et al.*, 1995).

1.3.4 $P2X_4$ receptors

Agonist-evoked currents mediated by $P2X_4$ receptors exhibit rapid activation and mild desensitisation kinetics (Figure 1.3) (Bo *et al.*, 1995; Buell *et al.*, 1996; Garcia-Guzman *et al.*, 1997a; Townsend-Nicholson *et al.*, 1999).

A functional role for the $P2X_4$ receptor has been described in a number of tissues. Schaffer collateral stimulation in the CA1 region of mouse hippocampal slices leads to long-term potentiation (LTP). At these synapses,

LTP is reduced in $P2X_4$ deficient mice, thus indicating a role in synaptic plasticity (Sim *et al.*, 2006). Studies in the vascular system showed that pre-constricted arterioles vasodilate in response to administration of ATP (Yamamoto *et al.*, 2006). Such vasodilation of arterioles from $P2X_4$ receptor deficient mice was suppressed, indicating that $P2X_4$ receptors are important in control of vascular tone. Adaptive vascular remodelling describes the decrease in vessel diameter in response to a decrease in blood flow. However, in $P2X_4$ deficient mice, the lumen diameter of the common carotid artery was not reduced in response to decreased blood flow, demonstrating a role for $P2X_4$ receptors in vascular remodelling (Yamamoto *et al.*, 2006). Furthermore, following nerve injury, $P2X_4$ receptor expression is increased in spinal cord microglia, and administration of antisense oligodeoxynucleotides against the $P2X_4$ receptor reduced tactile allodynia (Tsuda *et al.*, 2003).

1.3.5 $P2X_5$ receptors

Rat $P2X_5$ receptor mediated currents have fast activation kinetics and show little desensitization (Bo *et al.*, 2003; Chen *et al.*, 1995; Collo *et al.*, 1996; Garcia-Guzman *et al.*, 1996).

Activation of the $P2X_5$ receptor has been shown to be important in skeletal muscle differentiation (Ryten *et al.*, 2002). Following muscle damage, skeletal muscle satellite cells undergo differentiation to form new muscle. $P2X_5$ receptor activation is thought to inhibit satellite cell proliferation and increase cell differentiation. Indeed, $P2X_5$ receptor protein was only expressed in the satellite cells when they are grown in conditions that promote cell differentiation, and not in normal growth media (Ryten *et al.*, 2002).

1.3.6 $P2X_6$ receptors

ATP-induced currents in cells expressing $P2X_6$ receptors are fast to activate. Currents show little desensitisation, however recovery to baseline is slow following agonist removal (Collo *et al.*, 1996; Jones *et al.*, 2004). When cDNA encoding the $P2X_6$ receptor was transfected into HEK293 cells, ATP-evoked currents could only be recorded in less than 5% of the cells (Collo *et al.*, 1996). Furthermore, ATP-induced $P2X_6$ mediated currents could not be detected when expressed in *Xenopus* oocytes (Soto *et al.*, 1996). However, it

has been shown that extensive glycosylation of $P2X_6$ receptors is required for receptor function (Jones *et al.*, 2004).

1.3.7 P2X receptor of invertebrate species

Disruption of the *Dictyostelium discoideum* P2X receptor orthologue *Dd*p2xA led to cells that were unable to control their volume in hypotonic solutions, and cell swelling (Fountain *et al.*, 2007). This is the first evidence supporting an intracellular role for P2X receptors and raises the questions of what roles intracellular P2X receptors could play in mammalian cell physiology.

1.4 P2X structure

The crystal structure of a P2X receptor has recently been solved (Kawate *et al.*, 2009). Prior to this, studies utilised site-directed mutagenesis in conjunction with biochemical and functional studies to determine the stoichiometry and molecular mechanisms of P2X receptors. It has now become clear that inferences made from such studies were highly accurate (Browne *et al.*, 2010; Evans, 2010; Kawate *et al.*, 2009; Young, 2010). In this section, the findings of these structure-function experiments, and how they relate to the P2X crystal structure are discussed.

1.4.1 Crystallisation of the zebrafish $P2X_4$ receptor

The zebrafish $P2X_4$ receptor crystal structure has been solved in the closed state at a resolution of 3.1 Å (Kawate *et al.*, 2009). To increase suitability for crystallisation, a zebrafish $P2X_4$ construct, with amino (N-) and carboxyl (C-) terminal truncations and three mutations (C51F/N78K/N187R) to reduce non-native disulphide bond formation and glycosylation, was generated. Importantly, this construct was functional, albeit with smaller ATP-induced currents in comparison to WT (Kawate *et al.*, 2009).

1.4.2 P2X receptor subunit topology

Cloning of the P2X receptor subunits allowed predictions on the subunit topology to be made. Based on hydrophobicity analyses, each P2X subunit was predicted to contain two TM domains, a large extracellular domain, and intracellular C- and N-termini (Valera *et al.*, 1994). The crystal structure confirms this subunit topology (Kawate *et al.*, 2009). The shape of a single $P2X_4$

subunit is dolphin-like when viewed parallel to the membrane (Figure 1.4A) (Kawate *et al.*, 2009).

1.4.3 P2X receptor architecture

Evidence from biochemical and functional experiments consistently show that P2X receptors are trimers. Nicke *et al.* used blue native polyacrylamide gel electrophoresis (BN-PAGE) followed by Western blotting to show that the native $P2X_1$ receptor is a trimer (Nicke *et al.*, 1998). Furthermore, the use of cross-linking agents, followed by Western blotting, has shown that P2X receptor subunits cross-link into trimers (Barrera *et al.*, 2005; Nicke *et al.*, 1998). Imaging of antibody-decorated $P2X_2$ receptor by atomic force microscopy indicated that this receptor also assembles as a trimer (Barrera *et al.*, 2005). The subunit arrangement of P2X receptors has been studied. Mutations V48C at the extracellular end of the $P2X_2$ TM1, and I319C at the extracellular end of the $P2X_3$ TM2 allowed inter-subunit disulphide bonds to form between the two subunit subtypes (Jiang *et al.*, 2003). Subunits are in a 'head-to-tail' arrangement, with contacts made between the TM1 of one subunit and TM2 of another (Jiang *et al.*, 2003).

The crystal structure of the zebrafish $P2X_4$ receptor confirmed that P2X receptors are trimers (Figure 1.4B) (Kawate *et al.*, 2009). Detailed study of the crystal structure revealed that the TM region has an hour-glass shape and comprises six helices (two from each subunit), which are in a left-handed twist. The three TM2 domains line the pore and form the ion conducting pathway. The TM2 domains cross halfway through the membrane when the channel is closed, whereas the three TM1 domains were found to surround the TM2 domains. The extracellular regions of the three subunits wrap around each other in a right-handed twist, and there are extensive subunit-subunit interactions in this domain (Kawate *et al.*, 2009).

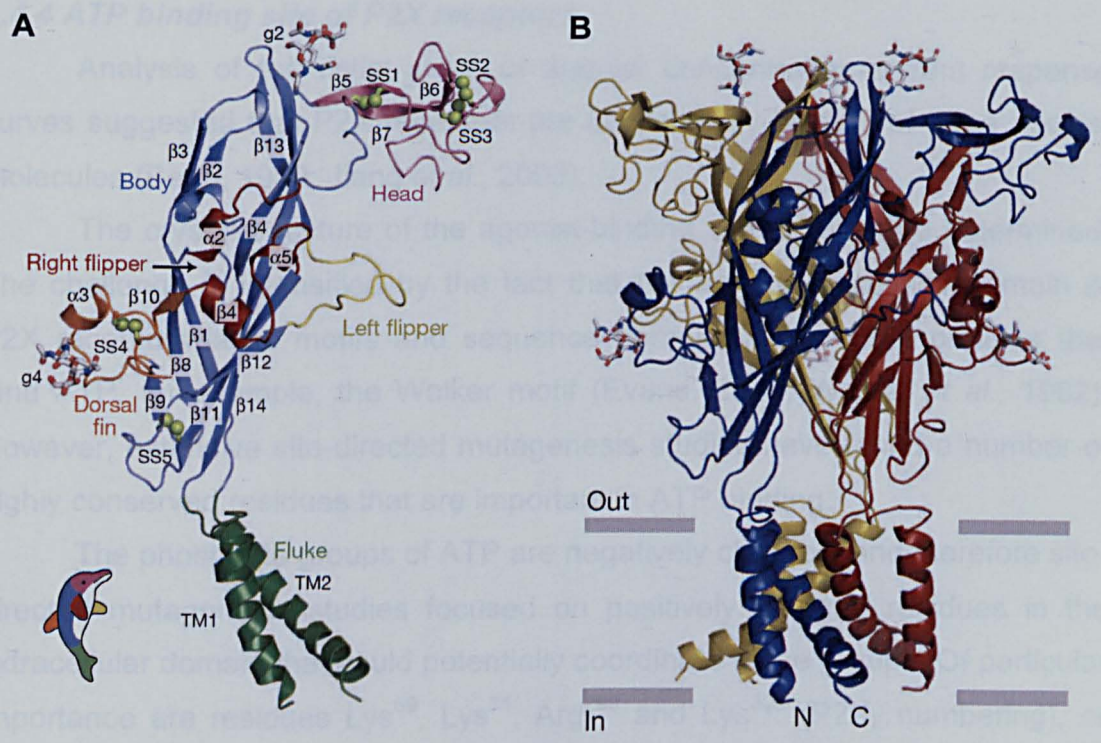

Figure 1.4 The subunit and trimeric structure of P2X receptors

(A) The zebrafish $P2X_4$ subunit is dolphin-like in shape. The α-helices, β-strands and attached glycans are indicated. Disulphide bonds are numbered SS1-5. (B) The structure of the zebrafish $P2X_4$ receptor viewed parallel to the membrane. Each subunit is in different colour and the grey lines represent the inner and outer leaflets of the plasma membrane. This figure has been taken from Kawate *et al.*, 2009.

1.4.4 ATP binding site of P2X receptors

Analysis of the initial slope of agonist concentration-current response curves suggested that P2X receptors are activated by binding of three agonist molecules (Bean, 1990; Jiang *et al.*, 2003).

The crystal structure of the agonist-binding site is yet to be determined. The challenge is intensified by the fact that the large extracellular domain of P2X receptors lacks motifs and sequence homology with other proteins that bind ATP, for example, the Walker motif (Evans, 2010; Walker *et al.*, 1982). However, extensive site-directed mutagenesis studies have found a number of highly conserved residues that are important in ATP binding.

The phosphate groups of ATP are negatively charged, and therefore site-directed mutagenesis studies focused on positively charged residues in the extracellular domain that could potentially coordinate these groups. Of particular importance are residues Lys^{69}, Lys^{71}, Arg^{290} and Lys^{308} ($P2X_2$ numbering), or the corresponding residues in $P2X_1$ and $P2X_4$ receptors (Table 1.1), the mutation of which reduced the potency of ATP (Ennion *et al.*, 2000; Jiang *et al.*, 2000b; Roberts and Evans, 2007; Roberts *et al.*, 2008; Zemkova *et al.*, 2007).

The aromatic residues in the extracellular domain have been investigated with respect to their potential interaction with the adenine ring of ATP. Mutation of residues Phe^{183} or Phe^{289} ($P2X_2$ receptor numbering) or equivalent residues in $P2X_1$ and $P2X_4$ receptors led to a reduction in the potency of ATP, implicating an importance in ATP binding (Table 1.1) (Roberts and Evans, 2004; Roberts and Evans, 2007; Roberts *et al.*, 2008; Zemkova *et al.*, 2007).

The effect of mutating uncharged polar residues of the extracellular loop has also been investigated. Mutation of Thr^{184} and Asn^{288} ($P2X_2$ numbering) or corresponding residues in $P2X_1$ and $P2X_4$ receptors has been shown to reduce the potency of ATP (Table 1.1) (Jiang *et al.*, 2000b; Roberts and Evans, 2006; Roberts and Evans, 2007; Roberts *et al.*, 2008; Roberts *et al.*, 2009).

To further investigate the ATP binding site, Jiang *et al.* introduced the I67C mutation to the $P2X_2$ receptor, and demonstrated inhibition of ATP-evoked currents by methanethiosulphate (MTS) compounds with different head group properties (different charges and size). The inhibition by negatively charged MTS compounds caused a rightward shift in the agonist dose response curve, and was overcome by increased ATP concentrations. Consistently, introduction of negative groups at this position by site-directed mutagenesis reduced the

Table 1.1 Amino acids predicted to be involved in ATP binding

$P2X_1$	$P2X_2$	$P2X_4$	References
Lys^{68}	Lys^{69}	Lys^{67}	Ennion *et al.*, 2000, Jiang *et al.*, 2000b, Roberts *et al.*, 2008, Zemkova *et al.*, 2007.
Lys^{70}	Lys^{71}	Lys^{69}	Ennion *et al.*, 2000, Jiang *et al.*, 2000b, Roberts *et al.*, 2008.
Phe^{185}	Phe^{183}	Phe^{185}	Roberts and Evans, 2004; Roberts *et al.*, 2008; Zemkova *et al.*, 2007.
Thr^{186}	Thr^{184}	Thr^{186}	Jiang *et al.*, 2000b, Roberts and Evans, 2006; Roberts *et al.*, 2008; Roberts *et al.*, 2009.
Asn^{290}	Asn^{288}	Asn^{293}	Jiang *et al.*, 2000b, Roberts and Evans, 2006; Roberts and Evans, 2007; Roberts *et al.*, 2008.
Phe^{291}	Phe^{289}	Phe^{294}	Roberts and Evans, 2004; Roberts *et al.*, 2008; Roberts and Evans, 2007; Zemkova *et al.*, 2007.
Arg^{292}	Arg^{290}	Arg^{295}	Ennion *et al.*, 2000; Jiang *et al.*, 2000b; Roberts *et al.*, 2008; Roberts and Evans, 2007; Zemkova *et al.*, 2007.
Lys^{309}	Lys^{308}	Lys^{313}	Ennion *et al.*, 2000; Jiang *et al.*, 2000b; Roberts and Evans, 2007.

The eight residues are predicted to be important in ATP-binding. Mutation of these residues reduced in ATP potency at $P2X_1$, $P2X_2$ and $P2X_4$ receptors.

affinity of the receptor for ATP. These observations indicate that Ile^{67} is in the region of the ATP binding site (Browne *et al.*, 2010, Jiang *et al.*, 2000b).

Wilkinson *et al.* found that the function of K69A or K308A but not K69A/K308A $P2X_2$ mutants could be rescued by co-expression with $P2X_3$ subunits, suggesting that the ATP binding site is located between neighbouring subunits rather than within the subunits (Wilkinson *et al.*, 2006). In a separate study, double cysteine substitution of Lys^{68} and Phe^{291} of the $P2X_1$ receptor, residues thought to be involved in ATP binding (see above), resulted in formation of trimers, which can be prevented by the presence of ATP. These residues are in close proximity, providing further evidence that the ATP binding sites are located at interfaces between adjacent subunits (Marquez-Klaka *et al.*, 2007).

The structure of the zebrafish $P2X_4$ receptor was solved in the absence of ATP, and therefore lacks direct evidence for the location of the ATP binding site (Kawate *et al.*, 2009). However, a model of the $P2X_2$ receptor, based on the zebrafish $P2X_4$ structure, shows there are inter-subunit grooves which contain the eight residues that have been shown to be important determinants of the actions of ATP (Lys^{69}, Lys^{71}, Phe^{183} and Thr^{184} from one subunit, and Asn^{288}, Phe^{289}, Arg^{290} and Lys^{308} from the other; $P2X_2$ numbering; Figures 1.5B and 1.5C) (Browne *et al.*, 2010; Kawate *et al.*, 2009). These residues are conserved between P2X receptors (Figure 1.6).

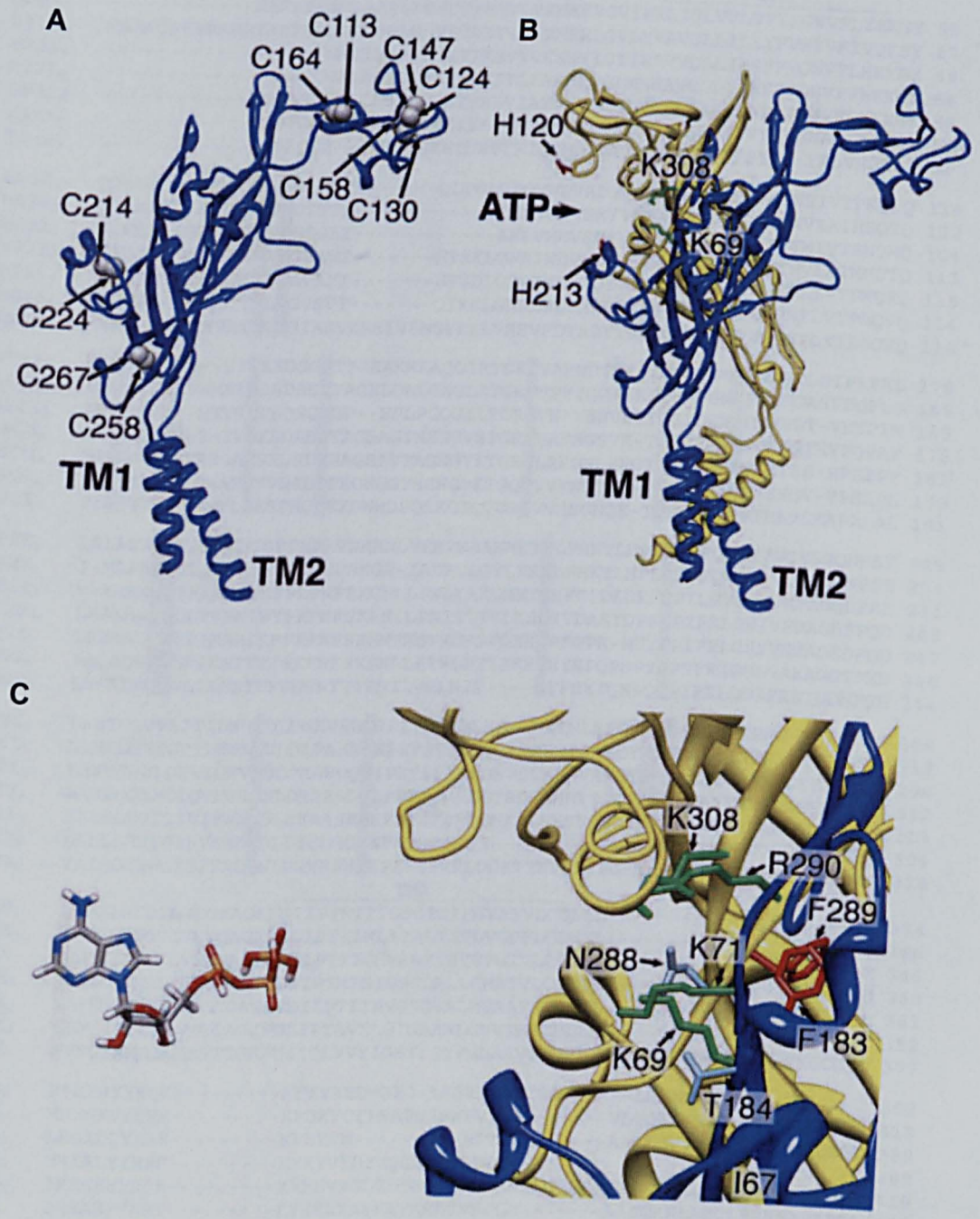

Figure 1.5 Structural model of the $P2X_2$ receptor

(A) A single subunit, viewed parallel to the membrane, showing the five disulphide bonds present within each subunit. (B) Diagram showing only two subunits to show the predicted ATP binding site (arrow), which is formed between the two subunits. (C) Predicted ATP binding site, showing the location of eight highly conserved residues shown to be important for ATP-induced receptor activation from site-directed mutagenesis studies. This figure has been taken from Browne *et al.*, 2010.

Figure 1.6 Amino acid sequence alignment of human P2X receptor subunits. Conserved cysteines are grey, and the 8 residues predicted to bind ATP (Table 1.1) are in pink. TM1 and TM2 are indicated. Accession numbers: X83688, AF190826, Y07683, Y07684, AF016709, O15547 and Y09561, respectively. Aligned using ClustalW.

1.4.5 Disulphide bonds

The extracellular loop of all mammalian P2X receptor subunits contains ten conserved cysteine residues (North, 2002). Clyne *et al* studied the effects of mutating these residues in the $P2X_2$ receptor on ATP sensitivity, ATP-induced peak current amplitude, zinc potentiation and the effects of extracellular pH (Clyne *et al.*, 2002). Ennion and Evans mutated each of these ten cysteines in $P2X_1$ receptor. If the mutated cysteine was usually involved in disulphide bond formation, mutational effects or the free cysteine, if accessible, would be labelled by MTSEA-biotin (2-aminoethyl methanethiosulfonate hydrobromide-biotin). Using these approaches, the two studies concluded that Cys^{113}-Cys^{164}, Cys^{124}-Cys^{147}, Cys^{130}-Cys^{158}, Cys^{214}-Cys^{224} and Cys^{258}-Cys^{267} ($P2X_2$ numbering) disulphide bonds exist (Ennion and Evans, 2002; Clyne *et al.*, 2002; Kawate *et al.*, 2009). The crystal structure of the zebrafish $P2X_4$ receptor shows these combinations of cysteines do indeed form disulphide bonds (Figure 1.4A and 1.5A) (Browne *et al.*, 2010; Clyne *et al.*, 2002; Ennion and Evans, 2002; Kawate *et al.*, 2009). In addition, disruption of Cys^{261}-Cys^{270} disulphide bond, or Cys^{117}-Cys^{165} and any other disulphide bond, disrupts $P2X_1$ receptor trafficking to the cell surface (Ennion and Evans, 2002).

The ten cysteine residues conserved among mammalian P2X receptors are not present in *Dictostelium discoideum* P2X receptors (with one exception) (Fountain *et al.*, 2007). Despite this, ATP-evoked currents of HEK293 cells expressing this P2X receptor can be recorded, showing that disulphide bonding is not essential for P2X receptor function (Fountain *et al.*, 2007).

1.4.6 Transmembrane region

The roles of the TM1 and TM2 domains in ion permeation have been investigated. Studies into the modification of introduced cysteines in the TM2 region of the $P2X_2$ receptor by thiol-reactive compounds and ions indicate that residues in this region are located in the ion permeation pathway (Browne *et al.*, 2010; Li *et al.*, 2008). For example, mutants T336C and T339C are modified much faster when the channel is open than in the closed state (Li *et al.*, 2008). Cadmium (Cd^{2+}) is a thiol-reactive metal with a similar radius to sodium and requires 3 cysteine residues for tight binding. Cd^{2+} inhibited ATP-evoked currents of T336C mutant only when the channel was in the open state,

suggesting that the region surrounding Thr^{336} lines the ion conducting pore (Li *et al.*, 2008).

Mutations in the TM2 domain have been shown to affect the spontaneous gating, unitary conductance and outward rectification of the $P2X_2$ receptor (Cao *et al.*, 2007; Cao *et al.*, 2009). Mutations introduced between residues Asn^{333} and Ser^{340} produced spontaneous channel activity. Furthermore, mutation of residues Asn^{333}, Thr^{336} and Ser^{340} to positively charged residues increased the amplitude of outward currents, indicating these side chains are important in ion permeation. Almost any amino acid substituted at Thr^{336} results in spontaneous activity of the channel, suggesting that movement of this residue is crucial for channel opening (Cao *et al.*, 2009).

Residues in the TM1 domain were mutated to cysteine, however ATP-evoked currents of relatively few mutants were modified by MTS reagents, suggesting that this domain does not line the ion permeation pathway (Browne *et al.*, 2010; Jiang *et al.*, 2001; Li *et al.*, 2008). When Val^{48} (TM1) and Ile^{328} (TM2) are both mutated to cysteine they are able to form a disulphide bond, leading to inhibition of ATP-evoked currents, which can be recovered by reducing agents. V48C becomes more accessible to MTS reagents when the channel is open, suggesting that movement of this part is important for gating of the ion channel (Jiang *et al.*, 2001). Furthermore, a chimera in which TM1 of $P2X_2$ receptor was replaced with that of $P2X_1$ receptor displayed increased αβmeATP sensitivity ($P2X_2$ receptor are insensitive to αβmeATP), showing that the TM1 domain has an important influence on the gating properties of the ion channel (Haines *et al.*, 2001).

The crystal structure of the zebrafish $P2X_4$ receptor shows that the narrowest part of the ion permeating pathway is at residue Ala^{344} (Thr^{336} of rat $P2X_2$) (Kawate *et al.*, 2009). This finding is consistent with structure-function studies (Li *et al.*, 2008). The extracellular boundary is composed of residues Leu^{340} and Asn^{341} (Ile^{332} and Asn^{333} in rat $P2X_2$), whilst the cytoplasmic gate is residues Ala^{347} and the Leu^{346} (Thr^{339} and Leu^{338} in rat $P2X_2$, respectively). A model of the rat $P2X_2$ receptor, based on the crystal structure of the zebrafish $P2X_4$ receptor, predicts that Val^{48} and Ile^{328} are in close proximity, inline with the structure-function data (Browne *et al.*, 2010; Jiang *et al.*, 2001).

1.4.7 Channel opening

A crystal structure of a protein is a snapshot in time, and, in the case of the zebrafish $P2X_4$ structure, this snapshot is in the closed state (Kawate *et al.*, 2009). However, the information gained from structure-function studies and the crystal structure allows predictions on the possible opening mechanism of the P2X receptor following agonist binding. Browne *et al.* predict that due to the positioning of Thr^{336}, Thr^{339} and Ser^{340}, channel opening is likely to involve a ≥50° anti-clockwise rotation of the TM2 domain and a steepening of the angle at which the TM2 domain crosses the membrane (Browne *et al.*, 2010). Cysteine mutation of Asp^{349} of the $P2X_2$ receptor lead to ATP-induced currents that were completely blocked by MTSEA (Rassendren *et al.*, 1997a). Asp^{349} is at the intracellular end of TM2, indicating that the intracellular parts of TM2, which are spread out in the closed state, must undergo substantial movement during channel opening (Browne *et al.*, 2010; Rassendren *et al.*, 1997a).

1.5 P2X Pharmacology

1.5.1 P2X receptor agonists

The physiological agonist for P2X receptors is ATP. All P2X receptors respond to ATP in the low micromolar (μM) range with the exception of $P2X_7$ that has a much lower sensitivity (Table 1.2). There are currently no P2X receptor subtype specific agonists. Several ATP analogues, however, show distinct potencies between receptor subtypes, although the difference is often limited.

αβmeATP most potently activates P2X receptors containing $P2X_1$ and $P2X_3$ subunits (Table 1.2). In contrast, the $P2X_2$ receptor is relatively insensitive to αβmeATP, thereby making this ATP analogue a useful tool for distinguishing these subtypes. αβmeATP acts as a partial agonist at human and mouse $P2X_4$ receptors, and antagonises the rat $P2X_4$ receptor (IC_{50} 4.6 μM) (Jones *et al.*, 2000). αβmeATP activates the human $P2X_5$ receptor, albeit with a relatively low potency, and is without effect at rat $P2X_5$ and $P2X_6$ and $P2X_7$ receptors at concentrations up to 100 μM (Collo *et al.*, 1996; Surprenant *et al.*, 1996). Benzoyl-benzoyl-ATP (BzATP), another ATP analogue (Table 1.2), is a more potent agonist at $P2X_7$ receptors than ATP (Surprenant *et al.*, 1996; Young *et al.*, 2007). BzATP, however, should not be used as a $P2X_7$ receptor specific

Table 1.2 Potencies of P2X receptor agonists and antagonists

P2X receptor	EC_{50} (μM)			IC_{50} (μM)		
	ATP	αβmeATP	BzATP	Suramin	PPADS	
$hP2X_1$	0.06*, 1, 0.8, 0.9	0.2*, 2.2	0.002*, 0.7	1-5, 0.9*	1-5, 1.8*	Bianchi *et al.*, 1999; Ennion *et al.*, 2000 ; Evans *et al.*. 1995.
$rP2X_1$	1		0.7	<10	<30, 0.09, 0.1	
$rP2X_2$	1.4*, 7.7, 60	<100*, >>100	5.5*, 23	1-5, 33*	1-5, 3.8*	Bianchi *et al.*, 1999; Brake *et al.*, 1994 ; Evans *et al.*,1995.
$hP2X_3$	0.3*	0.7*	0.08*	<100*	5.1*	Bianchi *et al.*, 1999; Chen *et al.*, 1995 ; Lewis *et al.*, 1995.
$rP2X_3$	0.3*, 0.5, 1.2	0.5*	0.03*	0.8*, 3	3.6*, 1.5	
$rP2X_{2/3}$	0.5*	3.4*	0.65*	0.8*	1.3*	Bianchi *et al.*, 1999.
$hP2X_4$	0.5*, 1.4	8.3*, 19	0.5*	<100*	<100*, 9.6	Bianchi *et al.*, 1999; Bo *et al.*, 1995; Jones *et al.*, 2000.
$rP2X_4$	5.5, 10	>100		>100	>100	
$mP2X_4$	2.3	7.1		>100	10.5	
$hP2X_5$	4.1	160	5.7	2.9	0.2	Bo *et al.*, 2003; Collo *et al.*, 1996.
$rP2X_5$	15	>100		4	2.6	
$rP2X_6$	12	>100		>100	>100	Collo *et al.*, 1996.
$hP2X_7$	96*	<100*	4.7*	<100*	4.6*	Bianchi *et al.*, 1999; Surprenant *et al.*, 1996; Young *et al.*, 2007.
$rP2X_7$	123, 115		3.6, 7			
$mP2X_7$	936		285			

*indicates EC_{50} values obtained using an intracellular calcium assay, as opposed to patch clamp recording.

agonist as it activates other P2X receptor subtypes such as $P2X_1$, $P2X_3$ receptors in the nanomolar range (Table 1.2) (Bianchi *et al.*, 1999).

1.5.2 P2X receptor antagonists

Pharmaceutical companies are making a huge effort to synthesise novel, potent and subunit selective P2X receptor antagonists, as reflected by the large number of recently patented compounds (Gunosewoyo and Kassiou, 2010). This section summarises the compounds that have been fully characterised.

Suramin was identified as an inhibitor of αβmeATP-evoked responses in the mouse vas deferens (Dunn and Blakeley, 1988). This compound inhibits a number of P2X receptors (Table 1.2) and P2Y receptors (Ralevic and Burnstock, 1998), making it of limited use in P2X receptor studies.

There are three analogues of suramin with improved selectivity and/or potency (NF023, NF279 and NF449). NF023 potently and reversibly inhibits $P2X_1$ receptors in a competitive manner with no effect on maximal current (Soto *et al.*, 1999). Of the receptor subtypes tested, NF023 is selective for $P2X_1$ receptors over $P2X_2$, $P2X_3$ and $P2X_4$ receptors. NF279 was reported as a potent P2X receptor antagonist when it was shown to antagonise αβmeATP-evoked smooth muscle contractions of rat vas deferens (Damer *et al.*, 1998). The compound blocks $P2X_1$ and $P2X_2$ receptors with a high potency and is also effective at $P2X_3$ receptors (Rettinger *et al.*, 2000). The $P2X_4$ receptor is relatively insensitive to NF279, with 300 μM only resulting in approximately 40% inhibition (Damer *et al.*, 1998). NF279 has so far been shown to be without effect on α1A-adrenoceptors, adenosine A1 and A2B, histamine H1, muscarinic M3 and nicotinic receptors (Soto *et al.*, 1999). Finally, NF449 has been reported as a highly potent $P2X_1$ receptor antagonist, and inhibits $P2X_1$ receptors in the picomolar range (Hulsmann *et al.*, 2003; Rettinger *et al.*, 2005).

PPADS (pyridoxyl-5'-phosphate-6-azo-phenyl-2,4-disulphonate) blocks a number of P2X receptor subtypes (Table 1.2), however, it is relatively ineffective at $P2X_4$ and $P2X_6$ receptors (Collo *et al.*, 1996; Jones *et al.*, 2000). It was initially identified as a P2X receptor antagonist by showing that it can block P2X receptor mediated responses in rat vas deferens (Lambrecht *et al.*, 1992). However, PPADS is now classed as a non-selective P2 antagonist since it can also block P2Y receptor responses (Ralevic and Burnstock, 1998).

Several analogues of PPADS that have been synthesised display increased potency. The first of these analogues, MRS2220, is a selective and reversible $P2X_1$ receptor antagonist (IC_{50} 10 μM) (Jacobson *et al.*, 1998). It is approximately 6-fold less potent at $P2X_3$ receptors (IC_{50} 58 μM), and shows no antagonistic properties at $P2X_2$ and $P2X_4$ receptors. Unlike PPADS, MRS2220 has no effect at $P2Y_1$, $P2Y_2$, $P2Y_4$ or $P2Y_6$ receptors as well as P1 receptors. The PPADS analogue PPNDS is also an antagonist at $P2X_1$ receptors, with 6 times greater potency than PPADS (IC_{50} 14 nM) (Lambrecht *et al.*, 2000).

IP_5I, a diinosine pentaphosphate, is a potent antagonist at $P2X_1$ receptors (IC_{50} 3 nM) (King *et al.*, 1999). The compound can also block $P2X_3$ receptors, albeit with approximately a 900-fold lower potency (IC_{50} 2.8 μM), and is ineffective at $P2X_2$ receptors. In contrast, IP_5I potentiates $P2X_4$ receptor responses (EC_{50} 2 nM) (King *et al.*, 1999).

2'3'-O-(2,4,6-trinitrophenyl)-substituted nucleotides have been described as potent antagonists at $P2X_1$, $P2X_3$ and $P2X_{2/3}$ receptors (Virginio *et al.*, 1998). The trinitrophenyl analogue of ATP (TNP-ATP) potently inhibits $P2X_1$, $P2X_3$ and $P2X_{2/3}$ receptors mediated responses (IC_{50} ~ 1 nM) (Virginio *et al.*, 1998). A similar potency is seen with trinitrophenyl analogues of ADP, AMP and GTP, but TNP-adenosine is ineffective. These compounds show a much lower potency of inhibiting $P2X_2$, $P2X_4$, $P2X_4$ and $P2X_7$ receptors (IC_{50} > 1 μM) (Burgard *et al.*, 2000).

A-317491 is a highly potent and selective inhibitor of $P2X_3$ and $P2X_{2/3}$ receptors. $P2X_3$ receptors expressed in 1321N1 cells are blocked by the S-enantiomer of A-317491 with a K_i of 22 nM (92 nM and 9 nM for rat $P2X_{2/3}$ and human $P2X_{2/3}$ respectively) (Jarvis *et al.*, 2002). The compound exhibits high affinity for $P2X_3$ and $P2X_{2/3}$ receptors compared to $P2X_1$, $P2X_2$, $P2X_4$, $P2X_7$ and $P2X_2$ receptors. Of these, A-317491 shows the highest affinity for $P2X_1$ receptors (IC_{50} 11 μM), and is >100-fold less potent than at $P2X_3$ and $P2X_{2/3}$ receptors. A-371344, the R-enantiomeric form of A-317491, is significantly less potent than A-317491. A-317491 antagonises $P2X_{2/3}$ mediated responses in a competitive manner. Radioligand binding studies show that [^{3}H] A-317491 can specifically label the $P2X_3$ subunit (Jarvis *et al.*, 2004).

When comparing receptor sensitivity to agonists or antagonists between studies, a number of factors should be taken into account. Firstly, the sensitivity of the assay used requires consideration. For example, the EC_{50} for the human

$P2X_1$ receptor was reported to be 0.002 μM using an Ca^{2+} uptake assay (Bianchi *et al.*, 1999), and 0.7 μM in a study using electrophysiology (Evans *et al.*, 1995) (Table 1.2). The composition of the recording solutions should also be taken into account. For example, the $P2X_7$ receptor mediated currents are inhibited by extracellular divalent cations and protons (see section 1.6.5) (Rassendren *et al.*, 1997; Surprenant *et al.*, 1996; Virginio *et al.*, 1997). Furthermore, current facilitation should be considered. For example, $P2X_7$ receptor mediated currents undergo facilitation when agonist application is prolonged or repeated (see section 1.6.6), and the receptor is more sensitive to agonist in the fully facilitated state (Roger *et al.*, 2008). In terms of antagonist potency, IC_{50} values depend on the concentration of agonist used, and the antagonist incubation time, both of which must be considered when comparing values between different studies.

$P2X_7$ receptor pharmacology is discussed in section 1.6.5.

1.6 The $P2X_7$ receptor

Prolonged application of ATP to macrophages results in cell permeabilisation, and this remarkable property was thought to result from activation of a receptor that was distinct from P2X and P2Y receptors, and was therefore named the P2Z receptor (Di Virgilio, 1995). However, molecular cloning and functional characterisation of the rat $P2X_7$ receptor indicated that prolonged activation of the $P2X_7$ receptor led to cell permeabilisation. Therefore the P2Z receptor is a member of the P2X receptor family (Surprenant *et al.*, 1996). The $P2X_7$ receptor has now been cloned from human macrophages, mouse microglial cells, guinea pig brain and dog heart (Chessell *et al.*, 1998; Fonfria *et al.*, 2008; Rassendren *et al.*, 1997; Roman *et al.*, 2009; Surprenant *et al.*, 1996), as well as zebrafish and *Xenopus laevis* (López-Castejón *et al.*, 2007; Paukert *et al.*, 2002). The gene for the human $P2X_7$ receptor (*P2RX7*) is located on chromosome 12q24 (Buell *et al.*, 1998). The mammalian $P2X_7$ subunit is 595 amino acid residues in length, with the exception of guinea-pig $P2X_7$, which is one residue shorter (Chessell *et al.*, 1998; Fonfria *et al.*, 2008; Rassendren *et al.*, 1997; Roman *et al.*, 2009, Surprenant *et al.*, 1996).

1.6.1 $P2X_7$ receptor tissue and cellular distribution

$P2X_7$ receptors are expressed in cells of hematopoietic origin, including monocytes, macrophages, B and T lymphocytes, mast cells and microglia (Boumechache *et al.*, 2009; Lister *et al.*, 2007; Solle *et al.*, 2001). Northern blotting has detected $P2X_7$ mRNA in the rat brain, lung, microglia, thymus, spleen, macrophages, pancreas, liver, heart and thymus (Collo *et al.,* 1997; Rassendren *et al.*, 1997). Furthermore, both osteoclasts, osteoblasts, lung, vas deferens, DRG and salivary glands have also been shown to express $P2X_7$ receptors (Gartland *et al.*, 2003; Ke *et al.*, 2003; Nicke, 2008).

Expression of $P2X_7$ receptors by neurons is a matter of continuing debate. Initial studies found little evidence of $P2X_7$ receptor RNA or protein in adult peripheral or central nerves (Collo *et al.*, 1997). However, a number of immunohistochemical experiments using antibodies against a C-terminal epitope of the $P2X_7$ receptor have shown expression in presynaptic terminals of neurons (Deuchars *et al.*, 2001; Armstrong *et al.*, 2002; Sperlágh *et al.*, 2002). However, the specificity of $P2X_7$ receptor antibodies has been brought into question by Sim *et al.* who analysed the expression of the $P2X_7$ receptor in the brain and found that antibodies targeting different epitopes of the receptor showed different patterns of immunoreactivity. $P2X_7$ receptor immunoreactivity in neurons from either $P2X_7$ knock out (KO) mouse was unchanged and Western blots from mouse brain showed bands of the expected size for $P2X_7$ protein in both WT and KO mice (Sim *et al.*, 2004).

In the study by Sim *et al.*, both published $P2X_7$-deficient mouse lines were used, one generated by Glaxo by the insertion of a *lac*Z transgene into exon 1, and the other by Pfizer by the insertion of a neomycin cassette into exon 13. However, a splice variant of the $P2X_7$ receptor ($P2X_7$(k)), which is functional in terms of both agonist-evoked current and dye uptake, has recently been identified (Nicke *et al.*, 2009). This variant has an alternative N-terminus and TM1 domain, and PCR, SDS-PAGE and BN-PAGE have shown it escapes gene deletion in the Glaxo KO mouse strain. Furthermore, cerebella from the Pfizer $P2X_7$-deficient mouse was shown by RT-PCR to express the $P2X_7$-specific sequences between Ala^{1737} and Ala^{1795} (downstream of the deleted sequence), but not the deleted sequence (Sánchez-Nogueiro *et al.*, 2005). A possible reason is that a splice variant that escapes deletion in the Pfizer KO mouse strain exists, although none of the currently identified splice variants

provide an explanation for these observations (Nicke *et al.*, 2009). It is therefore clear that further investigations into the neuronal expression of the $P2X_7$ receptor are required, and that such splice variants complicate studies that use $P2X_7$ receptor KO mice to study the role of the receptor in health and disease.

1.6.2 Biophysical properties of $P2X_7$ receptors

Like other members of the P2X family, the $P2X_7$ receptor is a ligand gated ion channel and upon ligand binding, the channel opens allowing the passage of small cations including Ca^{2+}. $P2X_7$ receptor mediated currents show relatively slow activation kinetics and no desensitisation (Figure 1.3) (North, 2002; Rassendren *et al.*, 1997; Surprenant *et al.*, 1996). The currents are carried by cations, and $P2X_7$ receptors show little evidence of chloride permeability, as evidenced by a lack of effect on reversal potentials when internal chloride is replace by aspartate (Rassendren *et al.*, 1997). $P2X_7$ receptor mediated currents are linearly dependent on membrane potential and reverse close to 0 mV (Rassendren *et al.*, 1997; Surprenant *et al.*, 1996). Electrophysiological experiments have shown that repeated or prolonged activation of the rat $P2X_7$ receptor leads to increased permeability of the large monovalent cation N-methyl-D-glucamine (NMDG), and fluorescent dyes such as YO-PRO-1 or ethidium (Et^+) can be seen to enter cells expressing the $P2X_7$ receptor (Rassendren *et al.*, 1997; Surprenant *et al.*, 18996; Virginio *et al.*, 1999). Deletion of an 18-amino acid juxamembrane cysteine-rich domain of the rat $P2X_7$ receptor led to loss of NMDG permeability, whilst agonist-evoked YO-PRO-1 uptake was unaffected, suggesting the NMDG and dye permeation pathways are different (Jiang *et al.*, 2005).

The molecular mechanism of dye uptake is still contentious. One idea is that the ion channel itself dilates, whereas an alternative hypothesis is that activation of the $P2X_7$ receptor leads to activation of a distinct protein that forms the dye-uptake pathway. In 2006 Pelegrin and Surprenant provided evidence that pannexin-1 forms the $P2X_7$ receptor mediated dye-uptake pathway (Pelegrin and Surprenant, 2006). Pannexin-1 is often referred to as a hemi channel because of structural similarity to connexins. mRNA for pannexin-1 was shown to be present in monocytes, macrophages, astrocytes and cell lines (e.g. HEK293 and HeLa) by RT-PCR. When over-expressed with $P2X_7$ receptors in HEK293 cells, pannexin-1 could interact with $P2X_7$ receptors. Furthermore,

siRNA targeting pannexin-1 and a pannexin-1 mimetic peptide inhibited ATP-induced dye uptake without effect on the ionic currents. HEK293 cells expressing pannexin-1 were shown to constitutively take up Et^+, however, cells co-expressing pannexin-1 and $P2X_7$ receptors required ATP application to take up Et^+. Therefore it has been proposed that pannexin-1 is the large pore-forming molecule that opens upon $P2X_7$ receptor activation, and that the $P2X_7$ receptor negatively regulates pannexin-1 (Pelegrin and Surprenant, 2006).

1.6.3 Molecular and biochemical properties

$P2X_7$ receptors share the membrane topology of P2X receptors, as discussed in section 1.4. The unique structural feature of the $P2X_7$ receptors is that its C-terminus is much longer than that of the other P2X receptors and is important for pore formation (Surprenant *et al.*, 1996). P2X subunits can assemble into homomeric receptors, but also interact with $P2X_{1-6}$ subunits to form heteromeric receptors (Murrell-Lagnado and Qureshi, 2008; Torres *et al.*, 1999). Evidence suggests native $P2X_7$ receptors form homotrimers (Boumechache *et al.*, 2009; Nicke, 1998), however there is also evidence that $P2X_7$ receptors can interact with $P2X_4$ receptors and functionally influence each one other (Guo *et al.*, 2007).

1.6.4 $P2X_7$ receptor trafficking

Cell surface expression of the $P2X_7$ receptor is under tight regulation. For example, $P2X_7$ receptor mRNA levels are similar between monocytes and macrophages, however differentiation from monocytes to macrophages occurs in parallel with an increase in $P2X_7$ receptor surface expression (Gudipaty *et al.*, 2001).

The $P2X_7$ receptor C-terminus contains residues/motifs important for its surface expression (Murrell-Lagnado and Qureshi, 2008). Point mutations within residues 551-581 prevent $P2X_7$ receptor expression at the plasma membrane (Smart *et al.*, 2003). In particular, mutation of Arg^{578} and Lys^{579} does not alter protein expression, but abolishes surface expression, suggesting this dibasic motif is important for $P2X_7$ receptor trafficking (Denlinger *et al.*, 2003). Furthermore, immunocytochemistry using an antibody against a C-terminal epitope has shown mutation I568N in the human $P2X_7$ receptor disrupts trafficking to the plasma membrane (Wiley *et al.*, 2003).

Palmitoylation is the reversible covalent linkage of a fatty acid palmitate group to cysteine side chains of proteins, resulting in increased hydrophobicity. Mutation of the cysteines within residues 371-377, 477-506, 572-573 or 572-573 in the C-terminus disrupted [^{3}H]-palmitic acid binding and led to retention of $P2X_7$ receptor in the endoplasmic reticulum (ER) and targeting to lysosomes (Gonnord *et al.*, 2009). Furthermore, disruption of palmitoylation reduced association of the receptor with detergent-resistant membranes. The study therefore demonstrates palmitoylation is important for $P2X_7$ surface expression and its association with lipid rafts.

1.6.5 $P2X_7$ receptor pharmacology

$P2X_7$ receptor agonists

As described in section 1.5.1, the physiological agonist for $P2X_7$ receptor is ATP. However, the $P2X_7$ receptor has a much lower sensitivity to ATP in comparison to other members of the P2X family, and requires concentrations in the submillimolar range for activation (Surprenant *et al.*, 1996; Young *et al.*, 2007). BzATP is a more potent agonist at $P2X_7$ receptors than ATP itself and therefore this unique property is a useful tool for distinguishing $P2X_7$ receptor responses from other P2X receptors (Anderson and Nedergaard, 2006).

In addition to ATP and BzATP, $P2X_7$ receptors can be activated by the covalent attachment of ADP-ribose at Arg^{125} (Adriouch *et al.*, 2007). ADP-ribosylation involves transfer of the ADP-ribose group from nicotinamide adenine dinucleotide to the $P2X_7$ receptor by ADP-ribosyltransferases. In the structural model, this residue is in close proximity to the predicted ATP binding site described in section 1.4.4 (Adriouch *et al.*, 2007; Browne *et al.*, 2010).

$P2X_7$ receptor antagonists

Oxidised ATP (oATP) was initially identified as an inhibitor of $P2X_7$ receptor mediated responses in J774 cells, including ATP-induced dye uptake and plasma membrane depolarisation, blebbing and cell swelling (Murgia *et al.*, 1993). The compound, however, is of limited use as high concentrations and prolonged incubation (hrs) are required for complete inhibition and the compound also inhibits ectonucleotidases enzymes and $P2X_1$ and $P2X_2$ receptors (Evans *et al.*, 1995; Murgia *et al.*, 1993).

Calmidazolium potently inhibits BzATP-evoked currents mediated by rat $P2X_7$ receptor (IC_{50} 13 nM), however it does not affect BzATP-induced YO-PRO-1 uptake (Virginio *et al.*, 1997). Inhibition is non-competitive, and recovery is partial and slow. Calmidazolium has no action at $P2X_2$ and $P2X_{2/3}$ receptors (Virginio *et al.*, 1997).

KN-62, an isoquinoline derivative, inhibits ATP-induced Et^+ uptake in cells expressing the human $P2X_7$ receptor, but shows only partial antagonism when BzATP is used as an agonist (Humphreys *et al.*, 1998). In contrast, KN-62 completely inhibits human $P2X_7$ receptor mediated currents whether ATP or BzATP is the agonist. Interestingly, KN-62 fails to inhibit the rat $P2X_7$ receptor. KN-62 is widely used as a Ca^{2+}/calmodulin-dependent protein kinase II (CaMKII) inhibitor. However, KN-04, a KN-62 structural analogue lacking CaMKII inhibitor activity, can also effectively block the human $P2X_7$ receptor, indicating inhibition of CaMKII activity is not involved in inhibition of the human $P2X_7$ receptor by KN-62 (Humphreys *et al.*, 1998).

A series of KN-62 related compounds have been synthesised by modifying the phenylpiperazine residues in an attempt to produce a more potent $P2X_7$ receptor antagonist (Baraldi *et al.*, 2003). The majority of the compounds blocked ATP-evoked Ca^{2+} influx in the nanomolar range, the most potent (compound 63) with an IC_{50} of 1.3 nM (Baraldi *et al.*, 2003).

Another analogue of KN-62, A-438079, was identified as a $P2X_7$ receptor antagonist via high throughput screening of a compound library and structure-activity relationship studies (Nelson *et al.*, 2006). Unlike KN-62, A-438079 acts in a competitive manner. The compound inhibits rat $P2X_7$ receptor with an IC_{50} of 320 nM, as determined by Ca^{2+} influx assay. A-438079 has weak or no antagonistic activity at $P2X_1$, $P2X_2$, $P2X_{2/3}$, $P2X_4$, $P2Y_1$ and $P2Y_2$ receptors, a range of G-protein coupled receptors, enzymes, transporters and ion channels (McGaraughty *et al.*, 2007).

Brilliant blue G (BBG) has been described as a selective inhibitor of the $P2X_7$ receptor (Jiang *et al.*, 2000a). The compound inhibits the rat $P2X_7$ receptor (IC_{50} 10 nM) more potently than human $P2X_7$ receptors (IC_{50} 265 nM). The inhibition was voltage independent, and non-competitive. BBG was found to prevent BzATP-induced YO-PRO-1 uptake and membrane blebbing in HEK293 cells expressing rat $P2X_7$ receptor. BBG is far less potent as an antagonist at other P2X receptors; it is ineffective at $P2X_1$, $P2X_3$, $P2X_{2/3}$ and

$P2X_{1/5}$ receptors, but inhibits $P2X_2$ receptor, albeit with a lower potency (IC_{50} 1.4 μM). (Jiang *et al.*, 2000a).

High throughput screening has revealed a series of cyclic imides that potently inhibit $P2X_7$ receptor activation-dependent Et^+ uptake in THP-1 cells, a human acute monocytic leukemia cell line (Alcaraz *et al.*, 2003). The action of one of these cyclic amides, AZ11645373, has been fully characterised (Stokes *et al.*, 2006). This compound is a potent inhibitor of ATP or BzATP-induced responses mediated by human $P2X_7$ receptors (agonist-induced current, Ca^{2+} influx, YO-PRO-1 uptake and interleukin-1β (IL-1β) release) with IC_{50}/k_B values of 5-90 nM. Inhibition was non-surmountable, indicating a non-competitive inhibitory mechanism. The compound, however, only weakly inhibits rat $P2X_7$ receptors, with 10 μM inhibiting agonist-induced currents by 40-50%. AZ11645373 has no agonistic or antagonistic action at $P2X_1$, $P2X_2$, $P2X_3$, $P2X_{2/3}$ receptors (Stokes *et al.*, 2006).

A-740003 is another new highly potent and selective antagonist at $P2X_7$ receptors (Honore *et al.*, 2006). This inhibitor is less species-specific than KN-62 and BBG, blocking rat and human $P2X_7$ receptors in the nM range (IC_{50} 18 nM and 40 nM, respectively). Schild analysis shows a slope close to unity, indicating competitive antagonism. A-740003 displays high specificity for $P2X_7$ receptors, with concentrations up to 100 μM having no effect on $P2X_1$, $P2X_2$, $P2X_{2/3}$, $P2X_4$, $P2Y_1$ and $P2Y_2$ receptors (Honore *et al.*, 2006).

Emodin has recently been identified as a $P2X_7$ receptor antagonist (Liu *et al.*, 2010). The compound is an anthraquinone derivative that has been isolated from *Rheum officinale Baill* (common name Chinese rhubarb). Emodin is able to inhibit BzATP-evoked currents in HEK293 cells expressing the rat $P2X_7$ receptor (IC_{50} 3 μM), and is much less potent in inhibiting rat $P2X_4$ receptors (IC_{50} >30 μM). Moreover, emodin is able to reduce ATP-evoked macrophage cell death, Et^+ dye uptake and BzATP-induced Ca^{2+} influx (Liu *et al.*, 2010).

Modulators of $P2X_7$

$P2X_7$ receptors are inhibited by extracellular protons and divalent cations such as Ca^{2+}, Mg^{2+}, Zn^{2+} and Cu^{2+} (Rassendren *et al.*, 1997; Surprenant *et al.*, 1996; Virginio *et al.*, 1997). The inhibition is voltage independent, therefore disfavouring an open channel block mechanism (Virginio *et al.*, 1997). For many

years it has been thought that the tetra-anionic form of ATP (ATP^{4-}) activates $P2X_7$ receptors, and the presence of divalent cations lowers the ATP^{4-} concentrations. However, inhibition of $P2X_7$ receptors by protons, Zn^{2+} and Cu^{2+} is at least in part due to their direct interaction with the receptor via allosteric modulation. Residues His^{62} and Asp^{197} are shown to be critical for Zn^{2+} and Cu^{2+} inhibition of $P2X_7$ receptors (Liu *et al.*, 2008). Similarly, several residues in the extracellular domain have been identified that contribute to inhibition by extracellular protons, with the most critical being Asp^{197} (Liu *et al.*, 2009).

1.6.6 Regulation by interacting proteins

Tyrosine phosphatase

A proteomic study has identified several proteins that interact with the $P2X_7$ receptor, including laminin α3, integrin β2, β-actin, α-actinin, supervillin, MAGuK, three heat shock proteins, phosphatidyl-inositol 4-kinase, and receptor protein tyrosine phosphatase-β (RPTP-β) (Kim *et al.*, 2001). The same study showed that repeated stimulation of rat $P2X_7$ receptors lead to rapid rundown in the current amplitude. This was preventable by application of phosphatase inhibitors or substitution of the phosphorylation site Tyr^{343} with phenylalanine in TM2. Therefore this rundown is thought to be due to dephosphorylation of $P2X_7$ receptor by RPTP-β (Kim *et al.*, 2001).

Calmodulin

Binding of Ca^{2+} to calmodulin (CaM) induces a conformational change, revealing a hydrophobic patch, which allows hydrophobic and salt bridge interactions with target proteins (Saimi and Kung, 2002). CaM acts as a Ca^{2+} sensor for a number of ion channels, and modulates their activity. The rat $P2X_7$ receptor sequence contains a CaM binding sequence in the C-terminus (Ile^{541}-Arg^{557}) (Roger *et al.*, 2008). It has been demonstrated, using co-immunoprecipitation, that $P2X_7$ receptors and CaM can interact, and that mutations I541T and S552C disrupt this interaction. ATP-evoked currents amplitudes were decreased by expression of a dominant negative CaM mutant. Therefore the study suggests that binding of CaM to the rat $P2X_7$ receptor increases current amplitudes and augments Ca^{2+} entry into cells (Roger *et al.*, 2008).

Agonist-evoked $P2X_7$ receptor currents undergo facilitation in response to prolonged or repeated receptor activation (Roger *et al.*, 2008). CaM inhibition by CaM inhibitory binding peptide, expression of a dominant negative CaM mutant, or intracellular Ca^{2+} chelation reduce current facilitation, demonstrating that rat $P2X_7$ receptor current facilitation is in part dependent on Ca^{2+}/CaM (Roger *et al.*, 2008).

1.6.7 Physiological functions of $P2X_7$ receptors

Cytokine release

IL-1β is a pro-inflammatory cytokine and is synthesised in response to inflammatory stimuli (e.g., lipopolysaccharide, or LPS). Proteolytic cleavage of the inactive precursor pro-IL-1β by caspase-1 is required to produce the mature, active IL-1β (Ferrari *et al.*, 2006). ATP-induced IL-1β release by LPS-primed human macrophages is completely inhibited by oATP (Ferrari *et al.*, 1997a). ATP-dependent release of IL-1β is completely absent in LPS-primed macrophages from $P2X_7$ receptor deficient mice, despite high levels of pro-IL-1β (Solle *et al.*, 2001). Furthermore, ATP-evoked IL-1β release from human LPS-primed monocytes expressing the functionally impaired E496A $P2X_7$ mutant receptor was reduced in comparison to WT subjects (Sluyter *et al.*, 2004b). Moreover, ATP-induced IL-18 release from LPS-primed human monocytes from subjects homozygous carrying the E496A mutation is also reduced in comparison to WT subjects (Sluyter *et al.*, 2004a). These studies show a critical role for $P2X_7$ receptors in release of IL-1β and IL-18.

Production of reactive oxygen species

A role for $P2X_7$ receptor in reactive oxygen species (ROS) generation has been demonstrated. BzATP-induced ROS production (measured indirectly as H_2O_2) in primary rat microglia was abolished by PPADS, BBG and oATP (Parvathenani *et al.*, 2003). Furthermore, ATP-induced ROS production by mouse macrophage RAW264.7 cells was reduced by KN-62 (Noguchi *et al.*, 2008; Parvathenani *et al.*, 2003). Inhibition of nicotinamide adenine dinucleotide phosphate (NADPH) oxidase, a generator of ROS at the plasma membrane, by apocyanin, suppresses BzATP-induced H_2O_2 production by rat microglia, and ATP-induced ROS generation by RAW264.7 cells (Noguchi *et al.*, 2008; Parvathenani *et al.*, 2003). p38 mitogen-activated protein kinase (p38 MAPK) is

activated by NADPH oxidase. The p38 MAPK inhibitor SB203580 reduced BzATP-induced H_2O_2 production by rat microglia (Parvathenani *et al.*, 2003). Furthermore, ATP- and BzATP-induced activation of p38 MAPK was reduced by KN-62 and BBG in RAW264.7 cells (Noguchi *et al.*, 2008). Therefore, $P2X_7$ dependent ROS production is via activation of the NADPH oxidase/p38 MAPK pathway.

A reduction in $P2X_7$ expression using siRNA knock-down reduced ATP-induced apoptosis (Noguchi *et al.*, 2008). Moreover, ATP-induced apoptosis was reduced by the antioxidant propyl gallate. Taken together, these studies suggest that the $P2X_7$ receptor mediates ROS production as a result of activation of NADPH oxidase and p38 MAPK, leading to apoptosis (Noguchi *et al.*, 2008; Parvathenani *et al.*, 2003).

Cell death

Cells death occurs via necrosis or apoptosis (Guimarães and Linden, 2004). Necrosis is characterised by swelling of the cytoplasm, organelle destruction and plasma membrane disruption, ultimately resulting in discharge of the cytoplasmic contents into the extracellular space and inflammation. Apoptosis is highly controlled, and characterised by cell shrinkage, membrane blebbing, maintenance of organelle integrity, DNA condensation and fragmentation, and finally, removal of cell by phagocytosis (Guimarães and Linden, 2004). Activation of $P2X_7$ receptors can cause cell death via necrosis or apoptosis (Ferrari *et al.*, 1999; Mackenzie *et al.*, 2005).

ATP-induced DNA fragmentation does not occur in cells that do not express $P2X_7$ receptors, and can be prevented by $P2X_7$ receptor antagonist oATP (Ferrari *et al.*, 1999). Furthermore, chromatin condensation can be prevented by inhibition of caspase activity. However, caspases are also involved in necrotic cell death, as caspase inhibitors can reduce ATP-induced lysis of these cells (Ferrari *et al.*, 1999).

Activation of the $P2X_7$ receptor induces rapid morphological changes such as membrane blebbing that occurs within 1 min of activation of $P2X_7$ receptor (Mackenzie *et al.*, 2005). Activation of $P2X_7$ receptor has also been shown to induce cytoskeletal rearrangements, including F-actin redistribution, focal adhesions disassembly and redistribution of α-tubulin. $P2X_7$ receptor activation can evoke depolarisation and swelling of mitochondria. However, if

the activation is within mins, membrane blebbing and mitochondrial disruption are reversible, and cytochrome c, which initiates apoptosis, is not released. Therefore, Mackenzie *et al.* have called this phenomenon "pseudoapoptosis" (Mackenzie *et al.*, 2005).

Cell growth and proliferation

A role for the $P2X_7$ receptor in cell proliferation has been demonstrated. Baricordi *et al.* observed that LG14 B-lymphoblastic cells and K562 leukemic cells over-expressing $P2X_7$ receptor were able to proliferate under serum-deprived conditions, whilst mock transfected cells were not (Baricordi *et al.*, 1999). Proliferation was preventable by apyrase, an ATP-hydrolysing enzyme. Furthermore, the luciferin-luciferase assay revealed that these cells release ATP. The study indicates that cells release ATP in an autocrine/paracrine fashion, leading to cell proliferation (Baricordi *et al.*, 1999). Therefore, depending on growth conditions, $P2X_7$ receptor can promote cell growth or death.

Investigations to identify the mechanisms by which the $P2X_7$ receptor mediates both cell growth and death have been performed. Under basal and serum-deprived conditions, cells expressing $P2X_7$ receptors are able to proliferate (Adinolfi *et al.*, 2005). HEK293 cells expressing $P2X_7$ receptors have high mitochondrial potentials, high Ca^{2+} concentrations in the mitochondria, and a high intracellular ATP concentration. The mechanism put forward is that under serum-free conditions, basal release of ATP activates the $P2X_7$ receptor and causes leak of Ca^{2+} into the mitochondria. The resulting increase in metabolic activity and ATP levels allows the cells to proliferate even when growth factors are lacking. However, application of supra-maximal concentrations of ATP is thought to lead to $P2X_7$ receptor-mediated increase in mitochondrial Ca^{2+} concentrations, collapse in mitochondrial potential, mitochondrial fragmentation and cell death (Adinolfi *et al.*, 2005).

Bone remodelling

Normal bone remodelling involves both osteoclast and osteoblast activities. Osteoclasts are multinucleated cells, resulting from the fusion of mononucleated phagocytes and are responsible for bone resorption. Osteoblasts are the cells responsible for depositing new bone. $P2X_7$ receptor

deficient mice have reduced total and cortical bone content, reduced periosteal circumference and bone formation, and increased bone resorption (Ke *et al.*, 2003). Furthermore, inhibition of the $P2X_7$ receptor by oATP or a $P2X_7$ receptor blocking monoclonal antibody prevents fusion of human mononucleated phagocytes into multinucleated osteoclasts (Gartland *et al.*, 2003). Taken together, these studies reveal an important role for $P2X_7$ receptors in bone remodelling.

Neuronal functions

Despite the challenges in interpreting immunohistological data of $P2X_7$ receptor expression in the brain, there is functional evidence that activation of $P2X_7$ receptors modulate synaptic transmission by promoting vesicular release of neurotransmitters (Armstrong *et al.*, 2002; Deuchars *et al.*, 2001; Sperlágh *et al.*, 2002). For example, Deuchars *et al.* have shown that application of BzATP to sympathetic preganglionic neurons of the spinal cord leads to depolarisation of the neurons, which can be prevented by BBG (2 μM) and the glutamate antagonists NBQX and AP-5 (Deuchars *et al.*, 2001). A separate study found that application of BzATP to rat hippocampal slices led to depression of transmission at mossy fibre–CA3 synapses (Armstrong *et al.*, 2002). Kukley *et al.* made similar findings, however this study also showed that BzATP-evoked depression of synaptic transmission at the mossy fibre-CA3 synapses was not different in the hippocampus of mice lacking the $P2X_7$ receptor (Kukley *et al.*, 2004). Furthermore, the same study showed that BzATP-induced inhibition of synaptic transmission in this region of the hippocampus could be prevented by pre-application of an A_1 receptor antagonist (Kukley *et al.*, 2004).

It is clear that the study of $P2X_7$ receptor expression and function in neurons is complex (Anderson and Nedergaard, 2006). Lack of $P2X_7$ receptor selective and specific agonists, antagonists and antibodies has hindered progress in this field. BzATP activates non-$P2X_7$ receptors with a very similar, or even higher, potency (Table 1.2). Unique to $P2X_7$ receptors is that BzATP is a more potent agonist at $P2X_7$ receptors than ATP, and so is only a useful tool for identifying $P2X_7$ receptor responses when its potency is compared to that of ATP. BBG is a rodent $P2X_7$ receptor selective antagonist with an IC_{50} of 10 nM. However, BBG can also inhibit other P2X receptors at μM concentrations (Jiang *et al.*, 2000a).

Neuron-glial interactions

Duan *et al.* have shown that ATP or BzATP induces a significant increase in release of [^{14}C]-glutamate and [^{3}H]-D-aspartate from preloaded astrocytes. This can be potentiated by removal of divalent cations from the extracellular solution and blocked by oATP, suggesting a role for $P2X_7$ receptors in mediating neurotransmitter release from astrocytes (Duan *et al.*, 2003).

There is also evidence supporting a role for $P2X_7$ receptors in neuron-glial communications. DRG nerve stimulation caused release of ATP, which activated $P2X_7$ receptors on satellite glial cells which release tumour necrosis factor-α (Zhang *et al.*, 2007). The same group have shown that the tonic activity of $P2X_7$ receptors inhibited expression of $P2X_3$ receptors in DRG (Chen *et al.*, 2008). The underlying mechanism is thought to involve activation of $P2X_7$ receptor-dependent release of ATP from satellite glial cells and activation of $P2Y_1$ receptors on DRG neurons by ATP (or possibly ADP), and inhibition of expression of $P2X_3$ receptors (Chen *et al.*, 2008).

NF-κB activation

NF-κB is a transcription factor that resides in the cytoplasm in an inactive complex with its inhibitory subunit IκB (Grossmann *et al.*, 1999). Phosphorylation of IκB induces a conformational change allowing binding of ubiquitin and subsequent degradation. The active NFκB then translocates into the nucleus and binds to target genes. A role for the $P2X_7$ receptor in NF-κB-DNA complex formation has been suggested (Ferrari *et al.*, 1997b). Application of ATP to mouse microglial N9 cells induced NF-κB-DNA complex formation. This was prevented by oATP, and did not occur in N9 clones that lack $P2X_7$ receptor (Ferrari *et al.*, 1997b). Target genes of NF-κB include those which encode inflammatory and chemotactic cytokines and cytokine receptors (Grossmann *et al.*, 1999).

1.6.8 Pathological functions

Inflammatory diseases

Rheumatoid arthritis describes a disease of the joint in which inflammation leads to destruction of cartilage and bone (Choy and Pabayi, 2001). Arthritic symptoms (paw swelling and inflammation) can be induced in mice by intraperitoneal injection of four mAbs against type II LPS (Labasi *et al.*, 2002). It was found that in $P2X_7$ receptor deficient mice the incidence of these symptoms and the severity of cartilage destruction were reduced (Labasi *et al.*, 2002). This suggests a role for the $P2X_7$ receptor is a potential therapeutic target for the treatment of arthritis.

Neurodegenerative diseases

Alzheimer's disease is characterised by formation of β-amyloid plaques and loss of cerebral cortex neurons (Apolloni *et al.*, 2009). In a transgenic mouse model of Alzheimer's disease (tg2576 with an amyloid precursor protein K670N/M671L mutation), or a rat model of Alzheimer's disease (induced by intrahippocampal β_{1-42} injection), $P2X_7$ receptor immunoreactivity was shown in close proximity to β-amyloid plaques, and localised to microglia (McLarnon *et al.*, 2006; Parvathenani *et al.*, 2003). Furthermore, $P2X_7$ protein expression was up regulated in the hippocampus in both these models of Alzheimer's disease (McLarnon *et al.*, 2006; Parvathenani *et al.*, 2003). Loss of rat hippocampal neurons following β_{1-42} injection was shown by reduced immunoreactivity of NeuN (neuronal marker), and was attenuated by BBG (Ryu and McLarnon, 2008). Taken together, these studies suggest that an increase in $P2X_7$ receptor expression in the hippocampus contributes to neuronal death in Alzheimer's disease.

Multiple sclerosis (MS) is an autoimmune disease in which the immune system attacks myelin in the CNS, leading to oligodendrocyte cell death, demyelination, and axonal damage (Apolloni *et al.*, 2009). Experimental autoimmune encephalomyelitis (EAE) describes a model of MS, in which injection of MOG_{35-55} (synthetic myelin oligodendrocyte glycoprotein peptide 35-55) results in neuronal demyelination in the CNS. Involvement of the $P2X_7$ receptor in MS was demonstrated in studies of the EAE mice model, in which ATP- and BzATP-induced demyelination and oligodendrocyte cell death is dramatically attenuated by oATP or BBG (Matute *et al.*, 2007). Studies of EAE

in $P2X_7$ receptor deficient mice show conflicting results. One investigation found axonal damage was greater in $P2X_7$ receptor deficient mice (Witting *et al.*, 2006). This was supported by another study showing $P2X_7$ receptor deficient mice had higher clinical scores for EAE (Chen and Brosnan, 2006). In contrast, Sharp *et al.* found that incidence of EAE, as well as axonal damage, was reduced in mice lacking the $P2X_7$ receptor (Sharp *et al.*, 2008). Therefore, the role of $P2X_7$ receptors in MS requires further investigation.

Pain

Hyperalgesia and allodynia are characteristic of chronic pain, and can occur because of neuronal injury (neuropathic pain) or inflammation (inflammatory pain). $P2X_7$ receptor deficient mice lacked thermal and mechanical hyperalgesia following partial ligation of the sciatic nerve. Furthermore, following intraplantar injection of Freund's Complete Adjuvant to induce inflammation, these mice failed to display mechanical hyperalgesia (Chessell *et al.*, 2005).

The role of $P2X_7$ receptor in nociception has also been demonstrated using $P2X_7$ receptor antagonists. A-740003 and A438079 (see section 1.6.5) dose-dependently reduced allodynic responses following sciatic or spinal nerve injury as well as pain responses following intraplantar injection of carrageenan or formalin to induce inflammation (Honore *et al.*, 2006; McGaraughty *et al.*, 2007).

Chronic lymphocytic leukaemia

Chronic lymphocytic leukaemia (CLL) is a hemopoietic tumour caused by monoclonal expansion of B lymphocytes, and as a result, $CD5^+$ B lymphocytes accumulate in the circulation (Matutes *et al.*, 1994). Progression of CLL is slow in patients with the indolent form and rapid in patients with the evolutive form of the disease. Both $P2X_7$ receptor protein expression and ATP-induced Ca^{2+} influx responses were lower in lymphocytes from patients with the indolent compared to the evolutive variant of the disease (Adinolfi *et al.*, 2002). As described above, expression of the $P2X_7$ receptor in leukemic cells allows proliferation under serum free conditions (Baricordi *et al.*, 1999). The results therefore suggest higher $P2X_7$ receptor expression may correlate with the more severity of CLL (Adinolfi *et al.*, 2002). The prevalence of the E496A

polymorphism is greater in CLL patients than healthy controls (Wiley *et al.*, 2002, but see Zhang *et al.*, 2003). The study also found agonist-induced Et^+ uptake and apoptosis were reduced in lymphocytes from CLL patients homozygous or heterozygous for the polymorphism. This suggests the $P2X_7$ receptor is required to remove lymphocytes from circulation via apoptosis, and that loss of receptor function results in lymphocyte accumulation in the circulation (Wiley *et al.*, 2002).

The two studies describe different roles for $P2X_7$ receptor in CLL. Both interpretations, however, are supported by a report that CLL survival was longer for patients heterozygous for the E496A polymorphism than WT subjects (Thunberg *et al.*, 2002). However, a separate study could not detect this association (Zhang *et al.*, 2003).

Killing intracellular mycobacteria

One role of macrophages is to engulf pathogens, such as bacteria, thereby removing them from the extracellular space. Application of ATP to bacille Calmette-Guérin (BCG)-infected macrophages leads death of the intracellular mycobacteria via fusion of phagosomes containing BCG with lysosomes (Fairbairn *et al.*, 2001). Neither ATP-dependent BCG death, nor phagosome-lysosome fusion occurs in macrophages from $P2X_7$ deficient mice (Fairbairn *et al.*, 2001). Furthermore, ATP-induced killing of BCG-infected macrophages from individuals heterozygous for the T357S or E496A polymorphisms is severely reduced in comparison to WT (Saunders *et al.*, 2003; Shemon *et al.*, 2006). Studies of two separate cohorts of individuals from Southeast Asia show that the E496A polymorphism is associated with extra pulmonary tuberculosis (Fernando *et al.*, 2007). However, this finding is not supported by a study of a separate cohort in the Chinese Han population (Xiao *et al.*, 2009).

Affective mood disorders

Association studies have identified chromosome 12q24.31, which encompasses the *P2RX7* gene, as a susceptibility locus for bipolar disorder (Barden *et al.*, 2006; Shink *et al.*, 2005) and major depressive disorder (Lucae *et al.*, 2006). One single nucleotide polymorphism (SNP) of the human *P2XR7* gene, 1405A>G, which leads to the Q460R mutation, was found to be

associated with bipolar disorder and major depressive disorder (Barden *et al.*, 2006; Lucae *et al.*, 2006; McQuillin *et al.*, 2008). This polymorphism has been shown have little, if any, effect of the functional expression of the $P2X_7$ receptor (see section 1.6.9) (Cabrini *et al.*, 2005; Roger et al., 2010a). However, the SNP 1405A>G lies in a haplotype with three gain-of-function SNPs of *P2RX7* (489C>T, 853G>A and 1068G>A) (Stokes *et al.*, 2010). Two recent studies, however, cannot confirm SNP 1405A>G is associated with bipolar disorder (Green *et al.*, 2009; Grigoroiu-Serbanescu *et al.*, 2009), and there is currently no clear insight into how SNPs of the *P2RX7* gene could cause increased susceptibility to bipolar disorder and major depressive disorder.

Due to the implication of the $P2X_7$ receptor in a number of diseases, as described above, pharmaceutical companies are keen to develop drugs to target the receptor, and $P2X_7$ receptor antagonists have now reached clinical trials (Guile *et al.*, 2009). The first compound to enter clinical trials was developed by AstraZeneca (AZD9056) (Astbury *et al.*, 2007), which has undergone phase II studies to test the efficacy of the compound for treatment of rheumatoid arthritis, osteoarthritis of the knee and chronic obstructive pulmonary disease (www.clinicaltrials.gov; www.astrazeneca.com). Pfizer are also undertaking phase II studies to investigate their $P2X_7$ receptor antagonist CE-224535 as a treatment for rheumatoid arthritis (www.clinicaltrials.gov).

1.6.9 Single nucleotide polymorphisms

There are extensive SNPs within the *P2RX7* gene. SNP mutations are either synonymous (no change in amino acid sequence) or non-synonymous (mutation of amino acid sequence). A number of non-synonymous SNP (ns-SNP) mutations have been identified in patients with mood disorders (Barden *et al.*, 2006; Lucae *et al.*, 2006; McQuillin *et al.*, 2008) or altered pathophysiology of CLL (Wiley *et al.*, 2002). This section focuses on some of the ns-SNP mutations previously studied. The research of ns-SNP mutations is important for two reasons. Investigation of these naturally occurring mutations can provide information into how the $P2X_7$ receptors operate at the molecular level, and such information can in turn help understand the molecular mechanisms responsible for the associated diseases.

The first ns-SNP studied in terms of it's effect on human $P2X_7$ receptor function is 1513A>C, which has an allele frequency of 0.08-0.23 (Barden *et al.*,

2006; Cabrini *et al.*, 2005; Gu *et al.*, 2001; Lucae *et al.*, 2006; Shemon *et al.*, 2006; Stokes *et al.*, 2010; Wiley *et al.*, 2002). This SNP leads to mutation E496A in the C-terminus of the receptor.

Results from experiments using two different heterologous expression systems show significant discrepancies. BzATP-induced Ca^{2+} influx was absent in HEK293 cells expressing the E496A mutant (Cabrini *et al.*, 2005). Likewise, agonist-induced Et^{+} uptake in HEK293 cells expressing the E496A mutant and in monocytes, B- and T-lymphocytes and NK cells from subjects homozygous for the E496A SNP was severely reduced or abolished (Denlinger *et al.*, 2005; Gu *et al.*, 2001; Saunders *et al.*, 2003; Wiley *et al.*, 2002). However, Boldt *et al.* found ATP-induced currents were unaltered by this mutation (Boldt *et al.*, 2003).

A further ns-SNP is 489C>T, has an allele frequency of 0.44-0.5 (Barden *et al.*, 2006; Cabrini *et al.*, 2005; Shemon *et al.*, 2006; Stokes *et al.*, 2010). This SNP introduces the H155Y mutation in the extracellular domain of the receptor. ATP-evoked Ca^{2+} influx was found to be increased in lymphocytes of CLL patients carrying this mutation (Cabrini *et al.*, 2005).

A third ns-SNP is 1068G>A, and has an allele frequency of 0.37-0.41 (Barden *et al.*, 2006; Cabrini *et al.*, 2005; Lucae *et al.*, 2006; Stokes *et al.*, 2010). This polymorphism results in mutation A348T. A recent study have demonstrated that monocytes and erthrocytes isolated from subjects homozygous for the mutation exhibit increased ATP-dependent Et^{+} uptake in comparison to those from WT subjects (Stokes *et al.*, 2010). Furthermore, LPS-primed monocytes from these subjects release more IL-1β in response to ATP.

The 946G>A SNP has an allele frequency of 0.01-0.013 and results in a R307Q mutation of the $P2X_7$ receptor (Shemon *et al.*, 2006; Stokes *et al.*, 2010). One study found ATP-induced Et^{+} uptake was abolished in lymphocytes from R307A heterozygous subjects (Gu *et al.*, 2004). Mutation of the equivalent residue in the rat $P2X_2$ receptor reduced the ATP sensitivity (Jiang *et al.*, 2000b). It is possible this residue plays a role in ATP binding (see section 1.4.4).

Another ns-SNP is 1096C>G, which has a minor allele frequency of 0.04-0.1 (Barden et al., 2006; Cabrini *et al.*, 2005; Lucae *et al.*, 2006; Stokes *et al.*, 2010; Shemon *et al.*, 2006), introduces T357S mutation. ATP induced Et^{+} uptake by lymphocytes, monocytes and macrophages from subjects polymorphic for the T357S mutation is reduced. Furthermore, in heterologous

systems, both ATP-evoked currents and Et^+ uptake are impaired by the mutation (Shemon *et al.*, 2006).

The final ns-SNP, 1729T>A has a minor allele frequency of 0.02-0.04, resulting in the I568N mutation (Stokes *et al.*, 2010; Wiley *et al.*, 2003; Shemon *et al.*, 2006). When expressed in HEK293 cells, the I568N mutant was non-functional in terms of ATP-induced Et^+ uptake. Moreover, lymphocytes from subjects polymorphic for the I568N mutation had reduced ATP-evoked Ba^{2+} uptake. The impaired function appeared to be due to a reduction in cell surface expression of the receptor as shown by flow cytometry and immunofluorescent staining (Wiley *et al.*, 2003).

Many of the studies into the effects of SNP mutations have used lymphocytes and macrophages from patients. However, Roger *et al.* studied twelve ns-SNP mutations identified in patients with mood disorders and CLL, by introducing the point mutations in the human $P2X_7$ receptor and performing functional studies upon expression in HEK293 cells (Barden *et al.*, 2006; Lucae *et al.*, 2006; Roger *et al.*, 2010a; Wiley *et al.*, 2002). Five mutations (V76A, R117W, L191P, T357S and E496A) reduced ATP-evoked currents and rate of Et^+ uptake, whilst two (Q460R and H521Q) had no effect. Using the same techniques, H155Y and A348T increased, whilst G150R, E186K and I568N abolished receptor function (Roger *et al.*, 2010a).

1.6.10 Species differences in $P2X_7$ receptors properties

Five mammalian $P2X_7$ receptor orthologues have been cloned and functionally characterised. These are, in order of the date they were cloned: rat, human, mouse, guinea pig and dog (Chessell *et al.*, 1998; Fonfria *et al.*, 2008; Rassendren *et al.*, 1997; Roman *et al.*, 2009; Surprenant *et al.*, 1996). Functional characterisation of the cloned $P2X_7$ receptors has revealed a number of striking species differences, which are discussed below.

Agonist potency

One difference is that the human $P2X_7$ receptor is less sensitive to ATP (10-fold) and BzATP (25-fold) than the rat $P2X_7$ receptor (Rassendren *et al.*, 1997). The mouse $P2X_7$ receptor is the least sensitive to both ATP and BzATP in comparison to the rat or human $P2X_7$ receptor (Hibell *et al.*, 2000; Young et

al., 2007). The dog $P2X_7$ receptor is equally sensitive to ATP and BzATP as the human $P2X_7$ receptor (Roman *et al.*, 2009).

The sensitivity of the $P2X_7$ receptor to agonist depends on the experimental conditions. $P2X_7$ receptors become more sensitive to agonist when the extracellular divalent cation concentration is lowered, or after the receptors are fully facilitated (see sections 1.6.5 and 1.6.6). Furthermore, EC_{50} values calculated from data obtained using different assays can differ significantly (Hibell *et al.*, 2001). Therefore, comparisons between the sensitivities of different $P2X_7$ receptor species orthologues to agonist should be under the same experimental conditions.

There are also differences between human and rat species in terms of the $P2X_7$ receptor mediated dye uptake pathway. The maximal uptake of YO-PRO-1 elicited by BzATP is greater by cells expressing the rat $P2X_7$ receptor in comparison to the human receptor (Rassendren *et al.*, 1997).

Activation and deactivation kinetics

The kinetics of the $P2X_7$ receptor activation and deactivation differ between species. The human, rat and mouse $P2X_7$ receptor are activated by BzATP very rapidly (within 1 s). However, the ATP- or BzATP-evoked current onset at dog $P2X_7$ receptor was much slower, and failed to reach the maximum within 2 s (Chessell *et al.*, 1998; Roman *et al.*, 2009). The deactivation kinetic of the rat $P2X_7$ receptor is considerably slow in external solution containing low concentrations of divalent cations, and progressively prolonged upon repeated agonist applications (Surprenant *et al.*, 1996). However, the deactivation of human and mouse $P2X_7$ receptors is much quicker, and does not change dramatically with repeated agonist applications (Chessell *et al.*, 1998; Rassendren *et al.*, 1997).

Antagonist sensitivity

BBG is a potent antagonist at rat $P2X_7$ receptor (see section 1.6.5); however, it has an approximately 20 times lower potency at human $P2X_7$ receptors (Jiang *et al.*, 2000a).

KN-62 is a potent antagonist at human $P2X_7$ receptors (Gargett and Wiley, 1997) (see section 1.6.5). Interestingly, KN-62 fails to inhibit rat $P2X_7$ receptors (Humphreys *et al.*, 1998). By constructing human and rat $P2X_7$

receptor chimeras, this species difference has been shown to depend on the extracellular part of the receptor (Humphreys *et al.*, 1998).

AZ11645373, is a potent antagonist at human and dog $P2X_7$ receptors. However, it is less potent at mouse and guinea pig $P2X_7$ receptors, and has low potency at rat $P2X_7$ receptors (Michel *et al.*, 2009; Stokes *et al.*, 2006). Introduction of F95L mutation in human $P2X_7$ receptor, which changes residue 95 in rat $P2X_7$ receptor, reduces the potency of AZ11645373 (Michel *et al.*, 2008; Michel *et al.*, 2009).

Current facilitation

Repeated or prolonged activation of $P2X_7$ receptors leads to an increase in current amplitude or facilitation (see section 1.6.6). The facilitation for rat $P2X_7$ receptors is much faster than human $P2X_7$ receptors. Facilitation of the rat $P2X_7$ receptor has a Ca^{2+}/CaM-dependent component (Roger *et al.*, 2008), which is absent for the human $P2X_7$ receptor as the latter does not contain a CaM binding site and does not associate with CaM. (Roger *et al.*, 2010b).

1.7 Aims of the study

There are numerous ns-SNP mutations of the human $P2X_7$ receptor, and two of these, H155Y and A348T, were of particular interest due to their gain-of-function effect. The molecular bases for these effects are not fully understood. In addition, these two mutations change residues in the human $P2X_7$ receptor to the corresponding ones in the rat $P2X_7$ receptor. The properties of $P2X_7$ receptors, including their functional expression and pharmacology, exhibit striking species differences. Therefore, the overall aim of the study was to investigate the molecular mechanisms responsible for the gain-of-function and whether the residues at these two positions contribute to the species-dependent properties. The specific objectives of this study, therefore, were:

1. To examine the gain-of-function effects of H155Y and A348T mutations singly or in combination, and determine the influence of side chains with different properties at position 155 and 348 (chapter 3).
2. To explore differences in functional expression of human and rat $P2X_7$ receptors, and particularly to determine the effects of introducing reciprocal mutations Y155H and T348A on the rat $P2X_7$ receptor (chapter 4).
3. To investigate the possible contribution of other non-conserved residues in the microdomains surrounding His^{155} and Ala^{348} to the functional expression and species-specific expression of the human and rat $P2X_7$ receptors (chapter 5).
4. The number of functional channels at the cell surface and the single channel properties (unitary conductance and open probability) together determine the functional expression of an ion channel. Therefore the effects of mutations at residues 155 and 348 on the total protein and surface expression of human and rat $P2X_7$ receptors was determined (chapter 6).
5. To characterise the monkey $P2X_7$ receptor in terms of sensitivity to agonists and antagonists, and compare its properties to those of the human $P2X_7$ receptor (chapter 7).

To address these aims, WT or mutant $P2X_7$ receptors were expressed in HEK293 cells, and receptor function was assessed by whole-cell patch-clamp recordings, and protein subcellular distribution and surface expression by immunocytochemistry and biotin labelling.

Chapter 2

Materials and methods

2.1 Chemicals, reagents and solutions

2.1.1 Chemicals and reagents

Chemicals and reagents were purchased at the appropriate grade from Sigma, unless otherwise stated.

2.1.2 Solutions

All solutions were prepared using Milli-Q deionised water and are shown in Table 2.1. Solutions used for DNA and tissue culture were sterilised by autoclaving or syringe filtering (0.22 µm).

2.1.3 Enzymes

Dpn I restriction enzyme, *PfuUltra* DNA polymerase and Benzonase nuclease were purchased from Promega, Stratagene and Sigma, respectively.

2.1.4 DNA purification kits

The QIAprep Spin Miniprep and Midiprep kits were purchased from Qiagen.

2.1.5 Antibodies, streptavidin beads, biotin, BCA kit and protein markers

Antibody suppliers are shown in Table 2.2. EZview red streptavidin affinity gel beads were purchased from Sigma. EZ-link sulfo-NHS-LC biotin and the bicinchoninic acid (BCA) Protein Assay kit were purchased from Pierce. Prestained protein markers (6-175 kDa) were purchased from New England Biolabs.

2.1.6 E. coli strains and growth media

Competent *Escherichia coli (E. Coli)* cells (α-Select bronze efficiency) used for site-directed mutagenesis were purchased from BioLine. Competent *E. coli* cells (DH5α strain) used for plasmid amplification were prepared as described in section 2.2.1, using cells originally purchased from GIBCOBRL. *E. coli* growth medium was purchased from Sigma (Table 2.1).

2.1.7 Cell culture media and transfection reagents

HEK293 cells were kindly provided by Prof. Annmarie Surprenant (University of Manchester). Dulbecco's modified Eagle's medium (DMEM) +

Glutamax™-1, foetal bovine serum (FBS), trypsin/ethylenediaminetetraacetic acid (EDTA), OPTI-MEM®-I serum reduced media and Lipofectamine™ 2000 were purchased from Invitrogen (Table 2.1).

2.1.8 Plasmids and oligonucleotides

Prof. Annmarie Surprenant (University of Manchester) kindly provided the cDNAs encoding the human or rat $P2X_7$ receptor with a C-terminal EYMPME (EE) tag and the cDNA encoding enhanced green fluorescent protein (eGFP). The gene encoding the *Macaca Mullata* $P2X_7$ receptor (LOC722096, www.ensembl.org) with a C-terminal EE tag was synthesised by Epoch Biolabs and cloned into *KpnI/NotI* digested pcDNA3.1(+) vector. Primers were custom made by Sigma. Amino acid sequences were aligned using online ClustalW software.

2.2 Molecular biology methods

2.2.1 Bacterial cell culture and transformation

Preparation of competent E. coli cells

The protocol for the preparation of competent *E. coli* cells was adapted from a method described previously (Hanahan, 1983). DH5α *E. coli* cells (stock stored at -80°C) were spread onto an LB agar plate (Table 2.1) without antibiotics and single colonies were grown overnight at 37°C. A single colony was used to inoculate 5 ml of LB growth media (Table 2.1) and was cultured overnight at 37°C with shaking (250 revolutions per minutes (rpm)). A sample of this culture (0.5 ml) was diluted in 100 ml of LB growth media and cultured overnight at 37°C with shaking (250 rpm). Cells were collected by centrifugation (2000 x *g* for 10 min at 4°C). After removal of the supernatant, the cell pellet was resuspended in 20 ml of chilled 0.1 M $CaCl_2$, and cells were pelleted again by centrifugation (2000 x *g* for 10 min at 4°C). Following removal of the supernatant, cells were resuspended in 4 ml of chilled transformation buffer (Table 2.1). The cells were then aliquoted and stored at -80°C.

Table 2.1 Solutions and media

E. coli growth media, transformation buffer and antibiotics	
LB growth media	10 g/l tryptone; 5 g/l yeast extract; 5 g/l NaCl.
LB agar plate	LB media supplemented with 15 g/l agar, autoclaved, cooled to ~ 60°C, then supplemented with 100 µg/ml ampicillin or 50 µg/ml kanamycin, if required.
Transformation buffer	0.1 M $CaCl_2$; 15% glycerol (v/v).
Ampicillin	50 mg/ml ampicillin, dissolved in water, filter sterilised (0.22 µm), stored -20°C.
Kanamycin	10 mg/ml kanamycin, dissolved in water, filter sterilised (0.22 µm), stored -20°C.
DNA preparation	
Buffer P1 (resuspension buffer)	50 mM Tris-HCl, pH 8.0; 10 mM EDTA; 100 µg/ml RNase A, stored at 4°C.
Buffer P2 (lysis buffer)	200 mM NaOH; 1% sodium dodecyl sulphate (SDS) (w/v).
Buffer P3 (neutralisation buffer)	3.0 M potassium acetate, pH 5.5.
Buffer QBT (equilibration buffer)	750 mM NaCl; 50 mM MOPS, pH 7.0; 15% isopropanol (v/v); 0.15% Triton® X-100 (v/v).
Buffer QC (wash buffer)	1 M NaCl; 50 mM MOPS, pH 7.0; 15% isopropanol (v/v).
Buffer QF (elution buffer)	1.25 M NaCl; 50 mM Tris-HCl, pH 8.5; 15% isopropanol (v/v).
Buffer EB (elution buffer)	10 mM Tris-HCl, pH 8.5.
Buffer N3, PE	Recipes unknown, purchased from Qiagen.
DNA gel electrophoresis	
TAE buffer	40 mM Tris-Oac; 0.114% glacial acetic acid (v/v); 1 mM EDTA; pH 8.0.

1% agarose gel	1% agarose (w/v) dissolved in TAE.
EtBr	10 mg/ml EtBr dissolved in water.
6 x DNA loading buffer	0.25% bromophenol blue (w/v); 40% sucrose (w/v), stored at 4°C.
Polymerase chain reaction (PCR)	
10 x *PfuUltra* DNA polymerase buffer	100 mM KCl; 100 mM $(NH_4)_2SO_4$; 200 mM Tris-HCl, pH 8.8; 20 mM $MgSO_4$; 1% Triton® X-100; 1 mg/ml nuclease-free BSA, stored -20°C.
dNTPs	2 mM dATP; 2 mM dCTP; 2 mM dGTP; 2mM dTTP, stored -20°C.
Tissue culture and transfection	
HEK293 culture media	DMEM + Glutamax™-1, supplemented with 10% FBS (v/v).
Trypsin/EDTA	0.5 g/l trypsin; 0.2g/l EDTA·4Na; 0.8 g/l NaCl in PBS.
Phosphate buffered saline (PBS)	137.93 mM NaCl; 2.67 mM KCl; 8.06 mM Na_2HPO_4; 1.47 mM KH_2PO_4.
Biotin labelling	
PBS	138 mM NaCl; 2.7 mM KCl; 8.1 mM Na_2HPO_4; 1.5 mM KH_2PO_4; 0.1 mM $CaCl_2$; 1 mM $MgCl_2$, pH 8.0.
PBS/glycine	100 mM glycine dissolved in PBS.
EZ-link sulfo-NHS-LC biotin	0.5 mg/ml EZ-link sulfo-NHS-LC biotin in PBS.
RIPA lysis buffer	150 mM NaCl; 20 mM Tris-HCl, pH 7.4; 1 mM $CaCl_2$; 1 mM $MgCl_2$.
Protease inhibitor	1.5 µg/ml chymotrypsin; 0.8 µg/ml thermolysin; 1 mg/ml papain; 1.5 µg/ml pronase; 15 µg/ml pancreatic extract; 0.2 µg/ml trypsin; made in RIPA buffer.
Benzonase nuclease	10 U/µl benzonase in 50% glycerol (v/v); 20 mM Tris-HCl, pH8.0; 20 mM NaCl; 2 mM $MgCl_2$.
2 x Electrophoresis buffer	12% SDS; 20% glycerol; 100 mM Tris-HCl, pH 6.8; 4 mM EDTA; 0.1% bromophenol blue.
BCA assay	
BCA reagent A	Sodium carbonate; sodium bicarbonate; bicinchoninic acid; sodium tartrate in 0.1 M sodium hydroxide.

BCA reagent B	4% cupric sulphate.
SDS-polyacrylamide gel electrophoresis (SDS-PAGE)	
SDS-PAGE running buffer	25 mM Tris; 192 mM glycine; 0.1% SDS (w/v).
Towbin transfer buffer	25 mM Tris; 192 mM glycine; 10% methanol (v/v).
Tris-buffered saline-Tween (TBST)	10 mM Tris-HCl, pH8.0; 150 mM NaCl; 0.05% Tween-20 (v/v).
Non-fat milk blocking buffer	5% skim milk powder (w/v) dissolved in TBST.
Immunocytochemistry	
PBS	137 mM NaCl; 2.7 mM KCl; 0.01 M phosphate buffer, pH 7.4.
Zamboni's fixative	15% (v/v) picric acid; 5.5% (v/v) formaldehyde in PBS.
Antibody dilution buffer	2% (v/v) Triton® X-100 in PBS.
Blocking solution	5% (v/v) goats serum in antibody dilution buffer.

Table 2.2 Antibody suppliers and dilutions

Primary antibodies			
Antibody	Supplier	Western blotting	Immunocytochemistry
Rabbit anti-EE	Bethyl	1:5000	1:1000
Mouse anti-GFP	Santa Cruz	1:2000	N/A
Secondary antibodies			
Bovine anti-rabbit-HRP	Santa Cruz	1:5000	N/A
Bovine anti-mouse-HRP	Santa Cruz	1:2000	N/A
Goat anti-rabbit Alexafluor 488	Invitrogen	N/A	1:2000 (rat $P2X_7$) 1:4000 (human $P2X_7$)

Antibodies were diluted in blocking solution (Table 2.1). HRP: horseradish peroxidise.

Heat shock transformation

Plasmid DNA (10-100 ng) or 1 µl of PCR product was mixed with 50 µl of thawed competent *E. coli* cells and incubated on ice for 30 min. Cells were heat shocked at 42°C for 45 s and returned to ice for 2 min. Prewarmed (37°C) LB growth media was then added (950 µl) and incubated for 1 hr at 37°C with shaking (250 rpm). A sample of the culture (100 µl) was spread on a LB agar plate containing 100 µg/ml ampicillin (or 50 µg/ml kanamycin for eGFP) and incubated overnight at 37°C to allow colonies to grow. Plates were stored at 4°C.

2.2.2 DNA preparation

Small scale isolation of plasmid DNA

For small-scale isolation of plasmid DNA (up to 20 µg), the QIAprep Spin Miniprep kit was used (see Table 2.1 for solutions) according to the suggested protocol and as follows. LB growth media (5 ml) containing 100 µg/ml ampicillin (or 50 µg/ml kanamycin for eGFP) was inoculated with a single colony of transformed *E. coli* cells and incubated overnight at 37°C with shaking (250 rpm). Cells were collected from 3 ml of the cell culture by centrifugation (14,000 x *g* for 4 min at room temperature (RT)) and resuspended in 250 µl of chilled buffer P1 by vortexing. Cells were lysed under alkaline conditions by adding 250 µl of buffer P2 and gently inverting the tube. Buffer N3 was added (350 µl) and cell debris was cleared by centrifugation (12,000 x *g* for 10 min at RT). The supernatant was then applied to a QIAprep spin column, containing a silica membrane, and centrifuged (12,000 x *g* for 1 min at RT). Follow-through was discarded and the column was washed with 0.75 ml of buffer PE, followed by further centrifugation (12,000 x *g* for 1 min at RT). Follow-through was discarded and DNA was eluted by adding 50 µl of prewarmed (37°C) elution buffer (buffer EB) to the column and allowing 1 min incubation. Purified DNA was collected from the column by centrifugation (12,000 x *g* for 1 min at RT). Plasmid DNA was stored at -20 °C until use.

Large scale isolation of plasmid DNA

For larger scale isolation of plasmid DNA (up to 100 µg), the Qiagen Midiprep kit was used (see Table 2.1 for solutions) according to the suggested protocol, which was as follows. LB growth media (10 ml) containing 100 µg/ml

ampicillin, or 50 µg/ml kanamycin for eGFP, was inoculated with a single colony of transformed *E. coli* cells and incubated for 8 hrs at 37°C with shaking (250 rpm). This culture was diluted in 90 ml of LB growth media containing 100 µg/ml ampicillin or 50 µg/ml kanamycin and grown overnight at 37°C with shaking (250 rpm). Cells were harvested by centrifugation (6,000 x *g* for 15 min at 4°C). After removal of the supernatant, cells were resuspended in 4 ml of buffer P1 by vortexing and lysed under alkaline conditions by adding 4 ml of buffer P2 and gently inverting the tube. After a 5 min incubation at RT, the lysate solution was neutralised by adding 4 ml of buffer P3 and then incubated on ice for 15 min. Cell debris was cleared by two centrifugation steps (13,000 x *g* for 45 min in total at 4°C). The supernatant was then applied to the QIAGEN-tip 100, which had been pre-equilibrated with 4 ml of buffer QBT, and allowed to enter by gravity flow. The tip was washed with 20 ml of buffer QC. DNA was eluted with 5 ml buffer QF and precipitated by adding 3.5 ml of isopropanol. Precipitated DNA was collected by centrifugation (5,000 x *g* for 60 min at 4°C). Supernatant was removed and the DNA pellet washed with 2 ml 70% ethanol (v/v) and centrifuged (13,000 x *g* for 10 min at 4°C). Supernatant was removed; the pellet was air-dried for 10 min and dissolved in 200 µl of buffer EB. Plasmid DNA was stored at -20 °C until use.

2.2.3 Analysis of DNA by gel electrophoresis

DNA samples were analysed by agarose gel electrophoresis. A 1% agarose gel solution (Table 2.1) was made by heating in a microwave. When cooled to approximately 60°C, EtBr was added (Table 2.1) to a final concentration of 0.5 µg/ml, and the solution was poured into a pre-assembled gel cast with a comb inserted, and left to solidify. A 6 µl DNA sample was prepared (1 µl of plasmid; 1 µl 6 x DNA loading buffer (Table 2.1); 4 µl water). Samples were loaded into the wells, with an additional well for the 1 kb DNA markers. Gel electrophoresis was carried out at 70 V for 90 min, and intercalated Et^+ was detected by fluorescence under UV light using a gel doc XR quantity system (Biorad, UK). To quantify the DNA yield, a sample of DNA (1 µl) was diluted 100-fold in buffer EB. A spectrophotometer (Eppendorf) was used to measure A_{260}, and used to calculate the DNA concentration (1 A_{260} = 50 µg/ml of DNA). To check DNA purity the ratio of the absorbance at 260 and 280 nm ($A_{260/280}$) was measured. $A_{260/280}$ of 1.8 indicates pure DNA.

2.2.4 Site-directed mutagenesis

Site-directed mutagenesis was used to introduce point mutations. The primers were designed to encode the desired mutation (Table 2.3). Each primer was 22- 41 bases in length with the mutated base approximately in the middle, and had a melting temperature of ≥78°C. The PCR reaction mix contained 0.75 µl of each primer (10 µM), 2 µl of 10 x *PfuUltra* DNA polymerase buffer (Table 2.1), 2.5 µl of 2 mM dNTP mix (Table 2.1), 0.5 µl (50 ng) of template plasmid DNA, 0.5 µl of *PfuUltra* high-fidelity DNA polymerase, and was adjusted to 25 µl using sterile deionised water. PCR was performed using an Eppendorf thermocycler. The first step, 95°C for 60 s, denatured the double stranded DNA, and was followed by 18 cycles, each comprising 3 steps of 95°C for 50 s, 60°C for 50 s and then 68°C for 20 min. A further incubation of 68°C for 20 min was allowed, and the samples were maintained at 4°C until collection.

A *Dpn* I digestion step is necessary. *Dpn* I restriction enzyme (10 U) was mixed with the PCR sample by pipetting, and incubated at 37°C for 60 min to digest the methylated, non-mutated parental DNA template.

PCR product was transformed into competent *E. coli* cells (section 2.2.1), and small scale isolation of plasmid DNA was performed (section 2.2.2). The presence of the desired mutation was confirmed using commercial DNA sequencing services (University of Leeds or Geneservice).

The following mutations in the human $P2X_7$ receptor were made by other members of the lab: H155Y and A348T.

Table 2.3 Primer sequences for site-directed mutagenesis

Mutation name	5' to 3' sequences
Human $P2X_7$:	
V153I forward primer	GACCGGAAGGTGTATAGTGCATGAAGGG
V153I reverse primer	CCCTTCATGCACTATACACCTTCCGGTC
V154P forward primer	GGAAGGTGTGTACCGCATGAAGGGAACCAGAAG
V154P reverse primer	CTTCTGGTTCCCTTCATGCGGTACACACCTTCC
V154Y forward primer	GGAAGGTGTGTATACCATGAAGGGAACCAG
V154Y reverse primer	CTGGTTCCCTTCATGGTATACACACCTTCC
H155Y forward primer	GGAAGGTGTGTAGTGTATGAAGGGAACCAGAAGA
H155Y reverse primer	TCTTCTGGTTCCCTTCATACACTACACACCTTCC
H155F forward primer	GAAGGTGTGTAGTGTTTGAAGGGAACCAGAAG
H155F reverse primer	CTTCTGGTTCCCTTCAAACACTACACACCTTC
H155R forward primer	GAAGGTGTGTAGTGCGTGAAGGGAACCAGAAG
H155R reverse primer	CTTCTGGTTCCCTTCACGCACTACACACCTTC
H155D forward primer	GAAGGTGTGTAGTGGATGAAGGGAACCAGAAG
H155D reverse primer	CTTCTGGTTCCCTTCATCCACTACACACCTTC
H155N forward primer	GAAGGTGTGTAGTGAATGAAGGGAACCAGAAG
H155N reverse primer	CTTCTGGTTCCCTTCATTCACTACACACCTTC
H155A forward primer	GAAGGTGTGTAGTGGCTGAAGGGAACCAGAAG
H155A reverse primer	CTTCTGGTTCCCTTCAGCCACTACACACCTTC
H155L forward primer	GAAGGTGTGTAGTGCTTGAAGGGAACCAGAAG
H155L reverse primer	CTTCTGGTTCCCTTCAAGCACTACACACCTTC
E156D forward primer	GGTGTGTAGTGCATGACGGGAACCAGAAG
E156D reverse primer	CTTCTGGTTCCCGTCATGCACTACACACC
E156Y forward primer	GGTGTGTAGTGCATTACGGGAACCAGAAG
E156Y reverse primer	CTTCTGGTTCCCGTAATGCACTACACACC
G157Q forward primer	GTGTAGTGCATGAACAGAACCAGAAGACCTG
G157Q reverse primer	CAGGTCTTCTGGTTCTGTTCATGCACTACAC
N158K forward primer	GTGCATGAAGGGAAGCAGAAGACCTGTG
N158K reverse primer	CACAGGTCTTCTGCTTCCCTTCATGCAC
Q159R forward primer	GTGCATGAAGGGAACCGGAAGACCTGTGAAG
Q159R reverse primer	CTTCACAGGTCTTCCGGTTCCCTTCATGCAC
A348G forward primer	CTTCGGTCTGGCCACTGTGTTCATCG

A348G reverse primer	CGATGAACACAGTGGCCAGACCGAAG
A348F forward primer	CTTCGGGCTAGCCTTTGTGTTCATCGACTTCC
A348F reverse primer	GGAAGTCGATGAACACAAAGGCTAGCCCGAAG
A348M forward primer	CTTCGGGCTAGCCATGGTGTTCATCGACTTCC
A348M reverse primer	GGAAGTCGATGAACACCATGGCTAGCCCGAAG
F350C forward primer	GCTAGCCGCTGTGTGCATCGACTTCCTCATCG
F350C reverse primer	CGATGAGGAAGTCGATGCACACAGCGGCTAGC
F353L forward primer	GTGTTCATCGACTTACTCATCGACACTTACTCCAG
F353L reverse primer	CTGGAGTAAGTGTCGATGAGTAAGTCGATGAACAC
L354I forward primer	GTGTTCATCGACTTCATCATCGACACTTACTCCAG
L354I reverse primer	CTGGAGTAAGTGTCGATGATGAAGTCGATGAACAC
D356N forward primer	GACTTCCTCATCAACACTTACTCCAGTAACTGCTG
D356N reverse primer	CAGCAGTTACTGGAGTAAGTGTTGATGAGGAAGTC
Rat $P2X_7$:	
Y155H forward primer	GCAGGTGTATACCTCACGACCAGAAGAG
Y155H reverse primer	CTCTTCTGGTCGTGAGGTATACACCTGC
T348A forward primer	CTATTTCGGTTTGGCCGCCGTGTGTATTGAC
T348A reverse primer	GTCAATACACACGGCGGCCAAACCGAAATAG
L353F forward primer	GTGTGTATTGACTTCATCATCAACACGTATGCC
L353F reverse primer	GGCATACGTGTTGATGATGAAGTCAATACACAC

2.2.5 Mammalian cell culture and transfection

Maintenance of HEK293 cells

HEK293 cells were used to express WT and mutant $P2X_7$ receptors. Cells were maintained in culture media (Table 2.1) at 37°C and 5% CO_2, and under humidified conditions.

Cells were passaged every 3-4 days by trypsinisation. Solutions used are shown in Table 2.1, and volumes of solutions used are shown in Table 2.4. When cells were confluent, the culture media was removed and cells were washed with PBS. Trypsin/EDTA was added and cells were incubated at 37°C for 1-2 min to lift the cells. An equal volume of culture media was added and cells were collected by centrifugation. Cells were replated in new dishes containing fresh culture media at a ratio of 1:5 or 1:10.

Preparation of HEK293 frozen cell stocks

Frozen cells kept in a liquid nitrogen cryostat were thawed quickly in a 37°C incubator and added to a 25cm^2 culture flask containing 5 ml of culture media. Following overnight incubation, the culture media was replaced to remove the dimethylsulphoxide (DMSO) in the freezing solution. Cells were grown to confluency and maintained as described above.

To replenish frozen stocks, cells with a low passage number were frozen in liquid nitrogen. Confluent cells from a 75cm^2 flask were collected by trypsinisation as described above. The cell pellet was resuspended in 1 ml FBS containing 10% DMSO (v/v) and divided between 2 freezing vials. The vials were placed in a box containing isopropanol, kept at -80°C overnight, and then transferred to a liquid nitrogen cryostat.

Table 2.4 Solution or media volumes used for tissue culture

	35 mm dish	25 cm^2 flask	75 cm^2 flask
PBS (ml)	1	5	10
Trypsin/EDTA (ml)	0.5	1	2
Culture media (ml)	2	5	15

Transient transfection

In order to express $P2X_7$ receptors, HEK293 cells were transiently transfected with plasmid DNA using Lipofectamine™ 2000, according to the manufacturer's recommendations. Cells were transfected in 35 mm dishes at 50-80% confluency (~10^6 cells). Plasmid DNA (1 µg for $P2X_7$ encoding plasmid, and 0.1 µg for eGFP, if required) was diluted in 100 µl of OPTI-MEM®-I. Lipofectamine™ 2000 reagent (3 µl per 1 µg plasmid) was diluted in 100 µl of OPTI-MEM®-I and incubated for 5 min at RT. The plasmid and lipofectamine™ 2000 mixes were combined and incubated for 20 min at RT to allow DNA-liposome complex formation and, after adding 800 µl of culture media, was transferred to the cells.

2.2.6 Biotin labelling and Western blotting

Biotin labelling

HEK293 cells prepared in 35 mm dishes were co-transfected (as described above) with $P2X_7$ receptor (or pcDNA3.1 vector as a negative control) and eGFP as an internal control for possible variations in cell preparation, transfection efficiency and sample handling, and used 48 hrs later. Two 35 mm dishes of cells were used for each sample. Cells were washed four times with chilled PBS (Table 2.1) and incubated in 1 ml of 0.5 mg/ml EZ-link sulfo-NHS-LC biotin (Table 2.1) for 30 min at 4°C. PBS/glycine (1 ml; Table 2.1) was then added and the cells collected by centrifugation (16,000 x *g* for 15 s at RT). The cell pellet was washed 4 times with 1 ml PBS/glycine and the same centrifugation step applied each time, and finally resuspended in 0.5 ml RIPA lysis buffer supplemented with protease inhibitor and 20 U benzonase nuclease (Table 2.1). After being cleared by centrifugation (15,000 x *g* for 10 min at 4°C), the lysate was transferred to a new tube.

Protein concentrations were determined using the BCA assay (Table 2.1) and bovine serum albumin (BSA) as standard. A sample of the cell lysate was diluted at 1:1 using RIPA lysis buffer supplemented with protease inhibitors (RIPA/PI). 200 µl of BCA reagent (2% reagent B in reagent A) plus 10 µl of samples or standards were added to each wells of 96-well plates. The plate was placed on a mixer for 1 min at RT and then incubated for 30 min at 37°C before the A_{540} values were taken using a POLARstar OPTIMA plate reader (BMG

Labtech). A standard curve was produced, from which the protein concentrations of the samples were determined.

Cell lysate was diluted in RIPA/PI to a protein concentration of 1 μg/μl. For analysis of total expression of the $P2X_7$ receptor, a sample was taken and an equal volume of 2 x electrophoresis buffer (Table 2.1) added (protein concentration 0.5 μg/μl). The sample was then boiled for 2 min. For analysis of surface expression of the $P2X_7$ receptor, 300 μg of cell lysate was mixed with 50 μl of EZview red streptavidin affinity gel beads and incubated overnight at 4°C. Beads were collected by centrifugation (2,000 x *g* for 2 min at 4°C) and washed 4 times with 1 ml RIPA lysis buffer and the same centrifugation step applied each time. The beads were resuspended in 50 μl of 1 x electrophoresis buffer and the samples boiled for 5 min. These protein samples were subject to Western blotting analysis as described below.

Western blotting

Proteins were separated using 1.5 mm thick 12% resolving gels. The resolving gel solution (Table 2.5) was prepared and applied to pre-assembled gel casts. After a layer of water was applied onto the top of gel solution, the gel was allowed to set at RT for 30 min. The water layer was removed and a 4% stacking gel solution (Table 2.5) added. A 10-lane comb was inserted and the gel left to set at RT for 30 min.

The gel was placed in the electrophoresis tank and the tank filled with SDS-PAGE running buffer (Table 2.1). After clearance by centrifugation (16,000 x *g* for 1 min at RT), equal amounts of total protein sample (10 μl (5 μg) or 20 μl (10 μg)) and equal amounts of biotin labelled protein sample (20 μl) prepared as described above were added to each well alongside 6 μl of prestained protein markers. Samples were run through the stacking gel for 30 min at 80 V to form condensed bands. The voltage was then increased to 120 V.

Proteins were transferred to a Protran nitrocellulose membrane (pore size 0.45 μm) under semi-dry transfer conditions. The gel, blotting paper and membrane were soaked in Towbin transfer buffer (Table 2.1) and stacked on the anode plate from the bottom: 2 layers of blotting paper, nitrocellulose membrane, gel, then 2 more layers of blotting paper. The stack was rolled with a 5 ml pipette tip to remove trapped air bubbles, and the cathode plate placed on the top. A constant current of 1 mA/cm^2 was applied for 2 hrs.

The membrane was then rinsed in TBST (Table 2.1) and incubated in 5% non-fat milk (Table 2.1) for 1-2 hrs at RT to block non-specific protein binding. The membrane was then cut between the 30 kDa and 46 kDa protein markers. The top part was incubated in rabbit anti-EE containing solution and the bottom part in mouse anti-GFP antibody containing solution (Table 2.2), overnight at 4°C. The membranes were washed 4 times, each time for 5 min, with TBST. The top part was then incubated in HRP-conjugated bovine anti-rabbit IgG (Table 2.2), and the bottom part in HRP-conjugated bovine anti-mouse IgG (Table 2.2) for 1 hr at RT. Again, the membranes were washed 4 times, each time for 5 min, with TBST.

Table 2.5 Reagents used for SDS-PAGE gel preparation

Gel	30% acrylamide (ml)	1.5 M Tris-HCl, pH8.8 (ml)	0.5 M Tris-HCl, pH 6.8 (ml)	10% APS (µl)	10% SDS (µl)	TEMED (µl)	H_20 (ml)
12%	3.2	2		80	80	3.2	2637
4%	0.408		0.6	24	24	2.4	1342

Protein detection by enhanced chemilluminescence

The membrane was placed on a layer of cling film and incubated in SuperSignal West Pico or Femto chemilluminescent substrate solution (Pierce) for 5 min at RT to allow the chemilluminescent signals to develop. Excess substrate solution was removed and the membranes covered in cling film and exposed to X-ray films (Kodak) for a period of 5 s to 2 min, depending on the signal strength. A number of films were exposed to the membrane for range of exposure times to ensure that the bands were not saturated due to over-exposure and that any differences in signal strength between bands could be detected. Band intensities were quantified using a gel doc XR quantity system (Biorad).

2.2.7 Immunostaining

HEK293 cells prepared in 35 mm dishes were transfected (as described above) with 1 µg of plasmid and, 24 hrs later, re-plated onto cover slips, and incubated for further a 24 hrs. Cells were washed with PBS before being fixed in Zamboni's fixative (Table 2.1) at RT for 30 min. Cells were permeabilised and blocked for 1 hr in the blocking solution (Table 2.1) at RT, and then incubated in blocking solution containing rabbit anti-EE primary antibody (Table 2.2) at 4°C overnight. After 5 PBS washes, the cells were incubated in blocking solution containing Alexa Fluor 488 anti-rabbit IgG secondary antibody (Table 2.2) for 2 hrs at RT. Following 5 washes in PBS, cover slips were mounted onto microscope slides using Antifade Reagent (Molecular Probes) and stored at 4°C. A Zeiss AxioVert 200M confocal microscope and LSM510 software were used to capture the fluorescent images.

2.3 Recording of $P2X_7$ receptor mediated currents

2.3.1 Principle of whole-cell patch-clamp recording

The patch-clamp recording technique is a powerful tool for the study of ion channel activity (Hamill *et al.*, 1981). A recording pipette, which is a blunt-ended glass capillary with a tip of approximately 1 µm, was filled with saline solution and placed onto the cell membrane. Light suction was applied to the pipette to form an electrically tight, gigaohm seal with the cell membrane. This is the cell-attached configuration (Figure 2.1A), and, from this point, a number of patch-clamp configurations are achievable. In this study, the whole-cell configuration was used, which enabled the membrane potential to be held at the desired values and the ionic currents through all the ion channels at the cell membrane to be measured. To obtain the whole-cell configuration, further suction was applied to rupture the patch of membrane beneath the pipette tip so that the contents of the pipette were in physical contact with the interior of the cell while the tight seal was intact (Figure 2.1A). A reference electrode was placed in the extracellular solution to form an electrical circuit. Activation of ion channels allows ions to move through the open channels along their electrochemical gradients and forms ionic currents. Figure 2.1B shows a schematic of the patch-clamp set-up.

2.3.2 Solutions used for $P2X_7$ receptor recordings

Standard extracellular solution contained: 147 mM NaCl, 2 mM KCl, 1 mM $MgCl_2$, 2 mM $CaCl_2$, 10 mM HEPES and 13 mM glucose. Divalent cations strongly inhibit $P2X_7$ receptors (see section 1.6.5). $P2X_7$ receptors and particularly the human $P2X_7$ receptor, the main subject of the study, exhibit a low sensitivity to ATP. It is difficult to obtain maximal current responses in standard extracellular solution, unless high concentrations of ATP are used (Roger *et al.*, 2010a). Therefore, unless otherwise stated in the Figure legend, current recordings were made in low divalent extracellular solution, which contained: 147 mM NaCl, 2 mM KCl, 0.3 mM $CaCl_2$, 10 mM HEPES and 22 mM glucose. The composition of pipette or intracellular solution was: 145 mM NaCl, 10 mM EDTA and 10 mM HEPES. Both extracellular and intracellular solutions were adjusted to pH 7.3 using 5 M NaOH and the osmolality was in the range of 300-315 mOsm. ATP stock solution (100 mM) was prepared in extracellular

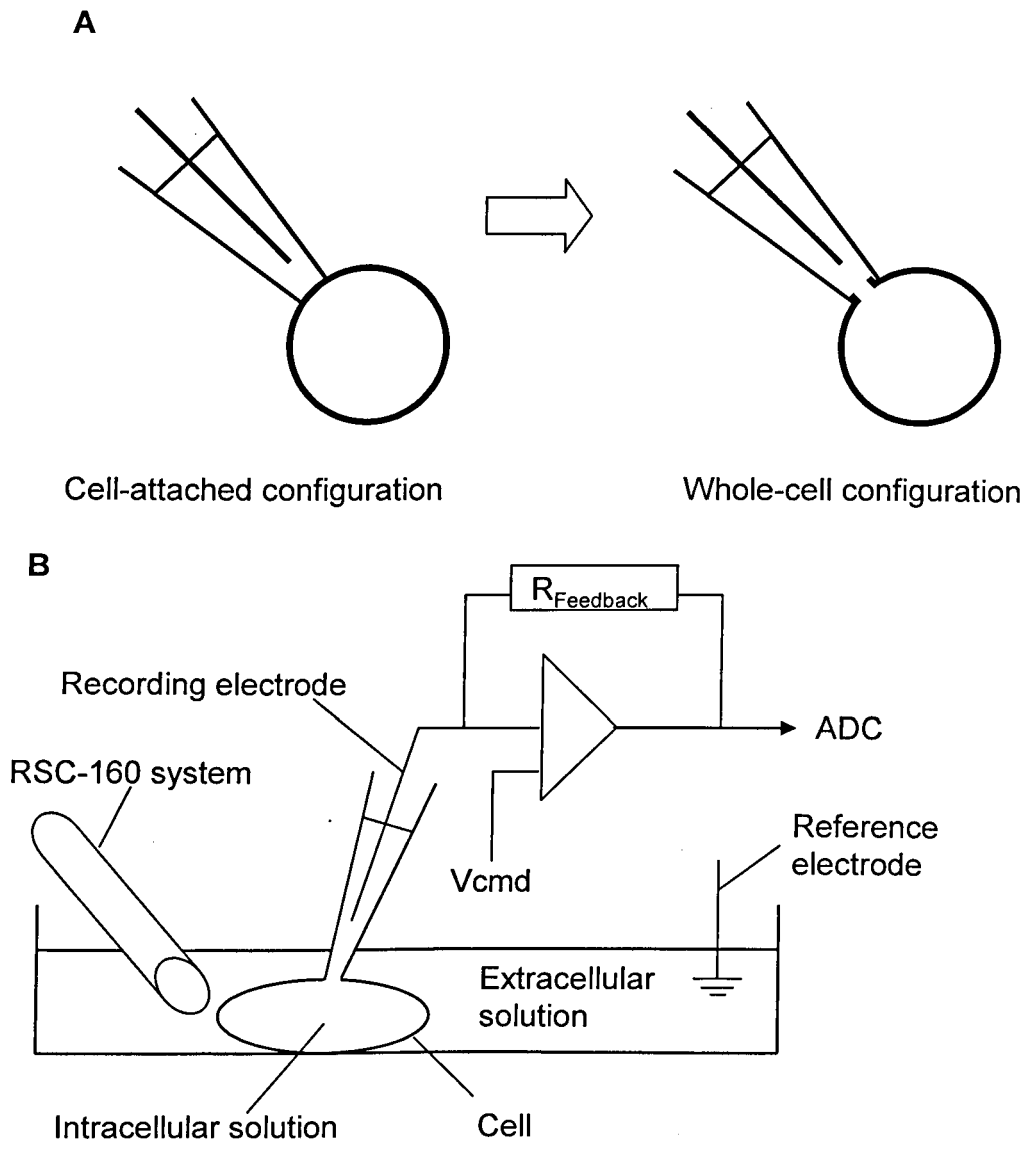

Figure 2.1 Whole-cell patch-clamp configuration and recording set-up
(A) The cell is placed in extracellular solution. The recording pipette, filled with intracellular solution, is manoeuvred to be form a gigaohm seal between the pipette and the cell membrane (cell-attached configuration). Suction is applied to rupture the membrane patch underneath the tip of the recording electrode, (whole-cell attached configuration). (B) The recording electrode is in physical contact with the inside of the cell, and the reference electrode is in contact with the extracellular solution. The voltage command (Vcmd) determines the voltage between the recording and reference electrode, and can be held at desirable values via a feedback resistor. The analogue/digital converter (ADC) converts analogue signals to digital signals or vice verse. The RSC-160 system was used to change the extracellular solutions.

solution and adjusted to pH 7.3 with 5 M NaOH, whilst BzATP stock solution (100 mM) was prepared in water. Stock solutions of antagonists (KN-62, AZ11645373 and A-438079, all 10 mM) were prepared in DMSO. In some experiments, where $P2X_7$ (particularly rat $P2X_7$) receptor mediated currents showed substantial run-down with repeated agonist applications, 100 μM bpV (bisperoxovanadium, an tyrosine phosphatase inhibitor) was used (Kim *et al.*, 2001a). bpV stock solutions (50 mM) were prepared in water.

2.3.3 Preparation of cells for patch-clamp recording

HEK293 cells prepared in 35 mm petri dishes were co-transfected with plasmid encoding the $P2X_7$ receptor and eGFP, as described in section 2.2.5. Cells were plated onto glass coverslips 24 hrs following transfection, and used 18-48 hrs later.

2.3.4 Preparation of recording and reference electrodes

The recording pipettes were made from borosilicate glass capillaries with an outer diameter of 1.5 mm and an inner diameter of 1.12 mm (World Precision Instruments). Pipettes were pulled in two stages using a vertical puller (PP-830, Narishige Scientific Instruments) to a tip of approximately 1 μm, and had a resistance of 3-5 MΩ in recording solutions. The pipettes were back-filled with intracellular solution and mounted onto a headstage (EPC-10, HEKA) via an AgCl coated Ag wire, which was connected to a HEKA EPC10 amplifier. The reference electrode was a silver chloride pellet, which was immersed in the extracellular solution and connected to the ground via the headstage.

2.3.5 Patch-clamp recording

Single, eGFP positive (identified under UV light) HEK293 cells were chosen for recordings. The recording pipette was lowered into the bath solution and the resistance was determined using a 5 mV test pulse. The pipette was manoeuvred until it is just in contact with the cell and a slight increase in the recording pipette resistance was detected. Negative pressure was then applied to form a gigaohm seal. The transient capacitative currents were compensated. Further suction was applied to break-through to the whole-cell configuration, as indicated by appearance of relatively slow capacitative currents. Series resistance and cell capacitance were measured and only the cells with series

resistance of <10 MΩ were used for recordings. The cells were held at -60 mV, and agonists and antagonists were applied for individually indicated durations using a rapid solution changer (RSC-160, Biological Sciences Instruments).

As described in previous studies (Roger *et al.*, 2008; Roger *et al.*, 2010b), a sub-maximal concentration of agonist was repeatedly applied (4 s every min or for 1 min with an 1 min interval) until the current amplitude was no longer increased. This was indicated by no change in the amplitude of currents subsequently evoked by 3 consecutive 4 s applications.

To obtain an agonist-dose response curve, 4 s applications of increasing concentrations of agonist were made at 1 min intervals, after the receptor was facilitated as described above. To measure antagonist concentration-dependent inhibition of agonist-evoked currents, antagonists were applied to the patched cells for 4 min (1 min for A-438079) before the currents were evoked by 4 s application of ATP. In the case of A-438079, A-438079 was also present during 4 s application of ATP. To measure the effect of antagonists on the ATP-dose response curve, ATP dose-response curves were obtained as described above, before and after a 4 min application of antagonist.

The peak current amplitudes were measured and converted to current density (pA/pF). For agonist dose-responses, the agonist concentration evoking half of the maximal response (EC_{50}) was determined by the least-square fit of the data from individual cells to the following Hill equation:

$$I/I_{MAX} = [A]^{nH}/([A]^{nH}+EC_{50}]^{nH}) \quad (1)$$

or:

$$I = 100\ [A]^{nH}/([A]^{nH}+[EC_{50}]^{nH}) \quad (2)$$

where I is the current evoked by the agonist concentration [A] and n_H is the Hill coefficient. I_{MAX} respresents the maximal response. For antagonist dose-inhibition curve, the antagonist concentration producing half of the maximal inhibition (IC_{50}) was determined by the least-square fit of the data from individual cells to the following Hill equation:

$$I = 100\ [IC_{50}]^{nH}/([B]^{nH}+[IC_{50}]^{nH}) \quad (3)$$

where I is the residual current in the presence of the antagonist concentration [B] as a percentage of the current in the absence of antagonist and n_H is the Hill coefficient. Where the inhibition was incomplete, the IC_{50} value was determined by using the following equation:

$$I = (100\text{-}C)\ [IC_{50}]^{nH}/([B]^{nH}+[IC_{50}]^{nH}) + C \quad (4)$$

where C is the antagonist-sensitive current component and the other parameters remain the same as in the equation 3. Sensitivity to agonist or antagonist was determined by calculating pEC_{50} ($-\log_{10}$ of the EC_{50} value), or pIC_{50} ($-\log_{10}$ of the IC_{50}) values, respectively. Dose response curves shown in the figures were fit to the mean current for all the cells recorded.

2.4 Statistical analysis

Origin software (version 7.5) was used for analysis of the data and preparation of figures. All data are presented as mean ± standard error of the mean (SEM). The number of independent experiments is indicated by 'n'. Comparisons were made using unpaired or paired Student's t-test. A probability (p) value of <0.05 was considered significant.

Chapter 3

Effect of mutations H155Y and A348T on human $P2X_7$ receptor function

3.1 Introduction

H155Y and A348T are ns-SNP mutations of the human $P2X_7$ receptor and were originally identified in patients with major depressive disorder and/or bipolar disorder (Barden *et al.*, 2006; Lucae *et al.*, 2006). Genetic linkage studies have so far shown that these SNPs are not associated with these conditions, however they are frequently co-inherited with Q460R, a polymorphism associated with affective mood disorders (see section 1.6.8) (Barden *et al.*, 2006; Lucae *et al.*, 2006; McQuillin *et al.*, 2008; Stokes *et al.*, 2010).

Previous studies have indicated both the H155Y and A348T mutations confer gain-of-function of the human $P2X_7$ receptor. The mutations increased either agonist-induced Et^+ dye uptake or Ca^{2+} influx (Cabrini *et al.*, 2005; Roger *et al.*, 2010; Stokes *et al.*, 2010), and ionic currents (Roger *et al.*, 2010; Stokes *et al.*, 2006).

These observations suggest that the residues at positions 155 and 348 may be important in the functional expression of the $P2X_7$ receptor. A model of the human $P2X_7$ receptor (Figure 3.1), based on the recently solved zebrafish $P2X_4$ structure, predicts His^{155} is located in the head region of the extracellular domain (Kawate *et al.*, 2009; Roger *et al.*, 2010a). In contrast, the model predicts Ala^{348} is located within TM2, on the intracellular side of the gate. In this chapter, the functional importance of residues His^{155} and Ala^{348} on human $P2X_7$ receptor function were investigated in detail using site-directed mutagenesis and whole-cell patch-clamp recording.

The results of this study have been presented in agonist dose-response curves, and the results have been analysed in terms of the maximal current amplitudes, the EC_{50} values and the Hill coefficients in order to gain insight into the functional effects of the $P2X_7$ receptor mutations, as well as the underlying mechanisms. A mutational effect on the maximal current amplitude may be caused by a change in the number of functional receptors expressed at the cell surface, or the single channel properties of the receptor. The EC_{50} value is a measure of the receptor sensitivity to agonist. Changes to the sensitivity of the receptor to agonist could reflect an alteration to agonist binding affinity, or to the conformational changes that lead to channel gating. A change in the Hill coefficient reflects a change in the cooperativity of ligand binding, with an increased Hill coefficient indicating increased cooperativity of binding.

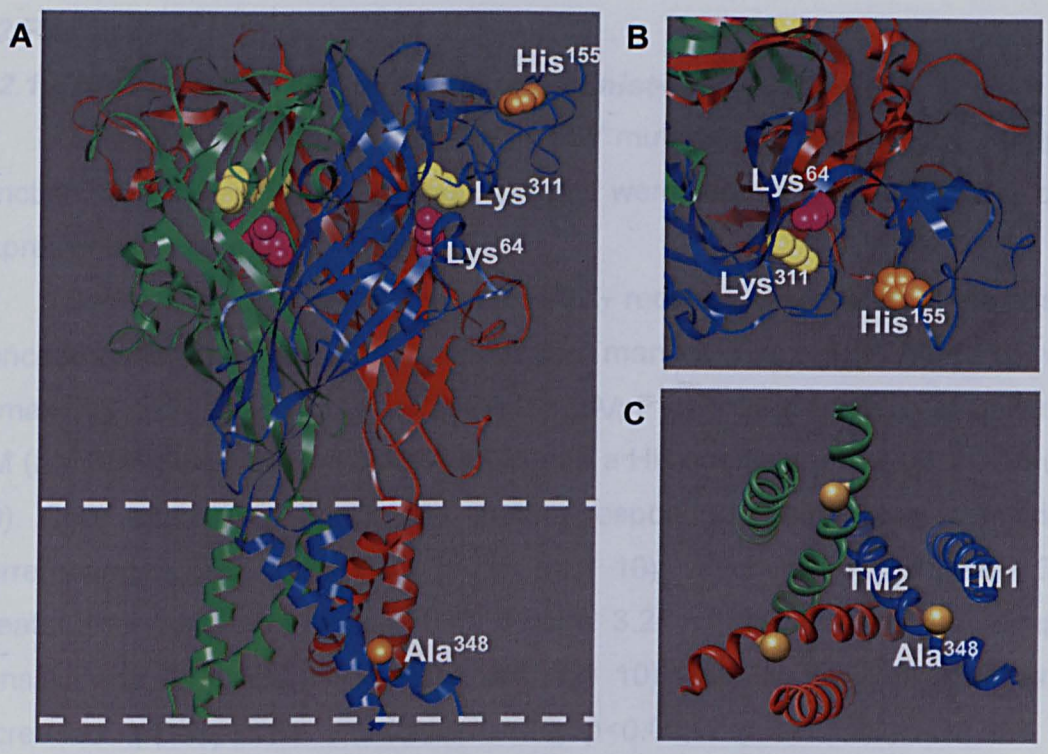

Figure 3.1 Structural model of the human $P2X_7$ receptor showing the location of His^{155} and Ala^{348}

The model is based in the crystal structure of the zebrafish $P2X_4$ receptor (Kawate *et al.*, 2009). (A) The trimeric complex showing the three subunits in green, red and blue. Lys^{64} and Lys^{311}, residues thought to form part of the agonist binding site, are pink and yellow, respectively. His^{155} and Ala^{348} are orange. Viewed parallel to the membrane. (B) Structure surrounding His^{155}, viewed from the extracellular side along the symmetrical axis. (C) Structure surrounding Ala^{348}, viewed from the intracellular side along the symmetrical axis. These figures were kindly provided by Prof. Steve Baldwin and Dr. Lin-Hua Jiang.

3.2 Results

3.2.1 Effect of the H155Y mutation on agonist-evoked currents

To investigate the effect of the H155Y mutation on human $P2X_7$ receptor function, agonist-evoked whole-cell currents were recorded from HEK293 cells expressing WT or mutant receptors.

Cells expressing the WT human $P2X_7$ receptor responded to increasing concentrations of ATP in a dose-dependent manner (Figures 3.2A and B), with a maximal current amplitude of 268 ± 12 pA/pF (n = 29), an EC_{50} of 397 ± 19 μM (n = 30) (pEC_{50} 3.42 ± 0.02, n = 30) and a Hill coefficient of 2.08 ± 0.06 (n = 30). Cells expressing the H155Y mutant responded to ATP with a maximal current amplitude of 391 ± 19 pA/pF (n = 10), which is approximately 50% greater than that of WT ($p<0.001$; Figure 3.2C). Furthermore, the receptor sensitivity to ATP (EC_{50} 313 ± 14 μM, n = 10) was slightly, yet significantly, increased (pEC_{50} 3.51 ± 0.02, n = 10; $p<0.05$; Figure 3.2D), but the Hill coefficient was unaltered (2.03 ± 0.07, n = 10; $p>0.05$; Figure 3.2E).

The effect of the H155Y mutation on BzATP-evoked current responses was investigated (Figure 3.3). The mutation significantly increased the maximal current amplitude from 244 ± 4.5 pA/pF (n = 4) for WT to 392 ± 51 pA/pF (n = 4) for the H155Y mutant ($p<0.05$; Figure 3.3C). The EC_{50} values were 36 ± 4.7 μM (n = 4) for WT and 27 ± 6.6 μM (n = 4) for H155Y. The mutation did not alter receptor sensitivity to BzATP (pEC_{50} 4.46 ± 0.05, n = 4 for WT, and 4.60 ± 0.11, n = 4 for H155Y; $p>0.05$; Figure 3.3D) or the Hill coefficient (2.06 ± 0.27, n = 4 for WT and 2.09 ± 0.14, n = 4 for H155Y; $p>0.05$; Figure 3.3E).

3.2.2 Effect of the H155Y mutation on antagonist inhibition

KN-62 is a potent antagonist at human $P2X_7$ receptors (see section 1.6.5; Humphreys *et al.*, 1998). The effect of the H155Y mutation on inhibition of ATP-evoked currents by KN-62 was investigated (Figure 3.4). KN-62 potently inhibited ATP-induced currents mediated by the WT receptor in a concentration dependent manner, with an IC_{50} of 127 ± 38 nM (n = 3). KN-62 showed similar inhibition of ATP-evoked currents mediated by the H155Y mutant (IC_{50} 129 ± 20 nM, n = 3). There was no difference in the potency of KN-62 at WT or mutant receptors (pIC_{50} 6.93 ± 0.12, n = 3 for WT, and 6.90 ± 0.06, n = 3 for H155Y; $p>0.05$; Figure 3.4C). The inhibition in both cases was largely irreversible (Figure 3.4A).

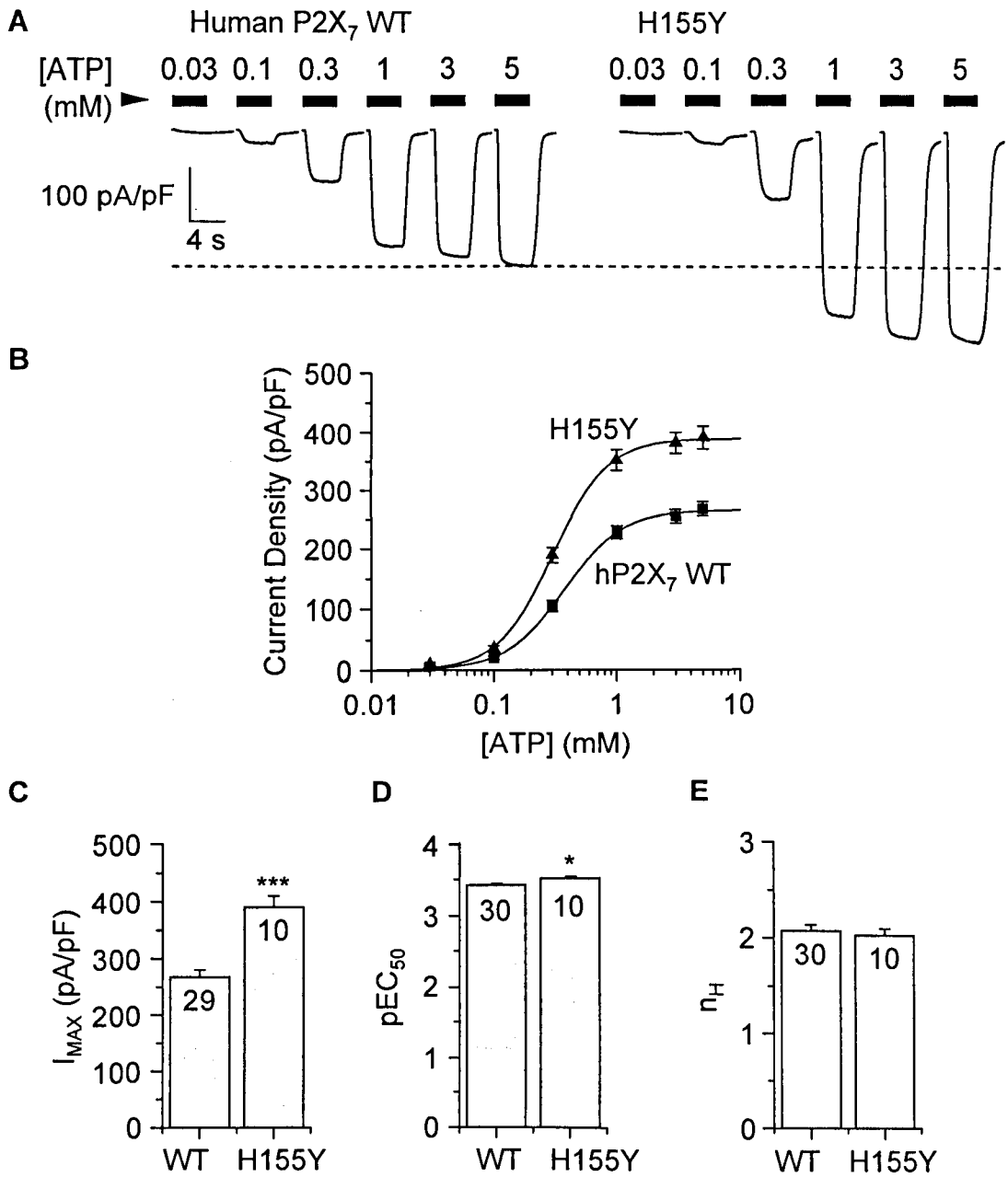

Figure 3.2 Effect of the H155Y mutation on ATP-evoked currents

(A) Representative ATP-evoked currents recorded from a HEK293 cell expressing WT (hP2X$_7$ WT; left) or mutant H155Y human P2X$_7$ receptors (right) at -60 mV. The black bars indicate the 4 s ATP application of the concentration shown, and ATP was applied at 1 min intervals. The dashed line indicates the maximal current for the WT receptor. (B) Mean ATP dose-response curves summarising the data from experiments shown in A: WT (squares) or H155Y (triangles). Smooth lines show the best fits to the Hill equation. (C) Mean maximal current amplitudes (I_{MAX}). (D and E) pEC_{50} and Hill coefficients calculated using the least-square fit to the Hill equation. The number of cells recorded is indicated in the bars. * $p<0.05$, *** $p<0.001$, compared to WT.

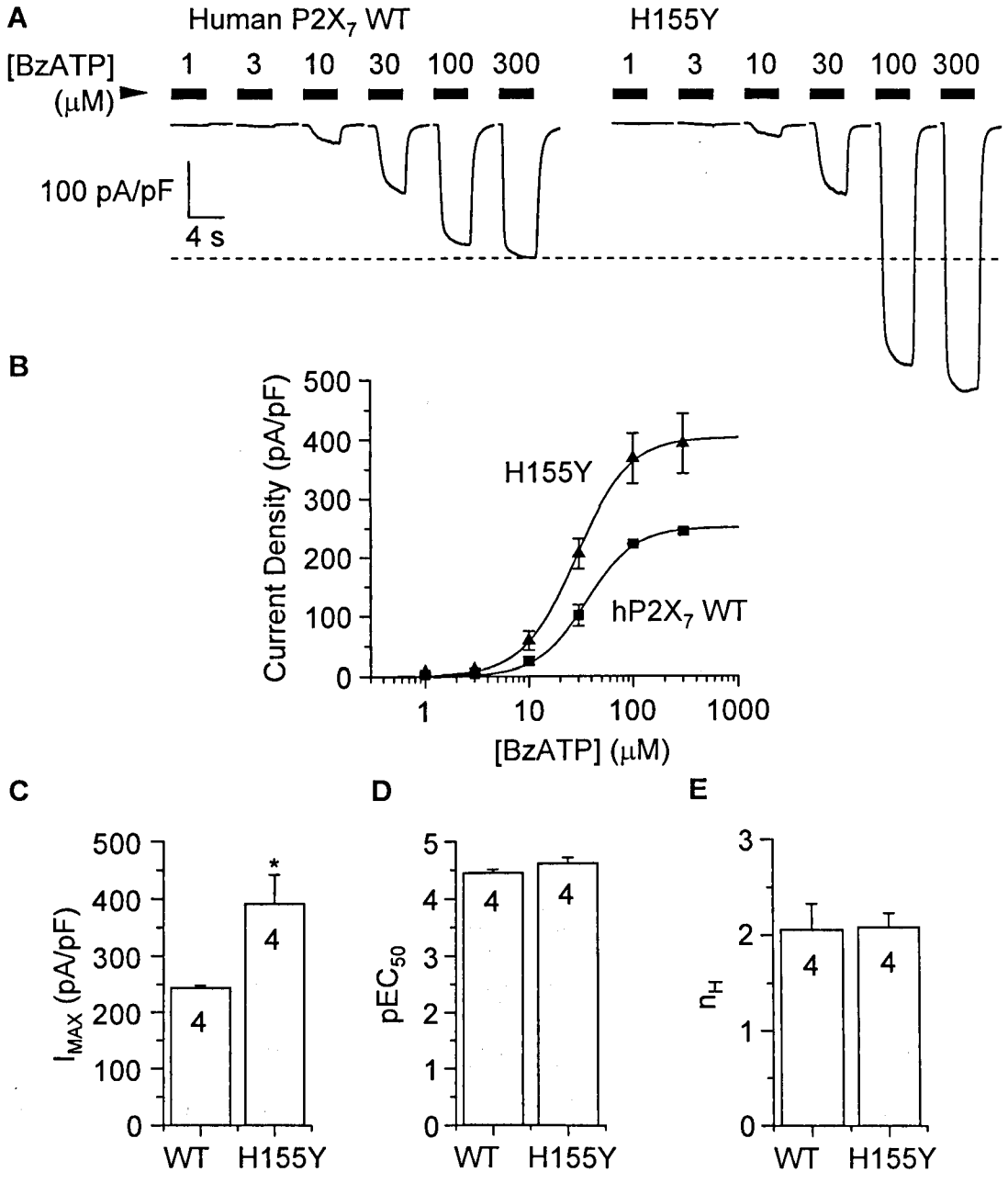

Figure 3.3 Effect of the H155Y mutation on BzATP-evoked currents

(A) Representative BzATP-evoked currents recorded from a HEK293 cell expressing WT (left) or mutant H155Y human $P2X_7$ receptors (right) at -60 mV. The dashed line indicates the maximal current for the WT receptor. (B) Mean BzATP dose-response curves summarising the data from experiments shown in A: WT (squares) or H155Y (triangles). Smooth lines show the best fits to the Hill equation. (C-E) Mean maximal current amplitudes (I_{MAX}), pEC_{50} and Hill coefficients. The number of cells recorded is indicated. * $p<0.05$, compared to WT.

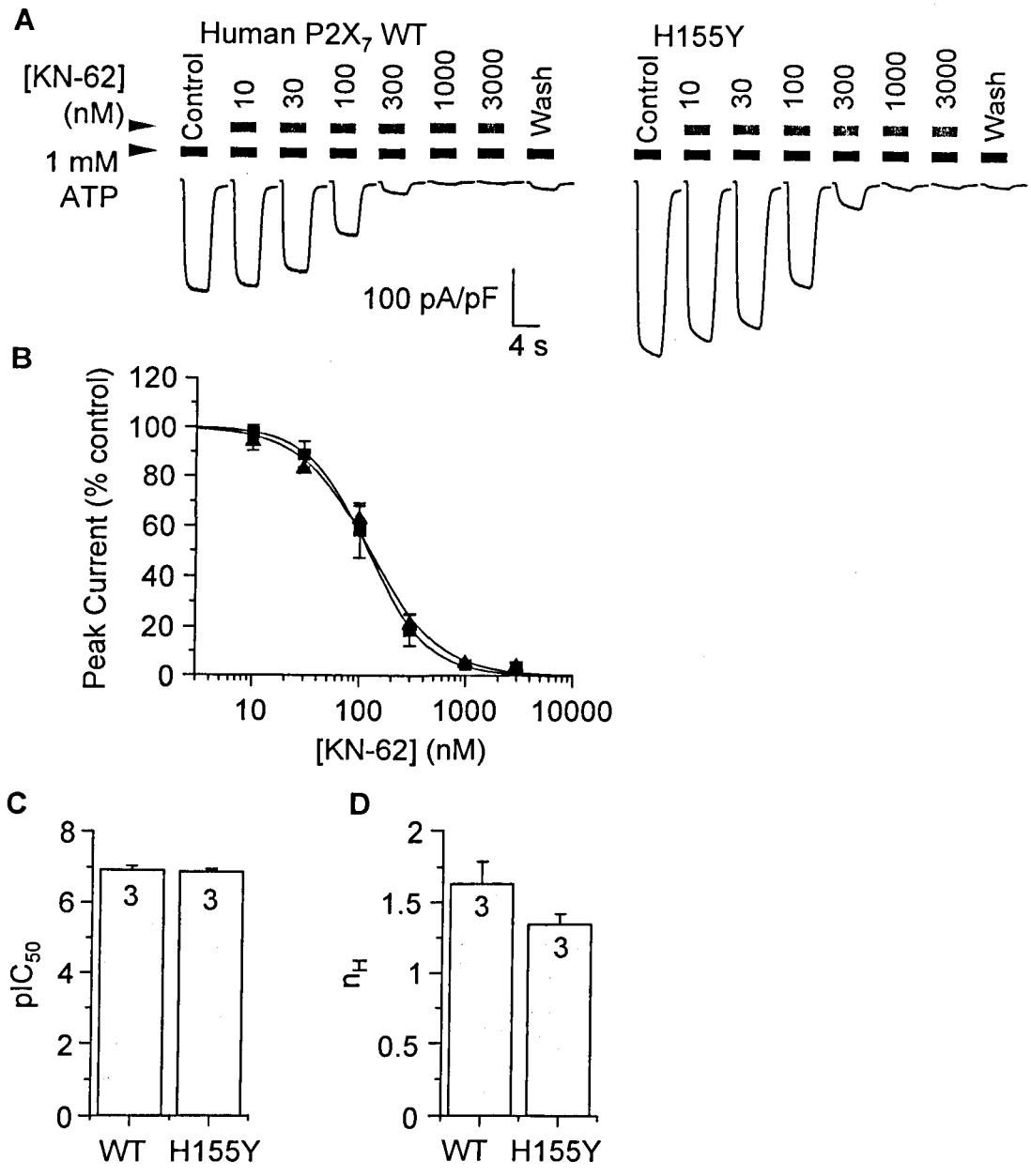

Figure 3.4 Effect of the H155Y mutation on antagonism of human $P2X_7$ receptor responses by KN-62

(A) Representative currents evoked by 1 mM ATP recorded in the absence (control) and presence of indicated concentrations of KN-62 from a HEK293 cell expressing WT (left) or mutant H155Y human $P2X_7$ receptors (right) at -60 mV. Washout was 20 min. (B) Mean KN-62 dose-inhibition curves summarising the data from experiments shown in A: WT (squares) or H155Y (triangles). Smooth lines show the best fits to the Hill equation using 2 parameters. (C-D) Mean pIC_{50} and Hill coefficients. The number of cells recorded is indicated. No significant differences were detected.

3.2.3 Effect of the A348T mutation on agonist-evoked currents

The effect of the A348T mutation on human $P2X_7$ receptor function was also investigated, firstly using ATP as the agonist (Figure 3.5). The mutation conferred a significant increase in the maximal current amplitude (268 ± 12 pA/pF, n = 29 for WT, and 324 ± 17 pA/pF, n = 12 for A348T; $p<0.05$; Figure 3.5C). The EC_{50} values were 397 ± 19 μM (n = 30) for WT, and 354 ± 26 μM (n = 12) for A348T. The mutation did not affect the sensitivity of the receptor to ATP (pEC_{50} 3.42 ± 0.02, n = 30 for WT, and 3.46 ± 0.03, n = 12 for A348T; $p>0.05$; Figure 3.5D). Furthermore, the mutation conferred a small, yet significant decrease in the Hill coefficient (2.08 ± 0.06, n = 30 for WT, and 1.80 ± 0.08, n = 12 for A348T; $p<0.05$; Figure 3.5E).

These experiments were also performed using BzATP as the agonist (Figure 3.6). The maximal current amplitude was significantly increased (244 ± 4.5 pA/pF, n = 4 for WT, and 447 ± 72 pA/pF, n = 3 for A348T; $p<0.05$; Figure 3.6C). EC_{50} values were 36 ± 4.7 μM (n = 4) for WT, and 31 ± 3.9 μM (n = 3) for A348T. The sensitivity to BzATP was not changed; pEC_{50} and Hill coefficients were 4.46 ± 0.05 and 2.06 ± 0.27 for WT (n = 4), and 4.51 ± 0.05 and 1.94 ± 0.14 for the mutant (n = 3; $p>0.05$; Figures 3.6D and E).

3.2.4 Effect of the double mutation H155Y/A348T on ATP-evoked currents

The effect of the double mutation H155Y/A348T on human $P2X_7$ receptor function was investigated using ATP as the agonist (Figure 3.7). The maximal current amplitude was significantly increased in comparison to WT, and H155Y and A348T mutations alone (268 ± 12 pA/pF, n = 29 for WT, and 473 ± 31 pA/pF, n = 7 for H155Y/A348T; $p<0.001$; Figure 3.7C). The EC_{50} values were 397 ± 19 μM (n = 30) for WT, and 360 ± 47 μM (n = 7) for H155Y/A348T. There was no effect on the sensitivity to ATP (pEC_{50} 3.42 ± 0.02, n = 30 for WT, and 3.47 ± 0.06, n = 7 for H155Y/A348T; $p>0.05$; Figure 3.7D). The Hill coefficient was decreased by the double mutation (2.08 ± 0.06, n = 30 for WT, and 1.73 ± 0.09, n = 7 for H155Y/A348T; $p<0.05$; Figure 3.7E).

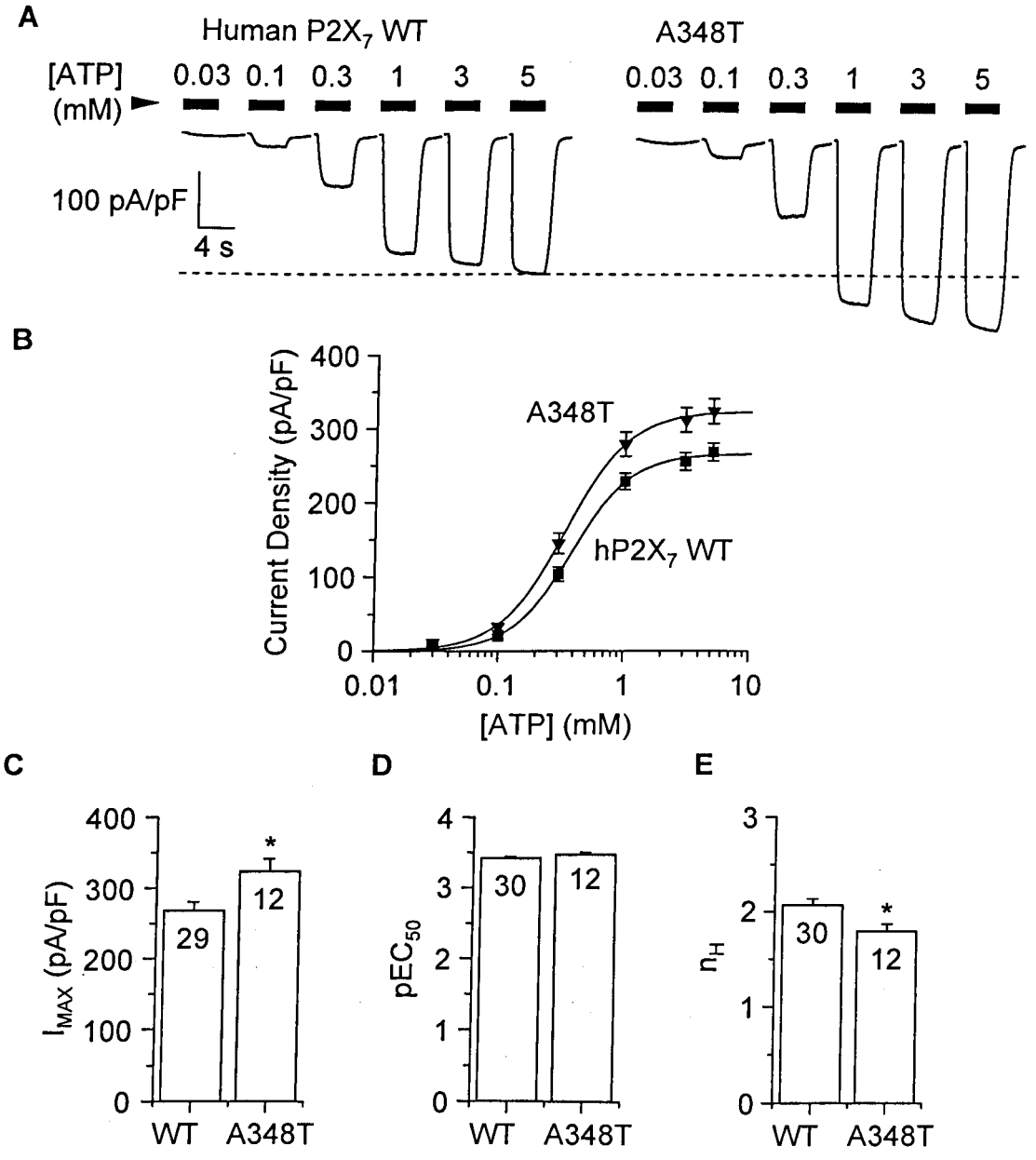

Figure 3.5 Effect of the A348T mutation on ATP-evoked currents

(A) Representative ATP-evoked currents recorded from a HEK293 cell expressing WT (left) or mutant A348T human $P2X_7$ receptors (right) at -60 mV. The dashed line indicates the maximal current for the WT receptor. (B) Mean ATP dose-response curves summarising the data from experiments shown in A: WT (squares) or A348T (triangles). Smooth lines show the best fits to the Hill equation. (C-E) Mean maximal current amplitudes (I_{MAX}), pEC_{50} and Hill coefficients. The number of cells recorded is indicated. * $p<0.05$, compared to WT.

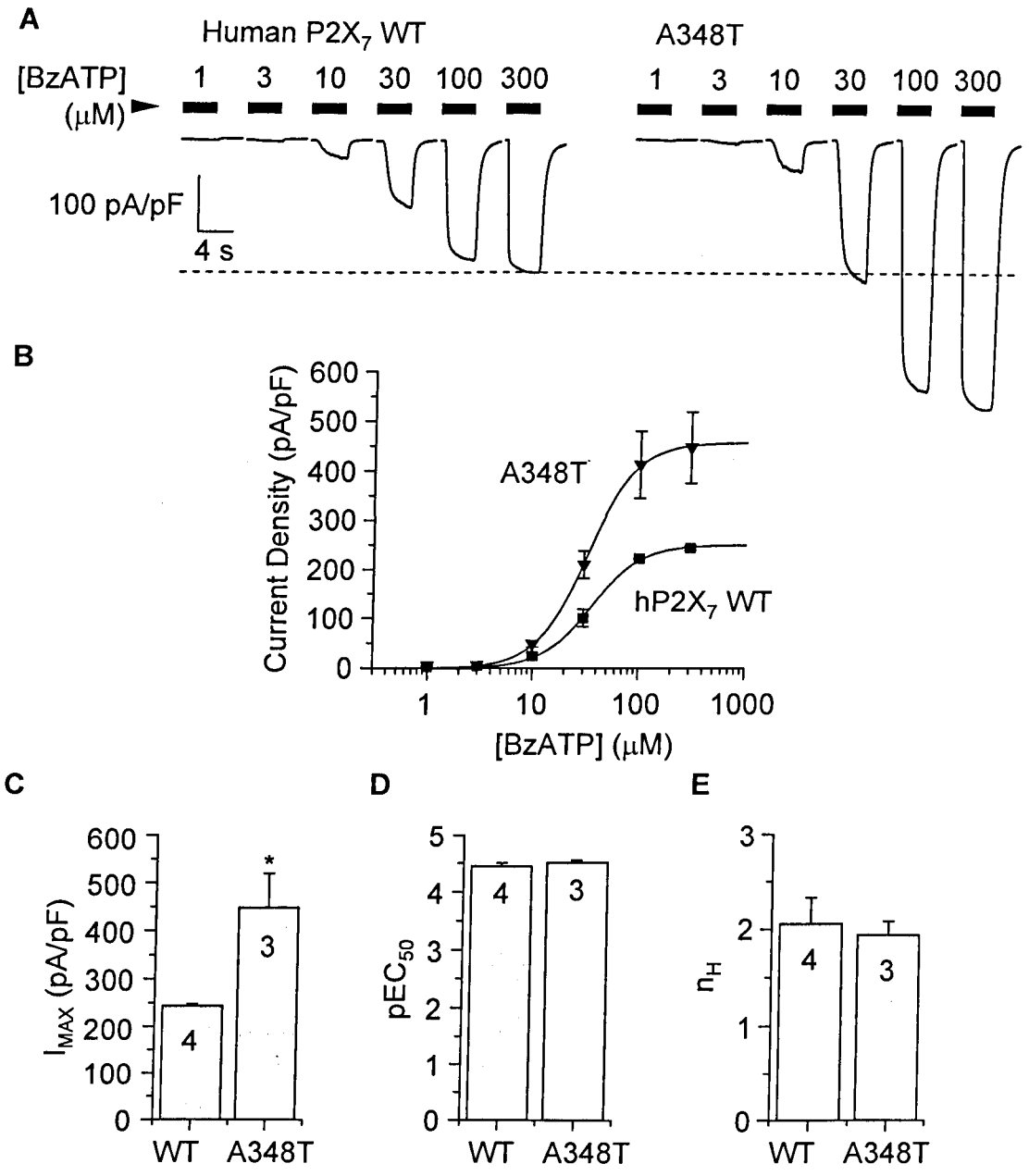

Figure 3.6 Effect of the A348T mutation on BzATP-evoked currents

(A) Representative BzATP-evoked currents recorded from a HEK293 cell expressing WT (left) or mutant A348T human $P2X_7$ receptors (right) -60 mV. The dashed line indicates the maximal current for the WT receptor. (B) Mean BzATP dose-response curves summarising the data from experiments shown in A: WT (squares) or A348T (triangles). Smooth lines show the best fits to the Hill equation. (C-E) Mean maximal current amplitudes (I_{MAX}), pEC_{50} and Hill coefficients. The number of cells recorded is indicated. * $p<0.05$, compared to WT.

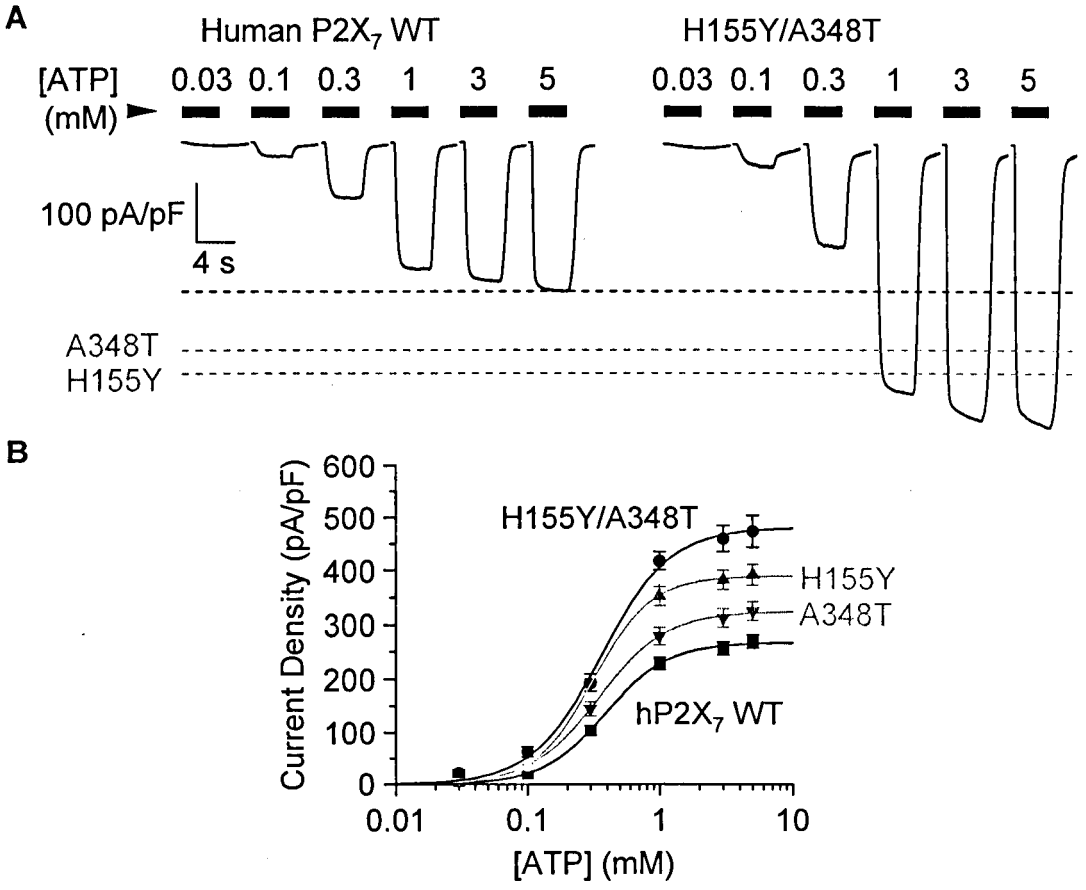

Figure continued on next page.

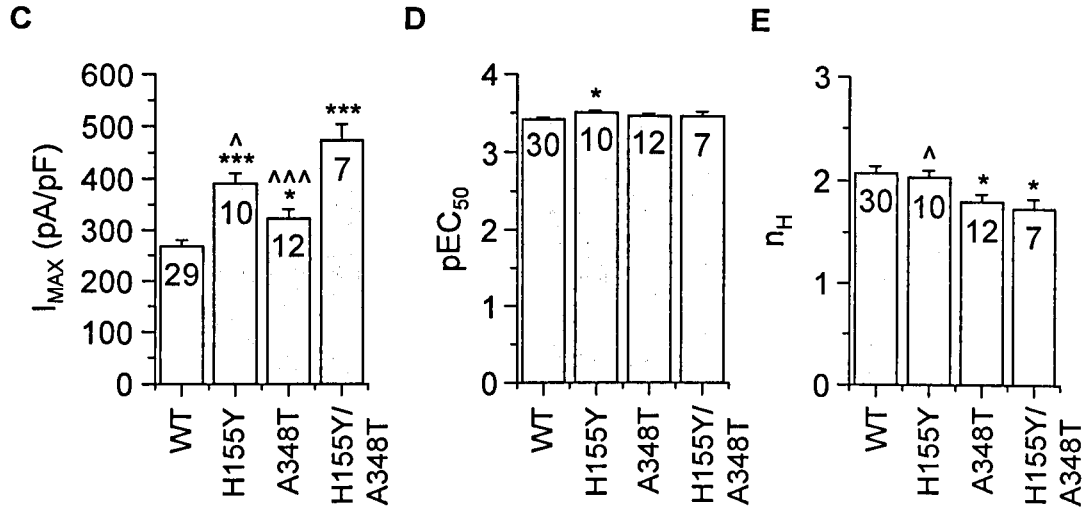

Figure 3.7 Effect of the double H155Y/A348T mutation on ATP-evoked currents

(A) Representative ATP-evoked currents recorded from a HEK293 cell expressing WT (left) or mutant H155Y/A348T human $P2X_7$ receptors (right) at -60 mV. The dashed line in black indicates the maximal current for the WT receptor, and in grey indicates the representative maximal currents for the H155Y (Figure 3.2A) and A348T (Figure 3.5A) single mutants. (B) Mean ATP dose-response curves summarising the data from experiments shown in A: WT (squares) or H155Y/A348T (circles). Smooth lines show the best fits to the Hill equation. (C-E) Mean maximal current amplitudes (I_{MAX}), pEC_{50} and Hill coefficients. The number of cells recorded is indicated. * $p<0.05$, *** $p<0.001$, compared to WT. ^ $p<0.05$, ^^^ $p<0.001$ compared to H155Y/A348T.

3.2.5 Effect of substituting His^{155} with other residues on ATP-evoked currents

To further study the functional role of His^{155} in the human $P2X_7$ receptor and particularly the role of the side chain, His^{155} was mutated to phenylalanine, arginine, aspartic acid, alanine and leucine. The mutational effects on ATP-evoked currents were investigated, and the results are shown in Figure 3.8. Mutations H155D and H155L led to a reduction in ATP-induced maximal currents (293 ± 13 pA/pF, n = 28 for WT, and 214 ± 25 pA/pF, n = 5; $p<0.05$ and 171 ± 29 pA/pF, n = 5; $p<0.001$ for H155D and H155L, respectively; Figure 3.8C). The EC_{50} values were 348 ± 14 μM (n = 28) for WT, and 228 ± 29 μM (n = 6) for H155R. The sensitivity to ATP was not altered by any of the mutations, with the exception of H155R (pEC_{50} 3.47 ± 0.02, n = 28 for WT, and 3.66 ± 0.06, n = 6 for H155R; $p<0.001$; Figure 3.8D). The H155A mutation significantly altered the Hill coefficient (1.89 ± 0.04, n = 28 for WT, and 2.20 ± 0.09, n = 5 for H155A mutant; $p<0.01$; Figure 3.8E).

3.2.6 Effect of substituting Val^{154} and Glu^{156} with tyrosine on ATP-evoked currents

To further determine the specificity of tyrosine at position 155, positions 154 and 156 in the human $P2X_7$ receptor were mutated to tyrosine (V154Y and E156Y; Figure 3.9). In comparison to WT (293 ± 13 pA/pF, n = 28), mutation V154Y had no effect on the ATP-induced maximal current (260 ± 15 pA/pF, n = 5; $p>0.05$), whilst mutation E156Y resulted in a significant reduction (137 ± 30, n = 6; $p<0.001$; Figure 3.9C). The EC_{50} value was 348 ± 14 μM (n = 28) for the WT receptor. The pEC_{50} and Hill coefficient values for the WT receptor were 3.47 ± 0.02 and 1.89 ± 0.04 (n = 28), respectively, and were not significantly altered by the V154Y or E156D mutations ($p>0.05$; Figures 3.9 D and E).

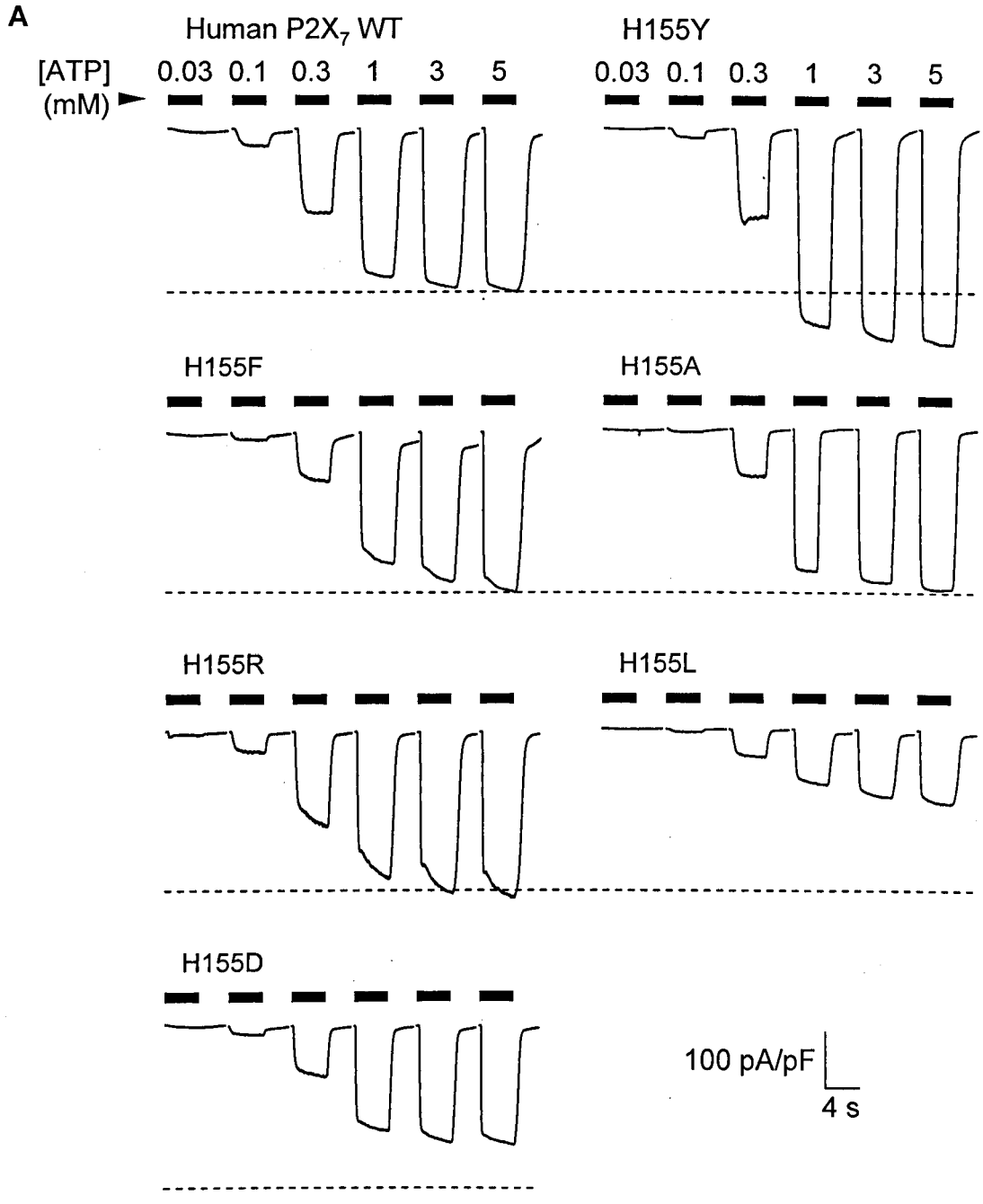

Figure continued on next page.

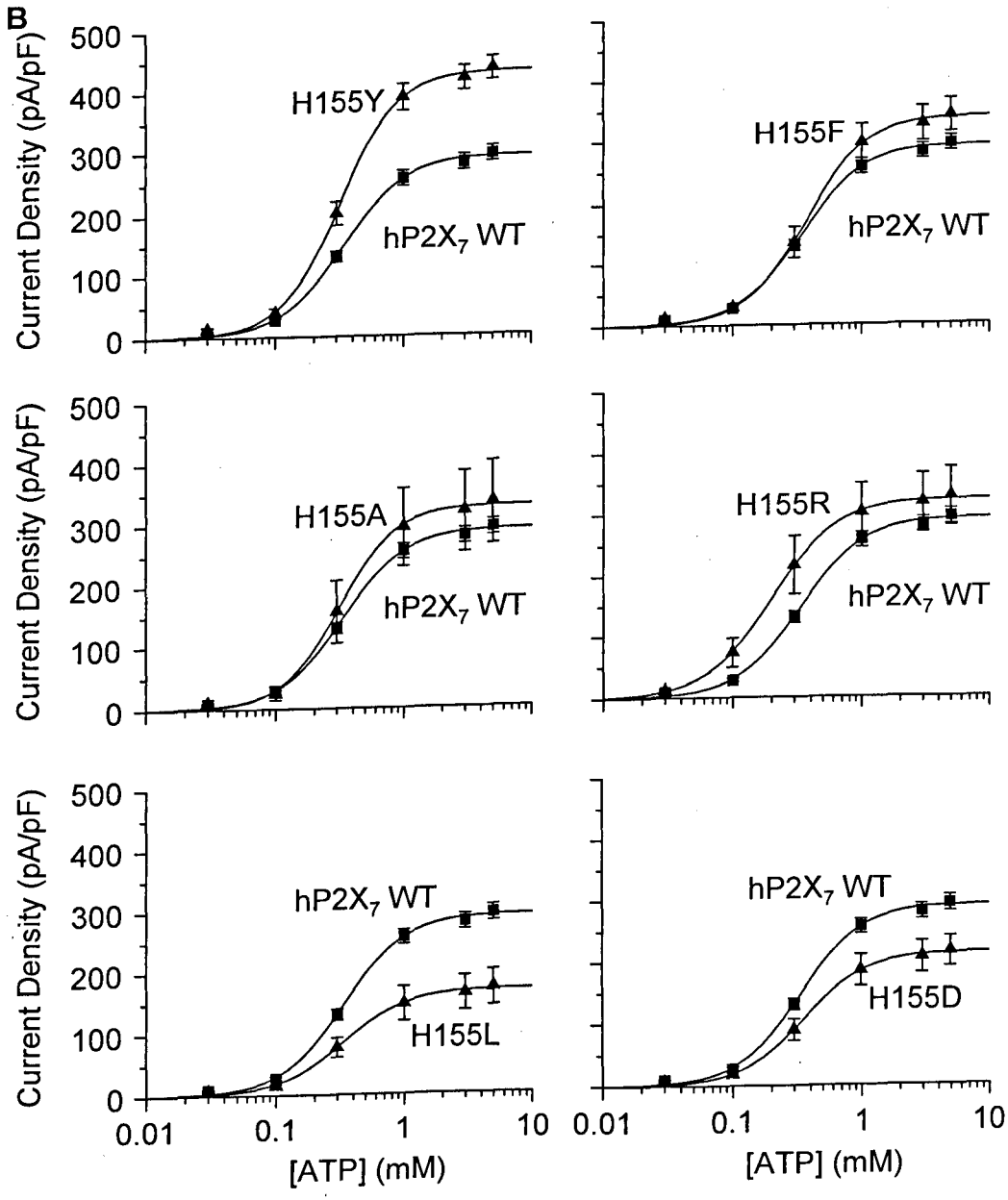

Figure continued on next page.

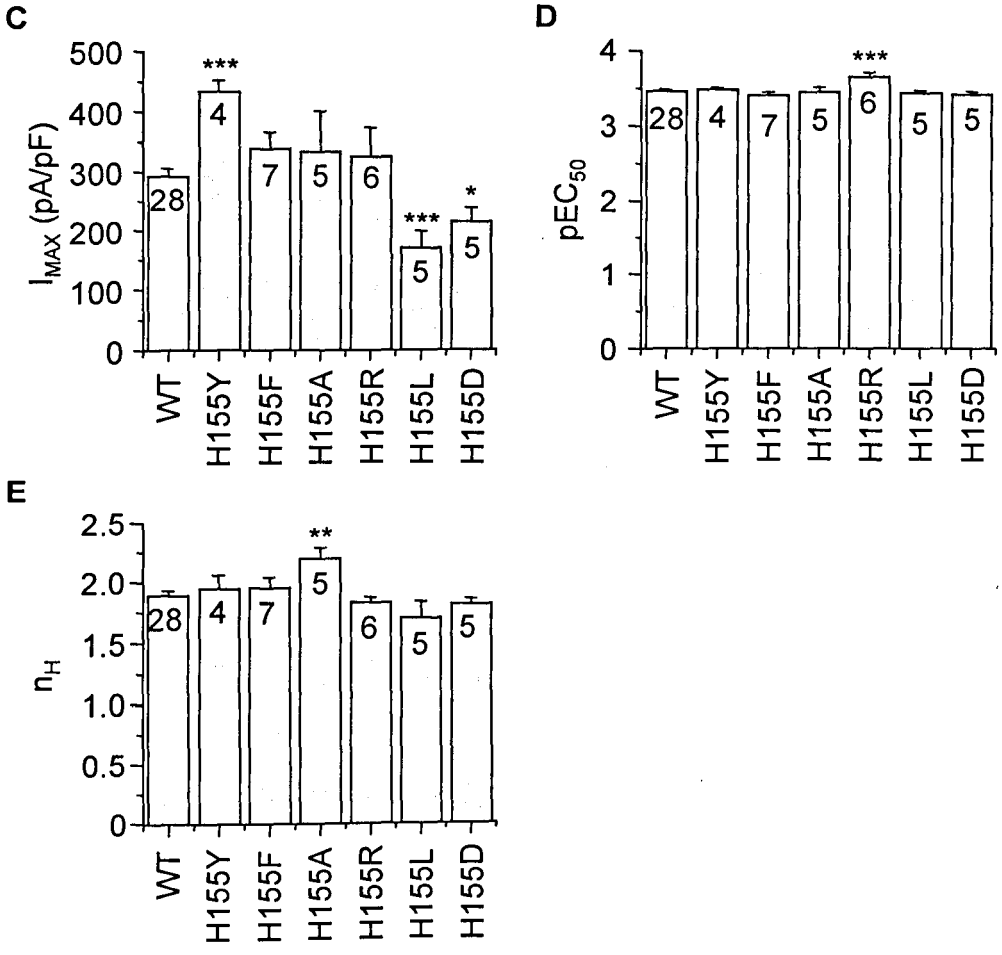

Figure 3.8 Effect of substituting His^{155} on ATP-evoked currents

(A) Representative ATP-evoked currents recorded from a HEK293 cell expressing WT or indicated mutant human $P2X_7$ receptors at -60 mV. The dashed line indicates the maximal current for the WT receptor. (B) Mean ATP dose-response curves summarising the data from experiments shown in A: WT (squares) or mutant (triangles). Smooth lines show the best fits to the Hill equation. (C-E) Mean maximal current amplitudes (I_{MAX}), pEC_{50} and Hill coefficients. The number of cells recorded is indicated. * $p<0.05$, ** $p<0.01$, *** $p<0.001$, compared to WT.

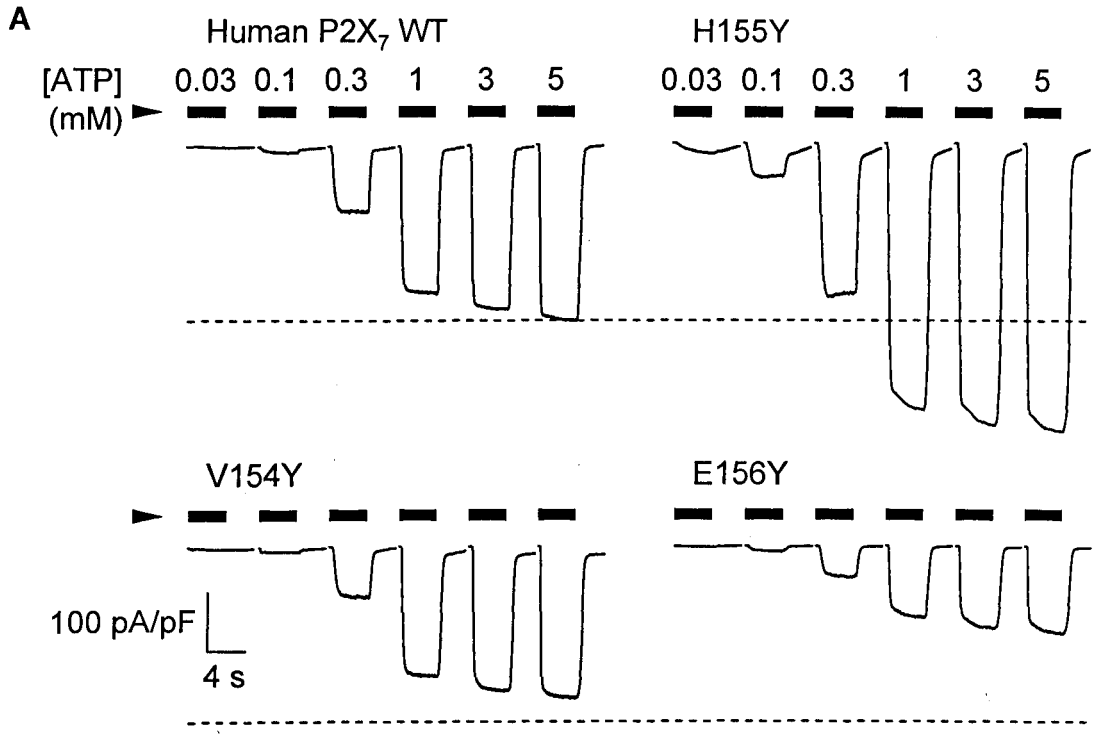

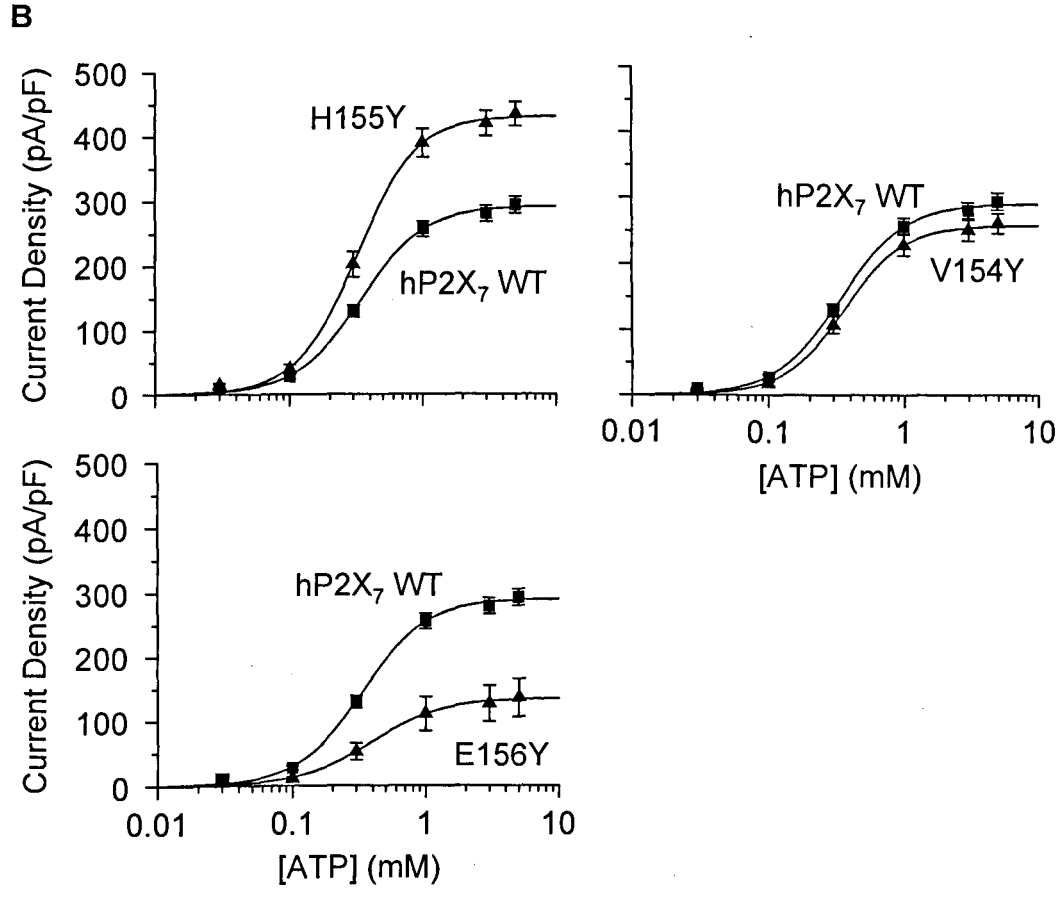

Figure continued on next page.

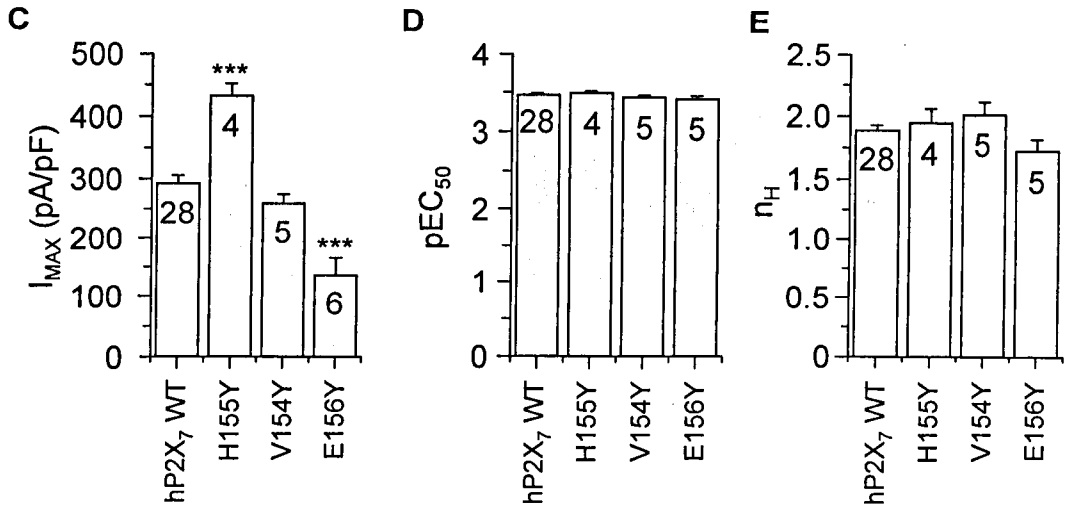

Figure 3.9 Effect of substituting Val^{154} and Glu^{156} with Tyr on ATP-evoked currents

(A) Representative ATP-evoked currents recorded from a HEK293 cell expressing WT or indicated mutant human $P2X_7$ receptors at -60 mV. The dashed line indicates the maximal current for the WT receptor. (B) Mean ATP dose-response curves summarising the data from experiments shown in A: WT (squares) or mutant (triangles). Smooth lines show the best fits to the Hill equation. (C-E) Mean maximal current amplitudes (I_{MAX}), pEC_{50} and Hill coefficient. The number of cells recorded is indicated. *** $p<0.001$, compared to WT.

3.2.7 Effect of substituting Ala^{348} with other residues on ATP-induced currents

Residue Ala^{348} in human $P2X_7$ receptor was substituted with other residues to study the importance of the side chain at this position (Figure 3.10). Ala^{348} was mutated to glycine, phenylalanine or methionine. In comparison to WT (257 ± 13 pA/pF, n = 18), the ATP-induced maximal currents were significantly increased by the A348G mutation (394 ± 19, n = 4; $p<0.001$; Figure 3.10C). The EC_{50} value was 392 ± 16 μM (n = 18) for WT, and 280 ± 25 μM, (n = 4) for A348G. The A348G mutation conferred an increase in sensitivity to ATP (pEC_{50} 3.41 ± 0.02, n = 18 for WT, and 3.56 ± 0.04, n = 4 for A348G; $p<0.01$; Figure 3.10D). Conversely, A348F and A348M significantly decreased the maximal current amplitude (143 ± 42 pA/pF, n = 4; $p<0.01$ and 178 ± 55 pA/pF, n = 5; $p<0.05$, respectively), and decreased the pEC_{50} (3.26 ± 0.05, n = 4; $p<0.01$, and 3.25 ± 0.07, n = 4; $p<0.01$, respectively; Figure 3.10D). Only A348F altered the Hill coefficient (2.14 ± 0.06, n = 18 for WT and 1.71 ± 0.11, n = 4 for A348F; $p<0.01$; Figure 3.10E).

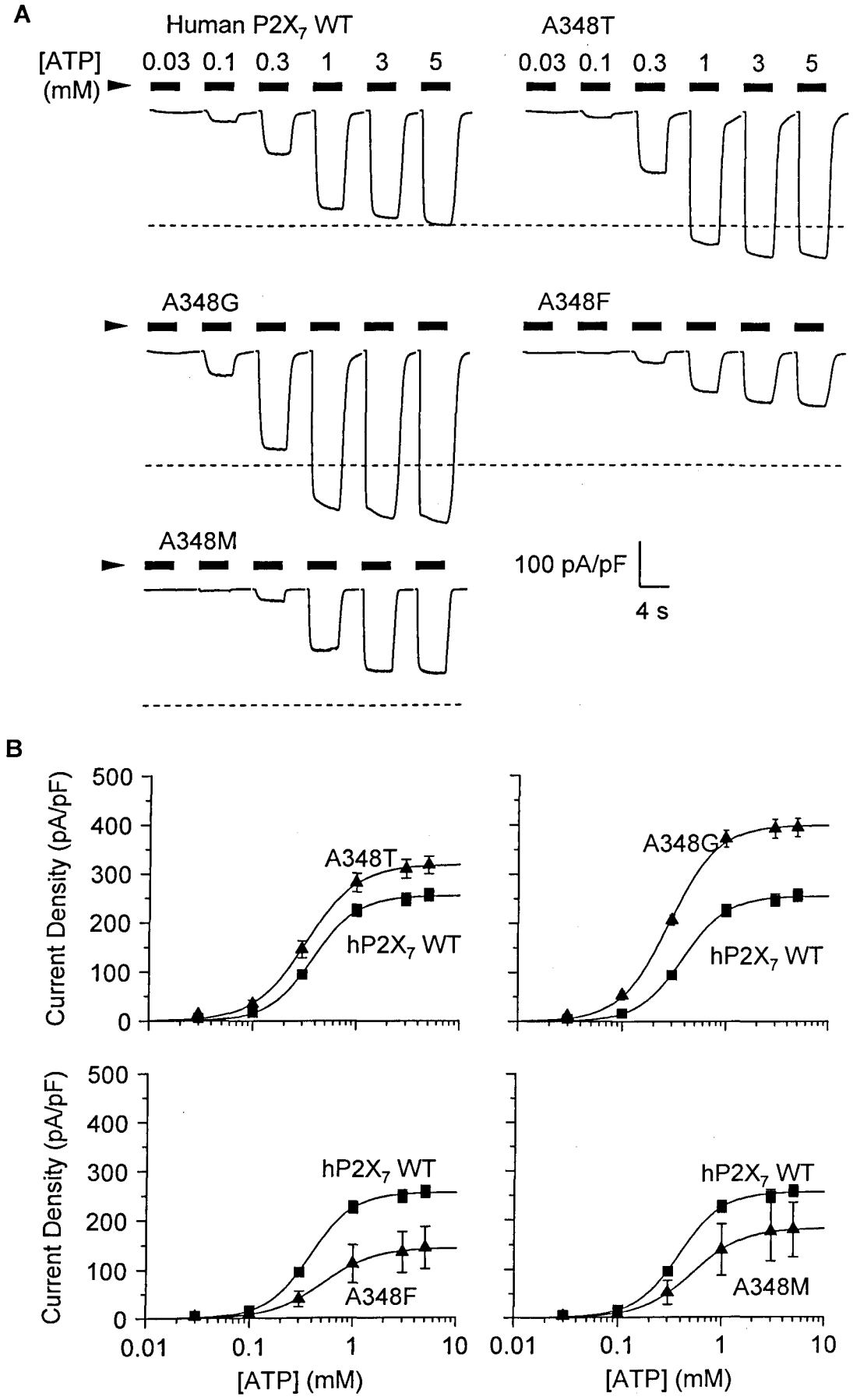

Figure continued on next page.

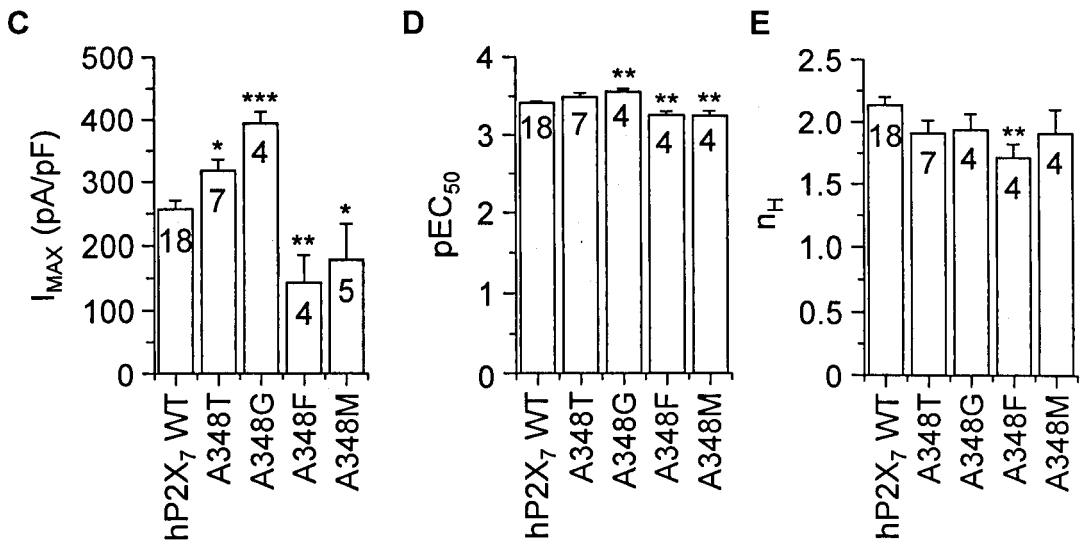

Figure 3.10 Effect of substituting Ala^{348} on ATP-evoked currents

(A) Representative ATP-evoked currents recorded from a HEK293 cell expressing WT or indicated mutant human $P2X_7$ receptors at -60 mV. The dashed line indicates the maximal current for the WT receptor. (B) Mean ATP dose-response curves summarising the data from experiments shown in A: WT (squares) or mutant (triangles). Smooth lines show the best fits to the Hill equation. (C-E) Mean maximal current amplitudes (I_{MAX}), pEC_{50} and Hill coefficients. The number of cells recorded is indicated. * $p<0.05$, ** $p<0.01$, *** $p<0.001$, compared to WT.

3.3 Discussion

In this chapter the effects of two ns-SNP mutations, H155Y and A348T, on human $P2X_7$ receptor functional expression were examined in detail. Both mutations conferred an increase in maximal current amplitudes, with little effect on agonist sensitivity. The size of the side chain at residue 348 is an important determinant of the functional expression of the receptor.

The H155Y mutation conferred an increase in maximal currents evoked by ATP or BzATP (Figures 3.2 and 3.3), confirming previous results (Roger *et al.*, 2010a), and consistent with studies showing increased Et^+ uptake and Ca^{2+} influx (Cabrini *et al.*, 2005; Roger *et al.*, 2010a). The A348T mutation also enhanced ATP- and BzATP-induced maximal currents (Figures 3.5 and 3.6), consistent with previous work (Roger *et al.*, 2010a) and in agreement with another study using patch-clamp (Stokes *et al.*, 2010) or dye uptake assays (Roger *et al.*, 2010a; Stokes *et al.*, 2010).

The importance of the side chain at 155 was examined by mutating His^{155} to other residues (Figure 3.8). Replacing the positively charged histidine with negatively charged aspartic acid (H155D) or hydrophobic leucine (H155L) reduced the maximal current. However, mutating to phenylalanine (differs from tyrosine by the lack of an OH group), arginine (similar properties to histidine) or alanine (smaller than tyrosine) had no such effect. Therefore, the particular residue at 155 is critical in determining human $P2X_7$ receptor function, however of the residues examined, only substitution with tyrosine conferred gain-of-function.

The effect of mutating His^{155} on ATP sensitivity was modest (H155Y and H155R) or lacking (H155F, H155A, H115L and H155D; Figures 3.2 and 3.8), and sensitivity to KN-62 was unaltered (Figure 3.4). These results suggest mutating His^{155} has little effect on the conformation of the ligand binding sites. Indeed, in the dolphin-like human $P2X_7$ receptor structural model (Figure 3.1), His^{155} is located in the head region and distant from both the proposed ATP binding site and ion permeating pathway (Kawate *et al.*, 2009; Roger *et al.*, 2010a). Therefore, mutation of His^{155} is unlikely to influence the ligand-bind site or single channel properties of the receptor.

The importance of the side chain at 348 on human $P2X_7$ receptor functional expression was also investigated (Figure 3.10). Mutating the small, hydrophobic alanine to threonine or glycine (also small) increased ATP-evoked

maximal currents, whilst mutating to methionine or phenylalanine (both bulky) had the opposite effect. The human $P2X_7$ receptor model predicts Ala^{348} is located in the TM2, and on the intracellular side of the channel gate (Figure 3.1). The zebrafish $P2X_4$ structure shows the TM2 region forms the ion permeating pathway (Kawate *et al.*, 2009). The TM2 α-helices are spread out on the intracellular side of the gate, and are predicted to undergo substantial movement during channel opening (Browne *et al.*, 2010; Kawate *et al.*, 2009). Such conformational changes may be affected by mutations at Ala^{348}. Considering this location, and the dependence of maximal current on the side chain size, mutation of Ala^{348} may affect the single channel properties of the ion channel. To examine these possibilities, single channel recordings are required. Altered surface expression is another possibility and is examined in chapter 6.

The double mutation H155Y/A348T further enhanced ATP-evoked maximal currents in comparison to single mutations (Figure 3.7). These ns-SNP mutations are frequently co-inherited with Q460R, an SNP mutation that has been associated with affective mood disorders (Barden *et al.*, 2006; Lucae *et al.*, 2006; McQuillin *et al.*, 2008; Stokes *et al.*, 2006). Q460R has little mutational effect on the functional expression of the human $P2X_7$ receptor (Roger *et al.,* 2010a), however, co-inheritance with H155Y and A348T SNP mutations may have a significant effect on the pathophysiology of affective mood disorders (Cabrini *et al.*, 2005; Roger *et al.*, 2010a; Stokes *et al.*, 2010). Indeed, Stokes *et al.* have shown that agonist-induced secretion of IL-1β by monocytes from subjects polymorphic for the A348T mutation is increased (Stokes *et al.*, 2010).

This study has shown that His^{155} and Ala^{348} are important for the functional expression of the human $P2X_7$ receptor, and are likely to be via different mechanisms (single channel properties for Ala^{348}, and a mechanism yet to be determined for His^{155}).

Chapter 4

Species differences between human and rat $P2X_7$ receptor functional responses

4.1 Introduction

The cloning and characterisation of the human and rat $P2X_7$ receptors has revealed striking differences in their functional expression (Rassendren *et al.*, 1997; Surprenant *et al.*, 1996) (see section 1.6.10). It is important to determine the differences in $P2X_7$ receptors properties between species. Pharmacological characterisations of $P2X_7$ receptors are frequently performed following heterologous expression of the rat $P2X_7$ receptor. Information from such work will be of limited use if the agonist and antagonist properties of $P2X_7$ receptors are very different. Furthermore, a large body of information gained on the physiological and pathophysiological roles for the $P2X_7$ receptor has been from laboratory animal studies. Inferring functional roles for the human $P2X_7$ receptor should bear in mind the differences in receptor properties between species.

It is clear that the rat $P2X_7$ receptor is more sensitive to ATP and BzATP than the human receptor (Rassendren *et al.*, 1997; Roman *et al.*, 2009). However, differences between the two species in terms of $P2X_7$ receptor mediated response to agonists are less well described. A previous study found that cells expressing the rat $P2X_7$ receptor have a higher BzATP-induced maximal uptake of YO-PRO-1 dye than those expressing the human $P2X_7$ receptor, however, surprisingly there was no significant difference in maximal BzATP-evoked currents (Rassendren *et al.*, 1997).

Studies described in chapter 3 show that mutations H155Y or A348T of the human $P2X_7$ receptor confer an increase in agonist-evoked maximal currents. Similar gain-of-function effects of these mutations on agonist-induced Ca^{2+} influx or dye uptake have also been reported (Cabrini *et al.*, 2005; Roger *et al.*, 2010a, Stokes *et al.*, 2010). These two mutations change the residues at 155 and 348 positions to those of the WT rat $P2X_7$ receptor. The particular residues at position 155 and 348 are therefore hypothesised to be important in determining the functional expression of the $P2X_7$ receptor, and particularly the difference between the human and rat species. Thus, in this chapter, the currents in HEK293 cells expressing human or rat $P2X_7$ receptors evoked by ATP and BzATP were re-examined. In addition, the reciprocal mutations, Y155H and T348A, of the rat $P2X_7$ receptor were introduced by site-directed mutagenesis, and their effects on rat $P2X_7$ receptor-mediated agonist-evoked currents was determined.

4.2 Results

4.2.1 Comparison of human and rat $P2X_7$ receptor mediated currents

The functional expression of human and rat $P2X_7$ receptors were compared. WT human and rat $P2X_7$ receptors were expressed in HEK293 cells and their current responses to ATP were compared by whole-cell patch-clamp recording. Figure 4.1 shows the results. Cells expressing the human $P2X_7$ receptor responded to ATP with a maximal current amplitude of 281 ± 18 pA/pF (n = 5), an EC_{50} of 304 ± 49 μM (n = 5), and a Hill coefficient of 2.03 ± 0.13 (n = 5). Cells expressing the rat $P2X_7$ receptor responded with larger maximal current amplitudes (458 ± 27 pA/pF, n = 5; $p<0.001$; Figure 4.1C). The EC_{50} value was 110 ± 6.1 μM (n = 5), and the rat receptor was more sensitive to ATP than the human (pEC_{50} 3.96 ± 0.02, n = 5, and 3.54 ± 0.07, n = 5, respectively; $p<0.001$; Figure 4.1D). The Hill coefficient was higher for the rat $P2X_7$ receptor (2.67 ± 0.18, n = 5; $p<0.05$; Figure 4.1E).

Figure 4.2 shows the dose-response curves constructed using BzATP as the agonist. Cells expressing the rat $P2X_7$ receptor responded to BzATP with a maximal current amplitude (282 ± 21 pA/pF, n = 12), and this was not significantly different to the human receptor (234 ± 24 pA/pF, n = 11; $p>0.05$; Figure 4.2C). The EC_{50} values were 1.9 ± 0.1 μM (n = 12) for the rat receptor, and 31 ± 3.7 μM (n = 11) for the human. The rat $P2X_7$ receptor was more sensitive to BzATP (pEC_{50} 5.72 ± 0.02, n = 12) than the human receptor (pEC_{50} 4.53 ± 0.05, n = 11; $p<0.001$; Figure 4.2D). The Hill coefficient was greater for the rat than the human receptor (3.59 ± 0.28, n = 12 and 2.73 ± 0.29, n = 11, respectively; $p<0.05$; Figure 4.2E).

The maximal current amplitudes recorded from cells expressing the human $P2X_7$ receptor were not significantly different whether ATP or BzATP were used as the agonist (281 ± 18 pA, n = 5 for ATP, and 234 ± 24 pA/pF, n = 11 for BzATP; $p>0.05$). However, the maximal current amplitudes recorded form cells expressing the rat $P2X_7$ receptor were significantly smaller when BzATP was used as the agonist (458 ± 27 pA/pF, n = 5 for ATP, and 282 ± 21 pA/pF, n = 12 for BzATP; $p<0.001$). These results indicate that BzATP is a full agonist at the human $P2X_7$ receptor, but only a partial agonist at the rat receptor. Note that these experiments were not performed in parallel.

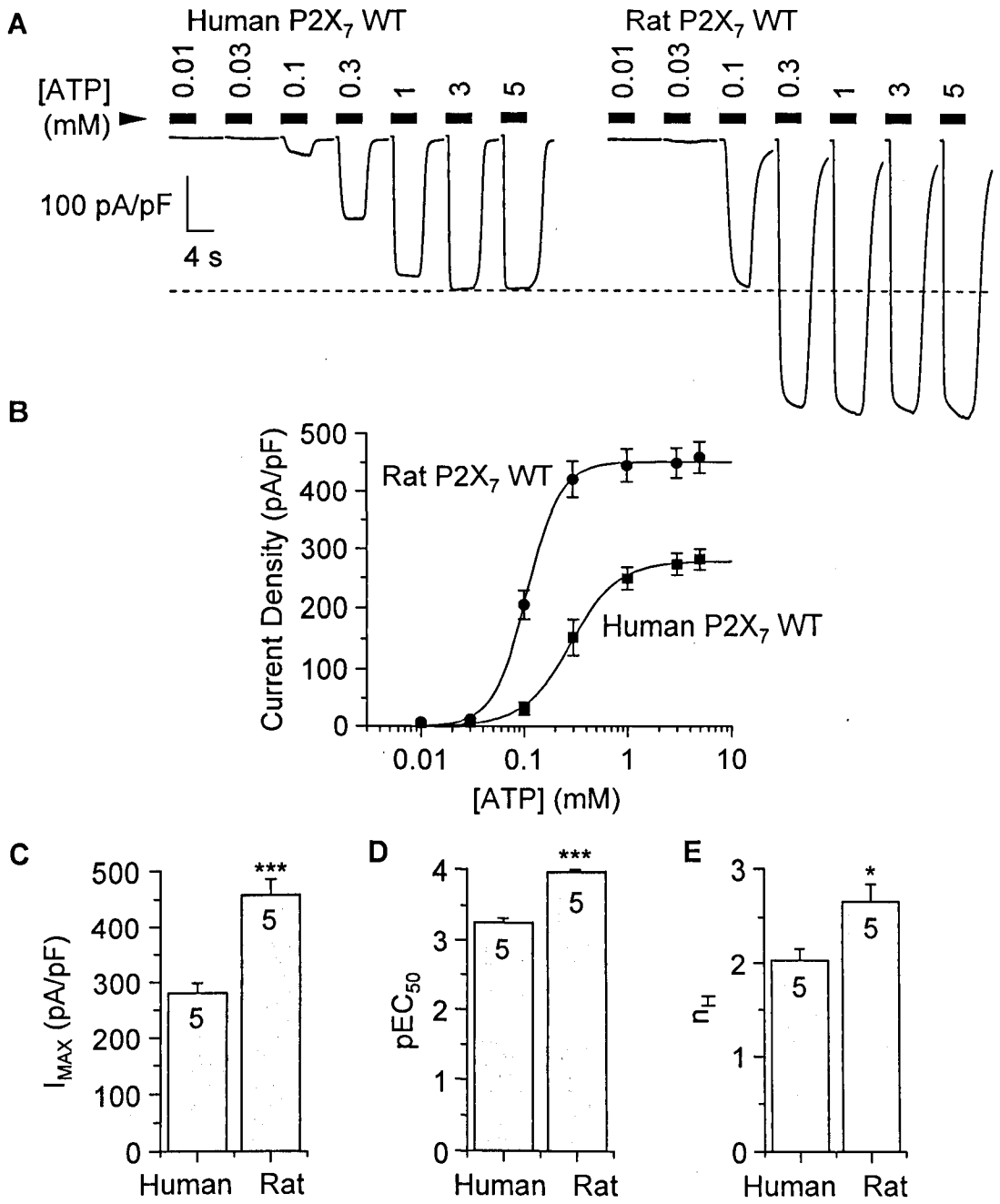

Figure 4.1 ATP-evoked human and rat $P2X_7$ receptor mediated currents recorded in low divalent extracellular solution

(A) Representative ATP-evoked currents recorded from a HEK293 cell expressing WT human (left) or rat $P2X_7$ receptors (right) at -60 mV. The dashed line indicates the maximal current for human $P2X_7$ receptor. (B) Mean ATP dose-response curves summarising the data shown in A: human (squares) or rat (circles). Smooth lines show the best fits to the Hill equation. (C-E) Mean maximal current amplitudes (I_{MAX}), pEC_{50} and Hill coefficients. The number of cells recorded is indicated. * $p<0.05$, *** $p<0.001$, compared to the human $P2X_7$ receptor.

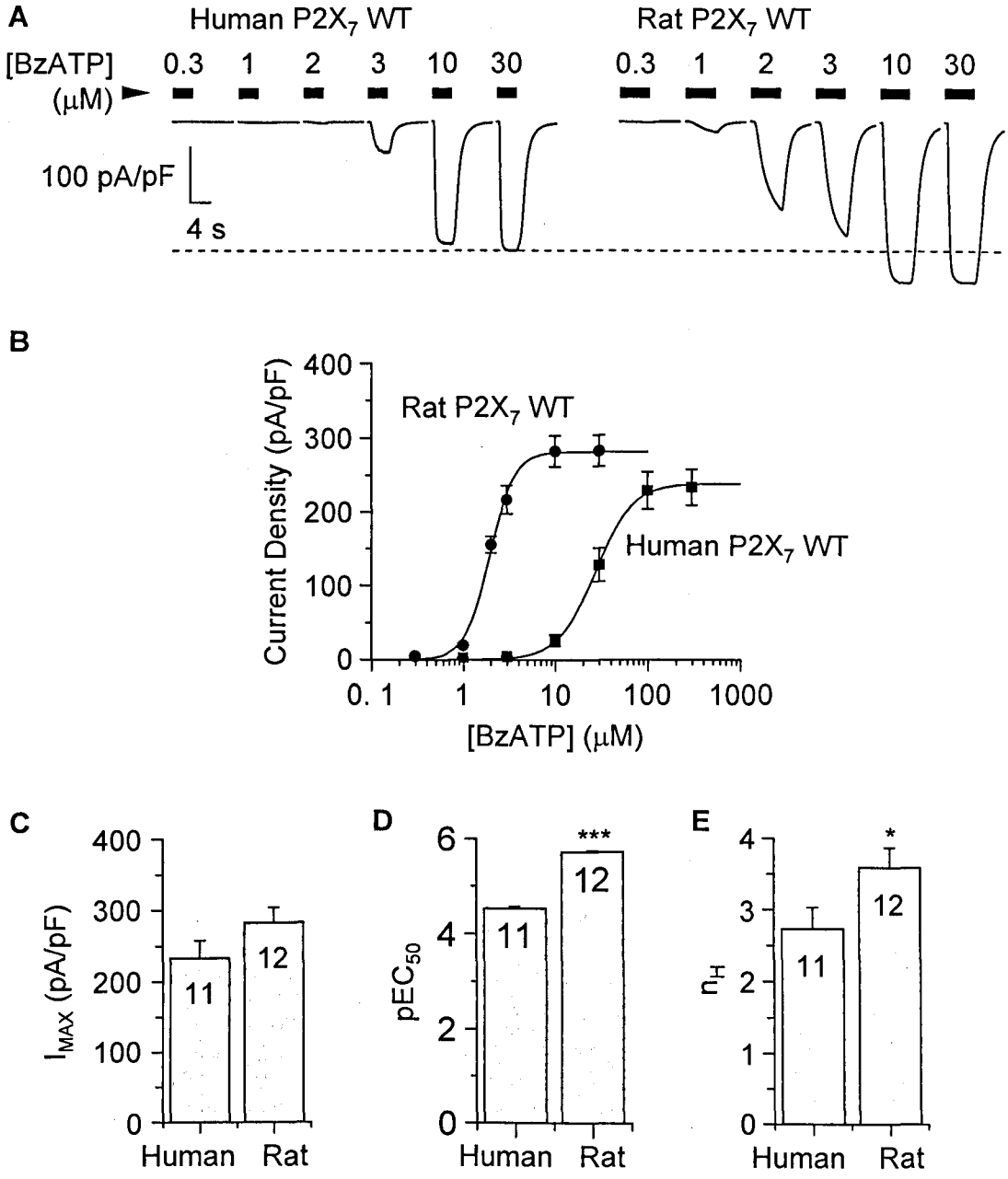

Figure 4.2 BzATP-evoked human and rat $P2X_7$ receptor mediated currents recorded in low divalent extracellular solution

(A) Representative BzATP-evoked currents recorded from a HEK293 cell expressing WT human (left) or rat $P2X_7$ receptors (right) at -60 mV. The dashed line indicates the maximal current for human $P2X_7$ receptor. (B) Mean ATP dose-response curves summarising the data shown in A: human (squares) or rat (circles). Smooth lines show the best fits to the Hill equation. (C-E) Mean maximal current amplitudes (I_{MAX}), pEC_{50} and Hill coefficients. The number of cells recorded is indicated. * $p<0.05$, *** $p<0.001$, compared to the human $P2X_7$ receptor.

4.2.2 Effect of the Y155H mutation on agonist-induced current responses of the rat $P2X_7$ receptor

In chapter 3 it was shown that the H155Y mutation confers increased ATP-evoked maximal current amplitudes (Figure 3.2). This mutation changes the residue at 155 to that of the WT rat $P2X_7$ receptor. The ATP-evoked current amplitudes mediated by the rat $P2X_7$ receptor were higher than the human receptor (Figure 4.1). Therefore, the effect of the reciprocal mutation Y155H on rat $P2X_7$ receptor function was investigated. Using low divalent cation extracellular solution (Figure 4.3), cells expressing the WT rat $P2X_7$ receptor responded to ATP with a maximal current amplitude of 444 ± 24 pA/pF (n = 10), and an EC_{50} of 104 ± 5.2 μM (n = 10). The Y155H mutation conferred a reduction in maximal current amplitude (211 ± 25 pA/pF, n = 7; $p<0.001$; Figure 4.3C) and in sensitivity to ATP (EC_{50} 286 ± 10 μM, n = 7) (pEC_{50} 3.99 ± 0.02, n = 10 for WT, and 3.55 ± 0.02 for Y155H, n = 7 for Y155H; $p<0.001$; Figure 4.3D). The Hill coefficient was unaltered (2.54 ± 0.07, n = 10 for WT and 2.40 ± 0.13, n = 7 for Y155H; $p>0.05$; Figure 4.3E).

These experiments were repeated using standard extracellular solution (Figure 4.4). Cells expressing the WT rat $P2X_7$ receptor responded to ATP with a maximal current amplitude of 411 ± 21 pA/pF (n = 5), which was reduced to 189 ± 37 pA/pF (n = 5; $p<0.001$) by the Y155H mutation (Figure 4.4C). The EC_{50} value was 1470 ± 33 μM (n = 5) for WT, and 2513 ± 114 μM (n = 4) for Y155H. The mutation conferred a significant decrease in sensitivity to ATP (pEC_{50} 2.83 ± 0.01, n = 5 for WT, and 2.60 ± 0.02, n = 4 for Y155H; $p<0.001$; Figure 4.4D). The mutation significantly increased the Hill coefficient (2.57 ± 0.18, n = 5 for WT, and 3.97 ± 0.13, n = 4 for Y155H; $p<0.001$; Figure 4.4E).

The effect of Y155H mutation on BzATP-evoked currents was also investigated (Figure 4.5). Cells expressing the WT rat $P2X_7$ receptor responded to BzATP with a maximal current amplitude of 294 ± 28 pA/pF (n = 7), an EC_{50} of 1.7 ± 0.06 μM (n = 7), and a Hill coefficient of 3.56 ± 0.19 (n = 7). The Y155H mutation reduced the maximal current amplitude (129 ± 15 pA/pF, n = 5; $p<0.01$; Figure 4.5C). The Y155H mutant responded to BzATP with an EC_{50} value of 8.0 ± 1.3 μM (n = 5). The mutation conferred a decrease in sensitivity to BzATP (pEC_{50} 5.78 ± 0.01, n = 7 for WT, and 5.12 ± 0.06, n = 5 for Y155H; $p<0.001$; Figure 4.5D) and decreased the Hill coefficient (2.78 ± 0.11, n = 5 for Y155H; $p<0.01$; Figure 4.5E).

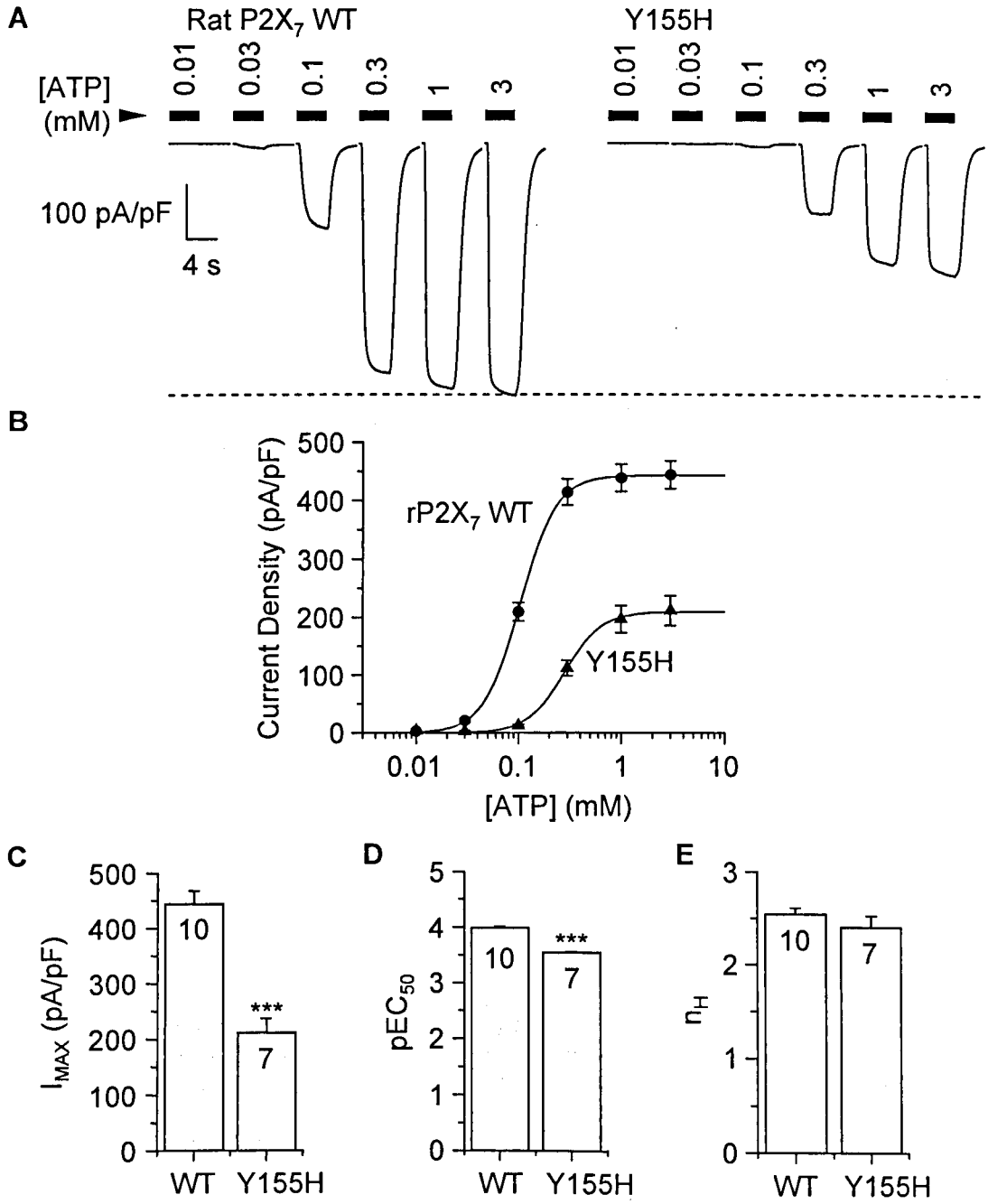

Figure 4.3 Effect of the Y155H mutation on ATP-evoked currents of the rat $P2X_7$ receptor recorded in low divalent extracellular solution

(A) Representative ATP-evoked currents recorded from a HEK293 cell expressing WT ($rP2X_7$ WT; left) or Y155H mutant rat $P2X_7$ receptors (right) at -60 mV. The dashed line indicates the maximal current for WT. (B) Mean ATP dose-response curves summarising the data shown in A: WT (squares) or Y155H (triangles). Smooth lines show the best fits to the Hill equation. (C-E) Mean maximal current amplitudes (I_{MAX}), pEC_{50} and Hill coefficients. The number of cells recorded is indicated. *** $p<0.001$, compared to WT.

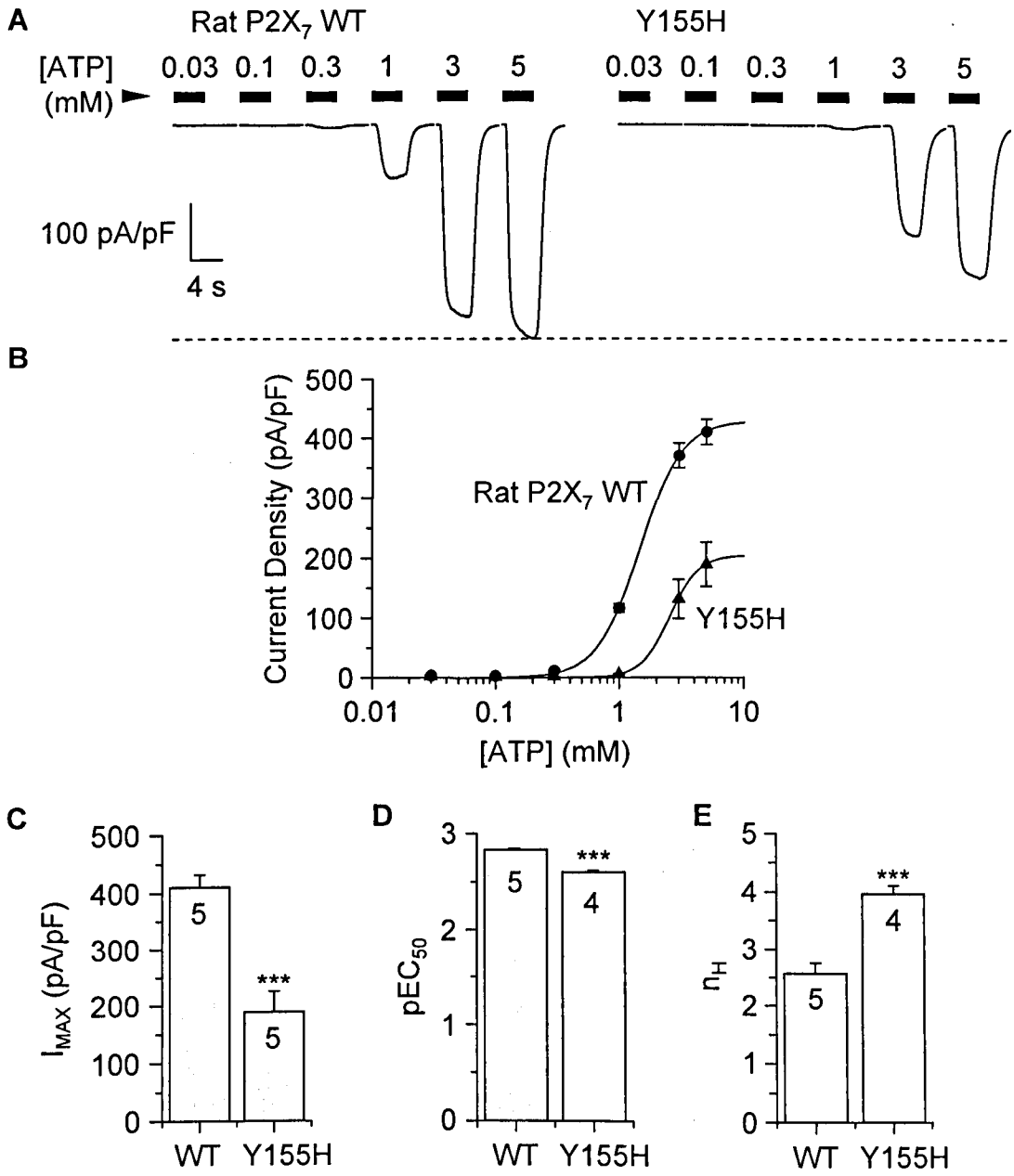

Figure 4.4 Effect of the Y155H mutation on ATP-evoked currents of the rat $P2X_7$ receptor recorded in standard extracellular solution

(A) Representative ATP-evoked currents recorded from a HEK293 cell expressing WT (left) or Y155H mutant rat $P2X_7$ receptors (right) in standard extracellular solution at -60 mV. The dashed line indicates the maximal current for WT. (B) Mean ATP dose-response curves summarising the data shown in A: WT (squares) or Y155H (triangles). Smooth lines show the best fits to the Hill equation. (C-E) Mean maximal current amplitudes (I_{MAX}), pEC_{50} and Hill coefficients. The number of cells recorded is indicated. *** $p<0.001$, compared to WT.

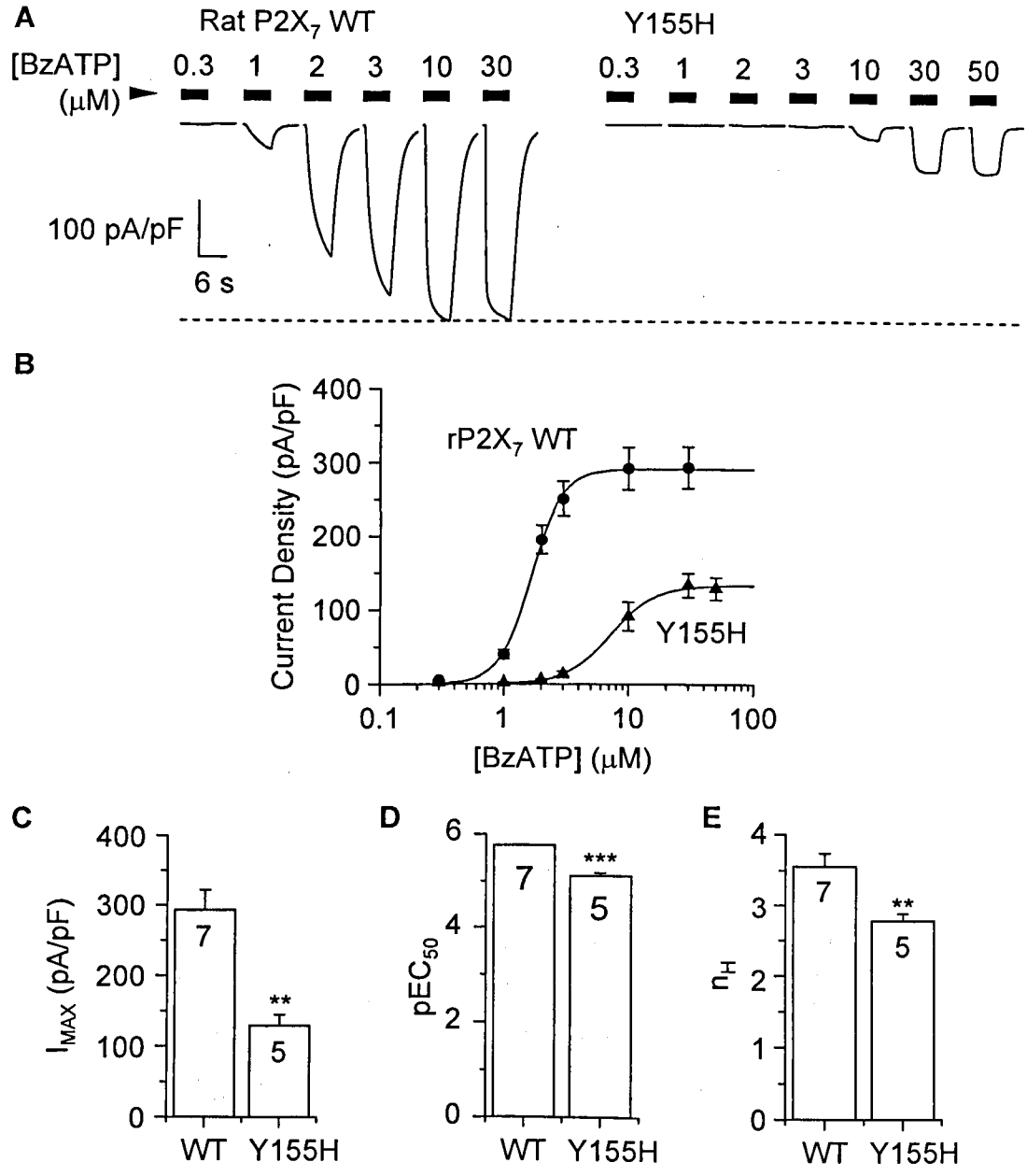

Figure 4.5 Effect of the Y155H mutation on BzATP-evoked currents of the rat $P2X_7$ receptor recorded in low divalent extracellular solution

(A) Representative BzATP-evoked currents (6 s) recorded from a HEK293 cell expressing WT (left) or Y155H mutant rat $P2X_7$ receptors (right) at -60 mV. The dashed line indicates the maximal current for WT. (B) Mean BzATP dose-response curves summarising the data shown in A: WT (squares) or Y155H (triangles). Smooth lines show the best fits to the Hill equation. (C-E) Mean maximal current amplitudes (I_{MAX}), pEC_{50} and Hill coefficients. The number of cells recorded is indicated. ** $p<0.01$, *** $p<0.001$, compared to WT.

4.2.3 Effect of the T348A mutation on agonist-induced current responses of the rat $P2X_7$ receptor

In chapter 3, it was shown that the A348T mutation confers increased ATP-evoked maximal current amplitudes (Figure 3.5). This mutation changes the residue at 348 to that of the WT rat $P2X_7$ receptor. Because the ATP-evoked current amplitudes mediated by the rat $P2X_7$ receptor were higher than the human receptor (Figure 4.1), the effect of the reciprocal mutation T348A on agonist-evoked receptor currents was investigated (Figure 4.6). Cells expressing the WT rat $P2X_7$ receptor responded to ATP with a maximal current amplitude of 444 ± 24 pA/pF (n = 10) in low divalent extracellular solution, which was reduced by the T348A mutation (326 ± 23, n = 7; $p<0.01$; Figure 4.6C). The WT receptor responded to ATP with an EC_{50} value of 104 ± 5.2 μM (n = 10), and 105 ± 5.4 μM for T348A, (n = 7). However, the T348A mutation does not alter the sensitivity to ATP (pEC_{50} 3.99 ± 0.02, n = 10 for WT, and 3.98 ± 0.02 for T348A, n = 7; $p>0.05$; Figure 4.6D). The Hill coefficient was unaffected (2.54 ± 0.07, n = 10 for WT, and 2.51 ± 0.18, n = 7 for T348A; $p>0.05$; Figure 4.6E).

These experiments were also performed using standard extracellular solution (Figure 4.7). Similarly, the T348A mutation conferred a decrease in maximal current amplitude (411 ± 21 pA/pF, n = 5 for WT, and 230 ± 8.1 pA/pF, n = 3 for T348A; $p<0.001$; Figure 4.7C). The WT receptor responded to ATP with an EC_{50} of 1470 ± 33 μM (n = 5), and the T348A mutant 1386 ± 142 μM. There was no significant effect on sensitivity to ATP (pEC_{50} 2.83 ± 0.01, n = 5 for WT, and 2.86 ± 0.04, n = 3 for T348A; $p>0.05$; Figure 4.7D). The Hill coefficient was unaltered (2.57 ± 0.18, n = 5 for WT, and 2.56 ± 0.26, n = 3 for T348A; $p>0.05$; Figure 4.7E).

The effect of the T348A mutation on rat $P2X_7$ receptor currents was further investigated using BzATP as the agonist and using low divalent extracellular solution (Figure 4.8). The T348A mutation decreased maximal current amplitude (294 ± 28 pA/pF, n = 7 for WT, and 191 ± 24 pA/pF, n = 5 for T348A; $p<0.05$; Figure 4.8D). The ATP EC_{50} value was 1.7 ± 0.06 μM (n = 7) for the WT receptor, and 1.7 ± 0.05 μM (n = 5) for T348A mutant. Receptor sensitivity to BzATP was unaltered (pEC_{50} 5.78 ± 0.01 μM, n = 7 for WT, and 5.77 ± 0.01, n = 5 for T348A; $p>0.05$; Figure 4.8D), and the Hill coefficient was also unaffected (3.56 ± 0.19, n = 7 for WT, and 3.48 ± 0.14, n = 5 for T348A; $p>0.05$; Figure 4.8E).

4.2.4 Effects of the Y155H/T348A mutation on ATP-induced current responses of the rat $P2X_7$ receptor

The Y155H/T348A double mutation was introduced to the rat $P2X_7$ receptor (Figure 4.9). Cells expressing the WT rat $P2X_7$ receptor responded to ATP with a maximal current amplitude of 444 ± 24 pA/pF (n = 10), which was reduced by the Y155H/T348A mutation (114 ± 18 pA/pF, n = 3; $p<0.001$). The maximal current amplitude for the Y155H/T348A double mutant receptor was significantly lower than that for the Y155H or T348A single mutant receptor. The ATP EC_{50} value was 104 ± 5.2 μM (n = 10) for WT, and 500 ± 161 μM (n = 3) for the Y155H/T348A mutant. The sensitivity to ATP was decreased by Y155H/T348A mutation in comparison to WT (pEC_{50} 3.99 ± 0.02, n = 10 for WT, and 3.34 ± 0.13, n = 3 for Y155H/T348A; $p<0.001$; Figure 4.9D). The Hill coefficient was decreased by the double mutation (2.54 ± 0.07, n = 10 for WT, and 1.72 ± 0.26, n = 3 for Y155H/T348A; $p<0.001$; Figure 4.9E).

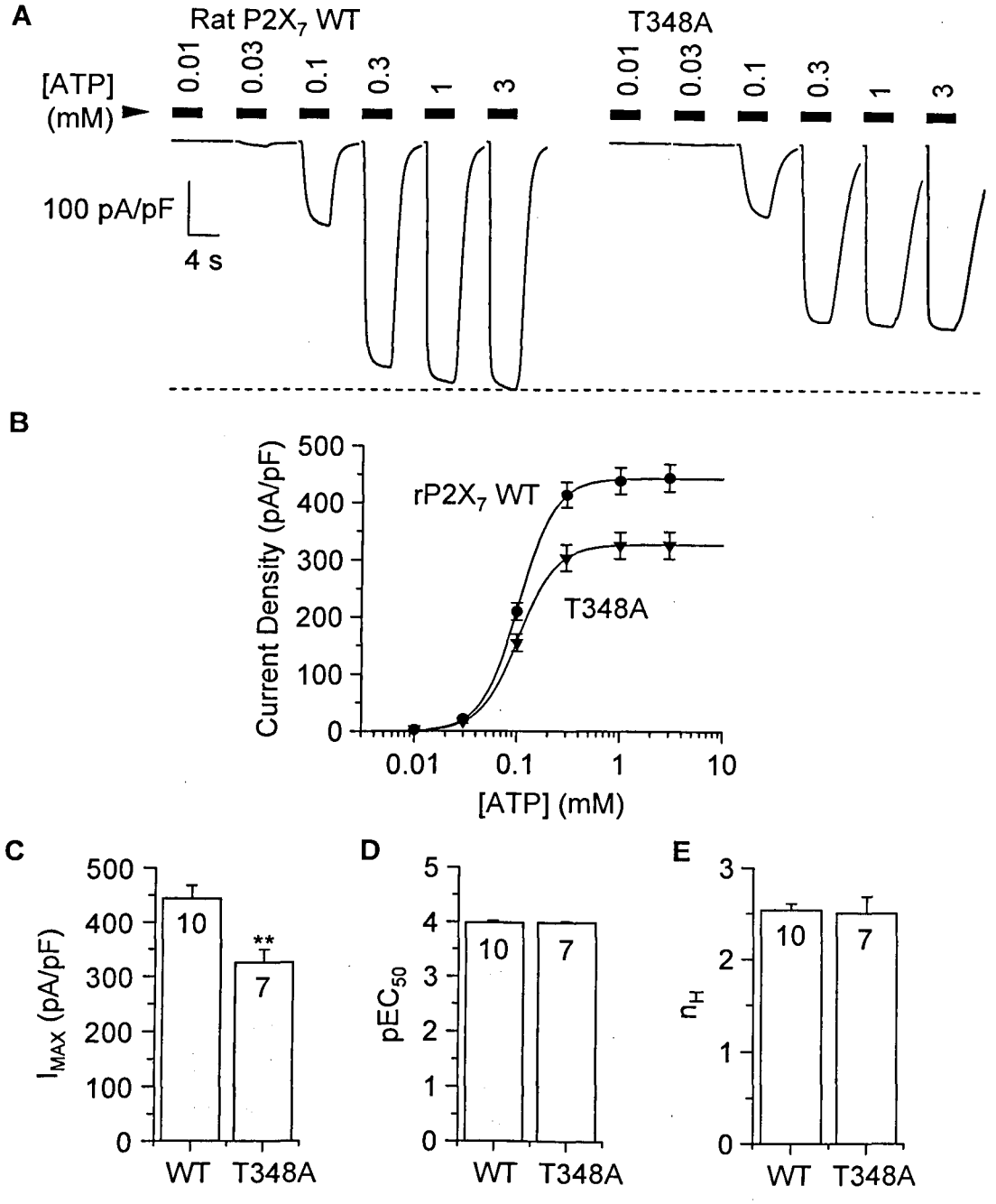

Figure 4.6 Effect of the T348A mutation on ATP-evoked currents of the rat $P2X_7$ receptor recorded in low divalent extracellular solution

(A) Representative ATP-evoked currents recorded from a HEK293 cell expressing WT (left) or T348A mutant rat $P2X_7$ receptors (right) at -60 mV. The dashed line indicates the maximal current for WT. (B) Mean ATP dose-response curves summarising the data shown in A: WT (squares) or T348A (triangles). Smooth lines show the best fits to the Hill equation. (C-E) Mean maximal current amplitudes (I_{MAX}), pEC_{50} and Hill coefficients. The number of cells recorded is indicated. ** $p<0.01$, compared to WT.

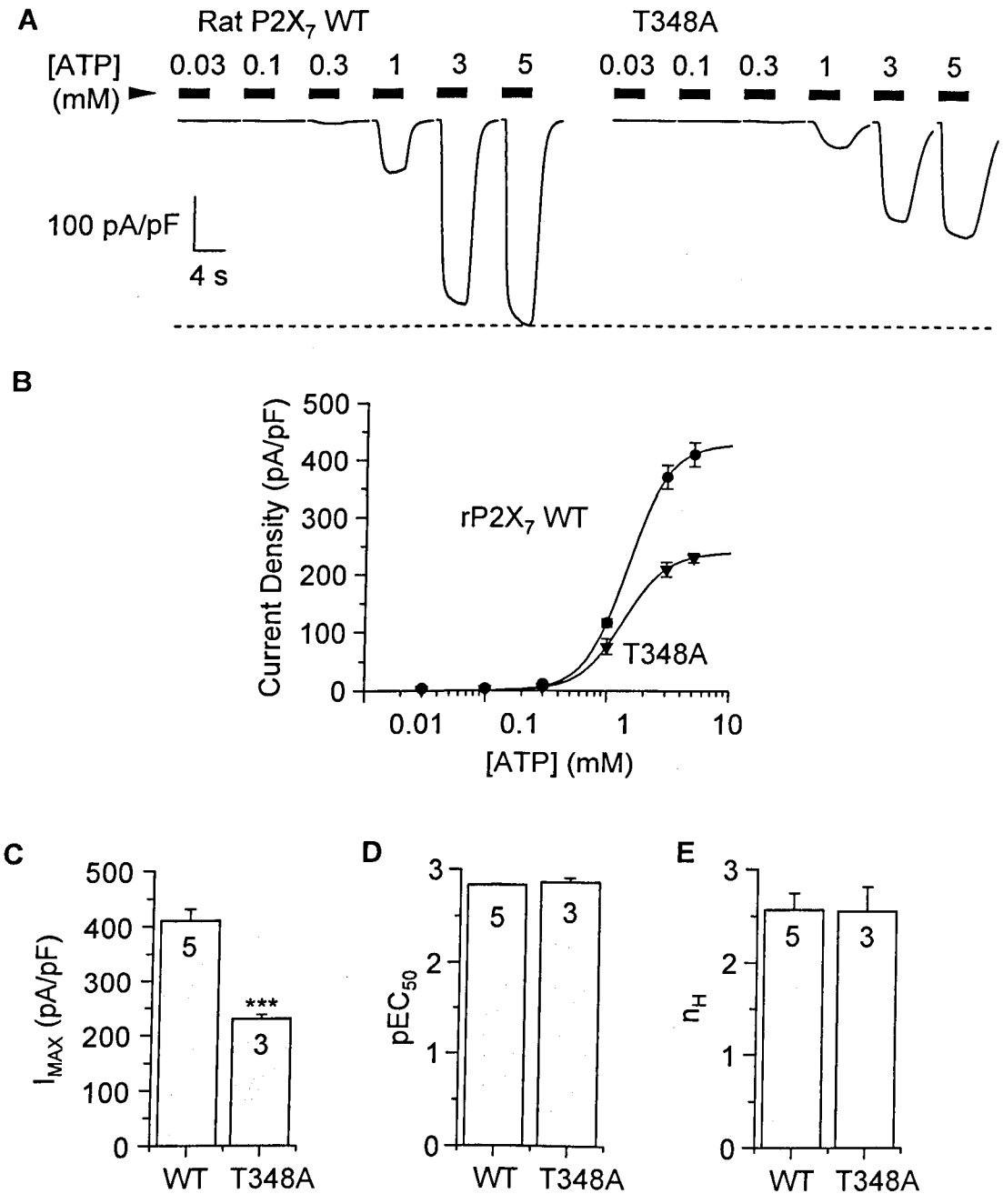

Figure 4.7 Effect of the T348A mutation on ATP-evoked currents of the rat $P2X_7$ receptor recorded in standard extracellular solution

(A) Representative ATP-evoked currents recorded from a HEK293 cell expressing WT (left) or T348A mutant rat $P2X_7$ receptors (right) in standard extracellular solution at -60 mV. The dashed line indicates the maximal current for WT. (B) Mean ATP dose-response curves summarising the data shown in A: WT (squares) or T348A (triangles). Smooth lines show the best fits to the Hill equation. (C-E) Mean maximal current amplitudes (I_{MAX}), pEC_{50} and Hill coefficients. The number of cells recorded is indicated. *** $p<0.001$, compared to WT.

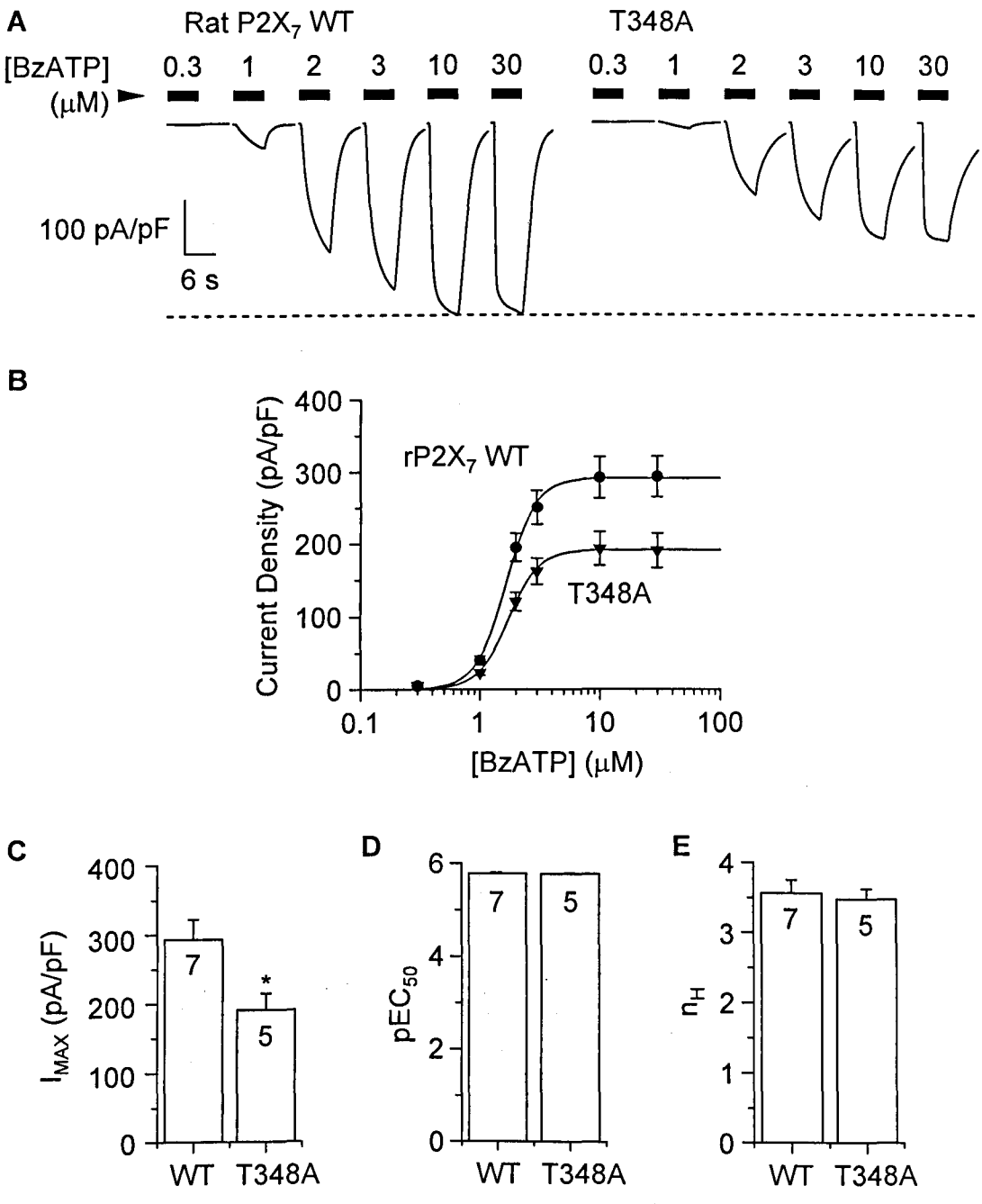

Figure 4.8 Effect of the T348A mutation on BzATP-evoked currents of the rat $P2X_7$ receptor recorded in low divalent extracellular solution

(A) Representative BzATP-evoked currents (6 s) recorded from a HEK293 cell expressing WT (left) or T348A mutant rat $P2X_7$ receptors (right) at -60 mV. The dashed line indicates the maximal current for WT rat $P2X_7$ receptor. (B) Mean BzATP dose-response curves summarising the data shown in A: WT (squares) or T348A (triangles). Smooth lines show the best fits to the Hill equation. (C-E) Mean maximal current amplitudes (I_{MAX}), pEC_{50} and Hill coefficients. The number of cells recorded is indicated. * $p<0.05$, compared to WT.

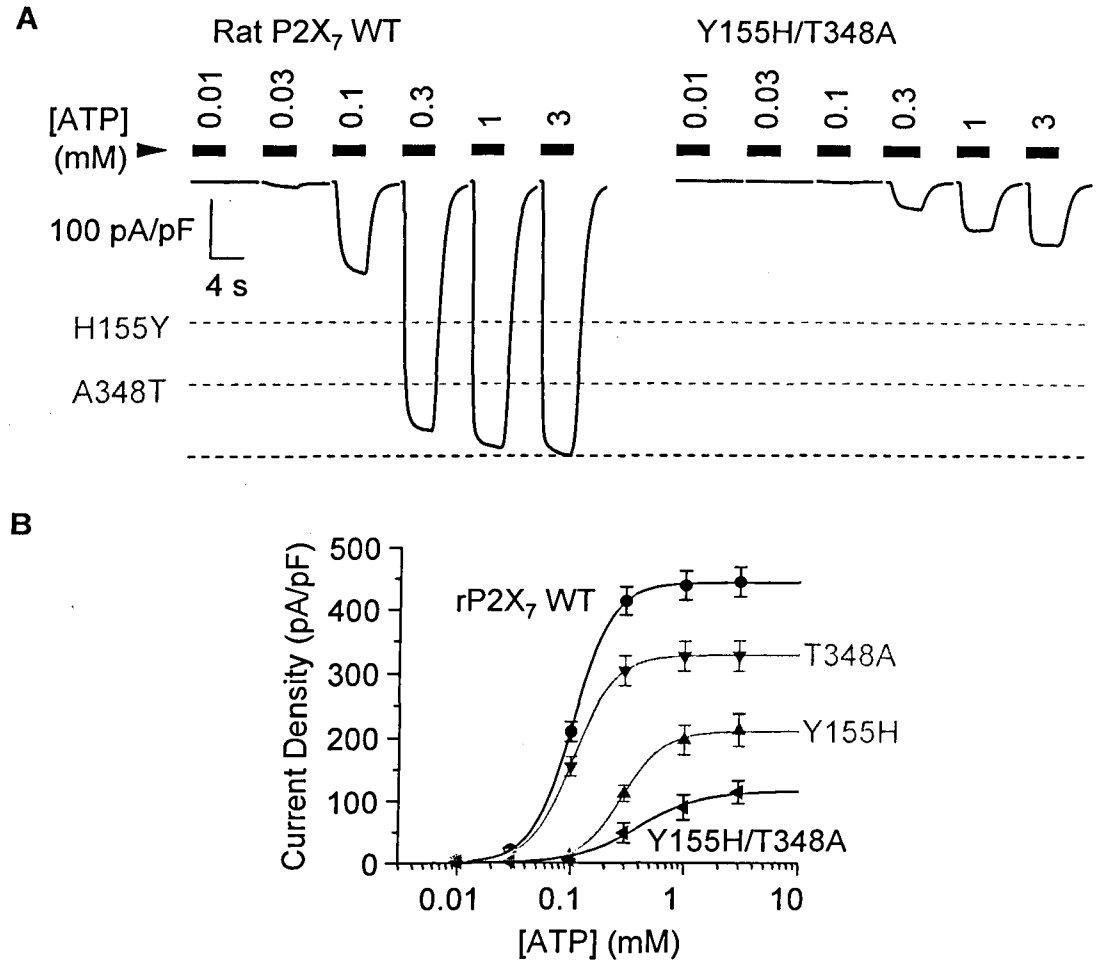

Figure continued on next page.

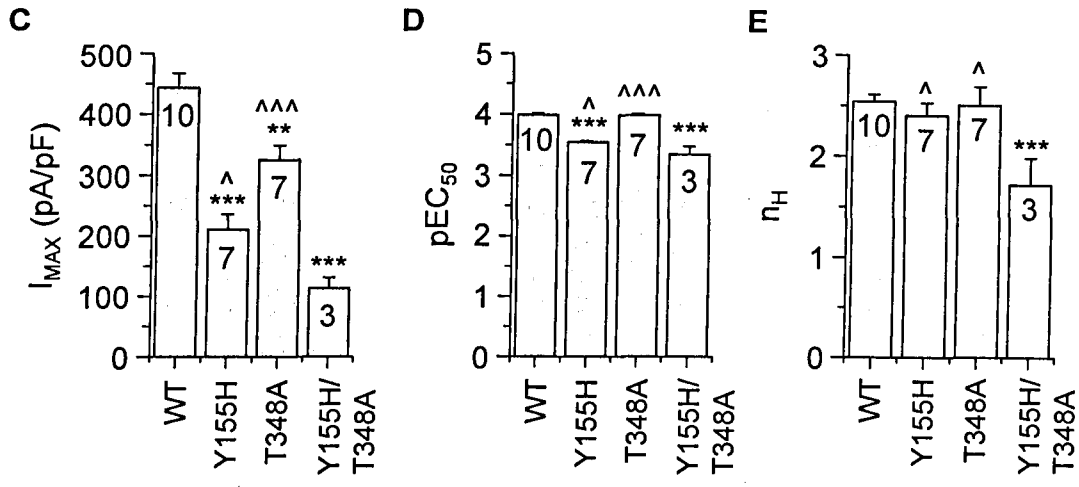

Figure 4.9 Effect of the Y155H/T348A mutation on ATP-evoked currents of the rat $P2X_7$ receptor recorded in low divalent extracellular solution

(A) Representative ATP-evoked currents recorded from a HEK293 cell expressing WT (left) or Y155H/T348A mutant rat $P2X_7$ receptors (right) at -60 mV. The black dashed line indicates the maximal current for the WT receptor, and in grey indicates the representative maximal currents for the Y155H (Figure 4.3A) and T348A (Figure 4.6A) single mutants. (B) Mean ATP dose-response curves summarising the data shown in A: WT (squares) or Y155H/T348A (triangles). Smooth lines show the best fits to the Hill equation. (C-E) Mean maximal current amplitudes (I_{MAX}), pEC_{50} and Hill coefficients. The number of cells recorded is indicated. ** $p<0.01$, *** $p<0.001$, compared to WT; ^ $p<0.05$, ^^^ $p<0.001$, compared to Y155H/T348A double mutant.

4.3 Discussion

The results presented in this chapter show that the ATP-induced maximal currents mediated by the rat $P2X_7$ receptor are greater than the human $P2X_7$ receptor (Figure 4.1), Furthermore, mutations Y155H and T348A of the rat $P2X_7$ receptor decrease agonist-induced maximal currents, with little or mild effect on agonist sensitivity (Figures 4.3 to 4.8).

Direct comparison of human and rat $P2X_7$ receptors shows that the rat $P2X_7$ receptor exhibits significantly greater sensitivity to ATP and BzATP than the human $P2X_7$ receptor (Figures 4.1 and 4.2), a finding that was reported by previous studies (Rassendren *et al.*, 1997, Roman *et al.*, 2009). Previous studies found that the amplitude of BzATP-evoked maximal currents mediated by the rat $P2X_7$ receptor was increased, in comparison to the human, but in this study there was no statistical difference detected (Figure 4.2) (Rassendren *et al.*, 1997). This is in striking contrast with the observation that BzATP-evoked YO-PRO-1 uptake was greater for cells expressing the rat $P2X_7$ receptor compared to the human receptor (Rassendren *et al.*, 1997). On the other hand, the results from this study have provided the first evidence that the amplitude of ATP-induced maximal currents was significantly greater in cells expressing the rat $P2X_7$ receptor than the human $P2X_7$ receptor (Figure 4.1). These observations suggest there is a species difference in functional expression of the $P2X_7$ receptors between human and rat, although such a difference only becomes apparent when ATP is used as the agonist. BzATP differs structurally from ATP due to the attachment of two benzoyls to the ribose group, and may interact with different sets of residues in the agonist-binding site. Therefore, it is likely the conformational changes that occur upon agonist binding differ depending on whether ATP or BzATP is bound. Indeed, Young *et al.* found that one residue (Asp^{284}) accounts for the difference in ATP sensitivity between rat and mouse $P2X_7$ receptors. However, two residues (Lys^{127} and Asn^{284}) are responsible for the difference in BzATP sensitivity (Young *et al.*, 2007). The finding in this study that BzATP was a full agonist at the human $P2X_7$ receptor, but only a partial agonist at the rat receptor, may also provide an explanation for the finding that a species difference in functional expression of the $P2X_7$ receptors between human and rat is only detectable when ATP is used as the agonist.

Results in chapter 3 show mutations H155Y and A348T, which change residues at 155 and 348 to those of the WT rat receptor, increase the amplitude of agonist-induced maximal currents mediated by the human $P2X_7$ receptor, with modest effects on agonist sensitivity. The results in this chapter show that reciprocal mutations, Y155H and T348A, of the rat $P2X_7$ receptor decrease the maximal current amplitude (Figures 4.3 to 4.8). Taken together, these results strongly suggest that residues at positions 155 and 348 are important for the differential functional expression of human and rat $P2X_7$ receptors. In summary, the study described in this chapter shows that ATP-induced maximal responses are greater for rat $P2X_7$ receptor than human $P2X_7$ receptor. Furthermore, the Y155H and T348A mutations of the rat $P2X_7$ receptor attenuates the functional expression. This provides further evidence that residues at positions 155 and 348 are important in determining the functional expression of the $P2X_7$ receptor, and particularly the species differences in functional expression of rat and human $P2X_7$ receptors.

Human and rat $P2X_7$ receptor sequences are 80% identical (Rassendren *et al.,* 1997). A number of species differences in the function of human and rat $P2X_7$ receptors have been reported (see general introduction, section 1.6.10). For example, the rat $P2X_7$ receptor sequence contains a CaM binding domain, which is not present in the human $P2X_7$ receptor sequence (Roger *et al.*, 2010b). Therefore, whilst the rat $P2X_7$ receptor has a Ca^{2+}/CaM component to current facilitation, the human $P2X_7$ receptors does not. Furthermore, the antagonist AZ11645373 has a greater potency at human than rat $P2X_7$ receptors (Michel *et al.*, 2009; Stokes *et al.*, 2006). Mutation F95L of the human $P2X_7$ receptor (changes the residue to that of the WT rat receptor) reduces the potency of AZ11645373 (Michel *et al.*, 2008; Michel *et al.*, 2009). Residues at positions 155 and 348 of the human and rat $P2X_7$ receptors adds to the list of sequence dissimilarities between these species that lead to differences in the functional expression of the receptors.

Chapter 5

Contribution of residues in microdomains surrounding 155 and 348 to the functional expression of human and rat $P2X_7$ receptors

5.1 Introduction

The results presented in the previous two chapters show that mutations H155Y and A348T of the human $P2X_7$ receptor lead to gain of receptor function and reciprocal mutations Y155H and T348A of the rat $P2X_7$ receptor reduce receptor function. This demonstrates residues at positions 155 and 348 are important in determining the species-specific functional expression of human and rat $P2X_7$ receptors.

According to the structural model of the human $P2X_7$ receptor, His^{155} is located in the head region of the extracellular domain (Figure 3.1) (Kawate *et al.*, 2009; Roger *et al.*, 2010a). Alignment of $P2X_7$ amino acid sequences shows that the six residues immediately surrounding 155 are not conserved between species (Figure 5.1). Results in chapter 3 found that mutation E156Y of the human $P2X_7$ receptor reduced ATP-evoked maximum currents (Figure 3.9), providing evidence that residues in the region surrounding position 155 may be important in $P2X_7$ receptor function.

The structural model of the human $P2X_7$ receptor indicates Ala^{348} is located in the TM2 region, on the intracellular side of the ion channel gate (Figure 3.1) (Kawate *et al.*, 2009; Roger *et al.*, 2010a)). The zebrafish $P2X_4$ structure shows that TM2 forms the ion conducting pathway and that, on the intracellular side of the gate, the TM2 α-helices spread out (Figure 1.5) (Kawate *et al.*, 2009). This region of TM2 is predicted to undergo substantial movement during channel opening (Browne *et al.*, 2010). Therefore, other residues in this region of the $P2X_7$ receptor may be important for receptor function, as demonstrated by the residue at 348. Alignment of $P2X_7$ receptor amino acid sequences shows all residues N-terminal to position 348 in TM2 are conserved (Figure 5.1). However, a number of residues C-terminal to position 348 in, or close to, the TM2 domain, are not conserved.

The potential contributions of the non-conserved residues in the microdomains surrounding positions 155 and 348 to the species-specific functional expression of human and rat $P2X_7$ receptors have been investigated. To this end, each of these residues of the human $P2X_7$ receptor were replaced in turn with the corresponding residue of the rat $P2X_7$ receptor, and the mutational effects on ATP-evoked currents have been examined in this chapter.

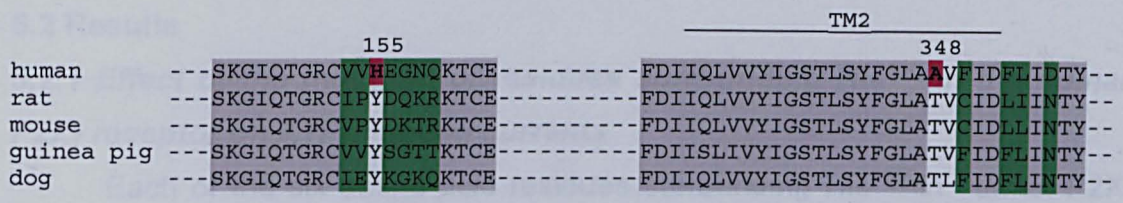

Figure 5.1 Microdomains surrounding positions 155 and 348 of $P2X_7$ receptors

Sequence alignments of the microdomains surrounding positions 155 and 348 in five cloned mammalian $P2X_7$ receptors. Conserved residues are highlighted in grey, residues 155 and 348 of the human $P2X_7$ receptor in pink, and residues studied in this chapter in green. The accession numbers are Y09561, X95882, AJ009823, EU275201 and EU334661, respectively. Aligned using ClustalW.

5.2 Results

5.2.1 Effect of the mutation of residues surrounding His^{155} in the human $P2X_7$ receptor on ATP-induced currents

Each of the six amino acid residues surrounding His^{155} in human $P2X_7$ receptor was replaced with the corresponding residue of the rat $P2X_7$ receptor, generating the following mutants: V153I, V154P, E156D, G157Q, N158K and Q159R. Figure 5.2A shows examples of ATP-elicited inward whole-cell currents in cells expressing individual mutants in HEK293 cells and Figure 5.2B shows the ATP dose-current response curves. Cells expressing WT human $P2X_7$ receptors responded to ATP with a maximal current amplitude of 276 ± 15 pA/pF (n = 23). Three mutations (V154P, E156D and Q159R) had no effect, but three other mutations (V153I, G157Q and Q159R) led to a reduction in maximal current amplitude (215 ± 19 pA/pF, n = 4; 197 ± 24 pA/pF, n = 5 and 184 ± 25 pA/pF, n = 6 respectively; $p<0.05$; Figure 5.2C). The WT EC_{50} value for ATP was 347 ± 24 μM (n = 24), and none of the mutations altered the sensitivity to ATP (pEC_{50} 3.48 ± 0.03, n = 24 for WT; Figure 5.2D) or Hill coefficient (2.04 ± 0.08, n = 24 for WT; Figure 5.2E).

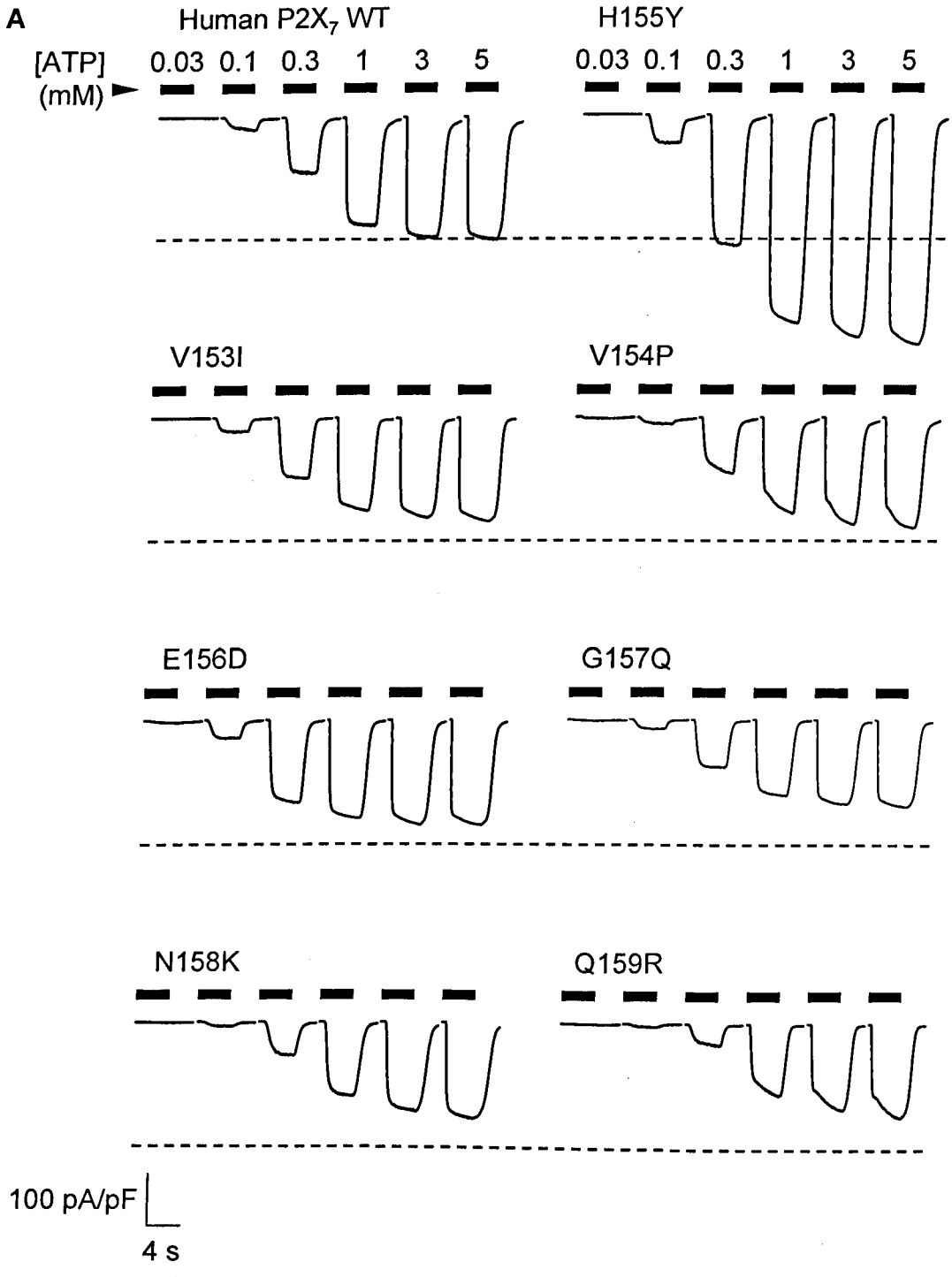

Figure continued on next page.

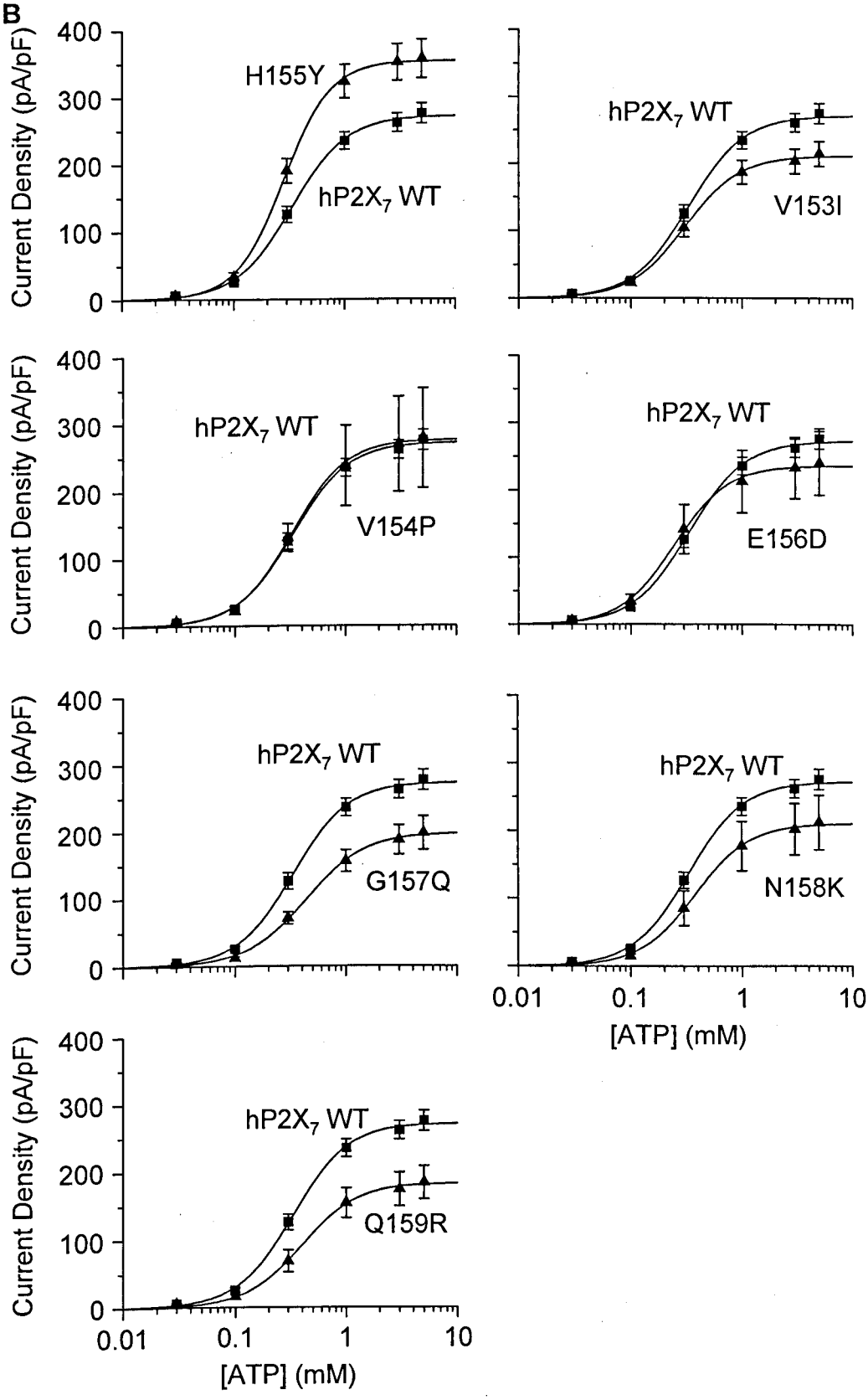

Figure continued on next page.

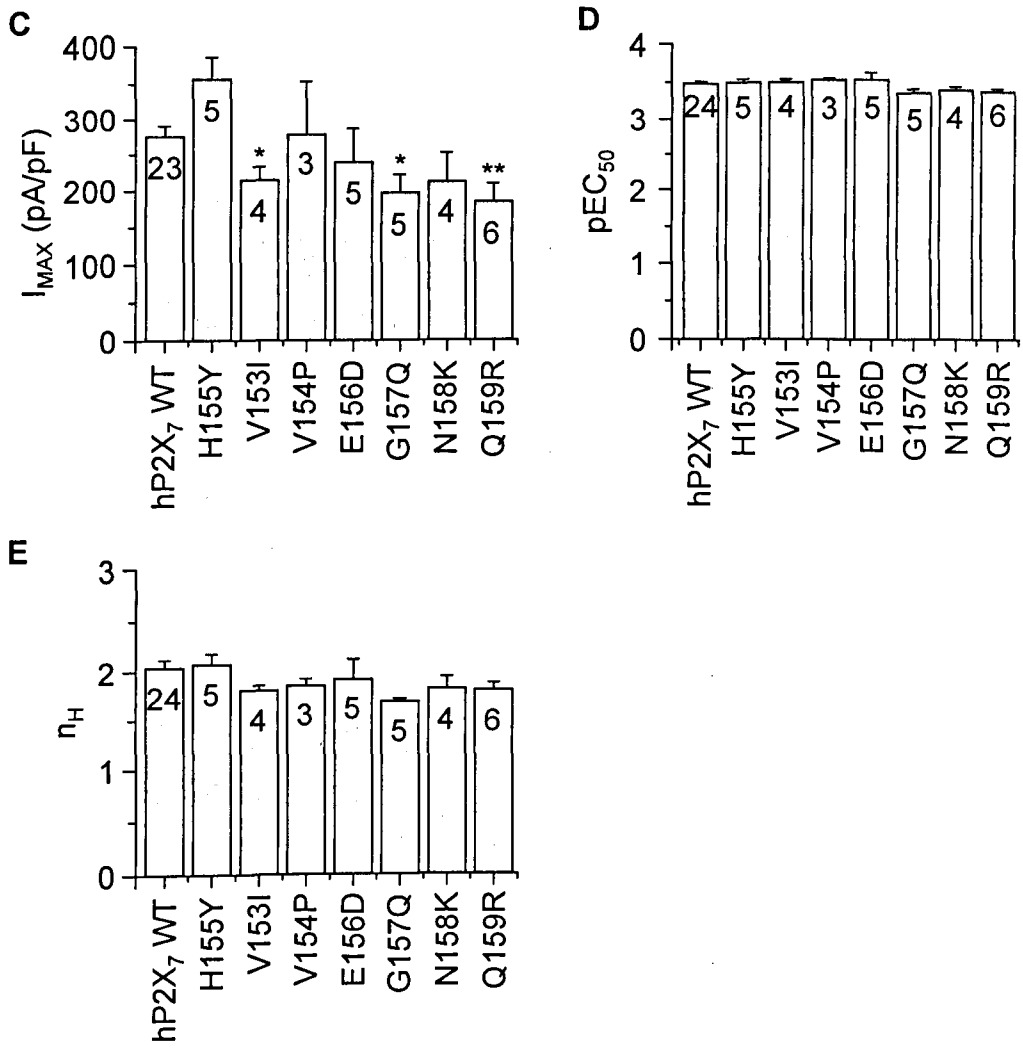

Figure 5.2 Effect of the mutation of residues in the microdomain surrounding His[155] of human $P2X_7$ receptor on ATP-evoked currents

(A) Representative ATP-evoked currents recorded from a HEK293 cell expressing WT or mutant human $P2X_7$ receptors at -60 mV. The dashed line indicates the maximal current for the WT receptor. (B) Mean ATP dose-response curves summarising the data from experiments shown in A: WT (squares) or mutant (triangles). Smooth lines show the best fits to the Hill equation. (C-E) Mean maximal current amplitudes (I_{MAX}), pEC_{50} and Hill coefficients. The number of cells recorded is indicated. * $p<0.05$, ** $p<0.01$, compared to WT.

5.2.2 Effect of the mutation of residues surrounding Ala^{348} in human $P2X_7$ receptor on ATP-induced currents

Each of the four non-conserved amino acids in the close vicinity of residue Ala^{348} in the human $P2X_7$ receptor was individually mutated to the corresponding residue in rat $P2X_7$ receptor. This lead to generation of four mutants: F350C, F353L, L354I and D356N. Individual mutants were expressed in HEK293 cells the ATP-induced whole-cell currents were recorded (Figure 5.3). Cells expressing the WT human $P2X_7$ receptor responded to ATP with a maximal current amplitude of 257 ± 13 pA/pF (n = 18), an EC_{50} of 392 ± 15 μM (n = 18), and a Hill coefficient of 2.14 ± 0.06 (n = 18). The F353L and D356N mutations had opposing effects on maximal current amplitude: F353L caused an increase (318 ± 23 pA/pF, n = 5; $p<0.05$), whilst D356N resulted in a decrease (191 ± 16 pA/pF, n = 4; $p<0.05$; Figure 5.3C). The maximal current amplitude was not altered by F350C or L354I mutations. The ATP EC_{50} values were 291 ± 32 μM (n = 4) and 291 ± 31 μM (n = 4) for the F350C and D356N mutants, respectively, and both mutations conferred an increase in receptor sensitivity to ATP (pEC_{50} 3.41 ± 0.02, n = 18 for WT, and 3.54 ± 0.05, n = 4 and 3.54 ± 0.05 for F350C and D356N, respectively; $p<0.01$; Figure 5.3D). The Hill coefficient was decreased by the F350C mutation (1.71 ± 0.20, n = 4; $p<0.05$; Figure 5.3E). For all other mutants, the EC_{50} and Hill coefficients were unaltered.

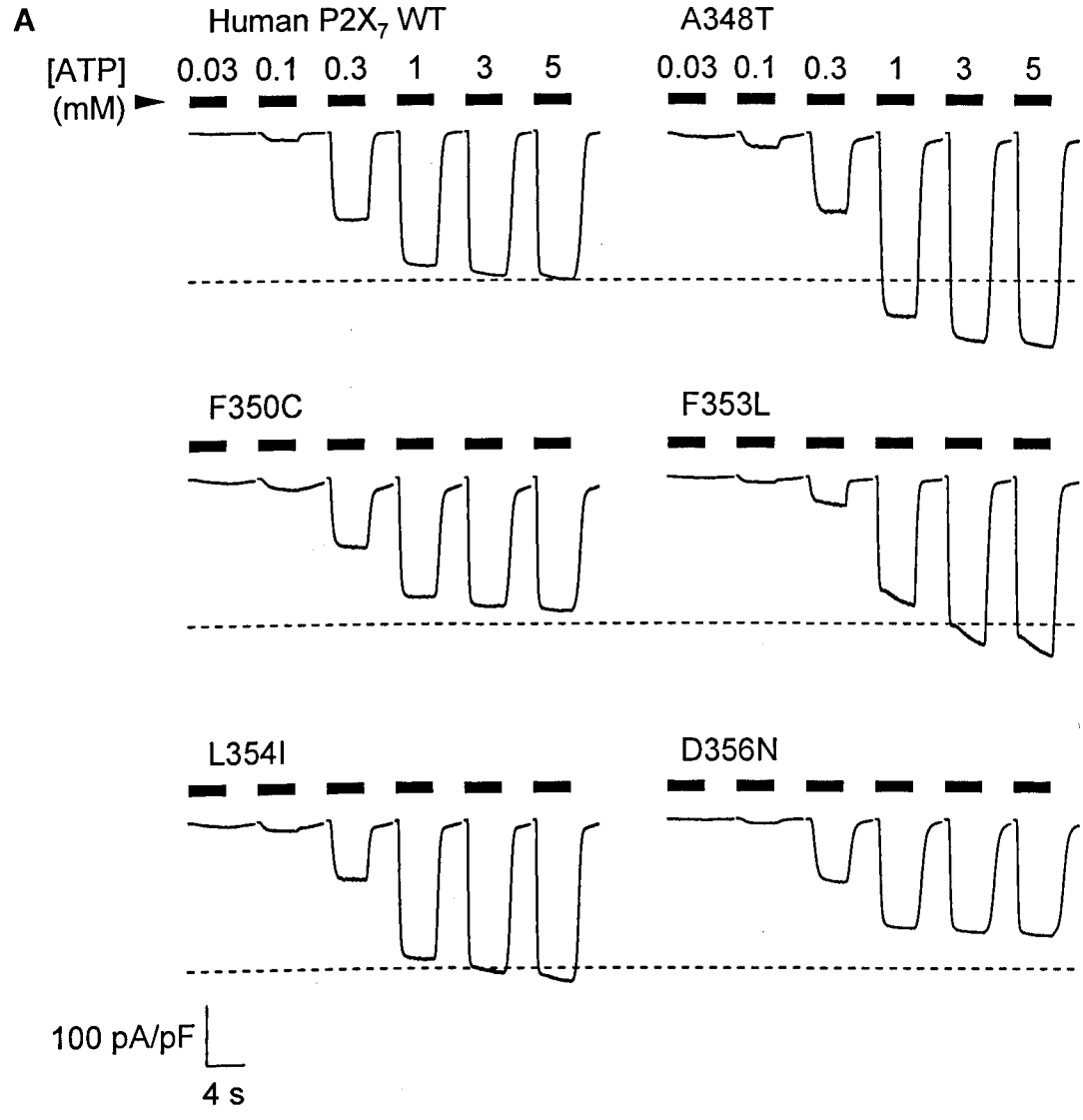

Figure continued on next page.

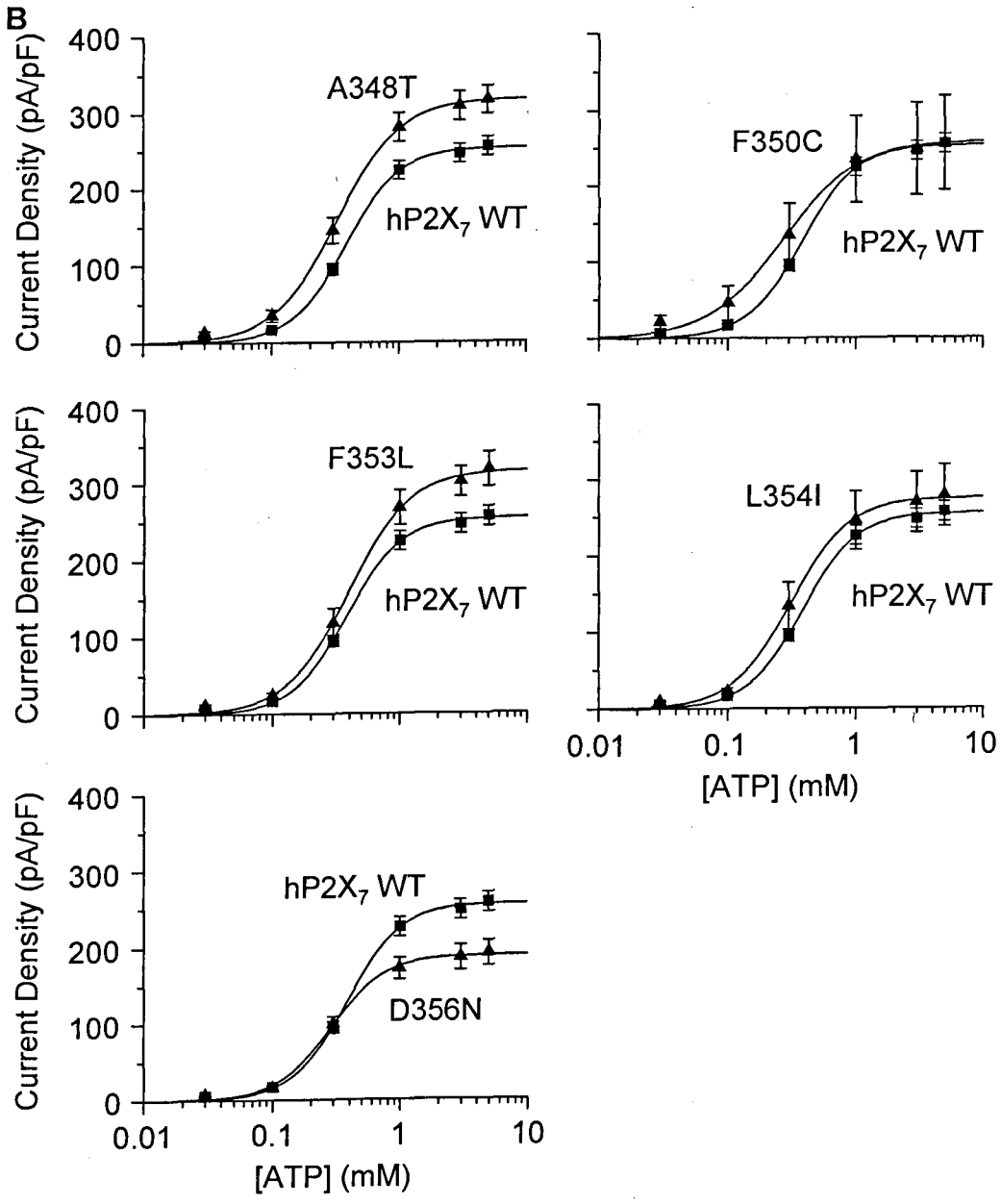

Figure continued on next page.

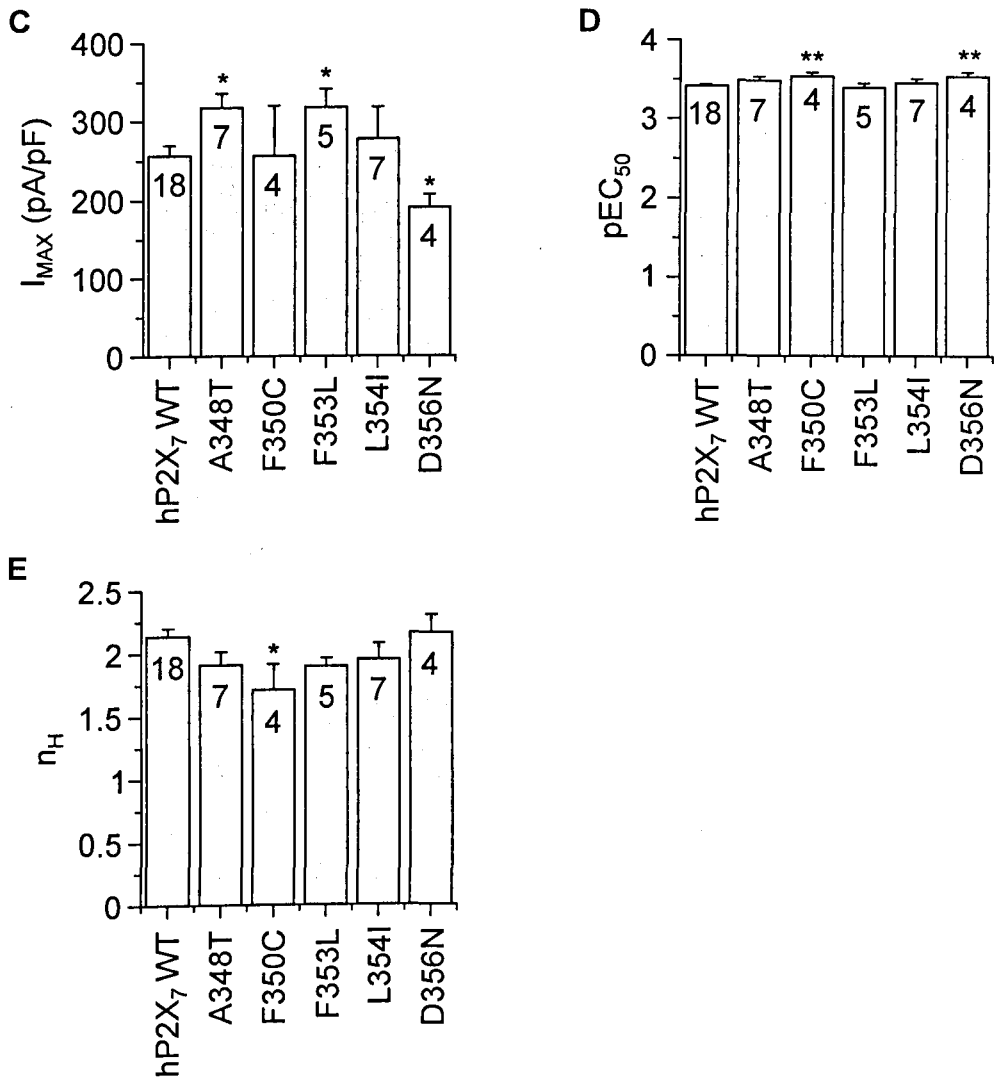

Figure 5.3 Effect of mutating residues close to Ala^{348} of the human P2X$_7$ receptor on ATP-evoked currents

(A) Representative ATP-evoked currents recorded from a HEK293 cell expressing WT (left) or mutant human P2X$_7$ receptors (right) at -60 mV. The dashed line indicates the maximal current for the WT receptor. (B) Mean ATP dose-response curves summarising the data from experiments shown in A: WT (squares) or mutant (triangles). Smooth lines show the best fits to the Hill equation. (C-E) Mean maximal current amplitudes (I_{MAX}), pEC_{50} and Hill coefficients. The number of cells recorded is indicated. * $p<0.05$, compared to WT.

5.2.3 Effect of the L353F mutation in the rat $P2X_7$ receptor on ATP-induced currents

Like A348T (Figures 3.5 and 5.3), mutation of Phe^{353} in the human $P2X_7$ to the corresponding leucine residue in the rat $P2X_7$ receptor increased the ATP-evoked maximal current amplitudes (Figure 5.3). The reciprocal mutation, L353F, was introduced to the rat $P2X_7$ receptor to see if this residue contributes to the species dependent functional expression in a similar way to 348 (chapter 4). Cells expressing WT rat $P2X_7$ receptors responded to ATP with a maximal current amplitude of 316 ± 29 pA/pF (n = 4), and was not significantly altered by the L353F mutation (371 ± 52 pA/pF, n = 4; $p>0.05$; Figure 5.4C). EC_{50} values were 108 ± 7 μM (n = 4) for WT, and 89 ± 13 μM (n = 4) for L353F. Receptor sensitivity to ATP was not altered by the mutation (pEC_{50} 3.97 ± 0.03, n = 4 for WT, and 4.07 ± 0.07, n = 4 for L353F; $p>0.05$; Figure 5.4D). The Hill coefficient was also not significantly altered by the L353F mutation (2.39 ± 0.13, n = 4 for WT, and 2.43 ± 0.15, n = 4 for L353F; $p>0.05$; Figure 5.4E).

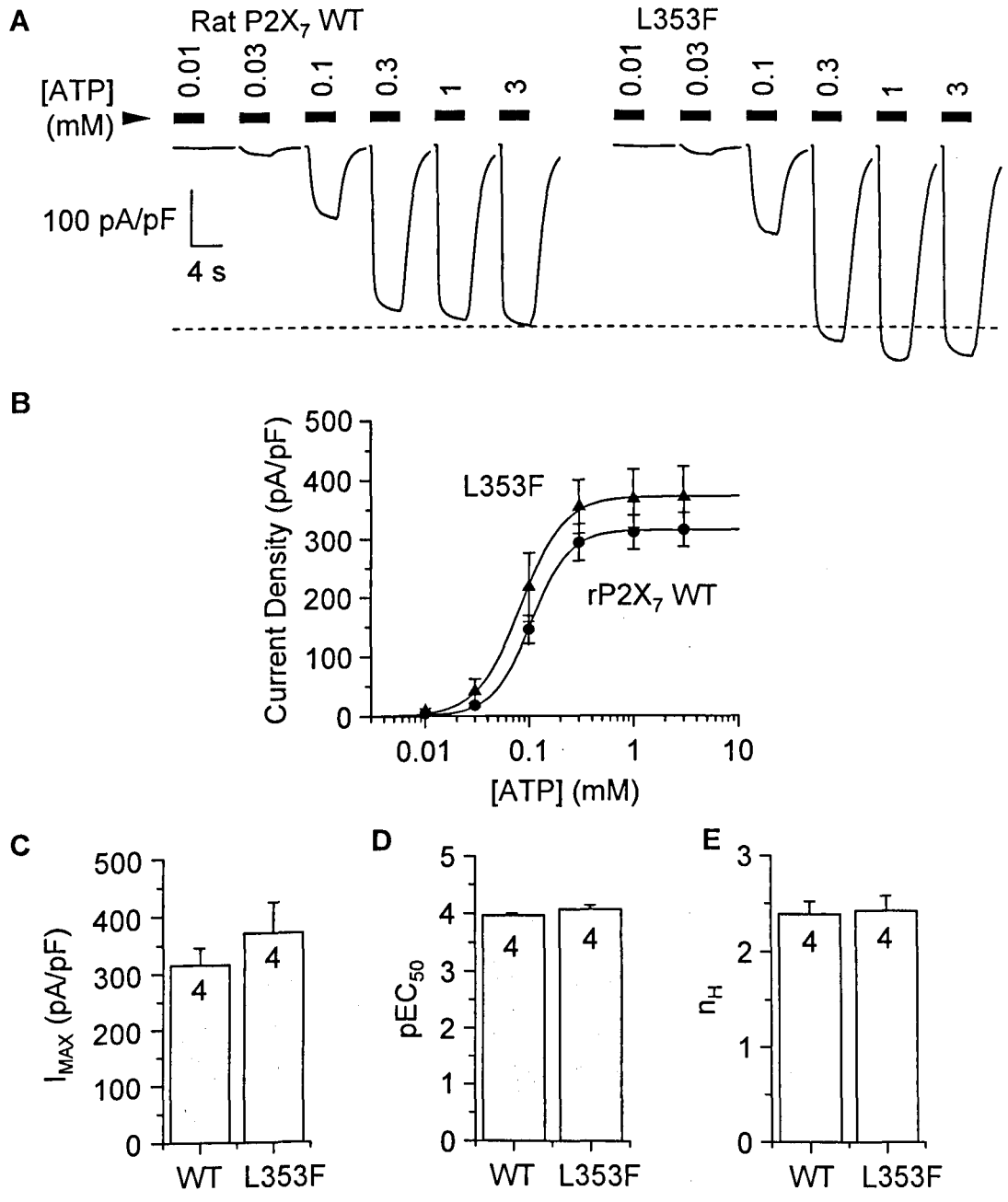

Figure 5.4 Effect of the L353F mutation in the rat $P2X_7$ receptor on ATP-evoked currents

(A) Representative ATP-evoked currents recorded from a HEK293 cell expressing WT (left) or L353F mutant rat $P2X_7$ receptors (right) at -60 mV. The dashed line indicates the maximal current for the WT receptor. (B) Mean ATP dose-response curve summarising the data from experiments shown in A: WT (squares) or L353F (triangles). Smooth lines show the best fits to the Hill equation. (C-E) Mean maximal current amplitudes (I_{MAX}), pEC_{50} and Hill coefficients. The number of cells recorded is indicated. No significant differences, compared to WT.

5.3 Discussion

In this chapter, the non-conserved residues in the microdomains surrounding residues His^{155} and Ala^{348} (Figure 5.1) in human $P2X_7$ receptor were investigated by individually mutating to the corresponding residues in rat $P2X_7$ receptor.

Among the six mutations introduced in the microdomain surrounding His^{155} of human $P2X_7$ receptor, V153I, G157Q and Q159R led to a significant reduction in the amplitude of maximal ATP-induced currents (Figure 5.2), suggesting Val^{153}, Gly^{157} and Gln^{159}, as well as His^{155}, in this microdomain are important for the human $P2X_7$ receptor functional expression. However, unlike H155Y, none of these six mutations increased the maximal current amplitude. Together, these results demonstrate that residue at position 155 has a unique role in this microdomain in contributing to the difference in functional expression between human and rat $P2X_7$ receptors.

For the four mutations in the microdomain close to Ala^{348}, F353L was interesting as, similar to A348T, this mutation conferred a significant increase in the amplitude of ATP-evoked maximal currents mediated by human $P2X_7$ receptor (Figure 5.3). However, the reciprocal mutation, L353F, did not alter the amplitude of ATP-induced maximal currents mediated by the rat $P2X_7$ receptor (Figure 5.4). Therefore, Leu^{353} is important for human $P2X_7$ receptor function, but it has little contribution to the species difference in $P2X_7$ receptor function between human and rat species. Furthermore, D356N mutation of the human $P2X_7$ receptor had the opposite effect to A348T, and decreased the maximal currents (Figure 5.3). Therefore, Asp^{356} also plays a role in determining the human $P2X_7$ receptor function.

Another approach to studying the contribution of the two microdomains to human $P2X_7$ receptor function and to the species differences between human and rat $P2X_7$ responses would be to use chimeras in which residues Val^{153} to Gln^{159} or Ala^{348} to Asp^{356} of the human $P2X_7$ receptor are replaced with the corresponding residues of the rat receptor. This would allow the contribution of the entire microdomains to the species-specific functional expression of the $P2X_7$ receptor to be determined. This technique, in conjunction with point mutations, proved useful in determining that Asn^{284} of the rat $P2X_7$ receptor accounts for the difference in ATP sensitivity between rat and mouse species,

and that Lys^{127} and Asn^{284} account for the differences in BzATP sensitivity (Young *et al.*, 2007).

In summary, the study presented in this chapter has identified residues Val^{153}, Gly^{157} and Gln^{159} in the microdomain surrounding His^{155} in the extracellular part and Phe^{353} and Asp^{356} close to Ala^{348} in TM2 are important for determining the human $P2X_7$ receptor function. However, none of the non-conserved residues in these microdomains contribute significantly to the species differences in ATP-evoked maximal currents or the functional expression of the $P2X_7$ receptors described in chapter 4.

Chapter 6

Effect of mutations at positions 155 and 348 on human and rat $P2X_7$ receptor protein expression

6.1 Introduction

The results presented in previous chapters show that H155Y and A348T mutations of the human $P2X_7$ receptor increase (chapter 3), whereas the reciprocal mutations Y155H and T348A of the rat $P2X_7$ receptor decrease (chapter 4), agonist-evoked maximal currents. The whole-cell currents are determined by the sum of the number of the functional receptors at cell surface (surface expression) and single channel conductance together with channel opening probability (single channel properties). Therefore, mutations of residues at these positions could alter surface expression of the $P2X_7$ receptor, or the single channel properties of the $P2X_7$ receptor, or both. In this chapter, the potential roles of the residues at positions 155 and 348 on the surface expression of human and rat $P2X_7$ receptor were investigated using immunocytochemistry and biotinylation.

6.2 Results

6.2.1. Effect of reciprocal mutations at position 155 on human and rat $P2X_7$ receptor protein expression and sub-cellular distribution

Both WT and mutant human and rat $P2X_7$ receptors contained a C-terminal EE tag. Thus the effect of mutations at position 155 on the sub-cellular localisation of human and rat $P2X_7$ receptors were studied by immunocytochemistry using an anti-EE antibody.

Figure 6.1 shows representative immunofluorescent confocal images. The immunoreactivity for the WT human $P2X_7$ receptor was diffuse throughout the cell, and for the WT rat receptor was more concentrated towards the cell surface. The H155Y mutant immunoreactivity was more concentrated towards the cell surface in comparison to WT. Conversely, the Y155H reciprocal mutation of the rat $P2X_7$ receptor reduced the surface localisation.

To further investigate the effect of mutations at position 155 on human and rat $P2X_7$ receptor total and surface expression, biotin labelling and Western blotting were performed. Figure 6.2 shows representative results. Strong expression of the WT receptor was consistently observed, and there was no detectable protein in cells transfected with the empty vector pcDNA3.1. WT and mutant $P2X_7$ receptors were co-expressed with eGFP, which was used as an internal control. Band sizes for eGFP were similar within experiments, indicating little variation in cell preparation, transfection efficiency, and sample handling. Biotin labelled eGFP was not detectable in any of the experiments, indicating that the biotin had not crossed the plasma membrane and labelled intracellular proteins. Both the human and rat $P2X_7$ receptor protein bands are close to the 58 kDa protein marker, and two protein bands are detected for the rat $P2X_7$ receptor (Figures 6.2A and B).

The H155Y mutation conferred a 74 ± 22% increase ($n = 5$; $p<0.001$; Figure 6.2D) in surface expression of the human $P2X_7$ receptor, and a 43 ± 8% increase ($n = 5$, $p<0.01$; Figure 6.2C) in total expression. The H155L mutation, which significantly decreased ATP-induced maximal currents of the human $P2X_7$ receptor (Figure 3.8), decreased both cell surface and total expression (Figure 6.2A). In contrast with the effect of H155Y in the human $P2X_7$ receptor, the reciprocal mutation Y155H of rat $P2X_7$ receptor decreased surface expression by 46 ± 2 % ($n = 4$; $p<0.01$; Figure 6.2D), and total expression by 27 ± 8 % ($n = 4$; $p<0.05$; Figure 6.2C).

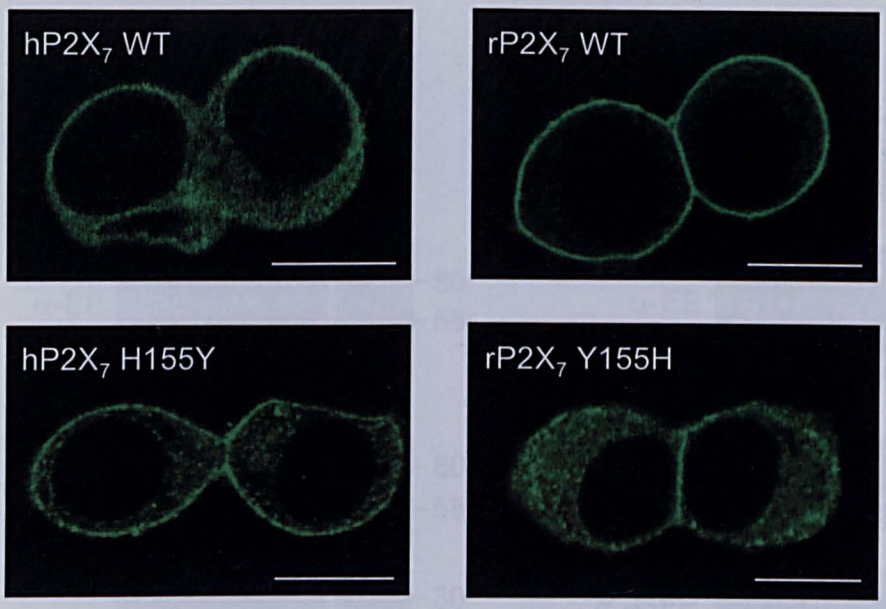

Figure 6.1 Effect of reciprocal mutations at position 155 on subcellular localisation of human and rat $P2X_7$ receptors

Representative immunofluorescent confocal images of HEK293 cells expressing the indicated EE-tagged WT or mutant human ($hP2X_7$) and rat ($rP2X_7$) $P2X_7$ receptors. The scale is 10 μm. Similar results were observed in three independent experiments.

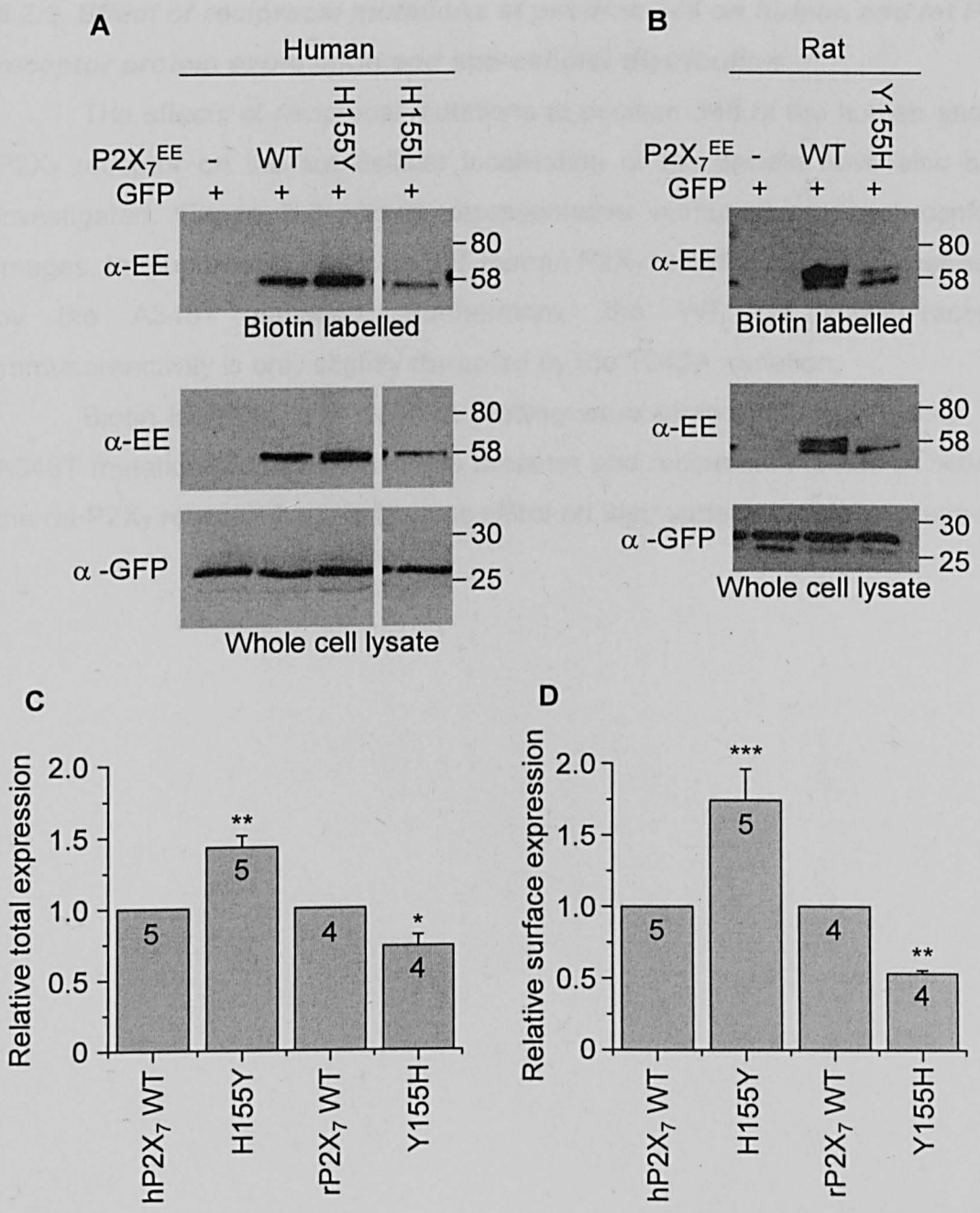

Figure 6.2 Effect of mutations at position 155 on surface and total protein expression of human and rat $P2X_7$ receptors

(A) and (B) Representative Western blots showing biotin labelled (surface) and whole-cell lysate (total) protein of the human ($hP2X_7$; A) or rat ($rP2X_7$; B) receptors. Total protein expression of GFP is also shown. Numbers on the right in each panel indicate the protein markers (kDa). (C) and (D) Relative total and surface expression of human (C) and rat (D) $P2X_7$ receptors, calculated from measurements of band intensities and normalised to that of the respective WT receptors in parallel experiments. The numbers in the bars indicate the number of experiments. * $p<0.05$, ** $p<0.01$ and ***, $p<0.001$, compared to WT.

6.2.2. Effect of reciprocal mutations at position 348 on human and rat $P2X_7$ receptor protein expression and sub-cellular distribution

The effects of reciprocal mutations at position 348 of the human and rat $P2X_7$ receptor on the sub-cellular localisation of the protein have also been investigated. Figure 6.3 shows representative immunofluorescent confocal images. Immunoreactivity for the WT human $P2X_7$ receptor is largely unaffected by the A348T mutation. Furthermore, the WT rat $P2X_7$ receptor immunoreactivity is only slightly disrupted by the T348A mutation.

Biotin labelling and Western blotting were performed (Figure 6.4). The A348T mutation of the human $P2X_7$ receptor and reciprocal mutation T348A of the rat $P2X_7$ receptor had no obvious effect on their surface or total expression.

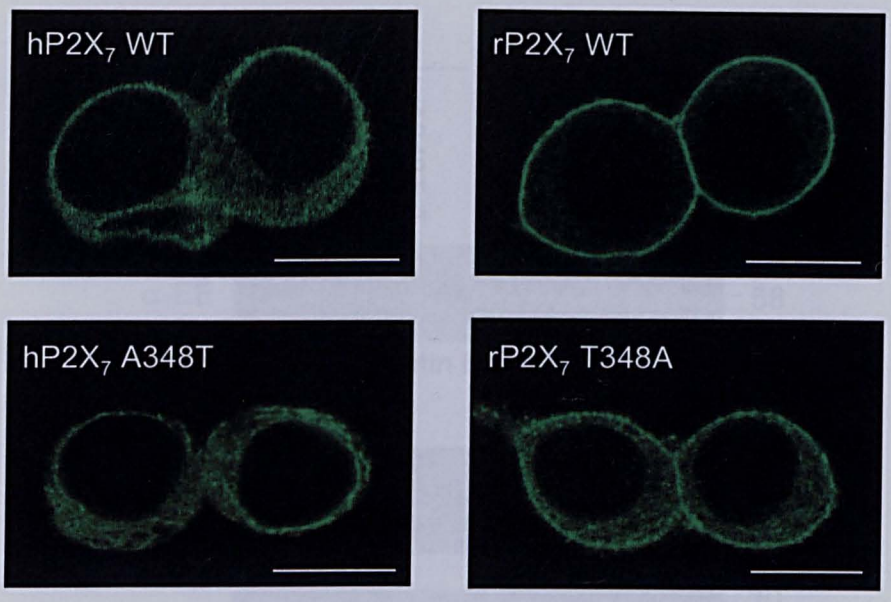

Figure 6.3 Effects of reciprocal mutations at position 348 on sub-cellular localisation of human and rat $P2X_7$ receptors

Representative immunofluorescent confocal images of HEK293 cells expressing the EE-tagged WT or mutant human ($hP2X_7$) and rat ($rP2X_7$) receptors. The scale is 10 μm. Similar results were observed in three independent experiments.

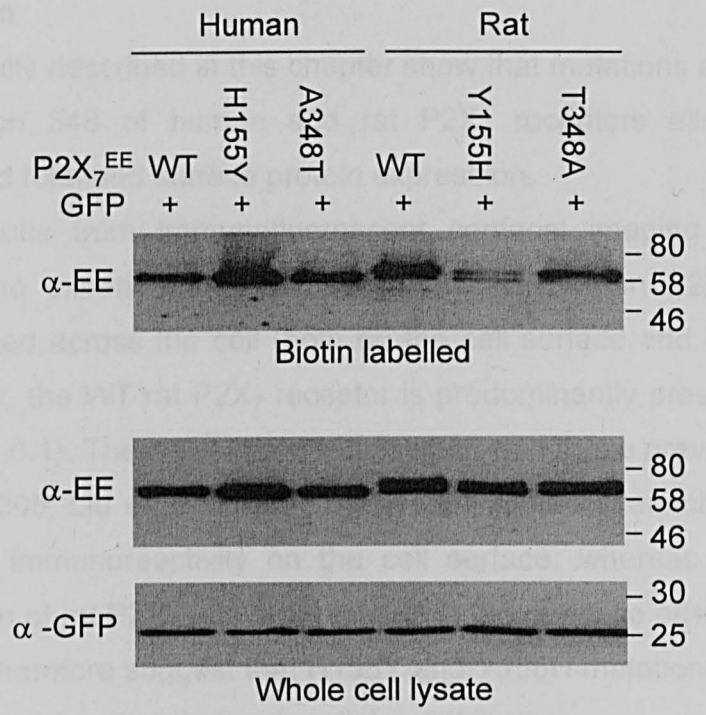

Figure 6.4 Effects of mutations at position 348 on surface and total protein expression of human and rat $P2X_7$ receptors

Representative Western blots showing biotin labelled (surface) and whole-cell lysate (total) protein of the WT or mutant human and rat $P2X_7$ receptors using an anti-EE antibody. Total protein expression of GFP is also shown. Numbers on the right in each panel indicate the protein markers (kDa). Representative of 2 experiments.

6.3. Discussion

The results described in this chapter show that mutations at position 155, but not position 348 of human and rat $P2X_7$ receptors alter sub-cellular localisation, and total and surface protein expression.

The results from immunofluorescent confocal imaging indicate that, under the same experimental conditions, the WT human $P2X_7$ receptor is evenly distributed across the cell (both on the cell surface and inside the cell) and, in contrast, the WT rat $P2X_7$ receptor is predominantly present on the cell surface (Figure 6.1). These results are consistent with those previously reported (Jiang *et al.*, 2005; Liu *et al.*, 2008). The H155Y mutation enriched the human $P2X_7$ receptor immunoreactivity on the cell surface, whereas the reciprocal Y155H mutation of rat $P2X_7$ receptor resulted in the opposite effect (Figure 6.1). These results therefore suggest that H155Y and Y155H mutations of the human and rat $P2X_7$ receptor alter their sub-cellular distribution.

In separate biotin labelling experiments, the H155Y mutation significantly increased surface expression of the human $P2X_7$ receptor, whereas the reciprocal mutation Y155H conferred a decrease in surface expression of the protein (Figure 6.2). These results provide consistent evidence suggesting that residue at position 155 is important in determining surface expression of the human and rat $P2X_7$ receptors. This appears to be, at least in part, due to changes in total protein expression, because Western blotting analysis showed that H155Y mutation of human $P2X_7$ receptor enhanced, whereas Y155H mutation of rat $P2X_7$ receptor reduced total protein expression, and to a comparable degree to surface expression. Thus, the change in total and particularly surface expression provides a reasonable explanation for the opposite effects resulting from reciprocal mutations of residue at position 155 on ATP-induced maximal current responses that are described in chapters 4 and 5. In addition, H155L mutation of the human $P2X_7$ receptor, which confers reduction in functional expression (Figure 3.8), attenuated the total and surface protein expression (Figure 6.2). This result provides further supporting evidence. It is worth mentioning the finding that the H155Y mutation of the human $P2X_7$ receptor increases surface expression of the protein is in disagreement with a previous study reporting no change in surface expression of H155Y mutant of the human $P2X_7$ receptor using flow cytometry (Cabrini *et*

al., 2005). Such differences may be due to the different assays used, which have different detection sensitivities.

Further experiments are required to determine the underlying mechanisms resulting in altered protein and surface expression conferred by mutations at position 155. Experiments should be performed to investigate possible changes in transcription and translation, protein folding and quality control in the ER and degradation, which contribute to total protein expression, as well as forward trafficking and endocytic retrieval that are important in determining the sub-cellular distribution and surface expression. For example, deletion mutation of Phe^{508} of CFTR (cystic fibrosis transmembrane conductance regulator) results in a dramatic reduction in total protein expression, due to protein misfolding in the ER and rapid degradation, and thereby surface expression (Cyr, 2005). The effects of mutating residue 155 could also change the single channel properties of the receptor. Although such a possibility cannot be completely ruled out, the contribution should be at most minor, considering the location of residue 155 is away from the ATP binding site, the channel gate and the ion conducting pore (Figure 3.1) (Kawate *et al.*, 2009; Roger *et al.*, 2010a)).

This study has shown that reciprocal mutations at position 348 of human and rat $P2X_7$ receptors have little detectable effect on receptor sub-cellular distribution (Figure 6.3). Furthermore, these mutations had little effect on the total and surface expression of the protein (Figure 6.4). Therefore, the changes in agonist-induced maximal current amplitudes conferred by these mutations (chapters 3 and 4) cannot be attributed to changes in surface expression of the protein. According to the model of the human $P2X_7$ receptor (Figure 3.1), residue 348 is located in TM2, and on the intracellular side of the ion channel gate. Considering this location, the next logical step would be to assess the single channel properties these mutants.

In this study, the $P2X_7$ receptor had a lower molecular weight (~58 kDa) than reported in the literature (~70-78 kDa) (Collo *et al.*, 1997; Sim *et al.*, 2004; Young *et al.*, 2007). An inaccuracy in the protein marker used in this study may be a possible reason for the discrepancy. The $P2X_7$ receptor is glycosylated (Young *et al.*, 2007; Lenertz *et al.*, 2010), and the two protein bands detected for the rat $P2X_7$ receptor may reflect two different glycosylation states of the receptor (Figure 6.2).

In conclusion, the results in this chapter support a significant role of residue at position 155 in determining the surface expression of the $P2X_7$ receptor, particularly human and rat $P2X_7$ receptors, and show that residue at position 348 have no or little effect on surface expression.

Chapter 7

Functional characterisation of the monkey $P2X_7$ receptor

7.1 Introduction

$P2X_7$ receptors are an attractive therapeutic target due to their role in release of the pro-inflammatory cytokine IL-1β, and their critical involvement in for example, inflammatory, neuropathic pain and rheumatoid arthritis (Chessell *et al.*, 2005; Ferrari *et al.*, 1997a; Labasi *et al.*, 2002; Solle *et al.*, 2001). Pharmaceutical industries are therefore making huge efforts to develop novel, highly potent and selective $P2X_7$ receptor antagonists (Donnelly-Roberts and Jarvis, 2007; Gunosewoyo and Kassiou, 2010). However, a number of compounds, including KN-62 and AZ11645373, show species specificity in inhibition of $P2X_7$ receptor responses (see sections 1.6.5 and 1.6.10) (Donnelly-Roberts *et al.*, 2009; Humphreys *et al.*, 1998; Stokes *et al.*, 2006). These species differences are useful in identifying the regions of the receptor that are important in $P2X_7$ receptor sensitivity to antagonists. More precisely, mutation of residue 95 of the human $P2X_7$ reduces sensitivity of the human $P2X_7$ receptor to KN-62 (Michel *et al.*, 2008). Furthermore, there are species differences in the potency and maximal responses to agonists (chapter 4 and section 1.6.10). However, the species-specificity of $P2X_7$ ligands is problematic as it hinders the development of compounds to treat human diseases based on rodent $P2X_7$ receptors or rodent disease models.

The human, rat, mouse, guinea pig and dog $P2X_7$ receptors have previously been cloned and their pharmacological properties characterised (Chessell *et al.*, 1998; Fonfria *et al.*, 2008; Rassendren *et al.*, 1997; Roman *et al.*, 2009; Surprenant *et al.*, 1996). Of these species, the human $P2X_7$ receptor shares the highest sequence homology of 85% to the dog $P2X_7$ receptor (Roman *et al.*, 2009). It is expected that primate $P2X_7$ receptors will share even higher sequence homology with the human $P2X_7$ receptor.

In this study, the monkey $P2X_7$ receptor has been characterised in terms of its sensitivity to agonists (ATP and BzATP) and antagonists (KN-62, AZ11645373 and A-438079). Comparisons between human and monkey responses have been made to determine whether their pharmacological profiles are similar between these species.

7.2 Results

7.2.1 Sequence similarity between monkey and other $P2X_7$ receptors

The monkey $P2X_7$ receptor is predicted to comprise of 595 amino acid residues. Figure 7.1 shows the sequence of the monkey $P2X_7$ receptor aligned with those of mammalian $P2X_7$ receptors that have previously been cloned (Chessell *et al.*, 1998; Fonfria *et al.*, 2008; Rassendren *et al.*, 1997, Roman *et al.*, 2009; Surprenant *et al.*, 1996). The monkey $P2X_7$ receptor shows the highest sequence similarity to the human $P2X_7$ receptor (96%; Table 7.1). Indeed, only 19 amino acids are different between these two species, five of which are in the extracellular domain where the agonist or antagonist binds (Figure 7.1). Chapters 4, 5 and 6 have investigated the contribution of residues at positions 155 and 348 to the species differences in the functional expression of human and rat $P2X_7$ receptors. Like the rat $P2X_7$ receptor, the monkey $P2X_7$ receptor has a tyrosine at 155 (Tyr^{155}) and a threonine at position 348 (Thr^{348}). The following experiments were designed to determine the pharmacological properties of the monkey $P2X_7$ receptor, and comparisons were also made to the properties of the human $P2X_7$ receptor.

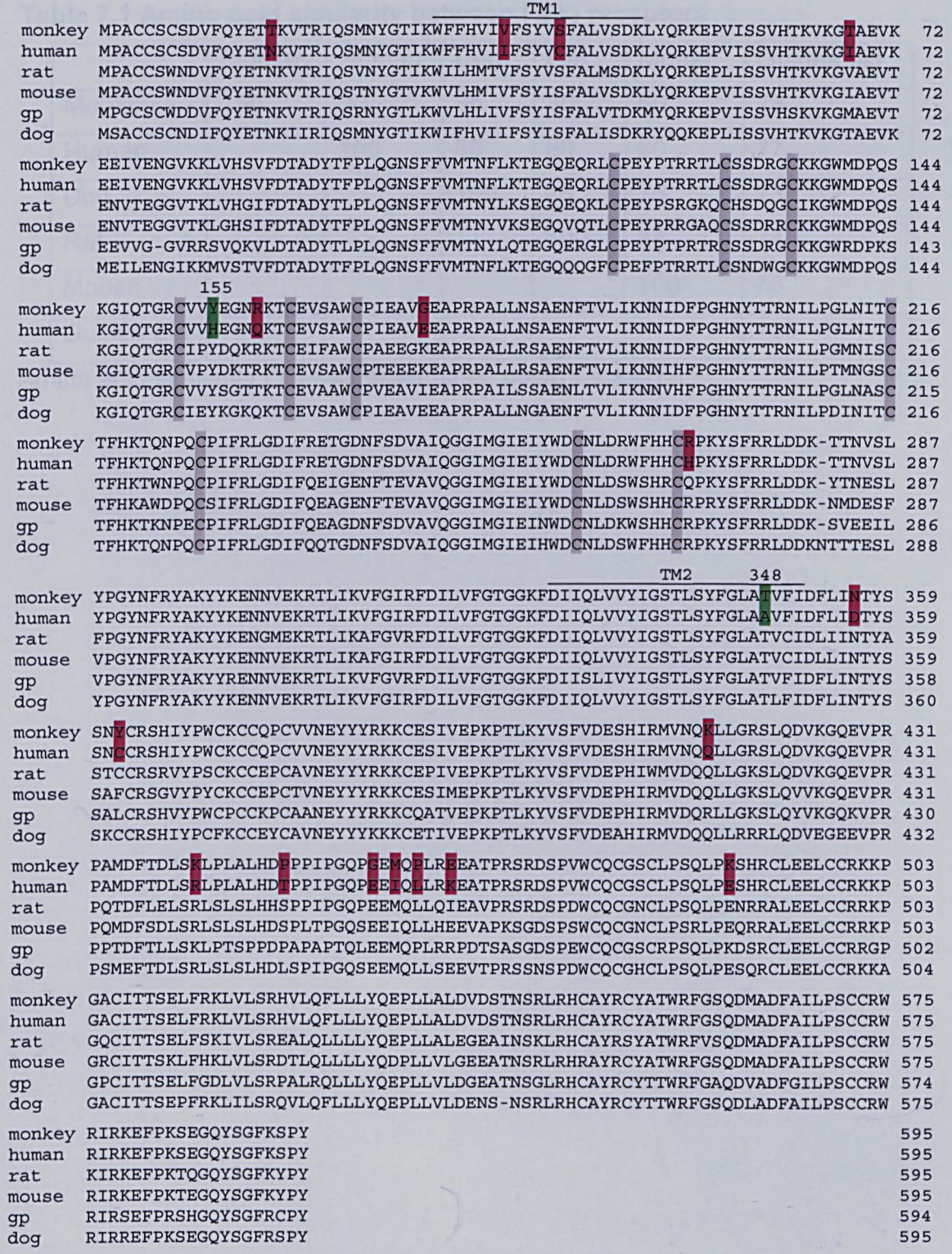

Figure 7.1 Amino acid sequence alignment of monkey, human, rat, mouse, guinea pig and dog $P2X_7$ receptors

Conserved cysteines are in grey, residues that differ between human and monkey are highlighted pink, and residues 155 and 348 are in green. TM1 and TM2 are indicated. The accession numbers for human, rat, mouse, guinea pig (gp) and dog are Y09561, X95882, AJ009823, EU275201 and EU334661, respectively. Aligned using ClustalW.

Table 7.1 Amino acid similarity between $P2X_7$ receptors

	Monkey	Human	Dog	Rat	Mouse	Guinea pig
Monkey	100	96	85	80	80	78
Human		100	85	80	80	77
Dog			100	76	76	73
Rat				100	84	74
Mouse					100	75
Guinea pig						100

Amino acid similarity (%) was determined using ClustalW.

7.2.2 Agonist-induced monkey $P2X_7$ receptor mediated currents

Firstly, cDNA encoding the monkey $P2X_7$ receptor was transfected into HEK293 cells, and agonist-evoked whole-cell currents were recorded in low divalent extracellular solution at -60 mV. Figure 7.2A shows representative inward currents induced by ATP and BzATP. Both ATP and BzATP activated the receptor dose-dependently. The receptor showed moderately fast activation and deactivation kinetics and little desensitisation during the 4 s agonist application. Dose-response analysis revealed that the EC_{50} for ATP was 802 ± 87 μM (n = 11), and for BzATP was 58 ± 4.2 μM (n = 6). BzATP was a significantly more potent agonist than ATP (pEC_{50} 4.24 ±0.03, n = 6 for BzATP, and 3.12 ± 0.04, n = 11 for ATP; $p < 0.001$; Figure 7.2D). The Hill coefficient was higher when BzATP was used as the agonist (1.23 ± 0.06, n = 11 for ATP, and 1.91 ± 0.08, n = 6 for BzATP; $p<0.001$; Figure 7.2E). The maximal amplitudes of currents evoked by ATP and BzATP were not significantly different (160 ± 22 pA/pF, n = 11 for ATP, and 220 ± 27 pA/pF, n = 4 for BzATP; $p>0.05$; Figure 7.2C).

The sensitivity of the monkey $P2X_7$ receptor to agonists was compared to that of the human $P2X_7$ receptor (Figures 7.3 and 7.4). The human $P2X_7$ receptor EC_{50} for ATP was 314 ± 24 μM, and the monkey $P2X_7$ receptor was significantly less sensitive to ATP than the human $P2X_7$ receptor (pEC_{50} 3.52 ± 0.04, n = 12 for human, and 3.12 ± 0.04, n = 11 for monkey; $p<0.001$; Figure 7.3C). The Hill coefficient was smaller for the monkey $P2X_7$ than the human $P2X_7$ receptor (1.92 ± 0.06, n = 12 for human; $p<0.001$; Figure 7.3D). ATP-induced maximal current amplitudes were larger for the human than the monkey P2X7 receptor (330 ± 22 pA/pF, n = 12 for human, and 160 ± 22 pA/pF, n = 11 for monkey; $p<0.001$).

The EC_{50} for BzATP was 30 ± 2.0 μM (n = 5) for human $P2X_7$ receptor, and the monkey $P2X_7$ receptor was slightly, yet significantly, less sensitive to BzATP than the human $P2X_7$ receptor (pEC_{50} 4.52 ± 0.03, n = 5 for human, and 4.24 ± 0.03, n = 6 for monkey; $p<0.001$; Figure 7.4C). There was no difference in the Hill coefficients (2.19 ± 0.16, n = 5 for the human $P2X_7$; $p>0.05$; Figure 7.4D). BzATP-induced maximal current amplitudes were not significantly different (310 ± 36 pA/pF, n = 5 for human, and 220 ± 27 pA/pF, n = 4 for monkey; $p>0.05$).

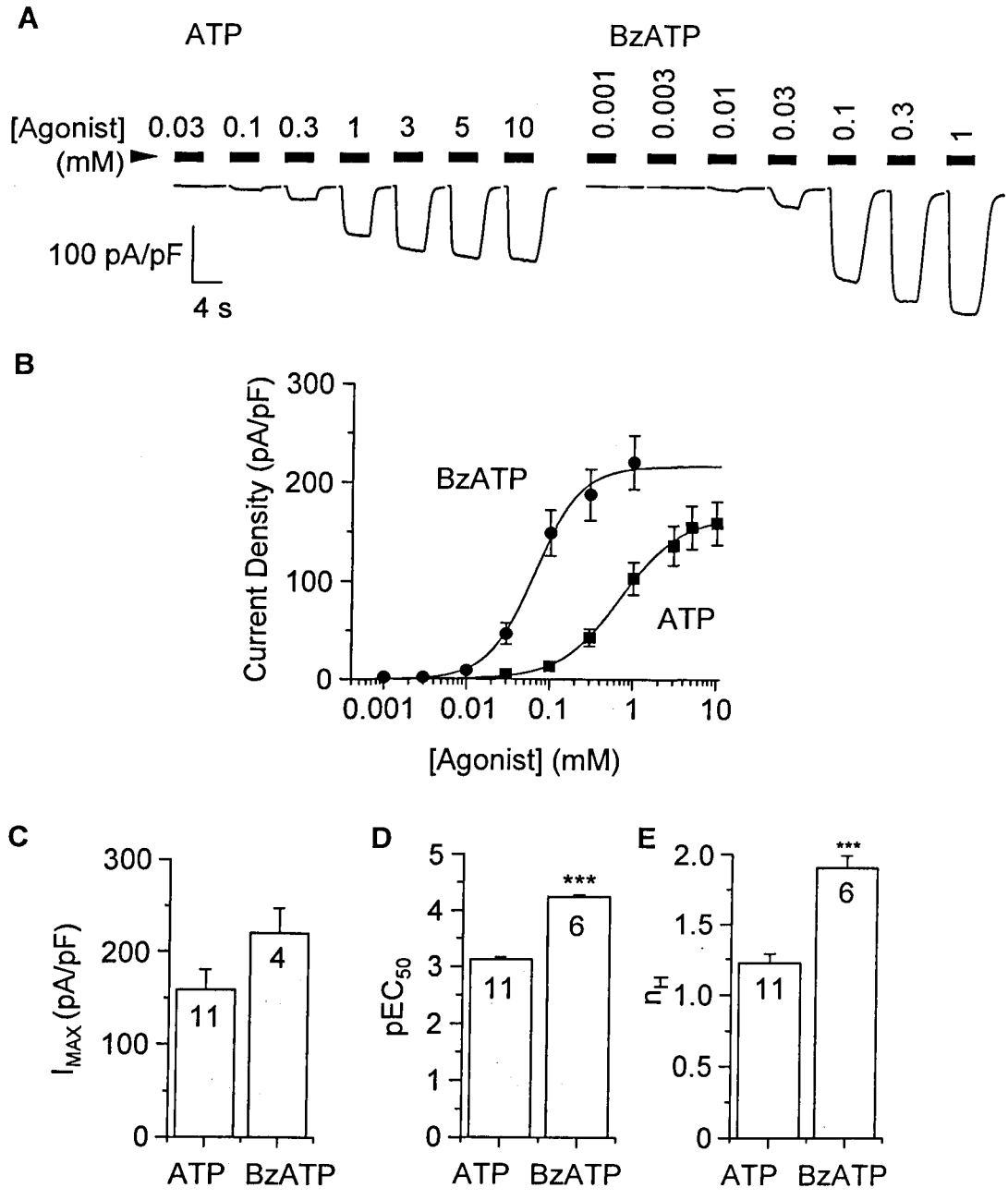

Figure 7.2 Agonist-evoked currents mediated by the monkey $P2X_7$ receptor

(A) Representative ATP- (left) and BzATP- (right) evoked currents recorded from a HEK293 cell expressing monkey $P2X_7$ receptors at -60 mV. (B) Mean dose-response curves summarising data from experiments shown in A: ATP (squares) or BzATP (circles). Smooth lines show the best fits to the Hill equation. (C-E) Mean maximal current amplitudes (I_{MAX}), pEC_{50} and Hill coefficients. The number of cells recorded is indicated. *** $p<0.001$, compared to ATP.

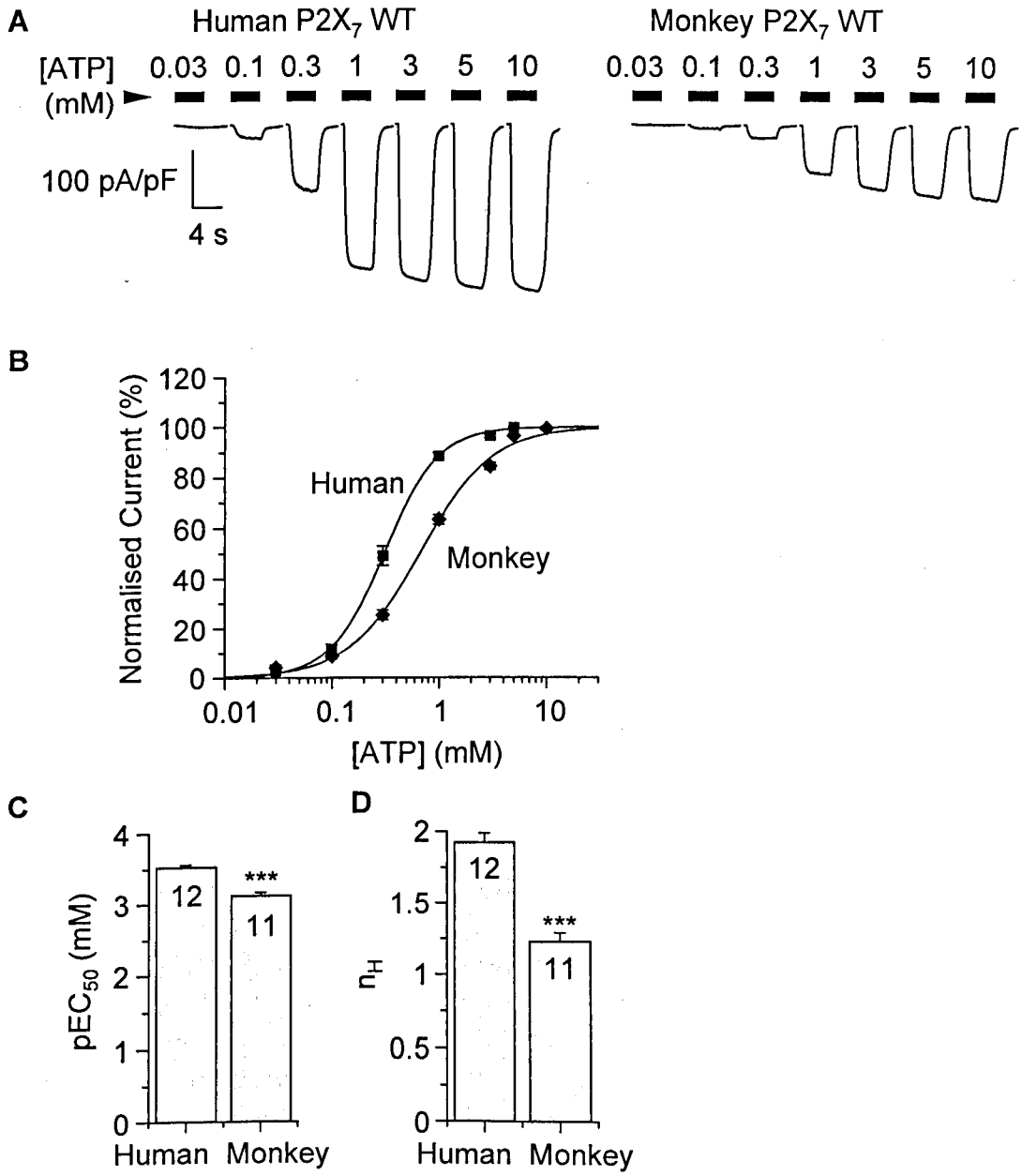

Figure 7.3 ATP-evoked monkey and human $P2X_7$ receptor mediated currents

(A) Representative ATP-evoked currents recorded from a HEK293 cell expressing human (left) or monkey (right) $P2X_7$ receptors at -60 mV. (B) Mean ATP dose-response curves summarising the data from experiments shown in A: human (squares) or monkey (diamonds). Smooth lines show the best fits to the Hill equation. (C-D) Mean pEC_{50} and Hill coefficients. The number of cells recorded is indicated. *** $p<0.001$, compared to human $P2X_7$.

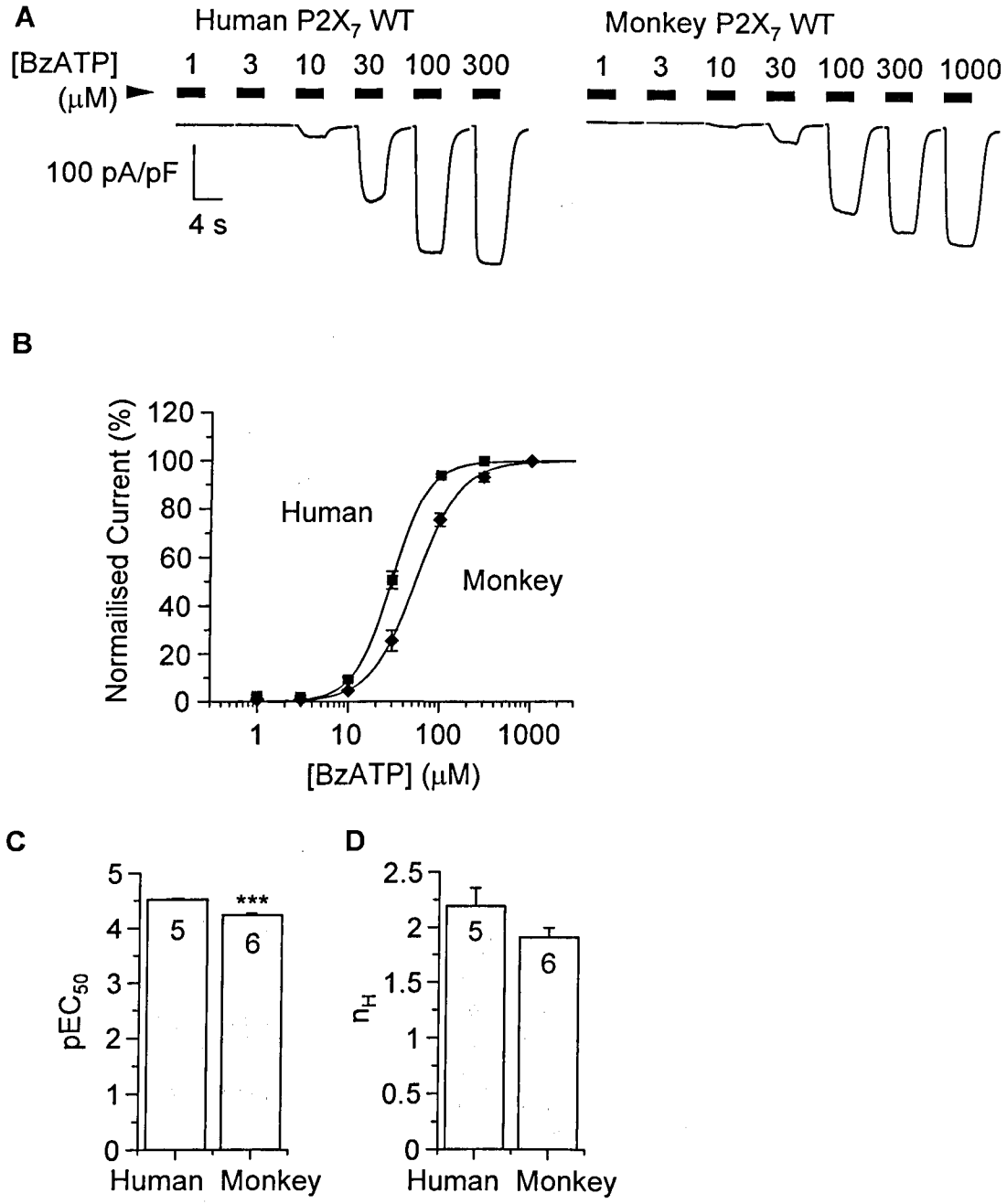

Figure 7.4 BzATP-evoked monkey and human $P2X_7$ receptor mediated currents

(A) Representative BzATP-evoked currents recorded from a HEK293 cell expressing human (left) or monkey (right) $P2X_7$ receptors at -60 mV. (B) Mean BzATP dose-response curves summarising the data from experiments shown in A: human (squares) or monkey (diamonds). Smooth lines show the best fits to the Hill equation. (C-D) Mean pEC_{50} and Hill coefficients. The number of cells recorded is indicated. *** $p<0.001$, compared to human $P2X_7$.

7.2.3 Inhibition of ATP-induced monkey $P2X_7$ receptor mediated currents by KN-62

The monkey $P2X_7$ receptor was also characterised in terms of its sensitivity to $P2X_7$ antagonists. KN-62 is a potent antagonist at human $P2X_7$ receptors (Humphreys *et al.*, 1998). KN-62 dose-dependently inhibited monkey $P2X_7$ receptor mediated currents and was largely irreversible following a 20 min washout (Figure 7.5A). However, the inhibition was noticeably incomplete; 16.8 ± 6.6% (n = 3) of ATP-induced current remained in the presence of the highest concentration of KN-62 used (3 μM). The data can be fit to the Hill equation using two parameters (see section 2.3.5), yielding an IC_{50} value of 86 ± 19 nM (n = 3; Figure 7.5B, grey line). However, because the inhibition is incomplete, it is more appropriate to fit using three parameters, resulting in an IC_{50} value of 54 ± 8.3 nM (n = 3; Figure 7.5B). However, there is no significant difference between the pIC_{50} values calculated using two or three parameters ($p>0.05$; Figure 7.5C).

Under the same experimental conditions, KN-62 was a potent antagonist of human $P2X_7$ receptor, with an IC_{50} value of 127 ± 38 nM (n = 3). The sensitivity to KN-62 is not significantly different between the monkey and human $P2X_7$ receptors (pIC_{50} 6.93 ± 0.12, n = 3 for human, and 7.28 ± 0.07, n = 3 for monkey; $p>0.05$; Figure 7.5C). There was no significant difference in the Hill coefficient between monkey and human $P2X_7$ receptors ($p>0.05$; Figure 7.5D).

To determine the nature of antagonism, monkey $P2X_7$ mediated ATP dose-current responses were recorded before and after a 4 min application of KN-62 (100 nM; Figure 7.6). The maximal current amplitude was significantly reduced (81 ± 1.2%; 192 ± 58 pA/pF for control, and 32 ± 7 pA/pF in the presence of KN-62, n = 3; $p<0.05$). The EC_{50} values were 0.68 ± 0.13 mM for control, and 0.46 ± 0.16 mM in the presence of KN-62 (n = 3). The sensitivity to ATP was not changed (pEC_{50} 3.18 ± 0.08 for control, and 0.40 ± 0.16 in the presence of KN-62, n = 3; $p>0.05$; Figure 7.6E). There was no significant difference in the Hill coefficients in the presence and absence of KN-62 (1.14 ± 0.02 for control, and 1.33 ± 0.22 in the presence of KN-62, n = 3; $p>0.05$; Figure 7.6F). These data point to KN-62 acting as a non-competitive antagonist at the monkey $P2X_7$ receptor.

The maximal current amplitude for the human $P2X_7$ receptor was also significantly reduced by the presence of KN-62 (344 ± 44 pA/pF for control, and

119 ± 18 pA/pF in the presence of KN-62, n = 6; $p<0.001$). However, the magnitude of inhibition was slightly less than for monkey $P2X_7$ receptors (65 ± 2.8%, n = 6; $p<0.01$; Figure 7.6D). The EC_{50} values were 0.28 ± 0.03 mM for control, and 0.25 ± 0.04 mM in the presence of KN-62 (n = 6). The sensitivity of the human $P2X_7$ receptors to ATP was unaffected by the presence of KN-62 (pEC_{50} 3.56 ± 0.06 for control, and 3.63 ± 0.06 in the presence of KN-62, n = 6; $p>0.05$; Figure 7.6E). The Hill coefficient was slightly reduced in the presence of KN-62 (1.83 ± 0.10 for control, and 1.43 ± 0.18 in the presence of KN-62, n = 6; $p<0.05$; Figure 7.6F).

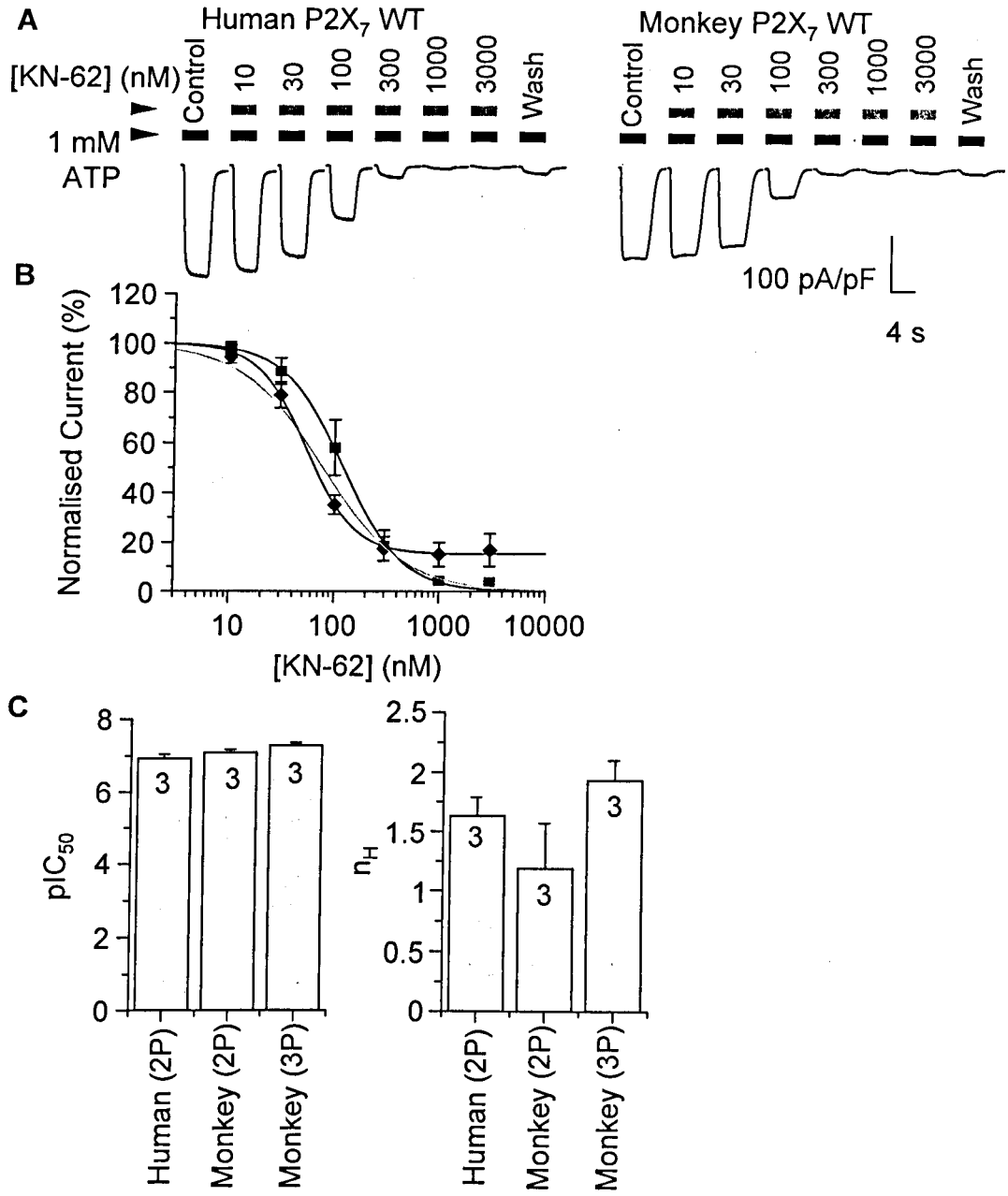

Figure 7.5 Inhibition of ATP-evoked monkey $P2X_7$ receptor currents by KN-62

(A) Representative ATP-evoked currents (1 mM ATP for human, 3 mM for monkey) recorded from a HEK293 cell expressing human (left) or monkey (right) $P2X_7$ receptors in the absence and presence of KN-62 at indicated concentrations at -60 mV (wash 20 min). (B) Mean KN-62 inhibition curve summarising the data from experiments in A: human (squares) and monkey (diamonds). Black smooth lines show the best fits to the Hill equation using 2 parameters (2P), and grey using 3 parameters (3P; for monkey $P2X_7$). (C-D) Mean pIC_{50} values and Hill coefficients from the data shown in B. The number of cells recorded is indicated. There are no differences among the three groups.

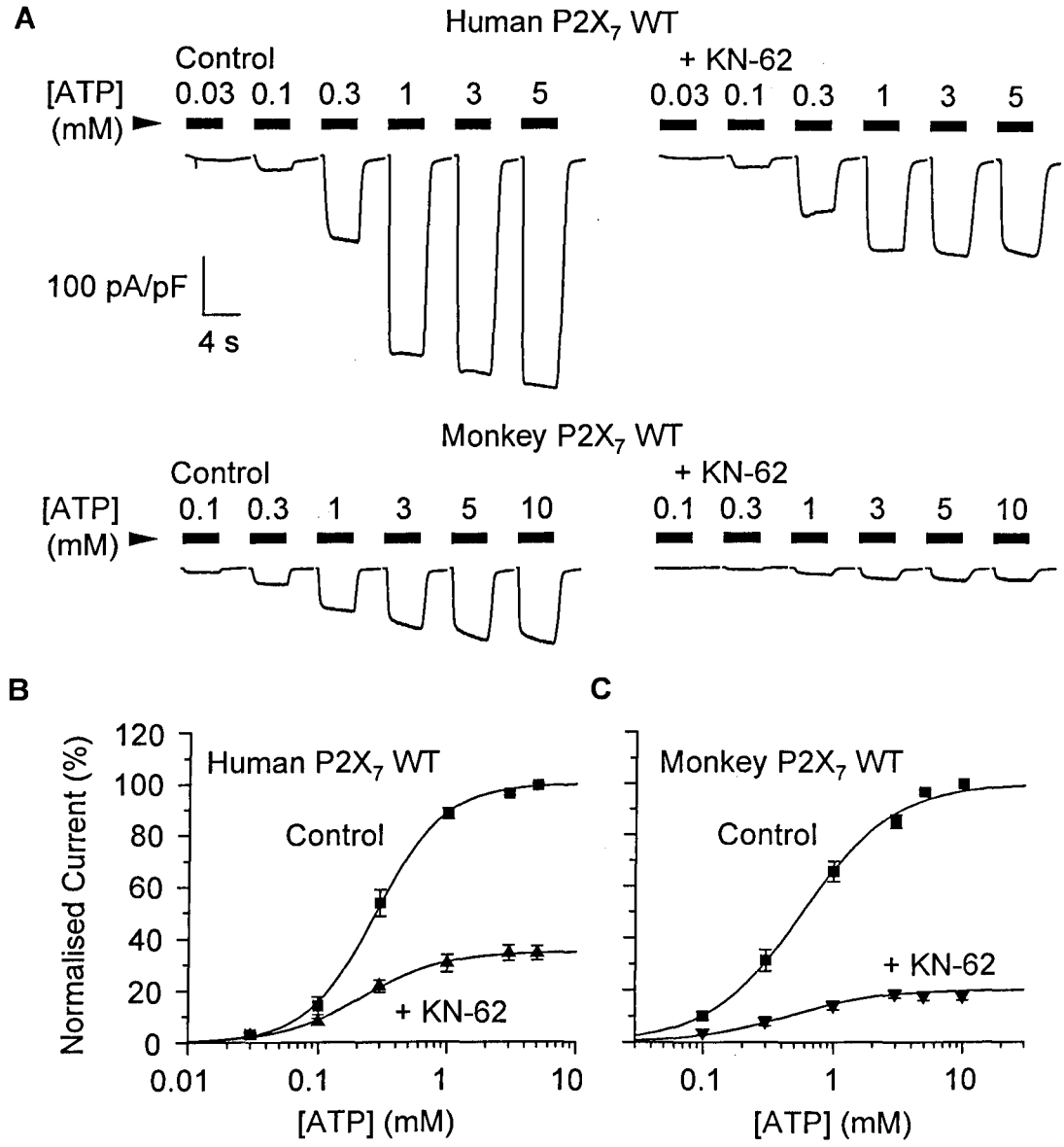

Figure continued on next page.

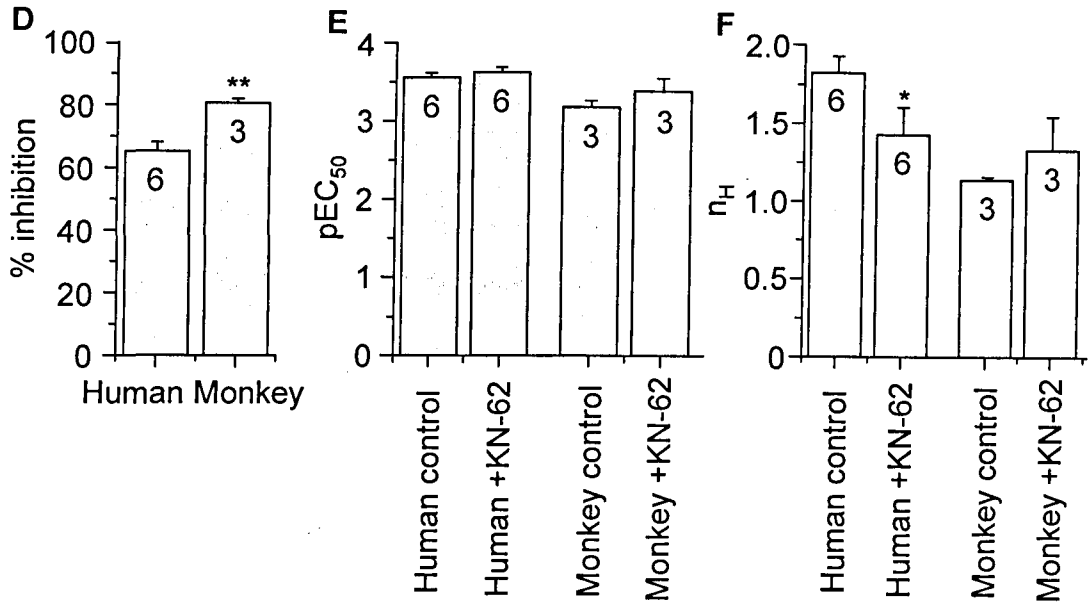

Figure 7.6 ATP-evoked human and monkey $P2X_7$ receptor mediated currents before and after of KN-62 treatment

(A) Representative ATP-evoked currents recorded from a HEK293 cell expressing human or monkey $P2X_7$ receptors before (left) and after (right) a 4 min application of 100 nM KN-62 at -60 mV. (B and C) Mean ATP dose-response curves summarising the data from experiments shown in A. Smooth lines show the best fits to the Hill equation. (D-F) Mean % inhibition, pEC_{50} and Hill coefficients. The number of cells recorded is indicated. In D: ** $p<0.01$, compared to human $P2X_7$. In E and F: * $p<0.05$ between control and presence of KN-62.

7.2.4 Inhibition of ATP-induced monkey $P2X_7$ receptor mediated currents by AZ11645373

Figure 7.7 shows that AZ11645373 was a potent antagonist inhibiting dose-dependently the ATP-induced currents (3 mM) in cells expressing monkey $P2X_7$ receptors (IC_{50} 23 ± 3.0 nM, n = 3). The compound also inhibited human $P2X_7$ receptor mediated currents with an equal potency to monkey $P2X_7$ currents (IC_{50} 31 ± 2.6 nM, n = 3) (pIC_{50} 7.52 ± 0.04, n = 3 for human, and 7.64 ± 0.06, n = 3 for monkey; $p>0.05$; Figure 7.7C). Inhibition was partly reversible following washout (Figure 7.7A).

To examine the mechanism of inhibition, the effect of AZ11645373 on ATP dose-response curves was determined (Figure 7.8). AZ11645373 (30 nM) dramatically reduced the maximal currents for monkey $P2X_7$ receptor (74 ± 8.1%; 214 ± 9 pA/pF for control, and 56 ± 19 pA/pF in the presence of AZ11645373, n = 3; $p<0.01$). The EC_{50} values were 0.70 ± 0.11 mM for control, and 1.67 ± 1.3 mM in the presence of AZ11645373 (n = 3). There was no effect on the receptor sensitivity to ATP (pEC_{50} 3.18 ± 0.08 for control, and 3.40 ± 0.16 in the presence of AZ11645373, n = 3; $p>0.05$; Figure 7.8E). The Hill coefficient was also unaffected (Figure 7.8F). AZ11645373 reduced the ATP-induced maximal current amplitude for human $P2X_7$ receptor (57 ± 12%; 329 ± 32 pA/pF for control, and 148 ± 52 pA/pF in the presence of AZ11645373, n = 3; $p<0.01$). The EC_{50} values for the human receptor were 0.29 ± 0.05 mM for control, and 0.36 ± 0.09 mM in the presence of AZ11645373 (n = 3). Moreover, the sensitivity of the human $P2X_7$ receptor to ATP was not changed by the presence of AZ11645373 (pEC_{50} 3.56 ± 0.06 for control, and 3.63 ± 0.06 in the presence of AZ11645373, n = 3; $p>0.05$; Figure 7.8E). The extent of inhibition of ATP-evoked maximal current amplitude by AZ11645373 was not significantly different between cells expressing human and monkey $P2X_7$ receptors ($p>0.05$; Figure 7.8D).

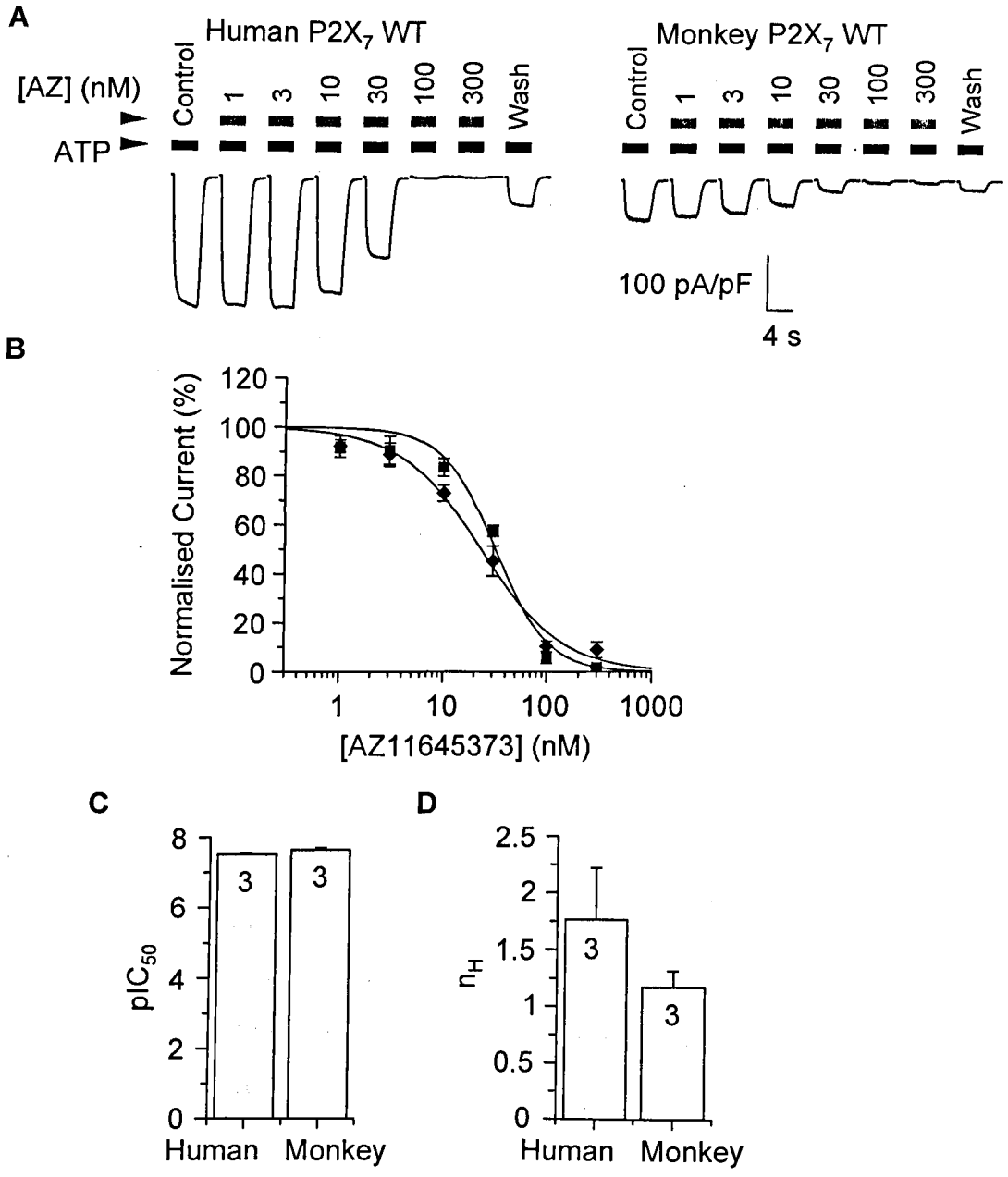

Figure 7.7 Inhibition of ATP-evoked monkey $P2X_7$ receptor currents by AZ11645373

(A) Representative ATP-evoked currents (1 mM ATP for human, 3 mM for monkey) recorded from a HEK293 cell expressing human (left) or monkey (right) $P2X_7$ receptors in the absence and presence of AZ11645373 at -60 mV (wash 15 min). (B) Mean AZ11645373 inhibition curve summarising the data from experiments shown in A: human (squares) and monkey (diamonds). Smooth lines show the best fits to the Hill equation. (C and D) Mean pIC_{50} and Hill coefficients. The number of cells recorded is indicated. No significant differences, compared to human $P2X_7$.

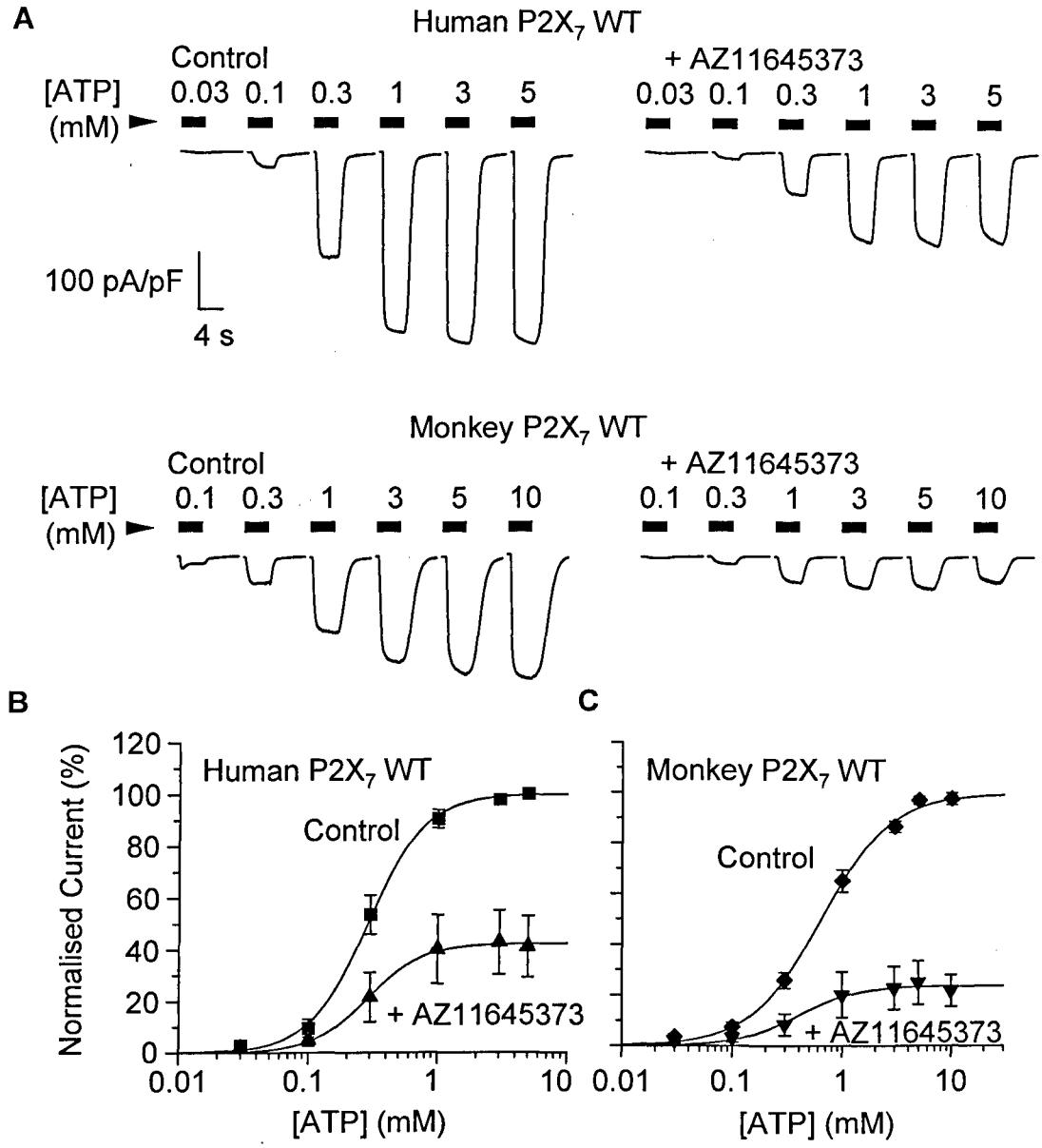

Figure continued on next page.

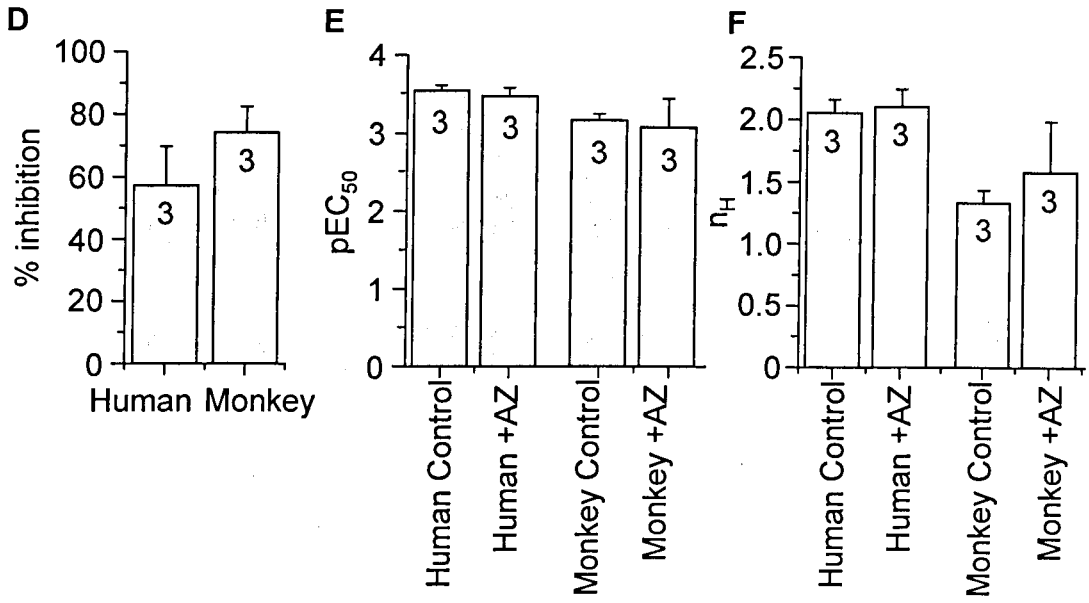

Figure 7.8 ATP-evoked human and monkey $P2X_7$ receptor mediated currents before and after of AZ11645373 treatment

(A) Representative ATP-evoked currents recorded from a HEK293 cell expressing human (top) or monkey (bottom) $P2X_7$ receptors at -60 mV before (control, left) and after (right) 4 min application of 30 nM AZ11645373 (AZ). (B and C) AZ11645373 inhibition curves summarising the data from experiments shown in A. Smooth lines show the best fits to the Hill equation. (D-F) Mean % inhibition, pEC_{50} and Hill coefficients. The number of cells recorded is indicated. In D: no difference, compared to human $P2X_7$. In E and F: no differences between control and presence of AZ11645373.

7.2.5 Inhibition of ATP-induced monkey $P2X_7$ receptor mediated currents by A-438079

A-438079 is reported as an antagonist at both human and rat $P2X_7$ receptors responses (McGaraughty *et al.*, 2007; Nelson *et al.*, 2006). The compound dose-dependently and completely inhibited ATP-evoked monkey $P2X_7$ receptor mediated currents (Figure 7.9). The monkey $P2X_7$ receptor was highly sensitive to A-438079 (IC_{50} 297 ± 24 nM, n = 6), and was equally potent at human $P2X_7$ receptors (IC_{50} 493 ± 94 nM, n = 6) (pIC_{50} 6.35 ± 0.09, n = 6 for human, and 6.53 ± 0.03, n = 6 for monkey; $p>0.05$; Figure 7.9C).

7.2.6 Total and surface expression of the monkey $P2X_7$ receptor

Monkey and human $P2X_7$ receptors contained a C-terminal EE tag. Therefore, biotin labelling and Western blotting were performed using an anti-EE antibody to assess total and surface expression of the monkey $P2X_7$ receptor. The expression of the human $P2X_7$ receptor was assessed for comparison. $P2X_7$ receptors were co-expressed with eGFP, used as an internal control for possible variations in cell preparation, transfection efficiency, and sample handling. Figure 7.10 shows representative results. There was significant surface and protein expression of the monkey $P2X_7$ receptor, and no obvious difference in the levels of expression between monkey and human $P2X_7$ receptors.

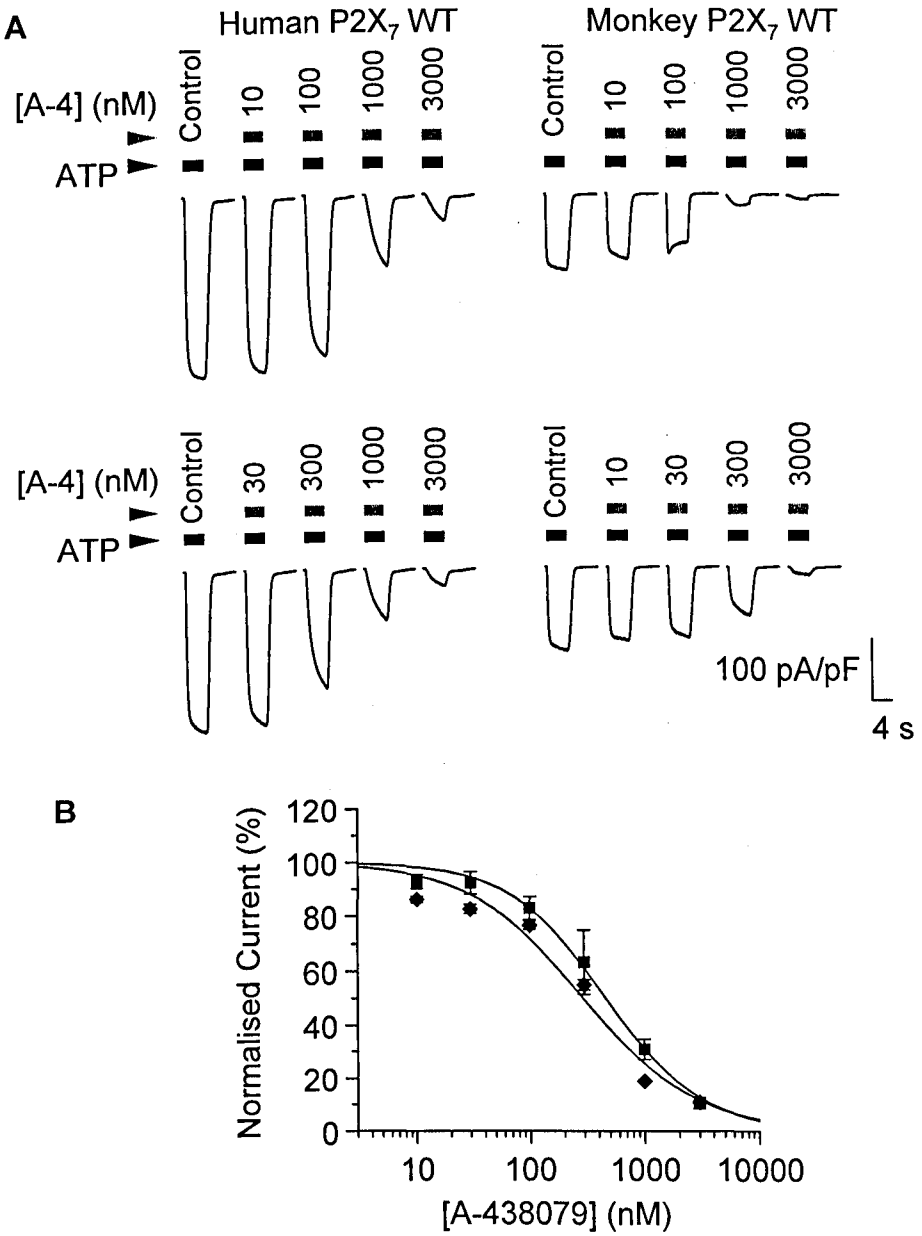

Figure continued on next page.

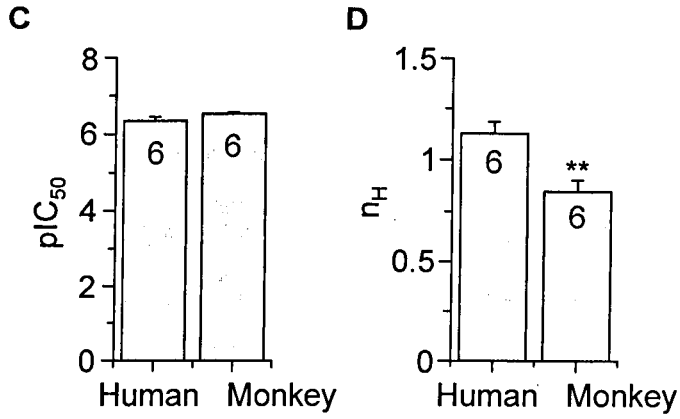

Figure 7.9 Inhibition of ATP-evoked monkey $P2X_7$ receptor currents by A-438079

(A) Representative ATP-evoked currents recorded from a HEK293 cell expressing human (left) or monkey (right) $P2X_7$ receptors in the absence and presence of A-438079 at -60 mV. (B) Mean A-438079 inhibition curve summarising the data from experiments shown in A: human (squares) and monkey (diamonds). Smooth lines show the best fits to the Hill equation. (C and D) Mean pIC_{50} and Hill coefficient. The number of cells recorded is indicated.

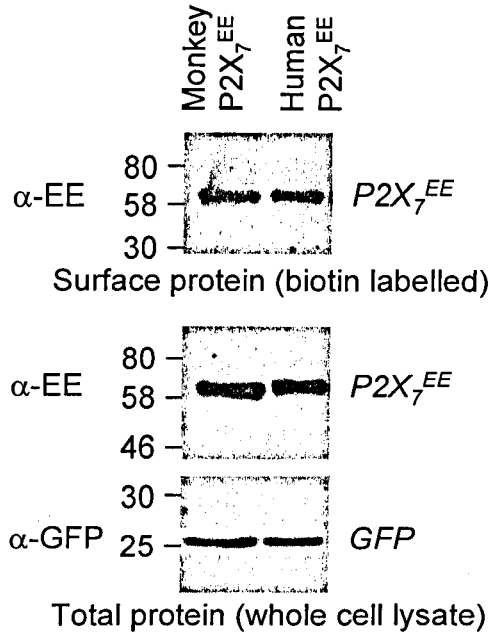

Figure 7.10 Total and surface expression of monkey $P2X_7$ receptors

Representative Western blots showing biotin labelled (surface) and whole-cell lysate (total) protein of the human or monkey $P2X_7$ receptors. Total protein expression of GFP is also shown. Numbers on the left in each panel indicate the protein markers (kDa). Similar results were observed in two independent experiments.

7.3 Discussion

This study found that both ATP and BzATP dose-dependently activate the monkey $P2X_7$ receptor (Figure 7.2). Furthermore, the receptor had a 14-fold higher sensitivity for BzATP over ATP. This was a significant finding because the higher potency of BzATP compared to ATP is a useful tool for distinguishing $P2X_7$ receptor mediated responses (Anderson and Nedergaard, 2006; North, 2002). The sensitivity of the monkey $P2X_7$ receptor to ATP and BzATP was slightly, yet significantly lower in comparison to human $P2X_7$ receptors (2.5- and 2-fold, respectively; Figures 7.3 and 7.4).

Human, rat, mouse, guinea pig and dog $P2X_7$ receptors have previously been characterised (Chessell *et al.*, 1998; Fonfria *et al.*, 2008; Rassendren *et al.*, 1997; Roman *et al.*, 2009; Surprenant *et al.*, 1996). The results from this study allow addition of the monkey $P2X_7$ receptor to this list of mammalian ATP- and BzATP-sensitive $P2X_7$ receptors (although the guinea-pig orthologues is relatively insensitive to BzATP) (Chessell *et al.*, 1998; Fonfria *et al.*, 2008; Rassendren *et al.*, 1997; Roman *et al.*, 2009; Surprenant *et al.*, 1996).

The present study has also provided insight into the antagonist pharmacology of the monkey $P2X_7$ receptor by investigating the sensitivity to KN-62, AZ11645373, and A-438079. It has been shown that KN-62 is a potent, nanomolar range inhibitor of ATP-induced currents mediated by monkey $P2X_7$ receptors, although the inhibition is incomplete (Figure 7.5). KN-62 inhibition of monkey $P2X_7$ receptor currents appeared to be non-competitive, evidenced by the insurmountable nature and lack of effect on the pEC_{50} for ATP (Figure 7.6). KN-62 was also shown to inhibit ATP-evoked currents mediated by the human $P2X_7$ receptor in the same concentration range, as previously reported (Humphreys *et al.*, 1998). The sensitivity of human and monkey $P2X_7$ receptors to KN-62 was virtually identical. Therefore, of the mammalian $P2X_7$ receptors functionally characterised, the rat $P2X_7$ receptor exhibits the lowest sensitivity to KN-62 (Donnelly-Roberts *et al.*, 2009; Hibell *et al.*, 2001; Humphreys *et al.*, 1998; Michel *et al.*, 2008; Roman *et al.*, 2009).

This work has also shown that AZ11645373 is a potent inhibitor of ATP-evoked monkey $P2X_7$ receptor currents in the high nanomolar range (Figure 7.7). The insurmountable nature of the inhibition and lack of effect on sensitivity to ATP indicates AZ11645373 is a non-competitive antagonist at the monkey $P2X_7$ receptor (Figure 7.8). The sensitivities of monkey and human $P2X_7$

receptors to AZ11645373 were identical. This is in agreement with a previous study, which found ATP- and BzATP-induced human $P2X_7$ receptor currents were potently inhibited by the compound (Stokes *et al.*, 2006). Furthermore AZ11645373 also acted as non-competitive antagonist at human $P2X_7$ receptors, in agreement with a previous studies showing non-surmountable inhibition of ATP-induced ionic currents, or ATP-induced Et^+ uptake mediated by the human $P2X_7$ receptor (Michel *et al.*, 2009; Stokes *et al.*, 2006). A previous study found AZ11645373 was an antagonist at dog $P2X_7$ receptors with a similar potency to the human receptor (Michel *et al.*, 2009). Moreover, the compound was an antagonist at mouse and guinea pig $P2X_7$ receptors, although with a lower potency. However, AZ11645373 a relatively low potency at rat $P2X_7$ receptors, with only 50% inhibition of BzATP-induced currents at 10 μM (Michel *et al.*, 2009; Stokes *et al.*, 2006).

In this study, A-438079 was a potent inhibitor of monkey $P2X_7$ receptor mediated currents (Figure 7.9). Furthermore, the monkey and human $P2X_7$ receptors were equally sensitive to inhibition by the compound. Unlike KN-62 and AZ11645373, A-438079 is an inhibitor of both the human and rat $P2X_7$ receptors (McGaraughty *et al.*, 2007; Nelson *et al.*, 2006).

Chapter 4 showed that the rat $P2X_7$ receptor has higher ATP-evoked maximal current amplitudes that the human receptor. It was shown that mutations H155Y and A348T (which change the amino acids to the corresponding one in the rat WT receptor) of the human $P2X_7$ receptor increased, whilst reciprocal mutations Y155H and T348A decreased agonist-evoked maximal current amplitudes. The WT monkey $P2X_7$ receptor, like the rat receptor, has tyrosine at position 155 (Tyr^{155}), and threonine at position 348 (Thr^{348}). Therefore, the finding that the ATP-induced maximal current amplitudes of the monkey $P2X_7$ receptor were significantly lower than the human was rather unexpected. The conclusion from chapter 6 was that the effect of H155Y and Y155H on maximal current amplitudes was at least in part due to changes in surface expression of the protein, and that changes in total protein expression contribute to this. However, the biotin labelling experiments shown in this chapter (Figure 7.10) found that the surface and total protein expression of human and monkey $P2X_7$ receptors were similar. Experiments to determine whether the residues at positions 155 and 348 are important in

determining the functional expression of the monkey $P2X_7$ receptor are required.

In conclusion, in terms of sensitivity to KN-62, AZ11645373 and A-438079, monkey $P2X_7$ receptors are virtually indistinguishable from human $P2X_7$ receptors. Sequence comparison showed that only 19 amino acids (5 in the extracellular domain) are different between the species orthologues (Figure 7.1). The results from this study therefore indicate that these 19 residues are not important for the antagonistic properties of these compounds at human and monkey $P2X_7$ receptors. The next step is to compare the antagonist profiles of monkey and dog $P2X_7$ receptors. By these systematic comparisons of antagonist profiles at different species orthologues, microdomains and residues that are important for antagonist binding could be identified. Furthermore, non-human primates have closer physiological, neurological and genetic similarities with humans than rodents, and therefore research is currently underway to develop transgenic non-human primate models for human diseases (Sasaki *et al.*, 2009; Yang *et al.*, 2008). The substantial similarities in the receptor pharmacology between monkey and human $P2X_7$ receptors shown in this study indicate the monkey could provide a good model for investigations into the roles of the $P2X_7$ receptors in human diseases.

Chapter 8

General discussion and conclusions

8.1 General discussion and conclusions

This study has provided information to improve the understanding of the mechanisms underlying the functional expression of $P2X_7$ receptors. WT or mutant $P2X_7$ receptors were expressed in HEK293 cells and the mutational effects were studied by whole-cell patch-clamp recording of agonist-evoked currents (results summarised in tables 8.1 and 8.2), and by assessing surface expression using immunostaining and biotin labelling. In this chapter, the main findings are summarised and discussed.

There are numerous ns-SNP mutations of the human $P2X_7$ receptor (Barden *et al*., 2006; Lucae *et al*, 2006; Wiley *et al.,* 2002). Two of these ns-SNP mutations, H155Y and A348T, are of particular interest because they confer gain-of-function in terms of agonist-induced currents (Roger *et al.*, 2010a; Stokes et al., 2010), Ca^{2+} influx (Cabrini et al., 2005) and dye uptake (Roger *et al.*, 2010a; Stokes et al., 2010), and were therefore further investigated in this thesis. These mutations increased the functional expression of the human $P2X_7$ receptor, as evidenced by greater ATP- and BzATP-evoked current amplitudes with no or small change in the agonist sensitivity (chapter 3). His^{155} and Ala^{348} in the human $P2X_7$ receptor were mutated to residues with different side chain properties. None of the residues introduced at His^{155} mimicked the gain-of-function effect of H155Y, however, in the cases of H155L and H155D, the ATP-evoked current amplitudes were reduced. Mutating Ala^{348} to bulky residues (A348M and A348F) decreased, whilst mutating to a small residue (A348G), increased the amplitude of ATP-evoked currents. Therefore, these results taken together with previous findings indicate that residues at 155 and 348 are important molecular determinants of functional expression of the human $P2X_7$ receptor.

These mutations were also of interest because they change the residues in the human $P2X_7$ receptor to the corresponding residues of the rat receptor. The results in chapter 4 have shown that ATP-evoked currents mediated by the rat $P2X_7$ receptor are larger than those by human $P2X_7$ receptors. Reciprocal mutations, Y155H and T348A, were introduced in the rat $P2X_7$ receptor and both mutations reduced the amplitude of ATP-evoked currents. The reciprocal mutations at 155 and 348 of human and rat $P2X_7$ receptors had opposite effects on BzATP-induced currents, as observed for ATP-induced currents. These results provide consistent evidence to show that residues at 155 and 348 are

important in determining the functional expression of human and rat $P2X_7$ receptors. In addition, the results suggest that the distinct residues at these two positions contribute to the difference in ATP-induced currents mediated by human and rat $P2X_7$ receptors.

It was shown in chapter 7 that the monkey $P2X_7$ receptor has smaller ATP-induced maximal current amplitudes than the human receptor. This was a surprising finding because the monkey $P2X_7$ receptor, like the rat $P2X_7$ receptor, has a tyrosine at position 155 (Tyr^{155}), and a threonine at position 348 (Thr^{348}). Further experiments are required to determine whether the particular residues at 155 and 348 are important in determining the functional expression of the monkey $P2X_7$ receptor.

The non-conserved residues in the microdomains surrounding positions His^{155} and Ala^{348} of the human $P2X_7$ receptor were investigated by mutating to the corresponding residues of the rat $P2X_7$ receptor (chapter 5). Four mutations, V153I, G157Q, Q159R and D356N reduced, whereas F353L increased, ATP-induced currents, indicating the importance of these residues in human $P2X_7$ receptor functional expression. The reciprocal mutation L353F was introduced into the rat $P2X_7$ receptor, however, the mutations conferred no significant effect on ATP-evoked currents. Therefore the residues 155 and 348 are unique in these microdomains in that the particular residues at these positions are important in determining the species differences between human and rat $P2X_7$ receptors.

There are three major mechanisms underlying changes in functional expression of an ion channel or agonist-induced currents. These are alterations to the single channel properties (open probability and conductance), and the number of functional receptors on the cell surface. A major advancement in the P2X receptor field was the determination of the zebrafish $P2X_4$ receptor crystal structure (Kawate *et al.*, 2009), which has greatly increased our understanding of the mechanisms underlying mutational effects on the receptor functions (Browne *et al.*, 2010, Evans, 2010; Young, 2010). A model of the human $P2X_7$ receptor, based on the zebrafish $P2X_4$ structure, indicates that His^{155} is located in the head region of the dolphin-like structure, and distant from the ion permeating pathway (Figure 3.1) (Kawate *et al.*, 2009; Roger *et al.*, 2010a), suggesting that this residue is unlikely to be critical in determining the single channel conductance. His^{155} is also away from the proposed agonist-binding

site. Consistent with such predictions, mutation of residue at 155 had little or minor effect on the sensitivity of both human and rat $P2X_7$ receptor to agonists (chapters 3 to 5). Furthermore, the human WT and H155Y mutant receptors are equally sensitive to KN-62, a potent human $P2X_7$ receptor antagonist (Humphreys *et al.,* 1998). These observations, taken together, strongly suggest mutations of residues at position 155 of $P2X_7$ receptors have little effect on the receptor conformation and channel gating properties. On the other hand, immunostaining and biotin labelling studies, shown in chapter 6, clearly demonstrated that H155Y mutation increased the expression level of human $P2X_7$ receptor at the cell surface, whilst reciprocal mutation Y155H decreased the membrane expression of rat receptor. The changes in surface expression appear to result from disrupted trafficking to the membrane as revealed by immunostaining, and altered total protein expression, as shown in Western blotting analysis. Furthermore, in comparison to WT, H155L mutation, which reduced ATP-evoked current amplitudes of the human $P2X_7$ receptor, had a reduced protein and surface expression. Therefore, the alterations in surface expression conferred by mutations at position 155 play a major role in determining the functional expression of $P2X_7$ receptors or the agonist-evoked currents. Further experiments are required to elucidate whether the effects of such mutations change protein folding and degradation. Additionally, it would be interesting to examine whether the mutations also affect the mechanisms of forward trafficking and endocytic retrieval.

The human $P2X_7$ receptor model predicts that Ala^{348} is located in the TM2 region, on the intracellular side of the ion channel gate (Figure 3.1) (Kawate *et al.,* 2009; Roger *et al.*, 2010a). TM2 forms the ion-permeating pathway, and residues on the intracellular side of the gate are proposed to undergo substantial movement during gating (Browne *et al.*, 2010; Kawate *et al.*, 2009). This concept is consistent with the observations described in this thesis (chapter 3) that the effects of mutating Ala^{348} in human $P2X_7$ receptors on ATP-evoked current amplitude were strongly dependent on the side chain size of the introduced residues. Immunostaining and biotin labelling showed that mutation A348T in the human $P2X_7$ receptor and reciprocal mutation T348A in rat $P2X_7$ receptor had little effect on the receptor surface expression (chapter 6). Taken together, these results suggest that residue 348 has an important role in defining the channel open probability and/or single channel conductance of

the $P2X_7$ receptor ion channel, and thereby ATP-induced currents. Single channel recording analysis of the WT and mutant receptors should provide direct evidence to confirm or refute such an interpretation.

The monkey $P2X_7$ receptor has been characterised of its pharmacological properties (chapter 7). ATP and BzATP activated the monkey $P2X_7$ receptor in a dose-dependent manner. Like human, rat, mouse and dog $P2X_7$ receptors, the monkey $P2X_7$ receptor is more sensitive to BzATP than ATP (Chessell *et al.*, 1998; Rassendren *et al.*, 1997; Roman *et al.*, 2009; Surprenant *et al.,* 1996). The monkey $P2X_7$ receptor was slightly, yet significantly less sensitive to ATP and BzATP than the human $P2X_7$ receptor, compared under the same experimental conditions. The sensitivity to $P2X_7$ receptor antagonists KN-62 (Humphreys *et al.*, 1998), AZ11645373 (Stokes *et al.,* 2006) and A-438079 (McGaraughty *et al.,* 2007; Nelson *et al.,* 2006) was also investigated. All three were potent antagonists at monkey $P2X_7$ receptors with IC_{50} values in the nanomolar range, and, in the case of AZ11645373 and A-438079, the inhibition was complete. Furthermore, the sensitivity of the monkey $P2X_7$ receptor to these compounds was not different from that of the human $P2X_7$ receptor. This receptor orthologue shares 96% amino acid sequence identity with the human $P2X_7$ receptors. There are 5 residues in the extracellular domain that are different between monkey and human $P2X_7$ receptors. Based on the results presented in this thesis, it can be concluded that these residues are not critically engaged in interacting with KN-62, AZ11645373 and A-438079. Additionally, the similar pharmacological profile of monkey and human $P2X_7$ receptors suggests that the monkey provides a good model for future studies of $P2X_7$ receptor involvement in human diseases. Non-human primates have closer physiological, neurological and genetic similarities with humans than rodents, and therefore research is currently underway to develop generate transgenic non-human primate models for human diseases (Sasaki *et al.*, 2009; Yang *et al.*, 2008).

In conclusion, the results presented in this thesis provide consistent and convincing evidence to suggest that residues at position 155 and 348 are important in determining the functional expression of human and rat $P2X_7$ receptors. Furthermore, the results suggest differential mechanisms underlie the contribution of these two residues; residue 155 is involved in determining surface expression of the $P2X_7$ receptor proteins, and residue 348 in single

channel properties of the $P2X_7$ receptors. The study has functionally characterised the pharmacological properties of the monkey $P2X_7$ receptor. Such information is useful in further studies to decipher the molecular basis underlying species-dependent properties. Comparisons made to human $P2X_7$ receptors have revealed similar agonist and antagonist properties between monkey and human $P2X_7$ receptors, suggesting that the monkey may provide a suitable model for the study of roles for $P2X_7$ receptors in human diseases.

8.2 Summary of future directions for the project

This work has increased our understanding of the expression and functional properties of human, rat and monkey $P2X_7$ receptors. However, there are a number of experiments that could be performed to enhance the conclusions that can be drawn, and these are summarised below.

In chapter 3 is was shown that the effects of mutating Ala^{348} of the human $P2X_7$ receptor on maximal current amplitude was dependent on the side chain size of the introduced residue, with larger side chains reducing and smaller side chains increasing maximal current amplitudes. According to the human $P2X_7$ receptor model (Figure 3.1), Ala^{348} is located in the TM2 domain of the receptor (Kawate *et al.*, 2009; Roger *et al.*, 2010a), and it was therefore hypothesised that mutation of Ala^{348} may affect the single channel properties of the human $P2X_7$ receptor. Single channel recording to assess the affect of mutation of Ala^{348} on single channel conductance and/or channel open probability of the human $P2X_7$ receptor would determine if this is indeed the case.

In chapter 6, it was shown using biotin labelling that the H155Y mutation of the human $P2X_7$ receptor increased, whilst the reciprocal mutation Y155H of the rat receptor decreased surface expression, and this appeared to be largely due to the changes in total protein expression. It would be useful to determine the mechanism by which mutation of residue 155 affects the total protein expression of the $P2X_7$ receptor. One possible mechanism is that the mutations affect the protein assembly in the ER. This could be tested by the use on BN-PAGE to determine whether the ratio of monomers: dimers: trimers is affected by mutations at position 155. Another possibility is changes in the level of protein degradation due to changes in rate of successful protein folding. Lower temperatures facilitate protein folding, and so cells could be incubated at a

lower temperature prior to Western blotting experiments to determine whether the total expression of the WT and mutant proteins are affected to a similar degree. For example, if the Y155H mutation of the rat $P2X_7$ receptor increases protein misfolding, it would be expected that a lower temperature would increase the total protein expression of the mutant.

The immunostaining experiments in chapter 6 showed that the WT rat $P2X_7$ receptor immunoreactivity was concentrated towards the cell surface, whereas the WT human receptor immunoreactivity was diffuse throughout the cell. It would be interesting to determine the subcellular compartments in which the human $P2X_7$ receptor is located. To achieve this, double immunostaining could be performed using markers for intracellular organelles, such as calreticulin (an ER protein marker), TGN46 (a *trans*-Golgi network protein marker), or LAMP1 (a lysosomal marker).

Based on the results shown in chapter 7, it can be concluded that the residues that are not conserved between human and monkey $P2X_7$ receptors are not critically engaged in interacting with KN-62, AZ11645373 and A-438079. The next step is to compare the antagonist profiles of monkey and dog $P2X_7$ receptors, which share 85% amino acid identity. This systematic comparison of antagonist profile between species will allow microdomains and residues important for antagonist binding to be identified.

The WT monkey $P2X_7$ receptor, like the rat receptor, has tyrosine at position 155 (Tyr^{155}), and threonine at position 348 (Thr^{348}). The finding that the ATP-induced maximal current amplitudes of the monkey $P2X_7$ receptor were significantly lower than the human was rather unexpected. It was shown in chapter 4 that mutations H155Y and A348T (which change the amino acids to the corresponding one in the rat WT receptor) of the human $P2X_7$ receptor increased, whilst reciprocal mutations Y155H and T348A decreased agonist-evoked maximal current amplitudes. Experiments to determine the effects of Y155H and T348A mutations of the monkey $P2X_7$ receptors are required to ascertain whether the particular residues at 155 and 348 are important determinants of the ATP-induced functional expression of the monkey $P2X_7$ receptor.

H155Y and A348T are ns-SNP mutations in the human *P2RX7* gene and have not yet been associated with disease conditions. However, a recent study has found that monocytes from individuals carrying the A348T SNP showed

enhanced ATP-evoked secretion of pro-inflammatory cytokine IL-1β (Stokes *et al.*, 2010). Further studies should be performed to determine the effect of these ns-SNP mutations on other ATP-evoked cell functions of the human $P2X_7$ receptor such as apoptosis, cell proliferation, neuron-glia interactions and bone remodelling (Baricordi *et al.*, 1999; Chen *et al.*, 2008; Ferrari *et al.*, 1999; Ke *et al.*, 2003; Zhang *et al.*, 2009). Furthermore, there is evidence for roles of the $P2X_7$ receptor in number of pathological conditions, including arthritis, CLL and pain (Chessell *et al.*, 2005; Labasi *et al.,* 2002; Wiley *et al.,* 2002). Thus, it would be interesting to examine by genetic linkage studies whether these ns-SNP mutations are associated with human diseases. The information provided by this study should be useful in understanding the pathological functions of the $P2X_7$ receptors and development suitable therapeutics.

Table 8.1 Summary of EC_{50}, pEC_{50}, Hill coefficient and maximal current amplitudes

Chapter	Agonist and EC used	$P2X_7$ receptor	EC_{50} (μM)	pEC_{50}	Hill coefficient	I_{MAX} (pA/pF)	n
3	ATP and LDEC	$hP2X_7$ WT	397 ± 19	3.42 ± 0.02	2.08 ± 0.06	268 ± 12	29-30
		H155Y	313 ± 14 *	3.51 ± 0.02 *	2.03 ± 0.07^	391 ± 19 *** ^	10
		A348T	354 ± 26	3.46 ± 0.03	1.80 ± 0.08 *	324 ± 17 * ^^^	12
		H155Y/A348T	360 ± 47	3.47 ± 0.06	1.73 ± 0.09 *	473 ± 31 ***	7
	BzATP and LDEC	$hP2X_7$ WT	36 ± 4.7	4.46 ± 0.05	2.06 ± 0.27	244 ± 4.5	4
		H155Y	27 ± 6.6	4.60 ± 0.11	2.09 ± 0.14	392 ± 51 *	4
		A348T	31 ± 3.9	4.51 ± 0.05	1.94 ± 0.14	447 ± 72 *	3
	ATP and LDEC	$hP2X_7$ WT	348 ± 14	3.47 ± 0.02	1.89 ± 0.04	293 ± 13	28
		H155Y	324 ± 15	3.49 ± 0.02	1.95 ± 0.11	434 ± 19 ***	4
		H155F	402 ± 42	3.41 ± 0.05	1.95 ± 0.08	339 ± 27	7
		H155A	364 ± 52	3.46 ± 0.06	2.20 ± 0.09 **	333 ± 68	5
		H155R	228 ± 29 ***	3.66 ± 0.06 ***	1.83 ± 0.04	325 ± 48	6
		H155L	368 ± 31	3.44 ± 0.04	1.70 ± 0.13	171 ± 29 ***	5
		H155D	388 ± 43	3.42 ± 0.05	1.82 ± 0.04	214 ± 25 *	5
	ATP and LDEC	$hP2X_7$ WT	348 ± 14	3.47 ± 0.02	1.89 ± 0.04	293 ± 13	28
		H155Y	324 ± 15	3.49 ± 0.02	1.95 ± 0.11	434 ± 19 ***	4
		V154Y	365 ± 22	3.44 ± 0.03	2.01 ± 0.10	260 ± 15	5
		E156Y	387 ± 30	3.42 ± 0.04	1.72 ± 0.09	137 ± 30 ***	6
	ATP and LDEC	$hP2X_7$ WT	392 ± 15	3.41 ± 0.02	2.14 ± 0.06	257 ± 13	18
		A348T	335 ± 34	3.49 ± 0.04	1.91 ± 0.10	318 ± 18 *	7
		A348G	280 ± 25 **	3.56 ± 0.04 **	1.94 ± 0.12	394 ± 19 ***	4
		A348F	568 ± 74 **	3.26 ± 0.05 **	1.71 ± 0.11 **	143 ± 42 **	4
		A348M	580 ± 77 ***	3.25 ± 0.07 **	1.91 ± 0.19	178 ± 55 *	4-5

4	ATP and LDEC	$hP2X_7$ WT	304 ± 49	3.54 ± 0.07	2.03 ± 0.13	281 ± 18	5
		$rP2X_7$ WT	110 ± 6.1 **	3.96 ± 0.02 ***	2.67 ± 0.18 *	458 ± 27 ***	5
	BzATP and LDEC	$hP2X_7$ WT	31 ± 3.7	4.53 ± 0.05	2.73 ± 0.29	234 ± 24	11
		$rP2X_7$ WT	1.9 ± 0.1 ***	5.72 ± 0.02 ***	3.59 ± 0.28 *	282 ± 21	12
	ATP and LDEC	$rP2X_7$ WT	104 ± 5.2	3.99 ± 0.02	2.54 ± 0.07	444 ± 24	10
		Y155H	286 ± 10 ***	3.55 ± 0.02 *** ^	2.40 ± 0.13 ^	211 ± 25 *** ^	7
		T348A	105 ± 5.4 ^^	3.98 ± 0.02 ^^^	2.51 ± 0.18 ^	326 ± 23 ** ^^^	7
		Y155H/T348A	500 ± 16 ***	3.34 ± 0.13 ***	1.72 ± 0.26 ***	114 ± 18 ***	3
	ATP and standard EC	$rP2X_7$ WT	1470 ± 33	2.83 ± 0.01	2.57 ± 0.18	411 ± 21	5
		Y155H	2513 ± 114 ***	2.60 ± 0.02 ***	3.97 ± 0.13 ***	189 ± 37 ***	4-5
		T348A	1386 ± 142	2.86 ± 0.04	2.56 ± 0.26	230 ± 8.1 ***	3
	BzATP and LDEC	$rP2X_7$ WT	1.7 ± 0.06	5.78 ± 0.02	3.56 ± 0.19	294 ± 28	7
		Y155H	8.0 ± 1.3 ***	5.12 ± 0.06 ***	2.78 ± 0.11 **	129 ± 15 **	5
		T348A	1.7 ± 0.05	5.77 ± 0.01	3.48 ± 0.14	191 ± 24 *	5

5	ATP and LDEC	$hP2X_7$ WT	347 ± 24	3.48 ± 0.03	2.04 ± 0.08	276 ± 15	23-24
		H155Y	285 ± 10	3.55 ± 0.02	2.08 ± 0.10	357 ± 29 *	5
		V153I	316 ± 32	3.51 ± 0.04	1.81 ± 0.05	215 ± 19 *	4
		V154P	314 ± 34	3.51 ± 0.05	1.86 ± 0.07	279 ± 74	3
		E156D	307 ± 65	3.55 ± 0.09	1.93 ± 0.19	240 ± 47	5
		G157Q	437 ± 47	3.37 ± 0.05	1.70 ± 0.03	197 ± 24 *	5
		N158K	400 ± 40	3.41 ± 0.05	1.83 ± 0.12	212 ± 40	4
		Q159R	415 ± 34	3.39 ± 0.04	1.82 ± 0.07	184 ± 25**	6
	ATP and LDEC	$hP2X_7$ WT	392 ± 15	3.41 ± 0.02	2.14 ± 0.06	257 ± 13	18
		A348T	335 ± 34	3.49 ± 0.04	1.91 ± 0.10	318 ± 18 *	7
		F350C	291 ± 32 *	3.54 ± 0.05 **	1.71 ± 0.20 *	257 ± 63	4
		F353L	408 ± 56	3.40 ± 0.05	1.90 ± 0.06	318 ± 23 *	5
		L354I	357 ± 42	3.46 ± 0.05	1.96 ± 0.12	278 ± 41	7
		D356N	291 ± 31 *	3.54 ± 0.05 **	2.16 ± 0.14	191 ± 16 *	4
	ATP and LDEC	$rP2X_7$ WT	108 ± 7	3.97 ± 0.03	2.39 ± 0.13	316 ± 29	4
		L353F	89 ± 13	4.07 ± 0.07	2.43 ± 0.15	371 ± 52	4
7	ATP and LDEC	$hP2X_7$	314 ± 24	3.52 ± 0.04	1.92 ± 0.07	330 ± 22	12
		$mP2X_7$	802 ± 87 ***	3.12 ± 0.04 ***	1.23 ± 0.06 ***	160 ± 22 ***	11
	BzATP and LDEC	$hP2X_7$	30 ± 2.0	4.52 ± 0.03	2.19 ± 0.16	310 ± 36	5
		$mP2X_7$	58 ± 4.2 ***	4.24 ± 0.03 ***	1.91 ± 0.08	220 ± 27	4-6

Summary of all the values calculated in the thesis. * $p<0.05$, ** $p<0.01$, and *** $p<0.001$, compared to WT. ^ $p<0.05$, ^^ $p<0.01$, and ^^^ $p<0.001$, compared to double mutant. EC: extracellular recording solution. LDEC: low divalent extracellular solution.

Table 8.2 Summary of IC_{50}, pIC_{50} and Hill coefficients

Chapter	Antagonist	$P2X_7$ receptor	IC_{50} (nM)	pIC_{50}	Hill coefficient	n
3	KN-62	$hP2X_7$ WT	127 ± 38	6.93 ± 0.12	1.63 ± 0.15	3
		H155Y	129 ± 20	6.90 ± 0.06	1.34 ± 0.07	3
7	KN-62	$hP2X_7$ WT	127 ± 38	6.93 ± 0.12	1.63 ± 0.15	3
		$mP2X_7$ WT	54 ± 8.3	7.28 ± 0.07	1.93 ± 0.17	3
	AZ11645373	$hP2X_7$ WT	31 ± 2.6	7.52 ± 0.04	1.77 ± 0.45	3
		$mP2X_7$ WT	24 ± 3.0	7.64 ± 0.06	1.17 ± 0.14	3
	A-438079	$hP2X_7$ WT	493 ± 94	6.35 ± 0.09	1.13 ± 0.05	6
		$mP2X_7$ WT	297 ± 24	6.53 ± 0.03	0.85 ± 0.06 **	6

** $p<0.01$. Summary of all the values calculated in the thesis. Low divalent extracellular solution was used.

References

ABBRACCHIO, M. P., BURNSTOCK, G., VERKHRATSKY, A. & ZIMMERMANN, H. (2009). Purinergic signalling in the nervous system: an overview. *Trends Neurosci,* 32: 19-29.

ADINOLFI, E., CALLEGARI, M. G., FERRARI, D., BOLOGNESI, C., MINELLI, M., WIECKOWSKI, M. R., PINTON, P., RIZZUTO, R. & DI VIRGILIO, F. (2005). Basal activation of the $P2X_7$ ATP receptor elevates mitochondrial calcium and potential, increases cellular ATP levels, and promotes serum-independent growth. *Mol Biol Cell,* 16: 3260-3272.

ADINOLFI, E., MELCHIORNI, L., FALZONI, S., CHIOZZI, P., MORELLI, A., TIEGHI, A., CUNEO, A., CASTOLDI, G., DI VIRGILIO, F. & BARICORDI, O. R. (2002). $P2X_7$ receptor expression in evolutive and indolent forms of chronic B lymphocytic leukemia. *Blood,* 99: 706-708.

ADRIOUCH, S., BANNAS, P., SCHWARZ, N., FLIEGERT, R., GUSE, A. H., SEMAN, M., HAAG, F. & KOCH-NOLTE, F. (2007). ADP-ribosylation at Arg^{125} gates the $P2X_7$ ion channel by presenting a covalent ligand to its nucleotide binding site. *FASEB J,* 22: 861-869.

AGBOH, K. C., WEBB, T. E., EVANS, R. J. & ENNION, S. J. (2004). Functional characterisation of a P2X receptor from *Schistosoma mansoni. J Biol Chem,* 279: 41650-41657.

ALCARAZ, L., BAXTER, A., BENT, J., BOWERS, K., BRADDOCK, M., CLADINGBOEL, D., DONALD, D., FAGURA, M., FURBER, M., LAURENT, C., LAWSON, M., MORTIMORE, M., MCCORMICK, M., ROBERTS, N. & ROBERTSON, M. (2003). Novel $P2X_7$ receptor antagonists. *Bioorg Med Chem Lett,* 13: 4043-4046.

ANDERSON, C. M. & NEDERGAARD, M. (2006). Emerging challenges of assigning $P2X_7$ receptor function and immunoreactivity in neurons. *Trends Neurosci,* 29: 257-262.

APOLLONI, S., MONTILLI, C., FINOCCHI, P. & AMADIO, S. (2009). Membrane compartments and purinergic signalling: P2X receptors in neurodegenerative and neuroinflammatory events. *FEBS J,* 27: 354-364.

ARMSTRONG, J. N., BRUST, T. B., LEWIS, R. G. & MACVICAR, B. A. (2002). Activation of presynaptic $P2X_7$-like receptors depresses mossy fiber-CA3

synaptic transmission through p38 mitogen-activated protein kinase. *J Neurosci,* 22: 5938-5945.

ASTBURY, C., BLAKEY, G. E., SPRAY, H. E., PERRETT, J. H. & LAWRENCE, P. (2007). Single dose safety, tolerability, pharmacokinetics and pharmacodynamics of AZD9056, a novel $P2X_7$ receptor antagonist, in healthy volunteers. Proceedings Annual Scientific Meeting of Am Coll Rheum Abtract 954: S397.

BARALDI, P. G., DEL CARMEN NUÃ±EZ, M., MORELLI, A., FALZONI, S., DI VIRGILIO, F. & ROMAGNOLI, R. (2003). Synthesis and biological activity of N-arylpiperazine-modified analogues of KN-62, a potent antagonist of the purinergic $P2X_7$ receptor. *J Med Chem,* 46: 1318-1329.

BARDEN, N., HARVEY, M., GAGNE, B., SHINK, E., TREMBLAY, M., RAYMOND, C., LABBE, M., VILLENEUVE, A., ROCHETTE, D., BORDELEAU, L., STADLER, H., HOLSBOER, F. & MULLER-MYHSOK, B. (2006). Analysis of single nucleotide polymorphisms in genes in the chromosome 12Q24.31 region points to $P2X_7$ as a susceptibilty gene to bipolar defective disorder. *Am J Med Gen B Neuropsychiatr Genet,* 141B: 374-382.

BARICORDI, O. R., MELCHIORRI, L., ADINOLFI, E., FALZONI, S., CHIOZZI, P., BUELL, G. & DI VIRGILIO, F. (1999). Increased proliferation rate of lymphoid cells transfected with the $P2X_7$ ATP receptor. *J Biol Chem,* 274: 33206-33208.

BARRERA, N. P., ORMOND, S. J., HENDERSON, R. M., MURRELL-LAGNADO, R. D. & EDWARDSON, J. M. (2005). Atomic force microscopy imaging demonstrates that $P2X_2$ receptors are trimers but that $P2X_6$ receptor subunits do not oligomerise. *J Biol Chem,* 280: 10759-10765.

BEAN, B. P. (1990). ATP-activated channels in rat and bullfrog sensory neurons: concentration dependence and kinetics. *J Neurosci,* 10: 1-10.

BIANCHI, B. R., LYNCH, K. J., TOUMA, E., NIFORATOS, W., BURGARD, E. C., ALEXANDER, K. M., PARK, H. S., YU, H., METZGER, R., KOWALUK, E., JARVIS, M. F. & VAN BIESEN, T. (1999). Pharmacological characterisation of recombinant human and rat P2X receptor subtypes. *Eur J Pharmacol,* 376: 127-138.

BO, X., JIANG, L.-H., WILSON, H. L., KIM, M., BURNSTOCK, G., SURPRENANT, A. & NORTH, R. A. (2003). Pharmacological and biophysical properties of the human $P2X_5$ receptor. *Mol Pharmacol,* 63: 1407-1416.

BO, X., ZHANG, Y., NASSAR, M., BURNSTOCK, G. & SCHOEPFER, R. (1995). A P2X purinoceptor cDNA conferring a novel pharmacological profile. *FEBS Lett,* 375: 129-133.

BODIN, P. & BURNSTOCK, G. (2001). Purinergic signalling: ATP release. *Neurochem Res,* 26: 959-969.

BOLDT, W., KLAPPERSTUCK, M., BUTTNER, C., SADTLER, S., SCHMALZING, N. & MARKWARDT, F. (2003). Glu^{496} Ala polymorphism of human $P2X_7$ receptor does not affect its electrophysiological phenotype. *Am J Physiol Cell Physiol,* 284: C749-C756.

BOUÉ-GRABOT, É., AKIMENKO, M. A. & SÉGUÉLA, P. (2000). Unique functional properties of a sensory neuronal P2X ATP-gated channel from zebrafish. *J Neurochem,* 75: 1600-1607.

BOUMECHACHE, M., MASIN, M., EDWARDSON, J. M., GÃRECKI, D. C. & MURRELL-LAGNADO, R. (2009). Analysis of assembly and trafficking of native $P2X_4$ and $P2X_7$ receptor complexes in rodent immune cells. *J Biol Chem,* 284: 13446-13454.

BRAKE, A. J., WAGENBACH, M. J. & JULIUS, D. (1994). New structural motif for ligand-gated ion channels defined by an ionotropic ATP receptor. *Nature,* 371: 519-523.

BROWNE, L. E., JIANG, L.-H. & NORTH, R. A. (2010). New structure enlivens interest in P2X receptors. *Trends Pharmacol Sci,* 31: 229-237.

BUELL, G., LEWIS, C., COLLO, G., NORTH, R. A. & SURPRENANT, A. (1996). An antagonist-insensitive P2X receptor expressed in epithelia and brain. *EMBO J,* 15: 55-62.

BUELL, G. N., TALABOT, F., GOS, A., LORENZ, J., LAI, E., MORRIS, M. A. & ANTONARAKIS, S. E. (1998). Gene structure and chromosomal localisation of the human $P2X_7$ receptor. *Receptors Channels,* 5: 347-354.

BURGARD, E. C., NIFORATOS, W., VAN BIESEN, T., LYNCH, K. J., KAGE, K. L., TOUMA, E., KOWALUK, E. A. & JARVIS, M. F. (2000). Competitive antagonism of recombinant $P2X_{2/3}$ receptors by 2',3'-O-(2,4,6-

trinitrophenyl) adenosine 5'-triphosphate (TNP-ATP). *Mol Pharmacol,* 58: 1502-1510.

BURNSTOCK, CAMPBELL, G., SATCHELL, D. & SMYTHE, A. (1970). Evidence that adenosine triphosphate or a related nucleotide is the transmitter substance released by non-adrenergic inhibitory nerves in the gut. *Br J Pharmacol,* 40: 668–688.

BURNSTOCK, G. (1972). Purinergic nerves. *Pharmacol Rev,* 24: 509-581.

BURNSTOCK, G. (1978). A basis for distinguishing two types of purinergic receptor. *Cell membrane receptors for drugs and hormones: A multidisciplinary approach*: 107-118.

BURNSTOCK, G. (2007). Purine and pyrimidine receptors. *Cell Mol Life Sci,* 64: 1471-1483.

CABRINI, G., FALZONI, S., FORCHAP, S. L., PELLEGATTI, P., BALBONI, A., AGOSTINI, P., CUNEO, A., CASTOLDI, G., BARICORDI, O. R. & DI VIRGILIO, F. (2005). A His^{155} to Tyr polymorphism confers gain-of-function to the human $P2X_7$ receptor of human leukemic lymphocytes. *J Immunol,* 175: 82-89.

CAO, L., BROOMHEAD, H. E., YOUNG, M. T. & NORTH, R. A. (2009). Polar residues in the second transmembrane domain of the rat $P2X_2$ receptor that affect spontaneous gating, unitary conductance, and rectification. *J Neurosci,* 29: 14257-14264.

CAO, L., YOUNG, M. T., BROOMHEAD, H. E., FOUNTAIN, S. J. & NORTH, R. A. (2007). Thr^{339}-to-Ser substitution in rat $P2X_2$ receptor second transmembrane domain causes constitutive opening and indicates a gating role for Lys^{308}. *J Neurosci,* 27: 12916-12923.

CHEN, C.-C., AKOPIAN, A. N., SIVILOTTIT, L., COLQUHOUN, D., BURNSTOCK, G. & WOOD, J. N. (1995). A P2X purinoceptor expressed by a subset of sensory neurons. *Nature,* 377: 428-431.

CHEN, L. & BROSNAN, C. F. (2006). Exacerbation of experimental autoimmune encephalomyelitis in $P2X_7R^{-/-}$ mice: evidence for loss of apoptotic activity in lymphocytes. *J Immunol,* 176: 3115-3126.

CHEN, Y., ZHANG, X., WANG, C., LI, G., GU, Y. & HUANG, L.-Y. M. (2008). Activation of $P2X_7$ receptors in glial satellite cells reduces pain through downregulation of $P2X_3$ receptors in nociceptive neurons. *Proc Natl Acad Sci USA*, 105: 16773-16778.

CHESSELL, I. P., HATCHER, J. P., BOUNTRA, C., MICHEL, A. D., HUGHES, J. P., GREEN, P., EGERTON, J., MURFIN, M., RICHARDSON, J., PECK, W. L., GRAHAMES, C. B. A., CASULA, M. A., YIANGOU, Y., BIRCH, R., ANAND, P. & BUELL, G. N. (2005). Disruption of the $P2X_7$ purinoceptor gene abolishes chronic inflammatory and neuropathic pain. *Pain,* 114: 386-396.

CHESSELL, I. P., SIMON, J., HIBELL, A. D., MICHEL, A. D., BARNARD, E. A. & HUMPHREY, P. P. A. (1998). Cloning and functional characterisation of the mouse $P2X_7$ receptor. *FEBS Lett,* 439: 26-30.

CHOY, E. H. & PANAYI, G. S. (2001). Cytokine pathways and joint inflammation in rheumatoid arthritis. *N Engl J Med*, 344: 907-916.

CLYNE, J. D., WANG, L.-F. & HUME, R. I. (2002). Mutational Analysis of the Conserved Cysteines of the Rat $P2X_2$ Purinoceptor. *J Neurosci,* 22: 3873-3880.

COCKAYNE, D. A., HAMILTON, S. G., ZHU, Q.-M., DUNN, P. M., ZHONG, Y., NOVAKOVIC, S., MALMBERG, A. B., CAIN, G., BERSON, A., KASSOTAKIS, L., HEDLEY, L., LACHNIT, W. G., BURNSTOCK, G., MCMAHON, S. B. & FORD, A. P. D. W. (2000). Urinary bladder hyporeflexia and reduced pain-related behaviour in $P2X_3$-deficient mice. *Nature,* 407: 1011-1015.

COLLO, G., NEIDHART, S., KAWASHIMA, E., KOSCO-VILBOIS, M., NORTH, R. A. & BUELL, G. (1997). Tissue distribution of the $P2X_7$ receptor. *Neuropharmacology,* 36: 1277-1283.

COLLO, G., NORTH, R. A., KAWASHIMA, E., MERLO-PICH, E., NEIDHART, S., SURPRENANT, A. & BUELL, G. (1996). Cloning of $P2X_5$ and $P2X_6$ receptors and the distribution and properties of an extended family of ATP-gated ion channels. *J Neurosci,* 16: 2495-2507.

COX, J. A., BARMINA, O. & VOIGT, M. M. (2001). Gene structure, chromosomal localisation, cDNA cloning and expression of the mouse ATP-gated ionotropic receptor $P2X_5$ subunit. *Gene,* 270: 145-152.

CYR, D. M. 2005. Arrest of CFTR[Delta]F508 folding. *Nat Struct Mol Biol,* 12: 2.

DAMER, S., NIEBEL, B., CZECHE, S., NICKEL, P., ARDANUY, U., SCHMALZING, G., RETTINGER, J., MUTSCHLER, E. & LAMBRECHT, G. (1998). NF279: a novel potent and selective antagonist of P2X receptor-mediated responses. *Eur J Pharmacol,* 350, R5-6.

DENLINGER, L. C., ANGELINI, G., SCHELL, K., GREEN, D. N., GUADARRAMA, A. G., PRABHU, U., COURSIN, D. B., BERTICS, P. J. & HOGAN, K. (2005). Detection of human $P2X_7$ nucleotide receptor polymorphisms by a novel monocyte pore assay predictive of alterations in lipopolysaccharide-induced cytokine production. *J Immunol,* 174: 4424-4431.

DENLINGER, L. C., SOMMER, J. A., PARKER, K., GUDIPATY, L., FISETTE, P. L., WATTERS, J. W., PROCTOR, R. A., DUBYAK, G. R. & BERTICS, P. J. (2003). Mutation of a dibasic amino acid motif within the C-terminus of the $P2X_7$ receptor results in trafficking defects and impaired function. *J Immunol,* 171: 1304-1311.

DEUCHARS, S. A., ATKINSON, L., BROOKE, R. E., MUSA, H., MILLIGAN, C. J., BATTEN, T. F. C., BUCKLEY, N. J., PARSON, S. H. & DEUCHARS, J. (2001). Neuronal $P2X_7$ receptors are targeted to presynaptic terminals in the central and peripheral nervous systems. *J Neurosci,* 21: 7143-7152.

DI VIRGILIO, F. (1995). The P2Z purinoceptor: an intriguing role in immunity, inflammation and cell death. *Immunol Today,* 16: 524-528.

DIAZ-HERNANDEZ, M., COX, J. A., MIGITA, K., HAINES, W., EGAN, T. M. & VOIGT, M. M. (2002). Cloning and characterisation of two novel zebrafish P2X receptor subunits. *Biochem Biophys Res Comm,* 295: 849-853.

DONNELLY-ROBERTS, D. L., NAMOVIC, M. T., HAN, P. & JARVIS, M. F. (2009). Mammalian $P2X_7$ receptor pharmacology: comparison of recombinant mouse, rat and human $P2X_7$ receptors. *Br J Pharmacol,* 157: 1203-1214.

DONNELLY-ROBERTS, D. L. JARVIS, M. F. (2007). Discovery of $P2X_7$ receptor-selective antagonists offers new insights into $P2X_7$ receptor function and indicates a role in chronic pain states. *Br J Pharmacol,* 151:571-579.

DORN, G., PATEL, S., WOTHERSPOON, G., HEMMINGS-MIESZCZAK, M., BARCLAY, J., NATT, F. J. C., MARTIN, P., BEVAN, S., FOX, A., GANJU, P., WISHART, W. & HALL, J. (2004). siRNA relieves chronic neuropathic pain. *Nucleic Acids Res,* 32: e49.

DRURY, A. N. & SZENT-GYÖRGYI, A. (1929). The physiological activity of adenine compounds with especial reference to their action upon the mammalian heart. *J Physiol,* 68: 213-237.

DUAN, S., ANDERSON, C. M., KEUNG, E. C., CHEN, Y., CHEN, Y. & SWANSON, R. A. (2003). $P2X_7$ receptor-mediated release of excitatory amino acids from astrocytes. *J Neurosci,* 23: 1320-1328.

DUNN, P. & BLAKELEY, A. (1988). Suramin: a reversible P2-purinoceptor antagonist in the mouse vas deferens. *Brit J Pharmacol,* 93: 243-245.

ENNION, S., HAGAN, S. & EVANS, R. J. (2000). The role of positively charged amino acids in ATP recognition by human $P2X_1$ receptors. *J Biol Chem,* 275: 29361-29367.

ENNION, S. J. & EVANS, R. J. (2002). Conserved cysteine residues in the extracellular loop of the human $P2X_1$ receptor form disulfide bonds and are involved in receptor trafficking to the cell surface. *Mol Pharmacol,* 61: 303-311.

EVANS, R. J. (2010). Structural interpretation of P2X receptor mutagenesis studies on drug action. *Brit J Pharmacol,* ahead of print.

EVANS, R. J., LEWIS, C., BUELL, G., VALERA, S., NORTH, R. A. & SURPRENANT, A. (1995). Pharmacological characterisation of heterologously expressed ATP-gated cation channels (P2X Purinoceptors). *Mol Pharmacol,* 48: 178-183.

FAIRBAIRN, I. P., STOBER, C. B., KUMARARATNE, D. S. & LAMMAS, D. A. (2001). ATP-mediated killing of intracellular Mycobacteria by macrophages is a $P2X_7$-dependent process inducing bacterial death by phagosome-lysosome fusion. *J Immunol,* 167: 3300-3307.

FERNANDO, S. L., SAUNDERS, B. M., SLUYTER, R., SKARRATT, K. K., GOLDBERG, H., MARKS, G. B., WILEY, J. S. & BRITTON, W. J. (2007). A polymorphism in the $P2X_7$ gene increases susceptibility to extrapulmonary tuberculosis. *Am J Respir Crit Care Med,* 175: 360-366.

FERRARI, D., CHIOZZI, P., FALZONI, S., DAL SUSINO, M., MELCHIORRI, L., BARICORDI, O. R. & DI VIRGILIO, F. (1997a). Extracellular ATP triggers IL-1β release by activating the purinergic P2Z receptor of human macrophages. *J Immunol,* 159: 1451-1458.

FERRARI, D., LOS, M., BAUER, M. K. A., VANDENABEELE, P., WESSELBORG, S. & SCHULZE-OSTHOFF, K. (1999). P2Z

purinoreceptor ligation induces activation of caspases with distinct roles in apoptotic and necrotic alterations of cell death. *FEBS Lett,* 447: 71-75.

FERRARI, D., PIZZIRANI, C., ADINOLFI, E., LEMOLI, R. M., CURTI, A., IDZKO, M., PANTHER, E. & DI VIRGILIO, F. (2006). The $P2X_7$ receptor: A key player in IL-1 processing and release. *J Immunol,* 176: 3877-3883.

FERRARI, D., WESSELBORG, S., BAUER, M. K. A. & SCHULZE-OSTHOFF, K. (1997b). Extracellular ATP activates transcription factor NF-κB through the P2Z purinoreceptor by selectively targeting NF-κB p65 (RelA). *J Cell Biol,* 139: 1635-1643.

FONFRIA, E., CLAY, W. C., LEVY, D. S., GOODWIN, J. A., ROMAN, S., SMITH, G. D., CONDREAY, J. P. & MICHEL, A. D. (2008). Cloning and pharmacological characterisation of the guinea pig $P2X_7$ receptor orthologue. *Brit J Pharmacol,* 153: 544-556.

FOUNTAIN, S. J. & BURNSTOCK, G. (2009). An evolutionary history of P2X receptors. *Purinergic Signal,* 5: 269–272.

FOUNTAIN, S. J., CAO, L., YOUNG, M. T. & NORTH, R. A. (2008). Permeation properties of a P2X receptor in the green algae *Ostreococcus tauri. J Biol Chem,* 283: 15122-15126.

FOUNTAIN, S. J., PARKINSON, K., YOUNG, M. T., CAO, L., THOMPSON, C. R. L. & NORTH, R. A. (2007). An intracellular P2X receptor required for osmoregulation in *Dictyostelium discoideum. Nature,* 448: 200-203.

GARCIA-GUZMAN, M., SOTO, F., GOMEZ-HERNANDEZ, J. M., LUND, P.-E. & STÃHMER, W. (1997a). Characterisation of recombinant human $P2X_4$ receptor reveals pharmacological differences to the rat homologue. *Mol Pharmacol,* 51: 109-118.

GARCIA-GUZMAN, M., SOTO, F., LAUBE, B. & STUHMER, W. (1996). Molecular cloning and functional expression of a novel rat heart P2X purinoceptor. *FEBS Lett,* 388: 123-127.

GARCIA-GUZMAN, M., STÜHMER, W. & SOTO, F. (1997b). Molecular characterisation and pharmacological properties of the human $P2X_3$ purinoceptor. *Brain Res Mol Brain Res,* 47: 59-66.

GARGETT, C. E. & WILEY, J. S. (1997). The isoquinoline derivative KN-62 a potent antagonist of the P2Z-receptor of human lymphocytes. *Br J Pharmacol,* 120: 1483-1490.

GARTLAND, A., BUCKLEY, K. A., BOWLER, W. B. & GALLAGHER, J. A. (2003). Blockade of the pore-forming $P2X_7$ receptor inhibits formation of multinucleated human osteoclasts. *Calcif Tissue Intl,* 73: 361-369.

GREEN, E. K., GROZEVA, D., RAYBOULD, R., ELVIDGE, G., MACGREGOR, S., CRAIG, I., FARMER, A., MCGUFFIN, P., FORTY, L., JONES, L., JONES, I., O'DONOVAN, M. C., Owen, M. J., KIROV, G. & CRADDOCK, N. (2009). *P2RX7*: A bipolar and unipolar disorder candidate susceptibility gene? *Am J Med Gen B Neuropsychiatr Gen*, 150: 1063-1069.

GODING, J. W., GROBBEN, B. & SLEGERS, H. (2003). Physiological and pathophysiological functions of the ecto-nucleotide pyrophosphatase/phosphodiesterase family. *Biochim Biophys Acta,* 1638: 1-19.

GONNORD, P., DELARASSE, C., AUGER, R., BENIHOUD, K., PRIGENT, M., CUIF, M. H., LAMAZE, C. & KANELLOPOULOS, J. M. (2009). Palmitoylation of the $P2X_7$ receptor, an ATP-gated channel, controls its expression and association with lipid rafts. *FASEB J,* 23: 795-805.

GRIGOROIU-SERBANESCU, M., HERMS, S., MÜHLEISEN, T. W., GEORGI, A., DIACONU, C. C., STROHMAIER, J., CZERSKI, P., HAUSER, J., LESZCZYNSKA-RODZIEWICZ, A., JAMRA, R. A., BABADJANOVA, G., TIGANOV, A., KRASNOV, V., KAPILETTI, S., NEAGU, A. I., VOLLMER, J., BREUER, R., RIETSCHEL, M., NÖTHEN, M. M., CICHON, S. & PROPPING, P. (2009) Variation in *P2RX7* candidate gene (rs2230912) is not associated with bipolar I disorder and unipolar major depression in four European samples. *Am J Med Gen B Neuropsychiatr Gen,* 150B: 1017-1021.

GROSSMANN, M., NAKAMURA, Y., GRUMONT, R. & GERONDAKIS, S. (1999). New insights into the roles of ReL/NF-κB transcription factors in immune function, hemopoiesis and human disease. *Intl J Biochem Cell Biol,* 31: 1209-1219.

GU, B. J., SLUYTER, R., SKARRATT, K. K., SHEMON, A. N., DAO-UNG, L. P., FULLER, S. J., BARDEN, J. A., CLARKE, A. L., PETROU, S. & WILEY, J. S. (2004). An Arg^{307} to Gln polymorphism within the ATP-binding site causes loss of function of the human $P2X_7$ receptor. *J Biol Chem,* 279: 31287-31295.

GU, B. J., ZHANG, W. Y., WORTHINGTON, R. A., SLUYTER, R., DAO-UNG, P., PETROU, S., BARDEN, J. A. & WILEY, J. S. (2001). A Glu^{496} to Ala polymorphism leads to loss of function of the human $P2X_7$ receptor. *J Biol Chem,* 276: 11135-11142.

GUDIPATY, L., HUMPHREYS, B. D., BUELL, G. & DUBYAK, G. R. (2001). Regulation of $P2X_7$ nucleotide receptor function in human monocytes by extracellular ions and receptor density. *Am J Physiol Cell Physiol,* 280: C943-953.

GUIMARÃES, C. A. & LINDEN, R. (2004). Programmed cell deaths. *Eur J Biochem,* 271: 1638-1650.

GUNOSEWOYO, H. & KASSIOU, M. (2010). P2X purinergic receptor ligands: recently patented compounds. *Exp Opin Ther Pat,* 20: 625-646.

GUO, C., MASIN, M., QURESHI, O. S. & MURRELL-LAGNADO, R. D. (2007). Evidence for functional $P2X_4/P2X_7$ heteromeric receptors. *Mol Pharmacol,* 72: 1447-1456.

HAINES, W. R., MIGITA, K., COX, J. A., EGAN, T. M. & VOIGT, M. M. (2001). The first transmembrane domain of the P2X receptor subunit participates in the agonist-induced gating of the channel. *J Biol Chem,* 276: 32793-32798.

HAINES, W. R., TORRES, G. E., VOIGT, M. M. & EGAN, T. M. (1999). Properties of the novel ATP-gated ionotropic receptor composed of the $P2X_1$ and $P2X_5$ isoforms. *Mol Pharmacol,* 56: 720-727.

HAMILL, O. P., MARTY, A., NEHER, E., SAKMANN, B. & SIGWORTH, F. J. (1981). Improved patch-clamp techniques for high-resolution current recording from cells and cell-free membrane patches. *Pflugers Arch,* 391: 85-100.

HANAHAN, D. (1983). Studies on transformation of *Escherichia coli* with plasmids. *J Mol Biol,* 166: 557-580.

HECHLER, B. A., LENAIN, N. G., MARCHESE, P., VIAL, C., HEIM, V. R., FREUND, M., CAZENAVE, J.-P., CATTANEO, M., RUGGERI, Z. M., EVANS, R. & GACHET, C. (2003). A role of the fast ATP-gated $P2X_1$ cation channel in thrombosis of small arteries *in vivo*. *J Expt Med,* 198: 661-667.

HIBELL, A. D., KIDD, E. J., CHESSELL, I. P., HUMPHREY, P. P. A. & MICHEL, A. D. (2000). Apparent species differences in the kinetic properties of $P2X_7$ receptors. *Br J Pharmacol,* 130: 167-173.

HIBELL, A. D., THOMPSON, K. M., XING, M., HUMPHREY, P. P. A. & MICHEL, A. D. (2001). Complexities of measuring antagonist potency at $P2X_7$ receptor orthologs. *J Pharmacol Exp Ther,* 296: 947-957.

HOLTON, P. (1959). The liberation of adenosine triphosphate on antidromic stimulation of sensory nerves. *J Physiol* , 145: 494-504.

HONORE, P., DONNELLY-ROBERTS, D., NAMOVIC, M. T., HSIEH, G., ZHU, C. Z., MIKUSA, J. P., HERNANDEZ, G., ZHONG, C., GAUVIN, D. M., CHANDRAN, P., HARRIS, R., MEDRANO, A. P., CARROLL, W., MARSH, K., SULLIVAN, J. P., FALTYNEK, C. R. & JARVIS, M. F. (2006). A-740003 [N-(1-{[(Cyanoimino)(5-quinolinylamino) methyl]amino}-2,2-dimethylpropyl)-2-(3,4-dimethoxyphenyl)acetamide], a novel and selective $P2X_7$ receptor antagonist, dose-dependently reduces neuropathic pain in the rat. *J Pharmacol Exp Ther,* 319: 1376-1385.

HULSMANN, M., NICKEL, P., KASSACK, M., SCHMALZING, G., LAMBRECHT, G. & MARKWARDT, F. (2003). NF449, a novel picomolar potency antagonist at human $P2X_1$ receptors. *Eur J Pharmacol,* 470: 1-7.

HUMPHREYS, B. D. & DUBYAK, G. R. (1996). Induction of the $P2Z/P2X_7$ nucleotide receptor and associated phospholipase D activity by lipopolysaccharide and IFN-γ in the human THP-1 monocytic cell line. *J Immunol,* 157: 5627-5637.

HUMPHREYS, B. D., VIRGINIO, C., SURPRENANT, A., RICE, J. & DUBYAK, G. R. (1998). Isoquinolines as antagonists of the $P2X_7$ nucleotide receptor: High selectivity for the human versus rat receptor homologues. *Mol Pharmacol,* 54: 22-32.

JACOBSON, K. A., KIM, Y. C., WILDMAN, S. S., MOHANRAM, A., HARDEN, T. K., BOYER, J. L., KING, B. F. & BURNSTOCK, G. (1998). A pyridoxine cyclic phosphate and its 6-azoaryl derivative selectively potentiate and antagonise activation of $P2X_1$ receptors. *J Med Chem,* 41: 2201-2206.

JARVIS, M. F., BIANCHI, B., UCHIC, J. T., CARTMELL, J., LEE, C.-H., WILLIAMS, M. & FALTYNEK, C. (2004). [3H]A-317491, a novel high-

affinity non-nucleotide antagonist that specifically labels human $P2X_{2/3}$ and $P2X_3$ receptors. *J Pharmacol Exp Ther,* 310: 407-416.

JARVIS, M. F., BURGARD, E. C., MCGARAUGHTY, S., HONORE, P., LYNCH, K., BRENNAN, T. J., SUBIETA, A., VAN BIESEN, T., CARTMELL, J., BIANCHI, B., NIFORATOS, W., KAGE, K., YU, H., MIKUSA, J., WISMER, C. T., ZHU, C. Z., CHU, K., LEE, C.-H., STEWART, A. O., POLAKOWSKI, J., COX, B. F., KOWALUK, E., WILLIAMS, M., SULLIVAN, J. & FALTYNEK, C. (2002). A-317491, a novel potent and selective non-nucleotide antagonist of $P2X_3$ and $P2X_{2/3}$ receptors, reduces chronic inflammatory and neuropathic pain in the rat. *Proc Nat Acad Sci USA,* 99: 17179-17184.

JIANG, L.-H., KIM, M., SPELTA, V., BO, X., SURPRENANT, A. & NORTH, R. A. (2003). Subunit arrangement in P2X receptors. *J Neurosci,* 23: 8903-8910.

JIANG, L.-H., MACKENZIE, A. B., NORTH, R. A. & SURPRENANT, A. (2000a). Brilliant blue G selectively blocks ATP-gated rat $P2X_7$ receptors. *Mol Pharmacol,* 58: 82-88.

JIANG, L.-H., RASSENDREN, F., MACKENZIE, A., ZHANG, Y.-H., SURPRENANT, A. & NORTH, R. A. (2005). N-methyl-D-glucamine and propidium dyes utilise different permeation pathways at rat $P2X_7$ receptors. *Am J Physiol Cell Physiol,* 289: C1295-1302.

JIANG, L.-H., RASSENDREN, F., SURPRENANT, A. & NORTH, R. A. (2000b). Identification of amino acid residues contributing to the ATP-binding site of a purinergic P2X receptor. *J Biol Chem,* 275: 34190-34196.

JIANG, L.-H., RASSENDREN, F. O., SPELTA, V., SURPRENANT, A. & NORTH, R. A. (2001). Amino acid residues involved in gating identified in the first membrane-spanning domain of the rat $P2X_2$ receptor. *J Biol Chem,* 276: 14902-14908.

JIANG, L.-H., RASSENDREN, F., MACKENZIE, A., ZHANG, Y.-H, SURPRENANT, A . & NORTH, A. (2005). N-methyl-D-glucamine and propidium dyes utilise different permeation pathways at rat $P2X_7$ receptors. *Am J Physiol Cell Physiol,* 289: 1295-1302.

JONES, C. A., CHESSELL, I. P., SIMON, J., BARNARD, E. A., MILLER, K. J., MICHEL, A. D. & HUMPHREY, P. P. A. (2000). Functional

characterisation of the $P2X_4$ receptor orthologues. *Br J Pharmacol,* 129: 388-394.

JONES, C. A., VIAL, C., SELLERS, L. A., HUMPHREY, P. P. A., EVANS, R. J. & CHESSELL, I. P. (2004). Functional regulation of $P2X_6$ receptors by N-linked glycosylation: Identification of a novel $\alpha\beta$-methylene ATP-sensitive phenotype. *Mol Pharmacol,* 65: 979-985.

JURANKA, P. F., HAGHIGHI, A. P., GAERTNER, T., COOPER, E. & MORRIS, C. E. (2001). Molecular cloning and functional expression of *Xenopus laevis* oocyte ATP-activated $P2X_4$ channels. *Biochim Biophys Acta,* 1512: 111-124.

KAWATE, T., MICHEL, J. C., BIRDSONG, W. T. & GOUAUX, E. (2009). Crystal structure of the ATP-gated $P2X_4$ ion channel in the closed state. *Nature,* 460: 592-598.

KE, H. Z., QI, H., WEIDEMA, A. F., ZHANG, Q., PANUPINTHU, N., CRAWFORD, D. T., GRASSER, W. A., PARALKAR, V. M., LI, M., AUDOLY, L. P., GABEL, C. A., JEE, W. S. S., DIXON, S. J., SIMS, S. M. & THOMPSON, D. D. (2003). Deletion of the $P2X_7$ nucleotide receptor reveals its regulatory roles in bone formation and resorption. *Mol Endocrinol,* 17: 1356-1367.

KHAKH, B. S. & NORTH, R. A. (2006). P2X receptors as cell-surface ATP sensors in health and disease. *Nature,* 442: 527-532.

KIM, M., JIANG, L. H., WILSON, H. L., NORTH, R. A. & SURPRENANT, A. (2001). Proteomic and functional evidence for a $P2X_7$ receptor signalling complex. *EMBO J,* 20: 6347-58.

KING, B. F., LIU, M., PINTOR, J., GUALIX, J., MIRAS-PORTUGAL, M. T. & BURNSTOCK, G. (1999). Diinosine pentaphosphate (IP5I) is a potent antagonist at recombinant rat $P2X_1$ receptors. *Br J Pharmacol,* 128: 981-988.

KUKLEY, M., STAUSBERG, P., ADELMANN, G., CHESSELL, I. P. & DIETRICH, D. (2004). Ecto-nucleotidases and nucleoside transporters mediate activation of adenosine receptors on hippocampal mossy fibers by $P2X_7$ receptor agonist 2'-3'-O-(4-Benzoylbenzoyl)-ATP. *J Neurosci,* 24: 7128-7139.

KUSNER, D. J. & ADAMS, J. (2000). ATP-induced killing of virulent Mycobacterium tuberculosis within human macrophages requires phospholipase D. *J Immunol,* 164: 379-388.

LABASI, J. M., PETRUSHOVA, N., DONOVAN, C., MCCURDY, S., LIRA, P., PAYETTE, M. M., BRISSETTE, W., WICKS, J. R., AUDOLY, L. & GABEL, C. A. (2002). Absence of the $P2X_7$ receptor alters leukocyte function and attenuates an inflammatory response. *J Immunol,* 168: 6436-6445.

LAMBRECHT, G., FRIEBE, T., GRIMM, U., WINDSCHEIF, U., BUNGARDT, E., HILDEBRANDT, C., BAUMERT, H. G., SPATZ-KUMBEL, G. & MUTSCHLER, E. (1992). PPADS, a novel functionally selective antagonist of P2 purinoceptor-mediated responses. *Eur J Pharmacol,* 217: 217-219.

LAMBRECHT, G., RETTINGER, J., BAUMERT, H. G., CZECHE, S., DAMER, S., GANSO, M., HILDEBRANDT, C., NIEBEL, B., SPATZ-KUMBEL, G., SCHMALZING, G. & MUTSCHLER, E. (2000). The novel pyridoxal-5'-phosphate derivative PPNDS potently antagonises activation of $P2X_1$ receptors. *Eur J Pharmacol,* 387: R19-21.

LÊ, K.-T., PAQUET, M., NOUEL, D., BABINSKI, K. & SÉGUÉLA, P. (1997). Primary structure and expression of a naturally truncated human P2X ATP receptor subunit from brain and immune system. *FEBS Lett,* 418: 195-199.

LENERTZ, L. Y., WANG, Z., GUADARRAMA, A., HILL, L. M., GAVALA, M. L. & BERTICS, P. J. (2010). Mutation of putative *N*-linked glycosylation sites on the human nucleotide receptor $P2X_7$ reveals a key residue important for receptor function. *Biochemistry*, 49: 4611-4619.

LEWIS, C., NEIDHART, S., HOLY, C., NORTH, R. A., BUELL, G. & SURPRENANT, A. (1995). Coexpression of $P2X_2$ and $P2X_3$ receptor subunits can account for ATP-gated currents in sensory neurons. *Nature,* 377: 432-435.

LI, M., CHANG, T.-H., SILBERBERG, S. D. & SWARTZ, K. J. (2008). Gating the pore of P2X receptor channels. *Nat Neurosci,* 11: 883-887.

LISTER, M., SHARKEY, J., SAWATZKY, D., HODGKISS, J., DAVIDSON, D., ROSSI, A. & FINLAYSON, K. (2007). The role of the purinergic $P2X_7$ receptor in inflammation. *J Inflamm,* 4: 5.

LIU, L., ZOU, J., LIU, X., JIANG, L.-H. & LI, J. (2010). Inhibition of ATP-induced macrophage death by emodin via antagonising $P2X_7$ receptor. *Eur J Pharmacol,* 640: 15-19.

LIU, X., MA, W., SURPRENANT, A. & JIANG, L.-H. (2009). Identification of the amino acid residues in the extracellular domain of rat $P2X_7$ receptor involved in functional inhibition by acidic pH. *Br J Pharmacol,* 156: 135-142.

LIU, X., SURPRENANT, A., MAO, H.-J., ROGER, S., XIA, R., BRADLEY, H. & JIANG, L.-H. (2008). Identification of key residues coordinating functional inhibition of $P2X_7$ receptors by zinc and copper. *Mol Pharmacol,* 73: 252-259.

LÓPEZ-CASTEJÓN, G., YOUNG, M. T., MESEGUER, J., SURPRENANT, A. & MULERO, V. (2007). Characterisation of ATP-gated $P2X_7$ receptors in fish provides new insights into the mechanism of release of the leaderless cytokine interleukin-1β. *Mol Immunol,* 44: 1286-1299.

LUCAE, S., SALYAKINA, D., BARDEN, N., HARVEY, M., GAGNE, B., LABBE, M., BINDER, E. B., UHR, M., PEAEZ-PEREDA, M., SILLABER, I., ISING, M., BRUCKL, T., LIEB, R., HOLSBOER, F. & MULLER-MYHSOK, B. (2006). *P2X7,* a gene coding for a purinergic ligand-gated ion channel, is associated with major depressive disorder. *Human Mol Genet,* 15: 2438-2445.

LUSTIG, K. D., SHIAU, A. K., BRAKE, A. J. & JULIUS, D. (1993). Expression cloning of an ATP receptor from mouse neuroblastoma cells. *Proc Natl Acad Sci USA,* 90: 5113-5117.

LYNCH, K. J., TOUMA, E., NIFORATOS, W., KAGE, K. L., BURGARD, E. C., VAN BIESEN, T., KOWALUK, E. A. & JARVIS, M. F. (1999). Molecular and functional characterisation of human $P2X_2$ receptors. *Mol Pharmacol,* 56: 1171-1181.

MACKENZIE, A. B., YOUNG, M. T., ADINOLFI, E. & SURPRENANT, A. (2005). Pseudoapoptosis induced by brief activation of ATP-gated $P2X_7$ receptors. *J Biol Chem,* 280: 33968-33976.

MARQUEZ-KLAKA, B., RETTINGER, J., BHARGAVA, Y., EISELE, T. & NICKE, A. (2007). Identification of an intersubunit cross-link between substituted cysteine residues located in the putative ATP binding site of the $P2X_1$ receptor. *J Neurosci,* 27: 1456-1466.

MATUTE, C., TORRE, I., PEREZ-CERDA, F., PEREZ-SAMARTIN, A., ALBERDI, E., ETXEBARRIA, E., ARRANZ, A. M., RAVID, R., RODRIGUEZ-ANTIGUEDAD, A., SANCHEZ-GOMEZ, M. & DOMERCQ, M. (2007). $P2X_7$ receptor blockade prevents ATP excitotoxicity in oligodendrocytes and ameliorates experimental autoimmune encephalomyelitis. *J Neurosci,* 27: 9525-9533.

MATUTES, E., OWUSU-ANKOMAH, K., MORILLA, R., GARCIA MARCO, J., HOULIHAN, A., QUE, T. H. & CATOVSKY, D. (1994). The immunological profile of B-cell disorders and proposal of a scoring system for the diagnosis of CLL. *Leukemia,* 8: 1640-1645.

MCGARAUGHTY, S., CHU, K. L., NAMOVIC, M. T., DONNELLY-ROBERTS, D. L., HARRIS, R. R., ZHANG, X. F., SHIEH, C. C., WISMER, C. T., ZHU, C. Z., GAUVIN, D. M., FABIYI, A. C., HONORE, P., GREGG, R. J., KORT, M. E., NELSON, D. W., CARROLL, W. A., MARSH, K., FALTYNEK, C. R. & JARVIS, M. F. (2007). $P2X_7$-related modulation of pathological nociception in rats. *Neuroscience,* 146: 1817-1828.

MCLARNON, J. G., RYU, J. K., WALKER, D. G. & CHOI, H. B. (2006). Upregulated expression of purinergic $P2X_7$ receptor in Alzheimer disease and amyloid-β peptide-treated microglia and in peptide-injected rat hippocampus. *J Neuropath Expt Neurol,* 65, 1090-1097.

MCQUILLIN, A., BASS, N. J., CHOUDHURY, K., PURI, V., KOSMIN, M., LAWRENCE, J., CURTIS, D. & GURLING, H. M. D. (2008). Case-control studies show that a non-conservative amino-acid change from a glutamine to arginine in the $P2X_7$ purinergic receptor protein is associated with both bipolar- and unipolar-affective disorders. *Mol Psychiatry,* 14: 614-620.

MICHEL, A. D., CLAY, W. C., NG, S. W., ROMAN, S., THOMPSON, K., CONDREAY, J. P., HALL, M., HOLBROOK, J., LIVERMORE, D. & SENGER, S. (2008). Identification of regions of the $P2X_7$ receptor that contribute to human and rat species differences in antagonist effects. *Br J Pharmacol,* 155: 738-751.

MICHEL, A. D., NG, S. W., ROMAN, S., CLAY, W. C., DEAN, D. K. & WALTER, D. S. (2009). Mechanism of action of species-selective $P2X_7$ receptor antagonists. *Br J Pharmacol,* 156: 1312-1325.

MULRYAN, K., GITTERMAN, D. P., LEWIS, C. J., VIAL, C., LECKIE, B. J., COBB, A. L., BROWN, J. E., CONLEY, E. C., BUELL, G., PRITCHARD, C. A. & EVANS, R. J. (2000). Reduced vas deferens contraction and male infertility in mice lacking $P2X_1$ receptors. *Nature,* 403: 86-89.

MURGIA, M., HANAU, S., PIZZO, P., RIPPA, M. & DIVIRGILIO, F. (1993). Oxidized ATP - an irreversible inhibitor of the macrophage purinergic P2Z receptor. *J Biol Chem,* 268: 8199-8203.

MURRELL-LAGNADO, R. D. & QURESHI, O. S. (2008). Assembly and trafficking of P2X purinergic receptors. *Mol Membr Biol,* 25: 321 - 331.

NAWA, G., URANO, T., TOKINO, T., OCHI, T. & MIYOSHI, Y. (1998). Cloning and characterisation of the murine P2XM receptor gene. *J Hum Genet.* , 43: 262-267.

NELSON, D. W., GREGG, R. J., KORT, M. E., PEREZ-MEDRANO, A., VOIGHT, E. A., WANG, Y., GRAYSON, G., NAMOVIC, M. T., DONNELLY-ROBERTS, D. L., NIFORATOS, W., HONORE, P., JARVIS, M. F., FALTYNEK, C. R. & CARROLL, W. A. (2006). Structure-activity relationship studies on a series of novel, substituted 1-benzyl-5-phenyltetrazole $P2X_7$ antagonists. *J Med Chem,* 49: 3659-3666.

NICKE, A., BÄUMERT, H. G., RETTINGER, J., EICHELE, A., LAMBRECHT, G., MUTSCHLER, E. & SCHMALZING, G. (1998). $P2X_1$ and $P2X_3$ receptors form stable trimers: a novel structural motif of ligand-gated ion channels. *EMBO J,* 17: 3016–3028.

NICKE, A. (2008). Homotrimeric complexes are the dominant assembly stateof native $P2X_7$ subunits. *Biochem Biophys Res Commun,* 377:803-808.

NICKE, A. (2009). A Functional $P2X_7$ splice variant with an alternative transmembrane domain 1 escapes gene inactivation in $P2X_7$ knock-out mice. *J Biol Chem*, 284:25813-25822.

NOGUCHI, T., ISHII, K., FUKUTOMI, H., NAGURO, I., MATSUZAWA, A., TAKEDA, K. & ICHIJO, H. (2008). Requirement of reactive oxygen species-dependent activation of ASK1-p38 MAPK pathway for extracellular ATP-induced apoptosis in macrophage. *J Biol Chem,* 283: 7657-7665.

NORTH, R. A. (2002). Molecular physiology of P2X receptors. *Physiol Rev,* 82: 1013-1067.

PARVATHENANI, L. K., TERTYSHNIKOVA, S., GRECO, C. R., ROBERTS, S. B., ROBERTSON, B. & POSMANTUR, R. (2003). $P2X_7$ mediates superoxide production in primary microglia and is up-regulated in a transgenic mouse model of Alzheimer's disease. *J Biol Chem,* 278: 13309-13317.

PAUKERT, M., HIDAYAT, S. & GRÜNDER, S. (2002). The $P2X_7$ receptor from *Xenopus laevis*: formation of a large pore in *Xenopus* oocytes. *FEBS Lett,* 513: 253-258.

PELEGRIN, P. & SURPRENANT, A. (2006). Pannexin-1 mediates large pore formation and interleukin-1 release by the ATP-gated $P2X_7$ receptor. *EMBO J,* 25: 5071-5082.

RALEVIC, V. & BURNSTOCK, G. (1998). Receptors for purines and pyrimidines. *Pharmacol Rev,* 50: 413-492.

RASSENDREN, F., BUELL, G. N., VIRGINIO, C., COLLO, G., NORTH, R. A. & SURPRENANT, A. (1997b). The permeabilising ATP receptor, $P2X_7$. CLONING AND EXPRESSION OF A HUMAN cDNA. *J Biol Chem,* 272: 5482-5486.

RETTINGER, J., BRAUN, K., HOCHMANN, H., KASSACK, M. U., ULLMANN, H., NICKEL, P., SCHMALZING, G. & LAMBRECHT, G. (2005). Profiling at recombinant homomeric and heteromeric rat P2X receptors identifies the suramin analogue NF449 as a highly potent $P2X_1$ receptor antagonist. *Neuropharmacology,* 48: 461-468.

RETTINGER, J., SCHMALZING, G., DAMER, S., MULLER, G., NICKEL, P. & LAMBRECHT, G. (2000). The suramin analogue NF279 is a novel and potent antagonist selective for the $P2X_1$ receptor. *Neuropharmacology,* 39: 2044-2053.

ROBERTS, J. A., DIGBY, H. R., KARA, M., AJOUZ, S. E., SUTCLIFFE, M. J. & EVANS, R. J. (2008). Cysteine substitution mutagenesis and the effects of methanethiosulfonate reagents at $P2X_2$ and $P2X_4$ receptors support a core common mode of ATP action at P2X receptors. *J Biol Chem,* 283: 20126-20136.

ROBERTS, J. A. & EVANS, R. J. (2004). ATP Binding at Human $P2X_1$ Receptors: CONTRIBUTION OF AROMATIC AND BASIC AMINO ACIDS REVEALED USING MUTAGENESIS AND PARTIAL AGONISTS. *J Biol Chem,* 279: 9043-9055.

ROBERTS, J. A. & EVANS, R. J. (2006). Contribution of conserved polar glutamine, asparagine and threonine residues and glycosylation to agonist action at human $P2X_1$ receptors for ATP. *J Neurochem,* 96: 843-852.

ROBERTS, J. A. & EVANS, R. J. (2007). Cysteine substitution mutants give structural insight and identify ATP binding and activation sites at P2X receptors. *J Neurosci,* 27: 4072-4082.

ROBERTS, J. A., VALENTE, M., ALLSOPP, R. C., WATT, D. & EVANS, R. J. (2009). Contribution of the region Glu^{181} to Val^{200} of the extracellular loop of the human $P2X_1$ receptor to agonist binding and gating revealed using cysteine scanning mutagenesis. *J Neurochem,* 109: 1042-1052.

ROGER, S., MEI, Z.-Z., BALDWIN, J. M., DONG, L., BRADLEY, H., BALDWIN, S. A., SURPRENANT, A. & JIANG, L.-H. (2010a). Single nucleotide polymorphisms that were identified in affective mood disorders affect ATP-activated $P2X_7$ receptor functions. *J Psych Res,* 44: 347-355.

ROGER, S., PELEGRIN, P. & SURPRENANT, A. (2008). Facilitation of $P2X_7$ receptor currents and membrane blebbing via constitutive and dynamic calmodulin binding. *J Neurosci,* 28: 6393-6401.

ROGER, S. B., GILLET, L., BAROJA-MAZO, A., SURPRENANT, A. & PELEGRIN, P. (2010b). C-terminal calmodulin-binding motif differentially controls human and rat $P2X_7$ receptor current facilitation. *J Biol Chem,* 285: 17514-17524.

ROMAN, S., CUSDIN, F., FONFRIA, E., GOODWIN, J., REEVES, J., LAPPIN, S., CHAMBERS, L., WALTER, D., CLAY, W. & MICHEL, A. (2009). Cloning and pharmacological characterisation of the dog $P2X_7$ receptor. *Brit J Pharmacol,* 158: 1513-1526.

RONG, W., GOURINE, A. V., COCKAYNE, D. A., XIANG, Z., FORD, A. P. D. W., SPYER, K. M. & BURNSTOCK, G. (2003). Pivotal role of nucleotide $P2X_2$ receptor subunit of the ATP-gated ion channel mediating ventilatory responses to hypoxia. *J Neurosci,* 23: 11315-11321.

RYTEN, M., DUNN, P. M., NEARY, J. T. & BURNSTOCK, G. (2002). ATP regulates the differentiation of mammalian skeletal muscle by activation of a $P2X_5$ receptor on satellite cells. *J Cell Biol,* 158: 345-355.

RYU, J. K. & MCLARNON, J. G. (2008). Block of purinergic $P2X_7$ receptor is neuroprotective in an animal model of Alzheimer's disease. *NeuroReport,* 19: 1715-1719.

SAIMI, Y. & KUNG, C. (2002). Calmodulin as an ion channel subunit. *Ann Rev Physiol,* 64: 289-311.

SANCHEZ-NOGUEIRO, J., MARIN-GARCIA, P. & MIRAS-PORTUGAL, M. T. (2005). Characterisation of a functional $P2X_7$-like receptor in cerebellar granule neurons from $P2X_7$ knockout mice. *FEBS Lett,* 579: 3783-3788.

SASAKI, E., SUEMIZU, H., SHIMADA, A., HANAZAWA, K., OIWA, R., KAMIOKA, M., TOMIOKA, I., SOTOMARU, Y., HIRAKAWA, R., ETO, T., SHIOZAWA, S., MAEDA, T., ITO, M., ITO, R., KITO, C., YAGIHASHI, C., KAWAI, K., MIYOSHI, H., TANIOKA, Y., TAMAOKI, N., HABU, S., OKANO, H. & NOMURA, T. (2009). Generation of transgenic non-human primates with germline transmission. *Nature,* 459: 523-527.

SAUNDERS, B. M., FERNANDO, S. L., SLUYTER, R., BRITTON, W. J. & WILEY, J. S. (2003). A loss-of-function polymorphism in the human $P2X_7$ receptor abolishes ATP-mediated killing of mycobacteria. *J Immunol,* 171: 5442-5446.

SHARP, A., POLAK, P., SIMONINI, V., LIN, S., RICHARDSON, J., BONGARZONE, E. & FEINSTEIN, D. (2008). $P2X_7$ deficiency suppresses development of experimental autoimmune encephalomyelitis. *J Neuroinflammation,* 5: 33.

SHEMON, A. N., SLUYTER, R., FERNANDO, S. L., CLARKE, A. L., DAO-UNG, L. P., SKARRATT, K. K., SAUNDERS, B. M., TAN, K. S., GU, B. J., FULLER, S. J., BRITTON, W. J., PETROU, S. & WILEY, J. S. (2006). A Thr^{357} to Ser polymorphism in homozygous and compound heterozygous subjects causes absent or reduced $P2X_7$ function and impairs ATP-induced mycobacterial killing by macrophages. *J Biol Chem,* 281: 2079-2086.

SHINK, E., HARVEY, M., TREMBLAY, M., GAGNE, B., BELLEAU, P., RAYMOND, C., LABBE, M., DUBE, M. P., LAFRENIERE, R. G. & BARDEN, N. (2005). Analysis of microsatellite markers and single nucleotide polymorphisms in candidate genes for susceptibility to bipolar affective disorder in the chromosome 12Q24.31 region. American

Journal of Medical Genetics Part B: Neuropsychiatric Genetics, 135: 50-58.

SIM, J. A., CHAUMONT, S., JO, J., ULMANN, L., YOUNG, M. T., CHO, K., BUELL, G., NORTH, R. A. & RASSENDREN, F. (2006). Altered hippocampal synaptic potentiation in $P2X_4$ knock-out mice. *J Neurosci,* 26: 9006-9009.

SIM, J. A., YOUNG, M. T., SUNG, H.-Y., NORTH, R. A. & SURPRENANT, A. (2004). Reanalysis of $P2X_7$ receptor expression in rodent brain. *J Neurosci,* 24: 6307-6314.

SLUYTER, R., DALITZ, J. G. & WILEY, J. S. (2004a). $P2X_7$ receptor polymorphism impairs extracellular adenosine 5 '-triphosphate-induced interleukin-18 release from human monocytes. *Genes Immunity,* 5: 588-591.

SLUYTER, R., SHEMON, A. N. & WILEY, J. S. (2004b). Glu^{496} to Ala polymorphism in the $P2X_7$ receptor impairs ATP-induced IL-1β release from human monocytes. *J Immunol,* 172: 3399-3405.

SMART, M. L., GU, B., PANCHAL, R. G., WILEY, J., CROMER, B., WILLIAMS, D. A. & PETROU, S. (2003). $P2X_7$ receptor cell surface expression and cytolytic pore formation are regulated by a distal C-terminal region. *J Biol Chem,* 278: 8853-8860.

SOLLE, M., LABASI, J., PERREGAUX, D. G., STAM, E., PETRUSHOVA, N., KOLLER, B. H., GRIFFITHS, R. J. & GABEL, C. A. (2001). Altered cytokine production in mice lacking $P2X_7$ receptors. *J Biol Chem,* 276: 125-132.

SOMERS, J. M., GOLDNER, E. M., WARAICH, P. & HSU, L. (2006). Prevalence and incidence studies of anxiety disorders: a systematic review of the literature. *Can J Psychiatry,* 51: 100-113.

SOTO, F., GARCIA-GUZMAN, M., KARSCHIN, C. & STUHMER, W. (1996). Cloning and tissue distribution of a novel P2X receptor from rat brain. *Biochem Biophys Res Comm,* 223: 456-460.

SOTO, F., GARCIA-GUZMAN, M. & STÜHMER, W. (1997). Cloned ligand-gated channels activated by extracellular ATP (P2X receptors). *J Mem Biol,* 60: 91-100.

SOTO, F., KRAUSE, U., BORCHARDT, K. & RUPPELT, A. (2003). Cloning, tissue distribution and functional characterisation of the chicken $P2X_1$ receptor. *FEBS Lett,* 533: 54-58.

SOTO, F., LAMBRECHT, G., NICKEL, P., STUHMER, W. & BUSCH, A. E. (1999). Antagonistic properties of the suramin analogue NF023 at heterologously expressed P2X receptors. *Neuropharmacology,* 38: 141-149.

SOUSLOVA, V., CESARE, P., DING, Y., AKOPIAN, A. N., STANFA, L., SUZUKI, R., CARPENTER, K., DICKENSON, A., BOYCE, S., HILL, R., NEBENIUS-OOSTHUIZEN, D., SMITH, A. J. H., KIDD, E. J. & WOOD, J. N. (2000). Warm-coding deficits and aberrant inflammatory pain in mice lacking $P2X_3$ receptors. *Nature,* 407: 1015-1017.

SOUSLOVA, V., RAVENALL, S., FOX, M., WELLS, D., WOOD, J. N. & AKOPIAN, A. N. (1997). Structure and chromosomal mapping of the mouse $P2X_3$ gene. *Gene,* 195: 101-111.

SPERLÁGH, B., KÖFALVI, A., DEUCHARS, J., ATKINSON, L., J. MILLIGAN, C., BUCKLEY, N. J. & VIZI, E. S. (2002). Involvement of $P2X_7$ receptors in the regulation of neurotransmitter release in the rat hippocampus. *J Neurochem,* 81: 1196-1211.

STOKES, L., FULLER, S. J., SLUYTER, R., SKARRATT, K. K., GU, B. J. & WILEY, J. S. (2010). Two haplotypes of the $P2X_7$ receptor containing the Ala^{348} to Thr polymorphism exhibit a gain-of-function effect and enhanced interleukin-1β secretion. *FASEB J,* 24: 2916-2927.

STOKES, L., JIANG, L. H., ALCARAZ, L., BENT, J., BOWERS, K., FAGURA, M., FURBER, M., MORTIMORE, M., LAWSON, M., THEAKER, J., LAURENT, C., BRADDOCK, M. & SURPRENANT, A. (2006). Characterisation of a selective and potent antagonist of human $P2X_7$ receptors, AZ11645373. *Br J Pharmacol,* 149: 880-887.

SURPRENANT, A., RASSENDREN, F., KAWASHIMA, E., NORTH, R. A. & BUELL, G. (1996). The cytolytic P2Z receptor for extracellular ATP identified as a P2X receptor ($P2X_7$). *Science,* 272: 735-738.

THUNBERG, U., TOBIN, G., JOHNSON, A., SODERBERG, O., PADYUKOV, L., HULTDIN, M., KLARESKOG, L., ENBLAD, G., SUNDSTROM, C., ROOS, G. & ROSENQUIST, R. (2002). Polymorphism in the $P2X_7$

receptor gene and survival in chronic lymphocytic leukaemia. *Lancet,* 360: 1935-1939.

TORRES, G. E., EGAN, T. M. & VOIGT, M. M. (1999). Hetero-oligomeric assembly of P2X receptor subunits. SPECIFICITIES EXIST WITH REGARD TO POSSIBLE PARTNERS. *J Biol Chem,* 274: 6653-6659.

TOWNSEND-NICHOLSON, A., KING, B. F., WILDMAN, S. S. & BURNSTOCK, G. (1999). Molecular cloning, functional characterisation and possible cooperativity between the murine $P2X_4$ and $P2X_{4a}$ receptors. *Mol Brain Res,* 64: 246-254.

TSUDA, M., SHIGEMOTO-MOGAMI, Y., KOIZUMI, S., MIZOKOSHI, A., KOHSAKA, S., SALTER, M. W. & INOUE, K. (2003). $P2X_4$ receptors induced in spinal microglia gate tactile allodynia after nerve injury. *Nature,* 424: 778-783.

URANO, T., NISHIMORI, H., HAN, H., FURUHATA, T., KIMURA, Y., NAKAMURA, Y. & TOKINO, T. (1997). Cloning of P2XM, a novel human P2X receptor gene regulated by p53. *Cancer Res.,* 57: 3281-3287.

VALERA, S., HUSSY, N., EVANS, R. J., ADAMI, N., NORTH, R. A., SURPRENANT, A. & BUELL, G. (1994). A new class of ligand-gated ion channel defined by P2X receptor for extracellular ATP. *Nature,* 371: 516.

VALERA, S., TALABOT, F., EVANS, R. J., GOS, A., ANTONARAKIS, S. E., MORRIS, M. A. & BUELL, G. N. (1995). Characterisation and chromosomal localisation of a human P2X receptor from the urinary bladder. *Receptors Channels,* 3: 283-289.

VIAL, C. & EVANS, R. J. (2000). P2X receptor expression in mouse urinary bladder and the requirement of $P2X_1$ receptors for functional P2X receptor responses in the mouse urinary bladder smooth muscle. *Brit J Pharmacol,* 131: 1489-1495.

VIAL, C. & EVANS, R. J. (2002). $P2X_1$ receptor-deficient mice establish the native P2X receptor and a $P2Y_6$-like receptor in arteries. *Mol Pharmacol,* 62: 1438-1445.

VIRGINIO, C., CHURCH, D., NORTH, R. A. & SURPRENANT, A. (1997). Effects of divalent cations, protons and calmidazolium at the rat $P2X_7$ receptor. *Neuropharmacology,* 36: 1285-1294.

VIRGINIO, C., ROBERTSON, G., SURPRENANT, A. & NORTH, R. A. (1998). Trinitrophenyl-substituted nucleotides are potent antagonists selective for

$P2X_1$, $P2X_3$, and Heteromeric $P2X_{2/3}$ Receptors. *Mol Pharmacol,* 53: 969-973.

VON KÜGELGEN, I. (2006). Pharmacological profiles of cloned mammalian P2Y-receptor subtypes. *Pharmacol Ther,* 110: 415-432.

WALKER, E., SARASTE, M., RUNSWICK, M. J. & GAY, N. J. (1982). Distantly related sequences in the alpha- and beta-subunits of ATP synthase, myosin, kinases and other ATP-requiring enzymes and a common nucleotide binding fold. *EMBO J,* 1: 945-951.

WEBB, T. E., SIMON, J., KRISHEK, B. J., BATESON, A. N., SMART, T. G., KING, B. F., BURNSTOCK, G. & BARNARD, E. A. (1993). Cloning and functional expression of a brain G-protein-coupled ATP receptor. *FEBS Lett,* 324: 219-225.

WILEY, J. S., DAO-UNG, L. P., GU, B. J., SLUYTER, R., SHEMON, A. N., LI, C. P., TAPER, J., GALLO, J. & MANOHARAN, A. (2002). A loss-of-function polymorphic mutation in the cytolytic $P2X_7$ receptor gene and chronic lymphocytic leukaemia: a molecular study. *Lancet,* 35: 1114-1119.

WILEY, J. S., DAO-UNG, L. P., LI, C. P., SHEMON, A. N., GU, B. J., SMART, M. L., FULLER, S. J., BARDEN, J. A., PETROU, S. & SLUYTER, R. (2003). An Ile^{568} to Asn polymorphism prevents normal trafficking and function of the human $P2X_7$ receptor. *J Biol Chem,* 278: 17108-17113.

WILKINSON, W. J., JIANG, L.-H., SURPRENANT, A. & NORTH, R. A. (2006). Role of ectodomain lysines in the subunits of the heteromeric $P2X_{2/3}$ receptor. *Mol Pharmacol,* 70: 1159-1163.

WITTING, A., CHEN, L., CUDABACK, E., STRAIKER, A., WALTER, L., RICKMAN, B., MÃLLER, T., BROSNAN, C. & STELLA, N. (2006). Experimental autoimmune encephalomyelitis disrupts endocannabinoid-mediated neuroprotection. *Proc Natl Acad Sci USA,* 103: 6362-6367.

WORTHINGTON, R. A., SMART, M. L., GU, B. J., WILLIAMS, D. A., PETROU, S., WILEY, J. S. & BARDEN, J. A. (2002). Point mutations confer loss of ATP-induced human $P2X_7$ receptor function. *FEBS Lett,* 512: 43-46.

www.atrazeneca.com. Homepage. Accessed 14th Jan 2011.

www.clinicaltrials.gov. Homepage. Accessed 14th Jan 2011.

XIAO, J., SUN, L., JIAO, W., LI, Z., ZHAO, S., LI, H., JIN, J., JIAO, A., GUO, Y., JIANG, Z., MOKROUSOV, I. & SHEN, A. (2009). Lack of association

between polymorphisms in the *P2X7* gene and tuberculosis in a Chinese Han population. *FEMS Immunol Med Micro,* 55: 107-111.

YAMAMOTO, K., SOKABE, T., MATSUMOTO, T., YOSHIMURA, K., SHIBATA, M., OHURA, N., FUKUDA, T., SATO, T., SEKINE, K., KATO, S., ISSHIKI, M., FUJITA, T., KOBAYASHI, M., KAWAMURA, K., MASUDA, H., KAMIYA, A. & ANDO, J. (2006). Impaired flow-dependent control of vascular tone and remodeling in $P2X_4$-deficient mice. *Nat Med,* 12: 133-137.

YANG, S.-H., CHENG, P.-H., BANTA, H., PIOTROWSKA-NITSCHE, K., YANG, J.-J., CHENG, E. C. H., SNYDER, B., LARKIN, K., LIU, J., ORKIN, J., FANG, Z.-H., SMITH, Y., BACHEVALIER, J., ZOLA, S. M., LI, S.-H., LI, X.-J. & CHAN, A. W. S. (2008). Towards a transgenic model of Huntington's disease in a non-human primate. *Nature,* 453: 921-924.

YEGUTKIN, G. G. 2008. Nucleotide- and nucleoside-converting ectoenzymes: Important modulators of purinergic signalling cascade. *Biochim Biophys Acta,* 1783: 673-694.

YOUNG, M. T. (2010). P2X receptors: dawn of the post-structure era. *Trends Biochem Sci,* 35: 83-90.

YOUNG, M. T., PELEGRIN, P. & SURPRENANT, A. (2007). Amino acid residues in the $P2X_7$ receptor that mediate differential sensitivity to ATP and BzATP. *Mol Pharmacol,* 71: 92-100.

ZEMKOVA, H., YAN, Z., LIANG, Z., JELINKOVA, I., TOMIC, M. & STOJILKOVIC, S. S. (2007). Role of aromatic and charged ectodomain residues in the $P2X_4$ receptor functions. *J Neurochem,* 102; 1139-1150.

ZHANG, L. Y., IBBOTSON, R. E., ORCHARD, J. A., GARDINER, A. C., SEEAR, R. V., CHASE, A. J., OSCIER, D. G. & CROSS, N. C. P. (2003). $P2X_7$ polymorphism and chronic lymphocytic leukaemia: lack of correlation with incidence, survival and abnormalities of chromosome 12. *Leukemia,* 17: 2097-2100.

ZHANG, X., CHEN, Y., WANG, C. & HUANG, L. Y. M. (2007). Neuronal somatic ATP release triggers neuron-satellite glial cell communication in dorsal root ganglia. *Proc Natl Acad Sci USA,* 104: 9864-9869.